Use of Fe isotopes to examine Fe cycling in Boreal Shield lakes: implications for cyanobacterial bloom development and ancient biogeochemical cycling

by

Kai Liu

A thesis
presented to the University of Waterloo
in fulfillment of the
thesis requirement for the degree of
Doctor of Philosophy
in
Earth Sciences

Waterloo, Ontario, Canada, 2024

© Kai Liu 2024

Examining Committee Membership

The following served on the Examining Committee for this thesis.

External Examiner	Dr. Bridget Bergquist Professor, University of Toronto
Supervisors	Dr. Sherry Schiff Professor, University of Waterloo
	Dr. Thai Phan Adjunct Assistant Professor, University of Waterloo
Internal Members	Dr. Fereidoun Rezanezhad Research Associate Professor, University of Waterloo
	Dr. Brian Kendall Associate Professor, University of Waterloo
Internal-external Member	Dr. Josh Neufeld Professor, University of Waterloo

Author's Declaration

This thesis consists of material all of which I authored or co-authored: see Statement of Contributions included in the thesis. This is a true copy of the thesis, including any required final revisions, as accepted by my examiners. I understand that my thesis may be made electronically available to the public.

Statement of Contributions

Chapter 2

All lake samples and 2011 stream samples were collected by Sherry Schiff, Jason Venkiteswaran and Richard Elgood. The 2016-2017 stream samples were collected by a sampling team that included Rachel Henderson, Jennifer Mead, Jared Wolfe, Jordyn Atkins, Emily Barber, Eric McQuay, Sherry Schiff, Jason Venkiteswaran and Richard Elgood. Geochemical data were measured by Sherry Schiff, Jason Venkiteswaran and Richard Elgood. Cyanobacterial biomass concentrations were provided by IISD-ELA. Microbial data were measured by Jackson Tsuji. The analysis of Fe isotope composition was conducted by Kai Liu. A version of this chapter has been published as:

> Liu, K.; Schiff, S. L.; Wu, L.; Molot, L. A.; Venkiteswaran, J. J.; Paterson, M. J.; Elgood, R. J.; Tsuji, J. M.; Neufeld, J. D. Large Fractionation in Iron Isotopes Implicates Metabolic Pathways for Iron Cycling in Boreal Shield Lakes. Environ Sci Technol 2022, 56 (20), 14840-14851. DOI: 10.1021/acs.est.2c04247.

Chapter 3

Lake water column samples were collected by a sampling team that included Rachel Henderson, Jennifer Mead, Jared Wolfe, Jordyn Atkins, Emily Barber, Eric McQuay, Sherry Schiff, Jason Venkiteswaran and Richard Elgood.
Geochemical data were measured by Richard Elgood. Cyanobacterial biomass concentrations and cell density were provided by IISD-ELA. Fe speciation, Fe concentration and Fe isotope composition data were performed by Kai Liu, under the supervision of Thai Phan.

Chapter 4

Lake water column samples were collected by the same sampling team mentioned in Chapter 3. Sediment core samples were collected by Mike Paterson, Cyndy Desjardins, Paul Faford, Stephen Paterson, Sherry Schiff, Richard Elgood and Kai Liu. Geochemical data were measured by Richard Elgood. Fe isotope composition data were conducted by Kai Liu and Thai Phan.

Abstract

Stable iron (Fe) isotopes have only been used recently to explore biogeochemical Fe processes in terrestrial and aquatic ecosystems. The $\delta^{56}Fe$ values in natural samples range from −4‰ to 4‰. An increasing number of studies have focused on Fe isotopes in marine settings. However, few studies have focused on lake systems and only in extreme environments such as meromictic ferruginous lakes. This thesis has applications in two distinct fields, freshwater eutrophic research and early Earth evolution. Phytoplankton blooms have been studied extensively in lake ecosystems. Despite the fact that macronutrients phosphorus and nitrogen are commonly known as dominant factors controlling the blooms, the critical role of micronutrient Fe has been proposed in recent studies. However, current understanding of the sources and availability of Fe for phytoplankton blooms and Fe cycling in lakes in general remains limited. Although the mechanisms that result in the deposition of banded iron formation in the Archean ocean remain a subject of debate, it is proposed that photoferrotrophy played a significant role in the oxidation of Fe(II) in anoxic Archean oceans. Studies investigating the occurrence and significance of photoferrotrophy have primarily focused on meromictic and ferruginous lakes. However, such lakes are thought to be rare on a global scale.

To explore the potential application of stable Fe isotopes for tracing biogeochemical Fe cycling in Boreal Shield lakes, $\delta^{56}Fe$ values of dissolved, particulate, and sediment Fe were measured in two small dimictic Boreal Shield headwater lakes: manipulated eutrophic Lake 227, with annual cyanobacterial blooms, and unmanipulated oligotrophic Lake 442. Within these small lakes, the range in $\delta^{56}Fe$ is large (ca. −0.9 to +1.8‰), spanning more than half the entire range of natural Earth surface samples. Two layers in the water column with distinctive $\delta^{56}Fe$ of dissolved (DFe) and particulate Fe (PFe) were observed in both lakes, despite large differences in trophic states. During cyanobacterial blooms in Lake 227, selective uptake of isotopically light Fe modifies $\delta^{56}Fe$, resulting in $\Delta^{56}Fe_{dis\text{-}part}$ of up to 1‰ between dissolved and particulate Fe in the epilimnion while little fractionation was observed in the epilimnion of Lake 442. In the anoxic layers in both lakes, upward flux from sediments dominates the dissolved Fe pool with an apparent $\Delta^{56}Fe_{dis\text{-}part}$ of −2.2 to −0.6‰. Large $\Delta^{56}Fe_{dis\text{-}part}$ and previously published metagenome sequence data suggest active Fe cycling

processes in anoxic layers, such as microaerophilic Fe(II) oxidation or photoferrotrophy, could regulate biogeochemical cycling. Large fractionation of stable Fe isotopes in these lakes provides a potential tool to probe Fe cycling and the acquisition of Fe by cyanobacteria, with relevance for understanding biogeochemical cycling of Earth's early ferruginous oceans.

To further explore the effect of phytoplankton blooms on biogeochemical Fe cycling in the epilimnion and metalimnion of L227, seasonal variations in Fe concentrations, Fe speciation and Fe isotope compositions of dissolved Fe (DFe), particulate Fe (PFe) and total Fe (TFe) were reported in the oxic layers of L227 and L442. Biological uptake of Fe by phytoplankton results in a decrease in DFe, an increase in PFe and a decrease in TFe in the oxic epilimnion and metalimnion during the blooms. The prevalence of Fe(II) in the particulate Fe coupled with the depletion of Fe(II) in the dissolved Fe during the blooms suggest that diazotrophic cyanobacteria and chlorophytes in L227 likely utilize dissolved inorganic Fe(II) rather than organic complexed Fe(III), highlighting the importance of Fe(II) during iron acquisition. Uptake of isotopically light Fe by phytoplankton results in a diagnostic change in the dissolved and particulate $\delta^{56}Fe$ in the oxic layers. As a result, dissolved $\delta^{56}Fe$ is more positive than particulate $\delta^{56}Fe$ in the oxic layers of L227, with $\Delta^{56}Fe_{dis\text{-}part}$ of 1.02 ± 0.33‰ (2σ) during the peak of the first bloom and $\Delta^{56}Fe_{dis\text{-}part}$ of 0.56 ± 0.05‰ (2σ) during the second bloom. The difference in $\Delta^{56}Fe_{dis\text{-}part}$ observed during the first bloom and the second bloom suggests that uptake of Fe by chlorophytes might produce distinct Fe isotope fractionation compared to diazotrophic cyanobacteria, possibly due to the differences in their uptake kinetics, the specific Fe-uptake mechanisms and associated enzymatic processes. The consistency in TFe concentration and Fe isotope composition of TFe ($\delta^{56}Fe_{TFe}$) in the epilimnion throughout the first and second blooms suggest that the settling flux of particulate Fe is limited during the blooms, likely due to efficient retention by phytoplankton. In contrast, during the decline of the bloom, the settling of isotopically light particulate Fe(II) associated with biomass to profundal sediment caused $\delta^{56}Fe_{TFe}$ in the epilimnion to become isotopically heavier. During the peak of the first bloom, the large $\Delta^{56}Fe_{dis\text{-}part}$, the more negative particulate $\delta^{56}Fe$, and the more particulate Fe concentrations in the metalimnion compared to what has been observed in the epilimnion suggest that cyanobacteria could migrate to the upper zone of the anoxic hypolimnion to uptake Fe under

Fe-limited conditions. Modelling results showed that isotopically light PFe and TFe measured in the metalimnion during the peak of the first bloom are best explained by the migration of cyanobacteria below the redox boundary for the uptake of dissolved Fe(II). The observed seasonal variation in Fe concentration, speciation and isotope compositions associated with the progression of two annual blooms show great potential in understanding the role of Fe in the formation of cyanobacterial bloom and determining the availability and source of Fe for cyanobacterial uptake.

To explore the Fe processes and Fe sources in the anoxic hypolimnia of Boreal Shield lakes, seasonal variation in Fe concentrations and Fe isotope compositions of dissolved Fe and particulate Fe in the anoxic hypolimnia along with the Fe concentrations and Fe isotope compositions of porewater Fe and bulk sediment Fe in bottom sediment cores were reported in four Boreal Shield lakes: one eutrophic Lake 227 and three oligotrophic Lake 221, Lake 304 and Lake 442. In the oxic layers of all lakes, dissolved δ^{56}Fe is more positive than particulate δ^{56}Fe, likely modified by a combination of multiple processes including biological uptake, photochemical reduction of particulate Fe(III), complexation of dissolved Fe and dissolved organic matter, photolysis and microbial decomposition. The observed $\Delta^{56}Fe_{dis\text{-}part}$ in the oxic layers of all lakes ranges from 0.06 ± 0.09‰ (2σ) to 1.02 ± 0.33‰(2σ), with the higher values likely arising from biological uptake. In contrast, the δ^{56}Fe values of dissolved and particulate Fe are reversed in the anoxic hypolimnia of all lakes, with negative $\Delta^{56}Fe_{dis\text{-}part}$ fractionations of −0.91 ± 0.58‰ (2σ) in L221, −0.87 ± 0.81‰ (2σ) in L227, −1.06 ± 0.26‰ (2σ) in L304 and −0.72 ± 0.25‰ (2σ) in L442. Particulate Fe from the epilimnia is likely reduced completely by dissimilatory iron-reducing bacteria at the redox boundary, supported by the similarity in δ^{56}Fe between dissolved Fe in the anoxic hypolimnia and particulate Fe in the epilimnia of all lakes. The highly positive δ^{56}Fe values of particulate Fe in the anoxic hypolimnion and the large $\Delta^{56}Fe_{dis\text{-}part}$ fractionations indicate *in situ* active Fe cycling in the anoxic hypolimnion. The most plausible explanation for the large $\Delta^{56}Fe_{dis\text{-}part}$ fractionations in the anoxic hypolimnion is microbial oxidation, possibly photoferrotrophy, supported by the 16S rRNA gene sequencing and genome-resolved metagenome sequencing analysis. An increase in the magnitude of $\Delta^{56}Fe_{dis\text{-}part}$ with depth and over time was observed in L221, L227 and L304, likely due to the variation of the oxidation rates, supported by

increased particulate Fe concentrations with depth and time. The high concentration and negative δ^{56}Fe values of porewater Fe(II) suggest that DIR dominates organic mineralization pathways in sediment cores from the bottoms of L227, L304 and L442. The DIR-produced porewater δ^{56}Fe is further modified by the diagenetic formation of siderite in the upper section of sediment cores and the diagenetic formation of pyrite in the deeper section. Temporal and spatial variation in Fe isotope fractionation in the anoxic hypolimnia, along with the Fe isotope signatures in the sediment, suggest active Fe cycling in four lakes, highlighting the potential of seasonally anoxic Boreal Shield lakes to serve as analogues of the late Archean ocean.

Acknowledgements

I would like to extend my deepest gratitude to Dr. Sherry Schiff, my supervisor, whose insightful ideas and constructive comments have been the driving force behind the progress of this project. From the sampling to the data interpretation, Dr. Schiff's guidance has been invaluable. I am especially thankful for her assistance during sediment sampling in ELA.

A heartfelt thank you to Dr. Thai Phan, my co-supervisor, for his unparalleled expertise in utilizing MC-ICP-MS and QQQ-ICP-MS for the analysis of Fe isotopes and elemental concentrations. His supervision in the clean lab has been essential to the success of this research.

I would like to express my gratitude to Dr. Liyan Xing for configuring the MC-ICP-MS instrument for Fe isotope analysis and for her valuable contributions to analyzing a subset of the Fe samples.

I am deeply grateful to Dr. Lingling Wu for her generous guidance and support during the initial stages of my research journey, where she played a crucial role in teaching and guiding me.

Many many many thanks you to Richard Elgood, for years of encouragement, unwavering support, the tons of geochemical data analyzed in the lab and so many other things. His contributions have made this journey not only incredibly productive but also thoroughly enjoyable.

I express my gratitude to Dr. Brian Kendall for generously allowing me to conduct my isotope work in the Metal Isotope Geochemistry Laboratory at the University of Waterloo. In addition, I am truly grateful for Dr. Brian Kendall's valuable insights into the implications of my research on early Earth aspects.

Special thank you to Rachel Henderson for her dedicated efforts in sampling water samples in ELA in 2016-2018, contributing significantly to the data collection process.

I would like to acknowledge Dr. Jackson Tsuji for his valuable insights into microbial data and consistent provision of excellent suggestions in the microbial aspect of the project.

I am greatly thankful to Josh Neufeld for his consistently excellent, detailed suggestions and comments on manuscripts during the publication process.

I would like to express my great thanks to all committee members, Dr. Sherry Schiff, Dr. Thai Phan, Dr. Fereidoun Rezanezhad and Dr. Brian Kendall, for their supportive and insightful comments, along with Dr. Bridget Bergquist for sharing her expertise as an external examiner. Their collective expertise has significantly enriched the depth and quality of this research.

We acknowledge that the IISD-ELA is situated on the traditional territory of the Anishinaabe Nations within Treaty #3 territory and the homeland of the Métis Nation. Additionally, we acknowledge that University of Waterloo is located on the traditional land of the Attawandaron, Anishinaabeg and Haudenosaunee peoples.

Table of Contents

Examining Committee Membership ii
Author's Declaration iii
Statement of Contributions iv
Abstract v
Acknowledgements ix
List of Tables xiii
List of Figures xiv

Chapter 1 Introduction 1
1.1. Literature review 1
1.1.1. Geochemistry of iron 1
1.1.2. Microbially mediated Fe redox processes 2
1.1.3. Iron acquisition and utilization in phytoplankton in aquatic ecosystems 5
1.1.4. Evolution of the biogeochemistry of ancient oceans 6
1.1.5. Deposition of banded iron formations 7
1.1.6. Archean ocean analogues: the occurrence and significance of photoferrotrophy 9
1.1.7. Fe isotope fractionation during biogeochemical Fe processes 10
1.1.8. Fe isotope variations in BIF 13
1.2. Thesis outline 14

Chapter 2 Large fractionation in iron isotopes implicates metabolic pathways for iron cycling in Boreal Shield lakes 17
2.1. Introduction 17
2.2. Materials and methods 19
2.2.1. Sites and sampling 19
2.2.2. Chemical analysis 22
2.2.3. Iron isotope analyses 22
2.3. Results and Discussion 23
2.3.1. Geochemistry of boreal streams and lake water column 23
2.3.2. Iron isotopic compositions in boreal streams in upland and wetland catchments 27
2.3.3. Iron isotope composition in L227 and L442 29
Dissolved and particulate δ^{56}Fe values in the epilimnia 30
Dissolved and particulate δ^{56}Fe values in oxic hypolimnion of L442 36
Dissolved and particulate δ^{56}Fe values in anoxic hypolimnia 37
2.3.4. Comparison of δ^{56}Fe profiles in L227 and L442 to other lakes 41

Chapter 3 Fe isotopes reveal distinct Fe cycling pathways during cyanobacterial blooms in Boreal Shield lakes 43

3.1. Introduction 43
3.2. Methods 45
3.2.1. Study site 45
3.2.2. Sample collection 47
3.2.3. Chemical analyses 49
3.2.4. Lake water column geochemical profiles 50
3.2.5. Iron isotope analyses 52
3.3. Results and Discussion 54
3.3.1. Biogeochemical cycling in the oxic layers of L227 and L442 54
3.3.2. Fe isotope fractionations between dissolved and particulate Fe near the redox boundary of L227 during the second bloom (Stage III) and the post bloom (Stage IV) 74
3.3.3. Effect of phytoplankton blooms on settling flux of particulate Fe in L22778
3.3.4. Migration of cyanobacteria for the uptake of dissolved Fe(II) during the peak of the first bloom 82
3.4. Conclusion 88

Chapter 4 Fe isotopes track microbial Fe cycling in the water column and sediments of Boreal Shield lakes 90
4.1. Introduction 90
4.2. Methods 92
4.2.1. Study site 92
4.2.2. Water sample collection 94
4.2.3. Sediment cores and porewater collection 95
4.2.4. Chemical analysis 96
4.2.5. Iron isotope analyses 97
4.2.6. Lake water column geochemical profiles 98
4.3. Results and Discussion 99
4.3.1. Fe concentrations in the water column 101
4.3.2. Fe isotopic compositions and associated Fe isotope fractionations in the oxic layers 103
4.3.3. Fe isotopic compositions and associated Fe isotope fractionations in anoxic hypolimnia 106
4.3.4. Fe cycling pathways in the profundal sediments at the bottom of lakes 119
4.3.5. Fe isotope compositions of porewater Fe and bulk sediment Fe reflect early diagenetic processes 127
4.3.6. The flux of Fe from sediments in the hypolimnion of L227 131
4.4. Conclusion 133

Chapter 5 Conclusions and recommendations 134
5.1. Major conclusions with implications 134
5.2. Recommendations for Future Research 141

References 143

Appendix A. 174

Appendix B. Use of muti-collector ICP-MS for studying biogeochemical metal cycling 181
Introduction 181
Methodology 185
Instrumentation 185
Interference 188
Sample material 189
Sample preparation 190
MC-ICP-MS Analysis 191
Data reporting 193
Reference standards 194
Precision and accuracy 195
Conclusion 195

List of Tables

Table 2-1 Saturation indices of Fe(II) minerals in the hypolimnia of L227 and L442 38
Table 3-1 Phytoplankton biomass (mg/L) and cell density (10^6 cell/mL) in the epilimnion and metalimnion of L227 during 2018 56
Table 4-1 Morphological characteristics and trophic state of ELA lakes 93

List of Figures

Figure 2-1 Location of Lake 227, 442, and proxy streams in the International Institute for Sustainable Development - Experimental Lakes Area (IISD-ELA). 20

Figure 2-2 Cyanobacterial biomass in the epilimnion and metalimnion of L227 in 2011 (A) and 2014 (B). 21

Figure 2-3 Geochemical profiles in the water column of L227 (sampled on 06/28/2011; 08/24/2011; 07/09/2014) and L442 (sampled on 06/27/2011). 24

Figure 2-4 Dissolved Fe versus DOC concentrations (A) and $\delta^{56}Fe$ versus dissolved Fe or DOC concentrations (B) in Boreal Shield streams of the IISD-ELA. 27

Figure 2-5 Iron isotope compositions of dissolved Fe in boreal streams sampled on different dates. 28

Figure 2-6 Iron isotope compositions of dissolved (Fe_{dis}) and particulate Fe (Fe_{spm}), and Fe isotope fractionations ($\Delta^{56}Fe_{dis\text{-}spm}$) for the water columns of L227 (A, B) and L442 (C, D). 29

Figure 2-7 Microbial community data from the water columns of Lakes 227 and 442. 31

Figure 2-8 Schematic diagram showing processes operating in L227 and L442 that could impact the Fe isotope compositions of dissolved and particulate Fe. 32

Figure 2-9 Unsupported ^{210}Pb (A), ^{226}Ra and ^{137}Cs activities (B), and age (C) versus depth profiles in a sediment core from L227 (March 2011). 36

Figure 2-10 Chlorophyll *a* (chl *a*) profiles in the water column of L227 (06/28/2011) and L442 (05/30/2011). 37

Figure 3-1 Phytoplankton biomass in the epilimnion (panel A) and metalimnion (panel B) of L227 in 2018. 46

Figure 3-2 Water column depth profiles of (A, G) dissolved oxygen (DO) and temperature (T); (B, H) pH and conductivity; (C, I) total dissolved sulfide (ΣS^{2-}) and sulfate (SO_4^{2-}) (D, J) Dissolved inorganic carbon (DIC) and dissolved organic carbon (DOC); (E, K) total dissolved nitrogen (TDN), ammonium (NH_4^+) and total dissolved phosphorus (TDP); (F, L) particulate organic carbon (POC) and suspended particulate phosphorus (SPP) in L227 (upper panel) and L442 (lower panel) during 2018. 52

Figure 3-3 $\delta^{56}Fe$ vs $\delta^{57}Fe$ for all lake samples, together with rock standards and test solutions. 53

Figure 3-4 Depth profiles of (A) Fe/Al molar ratio of suspended particulates and particulate Fe concentrations, and (B) chl a concentrations in L227 during 2018. 57

Figure 3-5 Dissolved Fe, particulate Fe, and total Fe concentrations in L227 (A-E) and L442 (F-J) during 2018. 58

Figure 3-6 Iron isotope compositions ($\delta^{56}Fe$) of dissolved and particulate Fe in the water column of L227 (A, B) and L442 (C, D). 59

Figure 3-7 The effect of oxidation-precipitation on dissolved Fe concentration and dissolved $\delta^{56}Fe$. 77

Figure 3-8 Iron isotope compositions of total Fe ($\delta^{56}Fe_{TFe}$) in the water column of L227..... 80
Figure 3-9 Weekly concentration profiles of phycocyanin and chlorophyll *a* in the water column of L227 during ice-free season of 2018. 83
Figure 3-10 Modelling of integrated intracellular particulate $\delta^{56}Fe$ at 4m contributed from non-migrating cyanobacteria and migrating cyanobacteria. 86
Figure 4-1 Location of the study lakes in the Sustainable Development - Experimental Lake Area (IISD-ELA) and the bathymetry of Lake 227, L304 and L442. 94
Figure 4-2 Water column depth profiles of (A-C) dissolved oxygen (DO) and temperature (T); (D-F) pH and conductivity; (G-I) total dissolved sulfide (ΣS^{2-}) and sulfate (SO_4^{2-}); (J-L) Dissolved inorganic carbon (DIC) and dissolved organic carbon (DOC); (M-O) total dissolved nitrogen (TDN), ammonium (NH_4^+) and total dissolved phosphorus (TDP); (P-R) particulate organic carbon (POC) and suspended particulate phosphorus (SPP) in L227 (upper panel), L442 (middle panel) and L221& L304 (lower panel) during 2018. 99
Figure 4-3 Profiles of dissolved Fe and particulate Fe in L227 (a, b), L442 (c, d), L221 (e, f) and L304 (g, h) during 2018. 100
Figure 4-4 Iron isotope compositions ($\delta^{56}Fe$) of dissolved and particulate Fe in water column of L227 (A, B), L442 (D, D), L221 (E, F) and L304 (G, H). 101
Figure 4-5 Depth profile of chlorophyll *a* (chl *a*) concentrations in L304 on July 26 2018. 104
Figure 4-6 Eh versus pH diagram for species of Fe at 4.5°C. 110
Figure 4-7 Light profiles of the water column of L227, L221 and L304 in 2018. 114
Figure 4-8 Microscopy images showing longitudinal sections of cyanobacterial cells in the surface sediment of one sediment core collected at the bottom of L227. 115
Figure 4-9 Average Fe concentrations of porewater (A) and average Fe/Al molar ratios of bulk sediment (B) in each sediment core versus the depth of the sediment core in L227, L304 and L442. 121
Figure 4-10 Fe concentrations of porewater and bulk sediments in the sediment core of L227 (A), L304 (B) and L442 (C). 122
Figure 4-11 Iron isotope composition of porewater and bulk sediments in the sediment core of L227 (A), L304 (B) and L442 (C). 128

Chapter 1
Introduction

1.1. Literature review

1.1.1. Geochemistry of iron

As the fourth most abundant element in the Earth's crust,[1] iron (Fe) forms complexes and reacts with many important elements such as oxygen (O), carbon (C), nitrogen (N), sulfur (S) and phosphorous (P) in natural environments.[2] As such, Fe redox transformations play an important or even a dominant role in the physicochemical processes involving these redox-sensitive elements, which together compose the main biogeochemical cycles in terrestrial and aquatic ecosystems.[3] Furthermore, Fe redox transformations provide important potential pathways to treat the contaminants in freshwater systems as Fe can either act as a catalyst in the reduction of metals (e.g., Cr, As),[4, 5] radionuclides (e.g., U)[6] and organic contaminants,[7, 8] or influence the mobility of these substances through sorption and co-precipitation,[9, 10] leading to subsequent precipitation and removal of these substances from aquatic environment (see review[11]).

Fe has two main redox states in natural environments: ferrous Fe (Fe(II)) and ferric Fe (Fe(III)). The chemical behaviour of Fe in aquatic systems depends strongly on physicochemical conditions (e.g., pH and Eh), dissolved organic matter (DOM) and inorganic substances that could interact with Fe.[12] Fe(II) is easily soluble under anoxic conditions, but it can react with dissolved sulfide, bicarbonate or phosphate, leading to the precipitation of Fe(II) minerals (e.g., FeS, siderite or vivianite) when these minerals are saturated. Fe(III) is thermodynamically stable under oxic conditions and tends to form poorly soluble Fe oxyhydroxides at circumneutral pH. A decrease in pH usually increases the solubility of Fe(III).[12] Decreasing pH can also promote the stability of Fe(II) in the presence of O_2, by slowing the rate of oxidation, making dissolved Fe(II) quite quasi-stable (pH<4.0).[12] Both Fe(II) and Fe(III) form strong complexes with DOM.[13-15] With the complexation of Fe with DOM leading to increased solubility of dissolved Fe(III) and the stability of dissolved Fe(II)[16-18], Fe(II)-DOM complexation can either accelerate or have no

effect on the rate of Fe(II) oxidation. The variable effects depend on the molecular composition of DOM and experimental system.[19] It is widely reported that Fe is intimately associated with DOM by strongly binding to organic ligands in aquatic environments.[20-24] Most of Fe(III) (>99%) is organically complexed Fe(III) in surface seawater[20-23] and likely also for surface freshwater systems.[24]

Abiotic redox reactions of Fe with redox species of other elements play a substantial role in environmental Fe cycling. Fe(II) is rapidly chemically oxidized to Fe(III) by O_2 at circumneutral pH, whereby the rate strongly depends on pH, temperature and oxygen concentrations.[25] The abiotic oxidation of Fe(II) by MnO_2 plays an important role in micro-oxic and anoxic environments such as freshwater and marine sediments.[26] Fe(II) can also be oxidized by NO_2^- and such reactions have a key role in the oxic-anoxic boundary zone.[27] Conversely, Fe(III) oxyhydroxides can be reduced abiotically by certain types of organic ligands (e.g., humic and fulvic acids) and hydrogen sulfide (H_2S), the latter of which has an important role in sulfate-rich environments where reduction of sulfate can produce a relatively high concentrations of sulfide.[28, 29] Fe(III) can also be photochemically reduced to Fe(II) in the presence of light, either via direct ligand-to-metal charge transfer (LMCT) or via indirect reactions with photochemically produced radicals.[30] Organically complexed Fe(III), the predominant Fe species in most surface aquatic systems with circumneutral pH, is readily reduced by photochemical reduction.[31] Consequently, photochemical Fe(III) reduction is a widespread pathway in sunlit freshwater and marine environments, producing inorganic dissolved Fe(II) in surface oxygenated water.[28]

1.1.2. Microbially mediated Fe redox processes

Fe plays an important role in the biosphere. Fe is intimately involved in various microbial metabolic processes, acting as an electron donor or acceptor.[32] Microbial Fe redox pathways are mediated by Fe(II)-oxidizing and Fe(III)-reducing microorganisms, which gain energy from Fe redox transformation.[28, 32, 33] Neutrophilic Fe(II)-oxidizing bacteria include microaerophilic Fe(II)-oxidizing bacteria, photoferrotrophs and nitrate-reducing Fe(II)-oxidizing bacteria.[28, 32, 33] In most cases, the products of biological Fe oxidation are

commonly thought to be poorly crystalline Fe(III) oxyhydroxides (e.g., ferrihydrite), which could mature into other crystalline Fe(III) minerals (e.g., goethite).[33]

Microaerophilic Fe(II)-oxidizing bacteria can oxidize Fe(II) in the presence of a trace amount of O_2 in aquatic systems and sediments.[34, 35] Microaerophilic Fe(II) oxidizing bacteria commonly inhabit oxic-anoxic interfaces, where O_2 is less than 50 μM,[36] or micro-oxic environments, where O_2 is at submicromolar concentrations,[37, 38] as the rate of microaerophilic Fe(II) oxidation needs to outcompete the rate of abiotic oxidation by O_2 at circumneutral pH.[39] The most notable examples of microaerophilic Fe(II)-oxidizing bacteria include freshwater genera *Gallionella*, *Sideroxydans*, *Ferriphaselus*, *Leptothrix* and marine genera *Mariprofundus* and *Ghiorsea*.[33]

Photoferrotrophs are primary producers that fix inorganic carbon into organic matter utilizing light as an energy source and Fe(II) as an electron donor.[40] Photoferrotrophs are thought to live mostly in aquatic environments as light can penetrate more than 100 m in the water column and only several millimeters in soil and sediments.[30, 41] Photoferrotrophy is identified in three taxonomic groups, including purple sulfur bacteria (PSB, phylum *Gammaproteobacteria*; e.g., *Thiodictyon* sp.), purple non-sulfur bacteria (PNSB, phylum *Alphaproteobacteria*; e.g., *Rhodobacter ferrooxidans*) and green sulfur bacteria (GSB, family *Chlorobiaceae*; e.g., *Chlorobium ferrooxidans*), although most of them are also able to utilize several electron donors other than Fe(II).[33] It has been suggested that GSB could inhabit deeper in the water column with low light availability compared to PSB and PNSB due to the lower light requirement and the shorter wavelengths utilized by GSB.[42, 43]

Nitrate-reducing Fe(II)-oxidizing bacteria (NRFeOx) can couple the oxidation of Fe(II) to the reduction of nitrate under anoxic conditions in various aquatic systems and in the upper few millimetres of sediments.[44] Only a few strains, called chemolithoautotrophic NRFeOx, can utilize Fe(II) as an electron donor and gain energy to fix inorganic carbon into biomass,[45, 46] while most other NRFeOx cannot grow autotrophically, hence requiring an organic co-substrate for Fe(II) oxidation.[47, 48] Although there is considerable debate on whether Fe(II) is enzymatically oxidized during metabolisms[47, 49] or Fe(II) is chemically oxidized by the reactive nitrogen species produced from heterotrophic denitrification,[50] nitrate-reducing Fe(II)-oxidizing bacteria may have played a key role in coupled Fe-N redox transformation (e.g., production of the greenhouse gas N_2O).

Fe(III)-reducing bacteria couple the reduction of Fe(III) substrates with the oxidation of inorganic compounds (H_2, NH_4), CH_4 or organic matter (OM), including fatty acids, amino acids and various aromatic compounds, in anoxic environments.[51] Examples of Fe(III)-reducing bacteria include *Geobacter* spp., *Shewanella* spp., *Albidoferax ferrireducens*, *Geothrix fermentans* and some hyperthermophilic archaea.[33] A variety of Fe(III) substances can be reduced by Fe(III)-reducing bacteria including dissolved Fe(III) complexes, poorly crystalline Fe(III) oxyhydroxides (e.g., ferrihydrite), crystalline Fe(III) oxides (e.g., goethite, hematite and magnetite) and Fe-rich clays (e.g., smectite).[52-54] The products of dissimilatory iron reduction (DIR), including siderite, magnetite, vivianite and green rust (i.e., mixed valence layered hydroxides), are influenced by factors such as the concentration of other anions, the concentration of Fe(III) substances, the Fe(II) supply rate and the bacterial species mediating Fe reduction.[55-57] Several Fe(III)-reducing species need direct contact with the surface of Fe(III) substances, whereas other species can utilize either extracellular conductive structures (e.g., conductive pili) or redox-reactive electron shuttles (e.g., humic substances) to transfer electrons to Fe(III) over distances of multiple μm to cm.[28, 33] Recent studies also highlight the important role of microbial Fe(III) reduction in the oxidation of ammonium and methane in anoxic environments.[33] It was suggested that Fe-ammox, which couples the reduction of Fe(III) with the oxidation of ammonium, can be mediated by some bacteria (e.g., *Acidimicrobiaceae* sp. A6)[58] in anoxic water-saturated soils such as riparian and wetlands.[59, 60] In addition, Fe(III)-dependent anaerobic methane oxidation that links the reduction of Fe(III) and methane oxidation was inferred in anoxic environments such as lakes, freshwater and marine sediments, and aquifers.[61-63]

Archaea also perform Fe reduction and Fe oxidation. Fe(II)-oxidizing archaea and Fe(III)-reducing archaea are widespread in natural environments.[64] Most of Fe(II)-oxidizing archaea are acidophiles (e.g., *Metallosphaera yellowstonensis*)[65] that are discovered in acidic environments. Fe(III)-reducing archaea include (hyper-)thermophilic archaea[66] and anaerobic methane-oxidizing archaea[67] that can couple the reduction of Fe(III) with the oxidation of H_2 or CH_4.

1.1.3. Iron acquisition and utilization in phytoplankton in aquatic ecosystems

Fe is a crucial element in nearly all living organisms as it is readily incorporated into various biological compounds, especially metalloproteins involved in metabolisms.[2] It is now well established that Fe is an essential micronutrient for phytoplankton, including eukaryotic algae and cyanobacteria.[68] Both cyanobacteria, the oldest oxygenic photoautotrophs responsible for the initial rise of atmospheric O_2 on early Earth, and eukaryotic algae are important primary producers in freshwater and marine systems.[69] Some cyanobacteria are capable of nitrogen fixation, hence playing an important role in the nitrogen cycle. It is widely accepted that phytoplankton, especially nitrogen-fixing cyanobacteria, have a greater Fe requirement than other heterotrophic bacteria.[70-72] However, Fe is typically scarce in oxic aquatic environments due to its limited solubility at circumneutral pH.[2] The constraints of Fe on phytoplankton growth were observed in some lakes and in certain high-nutrient, low-carbon areas of the ocean (e.g., the Southern Ocean, northeast Pacific Ocean and the equatorial Pacific Ocean), where the bioavailability of Fe could limit biological productivity.[73-77] Nevertheless, cyanobacteria and eukaryotic algae could either utilize adaptive mechanisms to optimize Fe uptake or decrease their requirement for Fe to survive in environments where Fe is extremely rare.[78] The bioavailability of Fe to phytoplankton is controlled not only by Fe redox processes, which influence the speciation, solubility and mobility of Fe, but also by the specific Fe-uptake pathways in each strain.[78] Considerable effort has been made to understand the mechanisms of Fe acquisition in phytoplankton, especially in cyanobacteria.[79, 80] The common Fe-uptake mechanisms include porin-mediated Fe uptake, siderophore-mediated Fe transport and reductive Fe uptake.[79, 80] It is commonly considered that dissolved inorganic Fe (Fe') is more bioavailable than organically complexed Fe in terms of Fe acquisition by cyanobacteria.[81, 82] Fe' can be transported through the outer membrane of cyanobacteria by porins, which are not permeable to organically complexed Fe.[83] The porin-mediated Fe uptake is proposed to be a common Fe transport pathway amongst cyanobacteria.[84] However, as most of Fe (>99%) is organically complexed Fe in aquatic systems,[20-23] the concentration of Fe' is extremely low. Siderophore mediated transport, which involves the complexation of Fe(III) with low molecular weight compounds (siderophore) and the transport of Fe(III)-siderophore complexes into the cell, is well characterized in both cyanobacteria and eukaryotic algae under Fe starvation.[85-87] An

alternative pathway of Fe acquisition that has been studied extensively in cyanobacteria and eukaryotic algae is reductive Fe uptake, which involves the reduction of Fe(III) before the transport of Fe through the plasma membrane. Cyanobacteria are thought to reduce Fe(III) to dissolved inorganic Fe(II) on the plasma membrane (or in the periplasm),[85, 88, 89] or generate superoxide to reduce Fe(III) to dissolved inorganic Fe(II) extracellularly.[90, 91] In addition, reduction/reoxidation Fe-uptake is proposed in some phytoplankton strains, which require the subsequent reoxidation of Fe(II) in the periplasm before Fe internalization.[92]

1.1.4. Evolution of the biogeochemistry of ancient oceans

The evolution of the ocean and atmosphere in early Earth is closely linked to the biogeochemistry of Fe.[93, 94] Despite current limited knowledge of the nature of ancient ocean chemistry, the Archean ocean (4.0-2.5 billion years ago, Ga) is considered to have been predominantly anoxic and ferruginous, with low sulfate concentrations[95, 96] and a high abundance of dissolved Fe(II) under the low-oxygen atmosphere.[97] However, studies on the geochemical proxies of the late Archean ocean suggest that while the deep ocean is likely characterized by anoxic ferruginous conditions, oxygenated or partially oxygenated surface oceans developed around 2.7-2.5 Ga,[98-101] prior to the Great Oxidation Event, which transferred the atmosphere from almost no oxygen to oxygenated about 2.4 Ga to 2.0 Ga.[97, 102] Anoxic ferruginous conditions of the deep ocean may persist throughout much of the Proterozoic until about 580 million years ago, with sulfate concentrations less than 400 μM.[103-106] Studies on the reconstruction of ocean redox conditions in the mid-Proterozoic suggest that euxinic conditions were widespread at mid-depth oceanic water in continental margins or restricted settings during this period.[94, 107, 108] Furthermore, recent findings suggest that ferruginous deep oceans may have even been prevalent into the Cambrian.[109] Such conditions in the Archean-Proterozoic oceans differ fundamentally from those prevailing in the modern ocean, suggesting that changes in the Fe cycle would have played an essential role in the biogeochemical and redox evolution of the ocean.[94, 97] However, the very low concentration of Fe in modern oxygenated oceans poses a challenge to studying the biogeochemistry and redox structure of ancient oceans.

Photoferrotrophy is most probably linked to primary production in the ancient ocean. Some studies have suggested that primary productivity in the Precambrian ocean may have been much lower than in modern oceans.[110, 111] Anoxygenic photosynthesis likely evolved before oxygenic photosynthesis and is supported by molecular phylogenetic analyses.[112-114] Consequently, anoxygenic photosynthesis likely accounted for much of the primary production in the Archean and possibly also early Proterozoic oceans.[115, 116] Photoferrotrophy, a Fe(II)-dependent anoxygenic photosynthesis, can link the production of organic carbon to the oxidation of ferrous Fe.[40] It has been proposed that photoferrotrophy could have been responsible for the majority of primary production in the photic layers of anoxic ferruginous ancient oceans prior to the evolution of oxygenic photosynthesis.[111, 117]

1.1.5. Deposition of banded iron formations

Sedimentary rocks precipitating from ancient oceans provide insight into the biogeochemistry and redox structure of the Precambrian oceans, the evolution of the atmosphere in early Earth, and Fe sources and sinks in the oceans. Banded iron formations (BIFs) are layered chemical sedimentary rocks that contain 15-40 weight percent (wt%) Fe and 40-60 wt% SiO_2 and consist of layers of Fe oxide, Fe carbonate and Fe silicate minerals.[118, 119] The majority of BIFs are deposited from the early Archean to the late Paleoproterozoic and thought to be indicative of prevalent anoxic ferruginous conditions in the ocean over this period.[119, 120] Although there are increasing findings of Neoproterozoic and Phanerozoic BIF,[121-123] the major BIF deposition is commonly considered to cease at ~1.8 Ga, suggesting the fundamental transitions from ferruginous to euxinic or oxic conditions.[119, 120] Considerable attention was devoted to understanding the possible explanations for this disappearance of BIF at 1.8 Ga. Early studies imply that the mild oxygenation of the deep ocean between 1.8 and 0.8 Ga caused the oxidation of dissolved Fe, resulting in the disappearance of BIF after 1.8 Ga.[97, 124, 125] An alternative interpretation is that the prevalent euxinic conditions in the deep ocean in mid-Proterozoic (~1.8-1.0 Ga) would have led to the precipitation of pyrite and reduced the availability of dissolved Fe for the deposition of BIFs, resulting in the termination of BIF deposition globally.[126, 127] However, recent studies have suggested that euxinic conditions were only developed in mid-

depth oceanic water in continental margins whereas anoxic ferruginous conditions are widespread and dominant in the deep ocean from Late Paleoproterozoic to Late Neoproterozoic (1.8 to 0.58 Ga).[94, 105-108] This inference is also supported by the recent discovery of Mesoproterozoic and Neoproterozoic BIFs.[121-123] Nevertheless, such euxinic conditions in mid-depth continental margins can suppress BIF deposition, as Fe(II) diffusing from anoxic ferruginous bottom could be titrated by sulfide along euxinic continental margins.

The massive deposition of BIFs requires large masses of dissolved Fe in the seawater, which could be transported into the ocean via continental and hydrothermal sources.[97, 128, 129] Hydrothermal fluids are commonly considered the dominant source for BIF deposition, supported by the similarity of rare earth element patterns between BIF and hydrothermal fluids,[130, 131] and Si isotope signatures.[132, 133] Benthic/diagenetic Fe sources mediated by DIR were also proposed as an important Fe source in BIF deposition.[134, 135] Other proposed continental sources, such as riverine input of dissolved Fe, are unlikely the predominant sources as riverine input of dissolved Fe was insufficient to sustain the concentration of Fe that is required for the precipitation of Fe minerals in the ocean and BIFs normally contain a low fraction of detrital components.[97, 136]

BIFs are commonly thought to be composed of oxide facies (magnetite and hematite), silicate facies (chert, greenalite and stilpnomelane), and carbonate facies (siderite, ankerite and ferroandolomite).[118, 119, 137] It is generally accepted that silica-associated Fe(III)-oxyhydroxides are the primary precipitates in BIF,[119] although some studies argue that greenalite might be the primary precipitate.[138-140] Despite the post-depositional alteration caused by the diagenetic and metamorphic processes after the initial deposition of BIFs, the presence of Fe oxides (e.g., magnetite and hematite) in BIF, interpreted to have originated from Fe(III) oxyhydroxides, requires the oxidation of ferrous Fe in Archean oceans where anoxic conditions are commonly considered to be prevalent.[119, 131] It is widely accepted that there are three possible Fe oxidation mechanisms involved in the deposition of BIFs in anoxic and ferruginous oceans: (1) biotic (microaerophilic Fe oxidation) or abiotic oxidation by O_2 that is produced by oxygenic photosynthesis;[141] (2) abiotic photo-oxidation by UV;[142] (3) microbial phototrophic Fe oxidation (photoferrotrophy).[40, 143, 144] Although the relative contribution of these proposed mechanisms is debated, it has been proposed that

photoferrotrophy may have played a substantial role in Fe(II) oxidation and BIF deposition in the anoxic and ferruginous seawater of Archean oceans.[138, 143-146] Furthermore, experimental studies demonstrate that photoferrotrophy has the capacity to produce sufficient supply of Fe(III) for the ferric oxides in BIFs.[143, 144]

1.1.6. Archean ocean analogues: the occurrence and significance of photoferrotrophy

Although the geological record in rocks provides valuable information for understanding biogeochemical processes occurring in past oceans, inferences solely based on the rock record (e.g., proxies) might be inaccurate or imprecise due to factors such as alteration through burial diagenesis or metamorphism, preservation bias, non-unique signatures and conflicting proxies.[147] To better understand the biogeochemical processes occurring in the past oceans, natural modern environments with analogy to different states of past oceans have been investigated. Modern ferruginous meromictic lakes are studied as Archean ocean analogues to explore the biogeochemical Fe processes, especially photoferrotrophy, shedding light on how photoferrotrophs could have shaped biogeochemical cycling of Fe in the Archean ocean.[148] A meromictic lake is permanently stratified into mixolimnion and monimolimnion with incomplete mixing between the two layers.[149] In ferruginous meromictic lakes, Fe concentrations in the monimolimnion are expected to be relatively high compared to the oxic mixolimnion.

Modern ferruginous meromictic lakes are rare globally.[148] To date, the occurrence and significance of photoferrotrophy have been investigated in a few ferruginous meromictic lakes, including Lake Matano (Indonesia), Lake La Cruz (Spain), Kabuno Bay of Lake Kivu (Democratic Republic of the Congo), Brownie Lake and Lake Svetloe (U.S.A.).[150-155] A population of anoxygenic phototrophs was detected in the anoxic photic zone of each of these lakes. However, the identification of anoxygenic phototrophic communities that are closely related to known photoferrotrophs by 16S rRNA gene sequencing or pigments analysis is insufficient to indicate the occurrence of photoferrotrophy since most of anoxygenic phototrophic bacteria can utilize electron donors other than Fe(II).[156] It is necessary to demonstrate that those anoxygenic phototrophic bacteria are performing Fe(II)-dependent

anoxygenic photosynthesis *in situ*. The activity of photoferrotrophy was confirmed only in Lake La Cruz and Kabuno Bay of Lake Kivu.[151, 155] Anoxygenic phototrophic GSB were detected in the photic chemocline of Lake Matano and were proposed to be sustained by photoferrotrophy.[152] However, a recent study suggested that these GSB, possessing sulfide-oxidizing genes, are likely S-oxidizing phototrophs rather than iron-oxidizing phototrophs, despite the very low concentration of sulfide in the anoxic chemocline of Lake Matano.[153] Anoxygenic phototrophic GSB were detected in the anoxic zone of Lake Svetloe, and the rate of anoxygenic photosynthesis was determined to be up to 0.69 μmol C L^{-1} d^{-1}, which significantly contributes to the total carbon fixation in the anoxic chemocline.[154] However, the occurrence of photoferrotrophy necessitates direct evidence (i.e., *in situ* activity of photoferrotrophy) despite the presence of *Chlorobium phaeoclathratiforme*, which are phylogenetically close to *Chlorobium ferrooxidans*.[154] Photoferrotrophs that are closely related to *Chlorobium ferrooxidans* were detected in the anoxic photic zone of Lake La Cruz.[155] Furthermore, the *in situ* activity of photoferrotrophy was observed in Lake La Cruz, and the rate of photoferrotrophic Fe oxidation has been estimated at 0.2-1.4 μmol Fe L^{-1} d^{-1}.[155] This is the first time that photoferrotrophic activity was confirmed in a modern ferruginous meromictic lake. *In situ* photoferrotrophy was reported in the illuminated chemocline of Kabuno Bay of Lake Kivu, where anoxygenic phototrophs contribute significantly to carbon fixation.[151, 157] In the anoxic chemocline of Kabuno Bay of Lake Kivu, the carbon fixation rates of photoferrotrophy (3.4 mol C m^{-2} y^{-1}) are comparable to the values predicted for primary production in ancient ferruginous oceans, and the photoferrotrophic Fe oxidation rates (100 μmol Fe L^{-1} d^{-1}) are sufficient to supply Fe(III) for the deposition of BIF in early ferruginous oceans.[151] *Chlorobium phaoferrooxidans,* a novel photoferrotroph belonging to the genus *Chlorobium*, was isolated from the water column of Kabuno Bay of Lake Kivu.[158] Another novel photoferrotroph, *Chlorobium* sp. strain BLA1, was also been isolated from the water column of Brownie Lake.[150]

1.1.7. Fe isotope fractionation during biogeochemical Fe processes

Natural Fe isotopes are a powerful tracer to understand the biogeochemical Fe processes in terrestrial and aquatic ecosystems. The variations in δ^{56}Fe values in natural

samples span a range of up to 8‰ (from ~ −4‰ to 4‰), with the largest variations recorded in Precambrian sedimentary rocks.[159, 160] Much effort has been made to investigate Fe isotope fractionations arising from different Fe processes in theoretical, experimental and natural environmental studies (see recent reviews).[159, 161-163] Fe isotope fractionations mainly result from slightly different efficiencies of the isotopes of Fe involved in biophysiochemical reactions, which is either caused by kinetic effects that refer to the different reaction rates for isotopes of Fe in a quasi-irreversible reaction, or equilibrium effects that refer to the distribution of isotopes between different phases or species in isotope exchange reactions.[164] Fe isotope fractionation occurs during various biogeochemical processes such as redox reactions, adsorption, ligand-complexation, precipitation and Fe acquisition.

Some of the largest Fe isotope fractionations are induced by Fe redox changes, including both abiotic and biotic reactions. The net Fe isotope fractionation between Fe oxides and aqueous Fe(II) reflect the combination of an equilibrium fractionation between aqueous Fe(III) and aqueous Fe(II) and a kinetic fractionation between Fe oxides and aqueous Fe(III) during precipitation.[159] The equilibrium fractionation $\Delta^{56}Fe_{Fe(III)–Fe(II)}$ between aqueous Fe(III) and aqueous Fe(II) is reported to be 3‰ at 22 °C.[165] Experimental studies also demonstrate the equilibrium fractionation $\Delta^{56}Fe_{ferrihydrite–Fe(II)}$ of 3.2‰ between poorly crystalline ferrihydrite and aqueous Fe(II) at 25 °C.[166] This fractionation could vary in the presence of Si (as a function of Fe/Si ratios), reflecting the differences in Fe-O bonds. Much work has been conducted on Fe isotope fractionation between Fe oxide minerals and aqueous Fe(II). Iron oxide minerals are commonly enriched in heavy isotopes relative to aqueous Fe(II), with the equilibrium $\Delta^{56}Fe_{goethite–Fe(II)}$ fractionation of up to 1.2‰,[167, 168] the $\Delta^{56}Fe_{hematite–Fe(II)}$ fractionation of up to 3.1‰[169-171] and the $\Delta^{56}Fe_{magnetite–Fe(II)}$ fractionation of up to 1.6‰.[172, 173]

Various biological experimental studies have investigated Fe isotope fractionation during microbially mediated redox reactions.[174-180] All biological iron-oxidizing experiments investigating photoferrotrophy, nitrate-reducing Fe(II) oxidation, Fe(II) oxidation by O_2 produced by cyanobacteria and acidophilic Fe(II) oxidation show that oxidized Fe(III) is isotopically heavier than co-existing Fe(II), similar to abiotic reactions.[174-180] The fractionation $\Delta^{56}Fe_{Fe(III)\ oxides–Fe(II)aq}$ between Fe(III) oxides and aqueous Fe(II) in these iron-oxidizing experiments vary between 1‰ and 3‰, reflecting an initial 3‰ equilibrium

fractionation between aqueous Fe(III) and aqueous Fe(II) overprinted by a kinetic fractionation during the precipitation of Fe oxides, the latter of which depends on oxidation rate and precipitation rate.[174-180] Experimental studies on Fe isotope fractionation arising from photoferrotrophy show that fractionation factors $\Delta^{56}Fe_{\text{Fe(III) oxide–Fe(II)aq}}$ between aqueous Fe(II) and Fe(III) oxides display variations depending on the oxidation rate,[177-180] with the smaller value of 1.5‰ for slow oxidation rate and the larger value of 2.5‰ for rapid oxidation rate (see recent review paper)[159]. The observed fractionation $\Delta^{56}Fe_{\text{Fe(III) oxide–Fe(II)aq}}$ induced by nitrate-reducing Fe(II) oxidation is reported to be ~2-3‰ in one study.[175] Acidophilic Fe(II) oxidation under low pH conditions also shows to produce a ~3.0‰ equilibrium fractionation between $Fe(III)_{aq}$ and $Fe(II)_{aq}$.[174] Moreover, one experimental study on the indirect Fe(II) oxidation by cyanobacteria demonstrated that Fe isotope fractionation between Fe(III) oxides and aqueous Fe(II) during microbially mediated Fe(II) oxidation by cyanobacteria is likely modified not only by oxidative precipitation but also by the adsorption of Fe on cells and Fe(III) minerals, the latter of which can induce sorbed Fe that is isotopically heavier than aqueous Fe(II).[176] Biological iron-reducing experiments investigating DIR show that enzymatically produced aqueous Fe(II) is isotopically lighter than ferric substances, with an equilibrium fractionation $\Delta^{56}Fe$ of ~−3‰ between enzymatically produced $Fe(II)_{aq}$ and Fe(III) oxyhydroxides, reflecting isotopic exchange among aqueous Fe(II), sorbed Fe(II) and reactive Fe(III) on the surface of ferric substances.[173, 181-183]

Fe isotope fractionation is also observed during uptake of Fe by microorganisms. One study on mineral dissolution by a siderophore-producing bacterium shows that bacterial cells assimilate isotopically heavy Fe^{3+}, leaving the dissolved phase enriched in lighter isotopes.[184] Furthermore, uptake by a diazotroph in a culture study results in cells with $\Delta^{56}Fe$ of +1.1‰ compared to the growth medium.[185] Recent study on the uptake by phytoplankton in ferrous solutions shows a fractionation factor of ~+0.8 to +3.1‰ between intracellular Fe and ferrous medium, likely resulting from a combination of uptake and metabolic oxidation of Fe(II).[186] The mass of extracellular Fe resulting from Fe adsorption on cells is approximately three times lower than that of intracellular Fe.[186]

Other processes could also fractionate Fe isotopes, but likely to a lesser degree. Adsorption of Fe on a solid surface could induce the enrichment of heavier isotopes in sorbed

Fe relative to aqueous Fe, with $\delta^{56}Fe$ of sorbed Fe being 0.3-1.2‰ heavier than that of aqueous Fe.[168, 181, 183, 187] Complexation of dissolved Fe and organic matter can lead to the enrichment of heavier isotopes in organic Fe complexes relative to inorganic Fe. An experimental study investigating the complexation of dissolved Fe(III) and desferrioxamine B (DFOB) ligand showed an equilibrium fractionation $\Delta^{56}Fe$ of 0.60 ± 0.15‰ between siderophore-Fe complexes and aqueous inorganic Fe(III).[188] Precipitation of Fe(II) minerals can also lead to Fe isotope fractionation between Fe(II) and Fe(II) minerals. The equilibrium fractionation $\Delta^{56}Fe_{Fe(II)aq-siderite}$ between aqueous Fe(II) and siderite is reported to be 0.48 ± 0.22‰ at 20 °C.[189] Precipitation of mackinawite (FeS) was reported to produce an equilibrium fractionation $\Delta^{56}Fe_{Fe(II)aq-mackinawite}$ of –0.32±0.29 ‰ (20 °C) between aqueous Fe(II) and mackinawite at near-neutral pH,[190] whereas at low pH (pH=4) the $\Delta^{56}Fe_{Fe(II)aq-mackinawite}$ fractionation between aqueous Fe(II) and mackinawite may result from kinetic isotope effects, with values ranging from 0.34 to 0.85‰.[191, 192]

1.1.8. Fe isotope variations in BIF

Iron isotopes are used to study Fe transport pathways during BIF formation. A wide range of $\delta^{56}Fe$ values, ranging from –2.5‰ to +1.5‰, are reported in BIFs, posing a challenge to constraining Fe pathways involved in BIF formation.[161, 193] There is still great debate over the origin of negative $\delta^{56}Fe$ values in BIFs. Some studies explain negative $\delta^{56}Fe$ values by partial oxidation of hydrothermal fluids,[194-196] whereas others argue that negative $\delta^{56}Fe$ values result from DIR.[193, 197, 198] One study examining the Fe isotope variations in the Hamersley BIFs (Australia, 2.5 Ga) reported a wide range of $\delta^{56}Fe$ values in BIFs, ranging from –0.83‰ to +1.3‰.[134] Based on the Fe-Nd isotope model, the authors proposed two Fe sources for the deposition of BIF: a hydrothermal component with positive $\delta^{56}Fe$ values and an isotopically light benthic Fe shuttle produced by DIR.[134] Much work has been conducted on the Fe isotope composition of Fe-bearing minerals in BIF to provide constraints on oxidative pathways involved in the deposition of BIF. One study on the Fe isotope variations of magnetite in the Hamersley BIFs (Australia, 2.5 Ga) reported a wide range of $\delta^{56}Fe$ values for magnetite, with the average value of –0.02‰, indicating complete oxidation in the upper

water column followed by diagenetic processes dominated by DIR.[199] In contrast, another study investigating the $\delta^{56}Fe$ of magnetite in the Isua BIFs (Greenland, 3.8 Ga) measured magnetite with positive $\delta^{56}Fe$ values, ranging from 0.4‰ to 1.1‰, suggesting an inherited origin from precursor Fe(III) oxyhydroxides that were formed through partial oxidation in the upper water column.[146]

1.2. Thesis outline

Stable Fe isotopes are powerful tracers for biogeochemical cycling in modern and ancient settings. However, only a few studies exit on lakes and only in extreme environments such as meromictic ferruginous lakes.[200-205] The work presented in this thesis has applications in two diverse areas that result in a broad appeal.

Harmful algal blooms, in most cases cyanobacterial blooms, are documented in lakes and reservoirs worldwide, posing a significant threat to human health and aquatic ecosystems. Nutrients phosphorus and nitrogen are commonly thought to be dominant factors in the formation of cyanobacterial blooms.[206, 207] In recent years, the critical role of Fe in controlling the dominance of cyanobacteria has been proposed, but the sources and availability of Fe for cyanobacterial uptake are not well understood.[208-210] Developing a better understanding of the confounding role of Fe in the formation of cyanobacterial blooms is a crucial step in helping assess, treat and manage cyanobacterial blooms in lakes and reservoirs.

Photoferrotrophy was proposed as one of the possible mechanisms regulating the deposition of banded iron formations in the Archean ocean. However, the study of photoferrotrophy in analogous modern freshwater systems is limited to rare meromictic ferruginous lakes. [150-155] One recent work proposed that Boreal Shield lakes with seasonal anoxia could potentially serve as Archean Ocean analogues to probe biogeochemical processes.[211]

The overall goal of this thesis is to evaluate the use of Fe isotopes to examine both the source of Fe for cyanobacterial blooms in freshwater and the biogeochemical Fe processes in anoxic water columns and sediments of stratified boreal lakes, providing valuable new insights into the Fe cycling in modern and ancient environments. This thesis is divided into

five chapters: an introduction and literature review chapter (Chapter 1), three main research chapters (Chapters 2-4) and a concluding chapter (Chapter 5). The objectives of each research chapter are presented below.

Chapter 2 was published in the *Environmental Science & Technology* and it is reproduced in this thesis. Fe concentrations and Fe isotope compositions were examined in boreal streams and two Boreal Shield lakes, consisting of a fertilized eutrophic lake that experiences a cyanobacterial bloom each summer and an oligotrophic lake without nutrient additions. This study investigates the biogeochemical Fe processes contributing to observed Fe isotope fractionation in modern lakes and explores the potential of Fe isotopes in Boreal Shield lakes to provide constraints on the availability of Fe for the formation of cyanobacterial blooms. Understanding the role of Fe in the formation of cyanobacterial blooms is essential for evaluating the risk of harmful algal blooms and for developing more effective management approaches. In addition, Fe isotope compositions of bulk sediments were also measured to assess the potential of $\delta^{56}Fe$ in sediment as an archive of the changes in Fe cycling in the water column.

Chapter 3 and Chapter 4 delve further into the initial concepts introduced in Chapter 2, where an overview of the importance of using Fe isotopes in dimictic boreal lakes was demonstrated. These two chapters present new data and interpretations. Chapter 3 focuses on the Fe processes in the oxic layers of dimictic boreal lakes. Seasonal variations in Fe speciation and Fe isotope compositions of dissolved Fe and particulate Fe are reported in dimictic boreal headwater lakes in relation to two annual cyanobacterial blooms. This study aims to (1) utilize Fe isotope and Fe speciation data to track the formation of annual cyanobacterial blooms with regard to the sources of Fe used by cyanobacteria and (2) test the hypothesis that cyanobacteria can migrate below the redox boundary to utilize dissolved Fe(II) under Fe-limited conditions during the bloom.

Chapter 4 focuses on the anoxic zone of stratified Boreal Shield lakes, including the hypolimnia and underlying sediments. Seasonal variations in Fe isotope fractionation between dissolved Fe and particulate Fe were reported in the anoxic hypolimnia of four small Boreal Shield lakes. Fe concentrations and Fe isotopic compositions were also measured for porewater and sediments collected from the bottom of each lake. This study aims to (1) use Fe isotopes and associated Fe isotope fractionations to determine the contribution of

biogeochemical Fe processes to Fe cycling in anoxic water columns and investigate the occurrence of microbial Fe oxidation, especially photoferrotrophy in the anoxic layers, (2) explore the source of Fe in the hypolimnion, (3) evaluate the role of Fe flux from sediments in controlling δ^{56}Fe of dissolved Fe in anoxic hypolimnia, (4) utilize Fe isotope signatures in porewaters and sediment Fe to explore the dominant Fe processes in the sediment and (5) explore the intensive Fe cycling in Boreal Shield lakes.

Chapter 2

Large fractionation in iron isotopes implicates metabolic pathways for iron cycling in Boreal Shield lakes

2.1. Introduction

Iron (Fe) plays a key role in the biogeochemistry and ecology of freshwater systems. In particular, the role of Fe in phosphorus (P) sequestration and internal loading has long been established.[149, 212] Fe is also an essential micronutrient for aquatic organisms.[149, 212] Cyanobacteria manufacture Fe complexing exudates or siderophores to aid in Fe acquisition.[213-215] and recent results indicate that Fe may promote harmful cyanobacterial blooms in lakes and reservoirs.[210] Even though the macronutrients P and nitrogen (N) remain important controllers of rates of primary productivity,[206, 207] access to reduced Fe may determine whether cyanobacteria are successful in competing with their eukaryotic algae counterparts across a range of trophic states.[210] Despite the far-reaching explanatory power of this new Fe-based conceptual model, the source of Fe(II) available to cyanobacteria is uncertain due to rapid oxidation of Fe(II) and low solubility of Fe(III) in oxygenated waters. A better understanding of Fe cycling in lakes is therefore required to enhance the predictive power of this model and further aid management of waters affected by harmful algal blooms.

Banded iron formations (BIFs) enable study of ancient Fe biogeochemical cycling, the composition of early Earth oceans, and the evolution of microbial metabolism in the Archean-Proterozoic oceans.[118, 119, 148, 216] Four Fe oxidation mechanisms could be involved in the deposition of BIFs in anoxic and ferruginous seawater: 1) biotic (microaerophilic Fe(II) oxidation) or abiotic oxidation by O_2 that is produced by oxygenic photosynthesis, 2) abiotic photo-oxidation by UV, 3) biotic oxidation coupled to nitrate reduction, and 4) photoferrotrophy, the light-driven biotic oxidation of Fe(II) by anoxygenic phototrophs. Although the relative contributions of these proposed mechanisms is debated, several studies suggest that biotic processes outside of oxygenic photosynthesis, including photoferrotrophy and microaerophilic Fe(II) oxidation, may have played a substantial role in the anoxic and ferruginous seawater of Archean oceans.[138, 145, 146, 151, 217] Photoferrotrophs have been found mostly in modern meromictic and ferruginous lakes, despite the scarcity of meromictic and

ferruginous lakes globally.[151, 155, 156, 204, 218] However, the ecological role of photoferrotrophs, their *in situ* activity, and the interaction between Fe biogeochemical cycling and photoferrotrophy remain poorly constrained. Similarly, microaerophilic Fe(II) oxidizing bacteria have only been identified in one modern meromictic ferruginous lake[219] and are poorly understood in terms of their ecology and the environmental conditions favourable to their growth.[217]

Iron isotopes have been used as a tracer for biogeochemical cycling of Fe in a variety of environments, including soils[220-222] and groundwater,[223-225] riverine[226-228] and marine systems,[229-231] and hydrothermal settings.[232-234] Stable Fe isotope compositions in natural environments span a range of up to 6‰ in δ^{56}Fe values.[235, 236] However, very few isotope studies have been conducted on lakes and only in extreme environments, such as Fe-rich meromictic lakes[200, 201] or one euxinic meromictic lake.[204] A meromictic lake is a lake that is permanently stratified with incomplete mixing.[149] Almost all previous work has focused on either dissolved Fe isotope values or particulate Fe isotope values[200-203] in the water column, and only one recent study investigated both dissolved and particulate Fe isotope values.[204] Further, only one study has investigated Fe isotopic fractionation in an oligotrophic dimictic lake but only in the sediments.[205] A dimictic lake is a lake which mixes from top to bottom twice per year.[237] Here we report the Fe isotope compositions of stream inflows, dissolved and particulate phases in the water column, and sediments in two small stratified boreal headwater lakes: a eutrophic lake that has been experimentally fertilized for the past 48 years and experiences a cyanobacterial bloom consistently each summer, and a reference oligotrophic lake without nutrient additions. Fe isotope compositions for the water column of both lakes have been previously published without detailed interpretation.[211] This study examines the processes and significance of Fe isotope fractionation, and thus the potential of Fe isotopes to unravel the complex biogeochemical processes of Fe cycling in Boreal Shield lakes with the implications for lake metabolism and management of cyanobacterial blooms.

2.2. Materials and methods

2.2.1. Sites and sampling

Lake 227 (L227) and Lake 442 (L442) are located in the International Institute for Sustainable Development - Experimental Lakes Area (IISD-ELA) in northwestern Ontario, Canada.[238] L227 has a surface area of 5.0 ha, a mean depth of 4.4 m, and a maximum depth of 10.0 m, whereas L442 is 16.0 ha with a mean depth of 9.6 m and a maximum depth of 17.8 m (Figure 2-1). Full water column mixing occurs in fall for both lakes, but mixing may be incomplete in spring for L227, if spring warming is very rapid and is not accompanied by storm activity, due to the smaller area and more wind-protected basin of the lake. During stratification in summer and winter, the lakes have two stable layers: an epilimnion (warm upper mixed layer) and a hypolimnion (cold bottom layer), separated by metalimnion, an intermediate layer which has a steep thermal gradient. We follow the IISD-ELA procedure of defining the bottom of the epilimnion as the depth where water temperature changes at a rate greater than 1°C m^{-1}, and the bottom of the metalimnion as the depth where 1% photosynthetically active radiation (PAR) is reached. This definition of metalimnion is different from the traditional one, which defines the metalimnion as the region where the thermal gradient is steep compared to nearby epilimnion and hypolimnion (usually accepted as a change of temperature >1°C m^{-1}).[149, 212] In L227, whole lake experimental addition of nutrients has been ongoing since 1969.[207] Since 1990, N additions were stopped and only P has been added. In the summer stratification period, water input from the terrestrial catchment is severely limited by shallow soils and evapotranspiration from growing vegetation. Lake outflow ceases in late spring in dry years. Oligotrophic L442 has only ever received natural sources of nutrients.

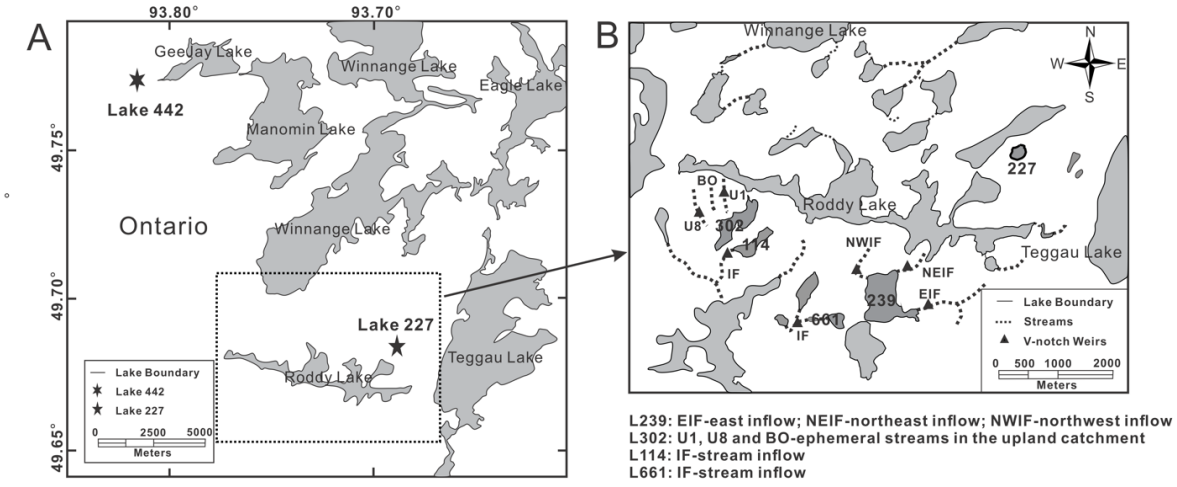


Figure 2-1 Location of Lake 227, 442, and proxy streams in the International Institute for Sustainable Development - Experimental Lakes Area (IISD-ELA).

Sampling in L227 occurred in June 2011 (during the peak of the cyanobacterial bloom), August 2011 (post bloom), and July 2014 (during bloom development), and sampling occurred in June 2011 in the reference Lake 442 (Figure 2-2). Lake samples were collected at different depths of both lakes using a gear pump from the centre of the lake. Particular attention was paid to avoid artificial oxidation during Fe sampling. Dissolved Fe samples were collected in 160 mL glass serum bottles capped by blue butyl rubber stoppers using a needle connected to the pump tubing. The empty glass serum bottles were acid-cleaned, vacuumed and then filled with N_2 gas. Dissolved samples were then filtered shortly after collection with 0.45-µm filters (Advantec, Dublin, CA). Particulate Fe samples were collected on the 0.45 µm membrane filters at various water depths. After filtration, 15 mL 6 M trace-metal grade hydrochloric acid (degassed with nitrogen) was added into glass serum bottles to acidify the water samples to a final concentration of 0.5 M. The particulate Fe samples were frozen until analysis. Dissolved Fe samples were stored at 4 °C until analysis.

Dissolved samples were filtered shortly after collection with 0.45-µm filters for measurement of dissolved Fe, sulfate, sulfide, dissolved organic carbon (DOC), and total dissolved P (TDP). Particulate organic matter (POM) collected by either 0.45-µm membrane filters or Whatman QMA quartz filters (1-µm nominal pore size) was analyzed for particulate

Fe, suspended particulate P (SPP), particulate organic N (PON), and particulate organic carbon (POC).

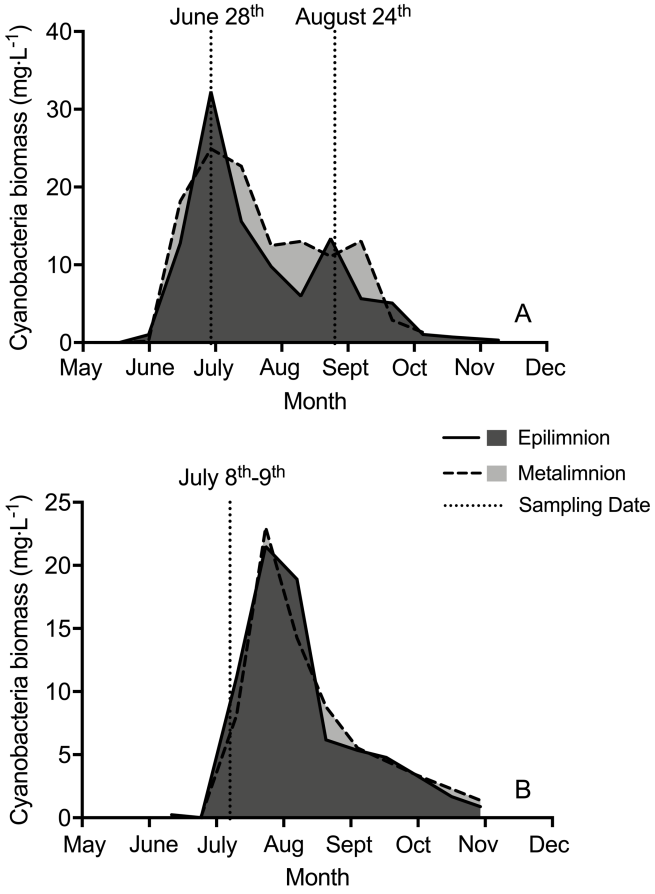


Figure 2-2 Cyanobacterial biomass in the epilimnion and metalimnion of L227 in 2011 (A) and 2014 (B).
Vertical dotted lines indicate different sampling events.

Samples from several streams were collected and filtered through 0.45-µm filters from 2011 to 2017 to examine iron isotopic values of lake inputs. Because there was no defined stream channel draining into L227, proxy streams were collected to analyze the range of terrestrial inputs (Figure 2-1). All streams described in this work are located < 4 km southwest of L227: EIF (East Inflow), NEIF (Northeast Inflow) and NWIF (Northwest Inflow) are the three main inflows that feed Lake 239; U1, U8 and BO (bedrock overflow) are ephemeral streams in the upland catchments located 40 m above Lake 302; and L114 IF and L661 IF are the stream inflows for Lake 114 and Lake 661, respectively. With the

exception of BO, where samples were collected from transient pools that formed along the bedrock surface, all stream samples were collected at a v-notch weir installed on each stream. It should be noted that the weirs for streams were removed in 2016 and stream samples were collected at the site of the weirs.

A lake sediment core was collected from ice-covered L227 on March 2011 by freeze coring, following a modified procedure,[239] at the deepest overlying water column depth. The sediment core was sectioned while frozen into 0.5 cm (to a depth of 11 cm) or 1 cm slices (after a depth of 11 cm). Additional surficial sediment samples were also collected at selected depths in L227 and L442 by subsampling sediment with intact surficial features obtained with an Eckman dredge in July 2010. Sediment samples were kept frozen until freeze-drying. Pb-210 dating was performed on the sediment core of L227.

2.2.2. Chemical analysis

Dissolved Fe was analyzed either directly after acidification or after drying 450 mL of filtered water and redissolving in 0.5 M HCl. Particulate Fe on 0.45-μm filters was first dissolved by 7 M HCl and then preserved in 0.5 M HCl through dilution. Both dissolved and particulate Fe were analyzed spectrophotometrically by the ferrozine method (detection limit: 0.05 μM).[240, 241] Sulfate, sulfide, DOC, POC, TDP, SPP, and PON concentrations in water samples were measured by standard methods.[242, 243]

2.2.3. Iron isotope analyses

Prior to Fe isotope analysis, Fe samples were purified using ion-exchange chromatography.[244] Iron isotope compositions of dissolved Fe, particulate Fe and sediments were measured by a MC-ICP-MS (Micromass IsoProbe) at the University of Wisconsin-Madison, following established protocols.[244] All Fe isotope data are reported as $\delta^{56}Fe$ values in per mil (‰):

$$\delta^{56}Fe = [(^{56}Fe/^{54}Fe_{sample})/(^{56}Fe/^{54}Fe_{standard}) - 1] \times 10^3$$

where $^{56}Fe/^{54}Fe_{standard}$ is the average of igneous rocks ($\delta^{56}Fe = 0.0 \pm 0.05$‰). Measured external precision for $\delta^{56}Fe$ was 0.04‰ (2σ; n = 55). The measured Fe isotope composition

of the IRMM-014 Fe isotope standard was –0.08 ± 0.05‰ (2σ; n = 49), which lies within error of the long-term value used in the lab of –0.09‰ relative to average igneous rocks.[244]

2.3. Results and Discussion

2.3.1. Geochemistry of boreal streams and lake water column

In both lakes, the water temperature decreased from ~12-21°C in the epilimnia to ~4°C in the hypolimnia in spring to summer months (Table A1, Figure 2-3). Epilimnetic oxygen concentrations in L227 and L442 were high (7-11 mg L^{-1}). In the L227 hypolimnion, O_2 was below detection limit (0.005 mg L^{-1}).[211] In L442, the hypolimnion became anoxic between 9 and 13 m, within 1-3 months following spring overturn. In 2011, anoxia in L442 developed early in the open-water season, but in some years, it may take longer. It should be noted that contemporaneous profiles of temperature (T) and dissolved O_2 were published previously.[211] Dissolved Fe in both lakes was at low concentrations (0.7-2.6 μM) in the epilimnia and metalimnia, and increased with depth in the anoxic hypolimnia, resulting from upward flux of Fe from anoxic sediments. In L227, the dissolved Fe reached ~80 to 110 μM at 8 m depth and up to 140 μM at 10 m depth. This high Fe concentration at the anoxic bottom of L227 shortly after spring overturn reflected large semi-annual fluxes in the internal Fe cycle. In L442, the dissolved Fe concentration was 10 μM at 13 m depth and reached ca. 100 μM at 16.5 m depth, typical of boreal lakes.[211]

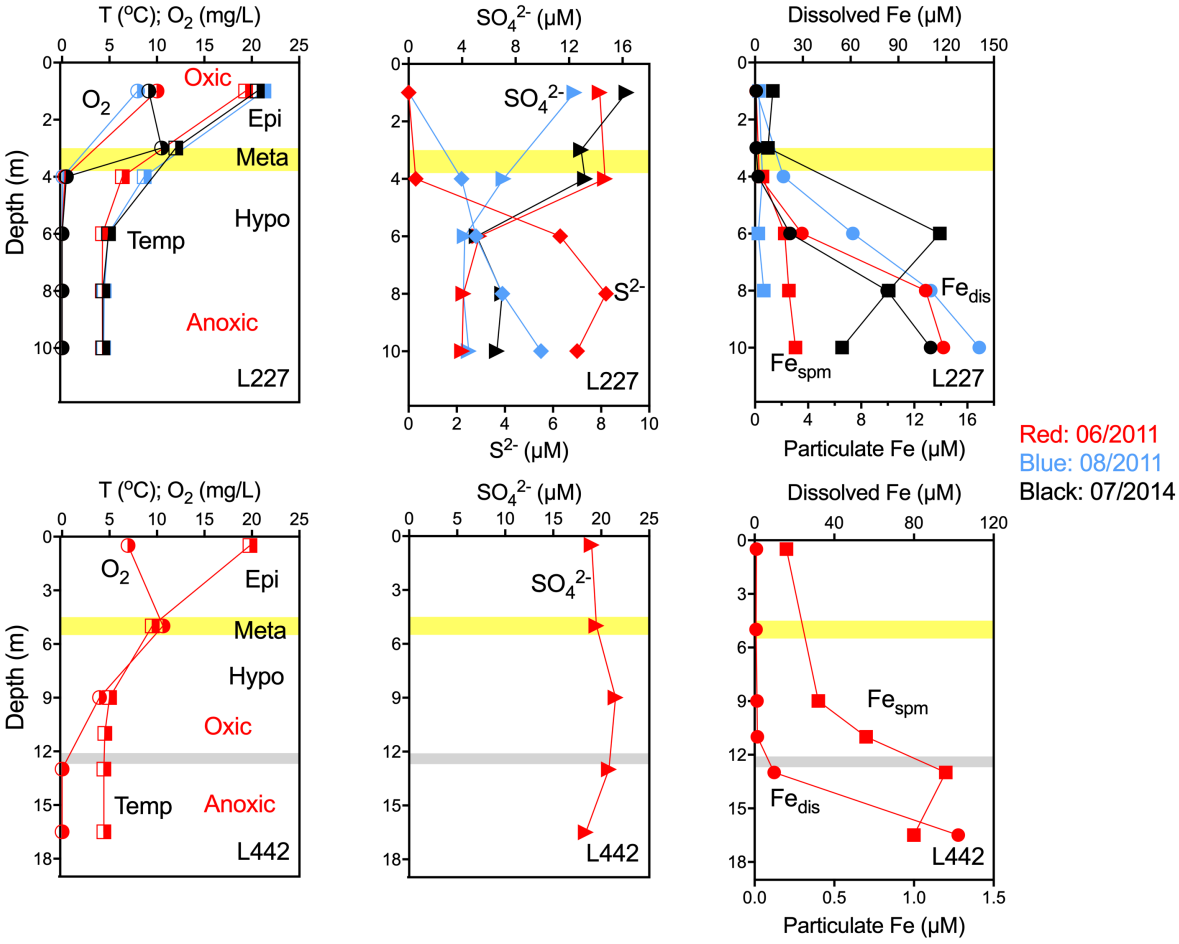


Figure 2-3 Geochemical profiles in the water column of L227 (sampled on 06/28/2011; 08/24/2011; 07/09/2014) and L442 (sampled on 06/27/2011).
Yellow bars indicate the approximate metalimnion depth. Grey bars indicate transition zones between oxic and anoxic hypolimnia in L442.

Sulfate concentrations in the epilimnion and metalimnion of L227 (Table A1, Figure 2-3) ranged from 12 to 16 μM (average: 14.0 ± 1.3 μM) and decreased to ~4 to 7 μM (average: 5.2 ± 1.2 μM) in the hypolimnion, accompanied by an increase in sulfide concentrations from near zero in the metalimnion to ~5 to 7 μM at 10 m depth (average for hypolimnion: 5.1 ± 2.1 μM). The amount of SO_4^{2-} lost is similar to S^{2-} produced at each depth of the hypolimnion. It should be noted that sulfide measured in this study is the total sulfide ($\sum S(II)=H_2S+HS^-+FeS$), which is the sum of free sulfide (H_2S, HS^-) and sulfide-bearing colloids/larger particles (FeS).[245] Free sulfide (H_2S, HS^-) concentrations by voltammetric analysis are generally one or two orders of magnitude less than total sulfide

(∑S(II)) concentrations.[218] Low sulfide concentrations and high dissolved Fe concentrations indicate that interaction with free sulfide plays a minor role in Fe cycling in the water column. In L227, all geochemical profiles are similar during different stages of algal succession and cyanobacterial bloom and between years (Table A1, Figure 2-3). In contrast to a decreasing trend of sulfate in L227, the water column of L442 showed almost no change in sulfate concentration across all depths (Figure 2-3, average: 19.8 ± 1.3 μM), suggesting that net sulfate reduction was almost absent in the hypolimnion.

Total dissolved phosphorus (TDP) was, in general, low in both fertilized L227 (range: 0.19 to 1.90 μM) and in pristine L442 (range: 0.03 to 0.10 μM; Table A1). The TDP was much lower in the hypolimnia of both lakes than the dissolved Fe concentrations at the corresponding depth. Suspended particulate P (SPP) concentrations were higher than those of dissolved P and comparable with those of particulate Fe. The SPP concentrations in the hypolimnion of L227 were much higher than in the epilimnion. The PON:SPP and POC:SPP molar ratios in the hypolimnion were much lower than in the epilimnion and metalimnion of L227. Collectively, these parameters suggest that POM in the hypolimnion of L227 is mostly formed *in situ* rather than settling down from the epilimnion consistent with the $\delta^{13}C$ and $\delta^{15}N$ values of the particulate in comparison to the values of the particulate in the overlying epilimnion.[211]

Continental weathering products transported by streams are the main Fe inputs to the study lakes as groundwater inputs are minimal due to the relatively impervious granitic bedrock of the boreal forest.[246] Subsurface inflow (e.g., lateral subterranean flow from surrounding wetlands)[247] could potentially occur in L442 during early summer, but not in L227 which is a perched and water-tight basin.[238] Contribution of Fe from atmospheric deposition is minor.[248, 249] These boreal streams have high DOC ranging from 13 to 64 mg C L^{-1} (Table A1), consistent with other boreal stream studies,[250-252] and dissolved Fe concentrations are also high (6 to 20 μM), supporting recent studies showing that organic-rich rivers generally have high dissolved Fe concentrations.[253, 254] Dissolved Fe concentrations in these oxic streams greatly exceed inorganic solubility and generally increase with DOC concentrations ($R^2 = 0.60$, $p < 0.0001$), implying strong binding of Fe by DOC (Figure 2-4A, Table A1). However, small variations in DOC versus Fe concentrations are found among different streams (Figure 2-4A), and the DOC/Fe molar ratios in three

inflows of Lake 239 [EIF (east inflow), NWIF (northwest inflow) and NEIF (northeast inflow)] differ (143 ± 22, 213 ± 18, and 262 ± 14, respectively; Table A1). Differences in DOC/Fe ratios in streams could reflect differences in DOC compositions, including variable amounts of oxygen-containing functional groups (e.g., carboxylic, phenolic, and carbonyl), which are thought to be the most reactive binding sites for organic Fe complexation.[14] A study of kinetic organic Fe complexation with dissolved organic matter (DOM) from different sources in marine coastal waters showed that the rate constant of Fe-DOC binding can change by several orders of magnitude among different DOM composition.[13] Spatial variations in DOC and Fe concentrations in IISD-ELA streams may reflect different DOC compositions involved in organic Fe complexation in these boreal streams, perhaps associated with different hydrologic flowpaths and consistent with a previous study that showed that the composition of DOC differs between upland and wetland streams at IISD-ELA.[255]

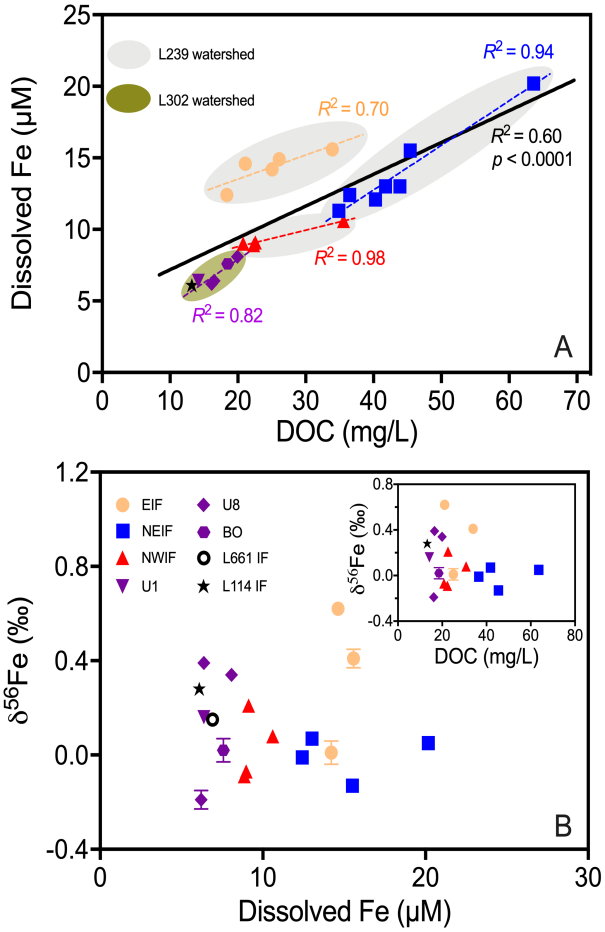


Figure 2-4 Dissolved Fe versus DOC concentrations (A) and δ^{56}Fe versus dissolved Fe or DOC concentrations (B) in Boreal Shield streams of the IISD-ELA.
The black line in panel (A) is the linear regression line for all stream samples. Error bars in panel (B) represent the standard deviation calculated from two measurements. Error bars not visible are contained within the symbols. EIF (East Inflow), NEIF (Northeast Inflow) and NWIF (Northwest Inflow) are three inflows of Lake 239. U1, U8 and BO (bedrock overflow) are ephemeral streams near Lake 302. L114 IF and L661 IF are inflows for Lake 114 and Lake 661, respectively. Both NEIF and NWIF are wetland streams. U1, U8, and BO are upland streams.

2.3.2. Iron isotopic compositions in boreal streams in upland and wetland catchments

The dissolved δ^{56}Fe in IISD-ELA stream waters span a large range of −0.19 to +0.62‰ [average δ^{56}Fe = +0.13 ± 0.43‰, 2σ, n = 18] (Table A1). Positive δ^{56}Fe values are contrary to early findings of isotopically negative riverine dissolved Fe, yet are consistent with more recent reports that, in tropical and temperate rivers, dissolved Fe associated with colloids and organic matter is isotopically more positive than the suspended load, which is enriched in Fe minerals.[226, 256, 257] The isotope systematics associated with Fe mobilization with natural DOC are largely unknown but may be dependent on colloidal size and characteristics of the organic matter. Organic matter complexation can fractionate Fe isotopes, but only a few studies with natural DOC have quantified this effect. For example, Fe bound to siderophores displays a more positive isotopic composition than inorganically bound Fe, with an average equilibrium fractionation factor at 25°C of +0.60 ± 0.15‰.[188] Systematic studies of Fe isotope compositions in different size fractions of boreal organic-rich surface waters (e.g., rivers, streams, and lakes) have further shown that small-size, C-rich colloids exhibit strong enrichment in the heavy isotope whereas large-size Fe particles are isotopically more negative,[258] and this effect was attributed to greater strength of Fe-O-C bonds in Fe-OC complexes than Fe-O-Fe bonds in Fe oxyhydroxides. A recent study about the impact of Fe-DOC complexation on the Fe isotopic composition of solutions of temperate wetland soil demonstrates that Fe binding to large biologically derived organic compounds causes Fe-DOC colloids (less than 0.2 μm) to be isotopically heavy in soil solution.[259] Thus, the observed positive values for dissolved Fe in our high DOC stream waters likely reflect the net effect of processes involved in DOC mobilization of Fe in these boreal streams. However, the δ^{56}Fe is not predictable from either Fe or DOC concentrations for a given site,

and there is no relationship for δ^{56}Fe with Fe or DOC concentrations within a site or between sites (Figure 2-4B), implicating involvement of other processes.

Dissolved δ^{56}Fe also varies seasonally within a single stream. Streams have higher DOC and dissolved Fe concentrations in early fall (September 2016) compared to early summer (June 2016), with seasonal variations of >0.17‰ in δ^{56}Fe between fall (September 2016) and summer (June 2016) observed in several boreal streams (NWIF, NEIF, EIF, U8; Figure 2-5, Table A1). September streamflows are, in general, lower than early summer streamflows, and the change in δ^{56}Fe may be due to a higher contribution from deeper hydrologic flowpaths. Two studies on podzolic and cambisolic soil profiles showed that bulk Fe and poorly crystalline Fe oxyhydroxides in the upper organic horizon were more isotopically negative than Fe phases in the lower mineral horizon, respectively.[220, 260] Biological processes (e.g., leaching of organic compounds, microbially mediated mineral dissolution and plant uptake) can produce isotopically light Fe in dissolved form, which can further enter into streams via porewater.[184, 227, 261]

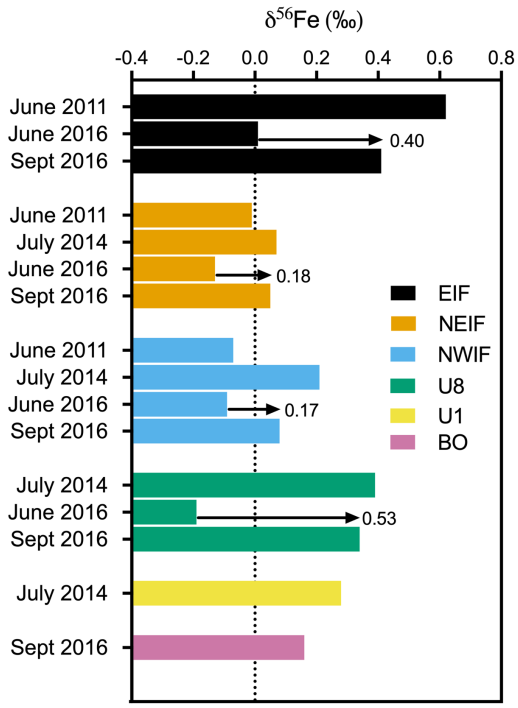


Figure 2-5 Iron isotope compositions of dissolved Fe in boreal streams sampled on different dates.
Arrows indicate the observed seasonal variations within one year.

2.3.3. Iron isotope composition in L227 and L442

Fe in the water columns of L227 and L442 exhibits a large range of $\delta^{56}Fe$ values (−0.9 to +1.8‰) for both dissolved and particulate Fe, spanning almost half of the known range (Figure 2-6).[235, 236] Distinct $\delta^{56}Fe$ of dissolved and particulate Fe were observed in different layers, but especially above and below the oxycline.

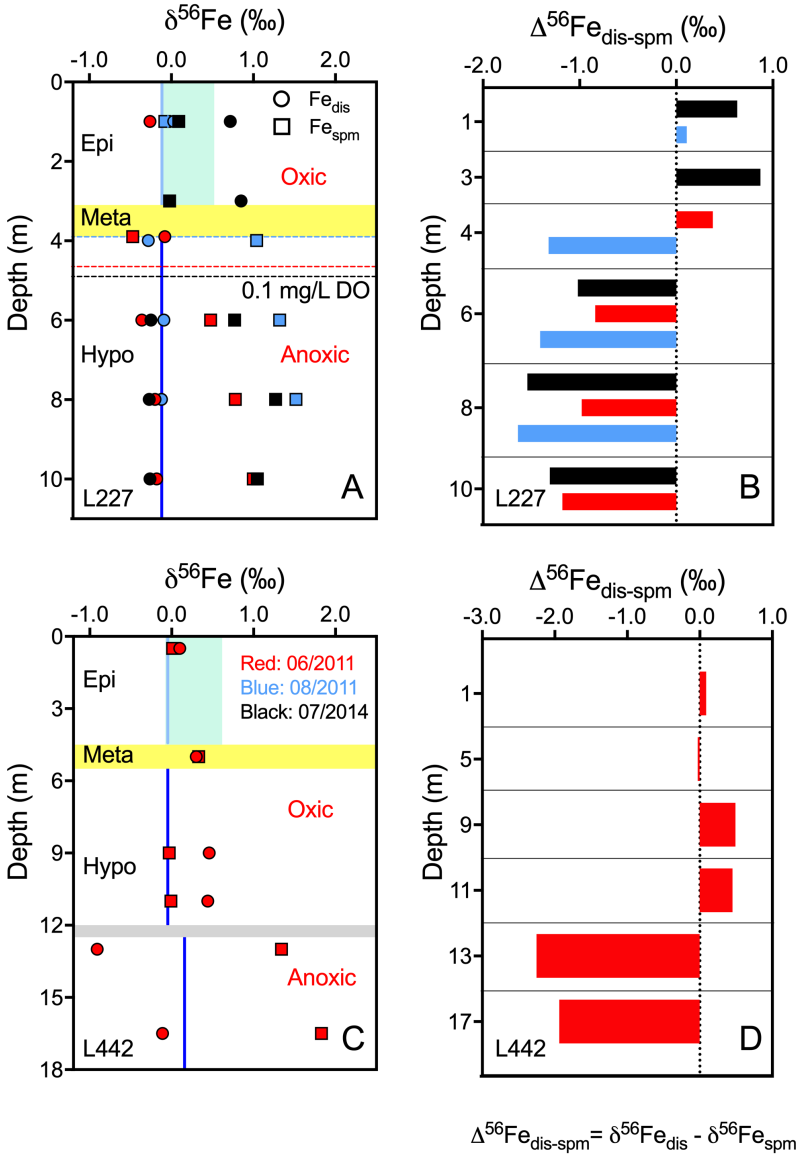


Figure 2-6 Iron isotope compositions of dissolved (Fe_{dis}) and particulate Fe (Fe_{spm}), and Fe isotope fractionations ($\Delta^{56}Fe_{dis\text{-}spm}$) for the water columns of L227 (A, B) and L442 (C, D).

Yellow bars indicate the approximate depth of the metalimnion. Red, blue and black horizontal dashed lines in panel A indicate depths of 0.1 mg L^{-1} dissolved oxygen for June 2011, August 2011, and July 2014, respectively. In panel C, the grey bar indicates the transition zone between the oxic and anoxic hypolimnion in L442 in June 2011. Blue vertical solid lines indicate $\delta^{56}Fe$ values for epilimnetic sediments (light blue) and profundal sediments (dark blue). Green boxes show the range of $\delta^{56}Fe$ values for stream waters.

Dissolved and particulate $\delta^{56}Fe$ values in the epilimnia

Following stream input, Fe isotopes are further fractionated in the epilimnia of Boreal Shield lakes. Dissolved Fe concentrations in the epilimnia of the lakes (0.7 to 0.9 μM) are a factor of 10 to 30 lower than streams (6 to 20 μM) because of the greater influence of Fe removal processes within lakes (Figures 2-3 and 2-4). In the epilimnion of L227, $\delta^{56}Fe$ spanned a larger range (−0.26 to 0.85‰) than stream input values (−0.19 to 0.62‰). Dissolved Fe generally had more positive $\delta^{56}Fe$ values than suspended particles, and isotopic variation between dissolved and particulate Fe was observed under different conditions (i.e., development of cyanobacterial bloom in July 2014 versus post bloom in August 2011; Figure 2-2 and Figure 2-6, Table A1). In the epilimnion of L442, dissolved Fe had slightly more positive $\delta^{56}Fe$ values than the suspended particles and $\delta^{56}Fe$ values of dissolved and particulate Fe were within stream input ranges, indicating that fewer in-lake processes modified $\delta^{56}Fe$ in the epilimnion of L442 compared to L227. The concentrations of chlorophyll *a* were >15-fold lower in the epilimnion of L442 compared to L227, implying that the activity of oxygenic phototrophs was comparatively low in the epilimnion of L442 (Figure 2-7). Operational taxonomic units (OTUs) associated with cyanobacteria and chloroplasts of eukaryotic algae also had lower diversity in the epilimnion of L442 compared to L227 based on previous 16S rRNA gene sequencing data (Figure 2-7). These measures of phototroph abundance and diversity support that fewer microbial processes that could mediate iron fractionation were likely active in the epilimnion of L442 compared to L227.

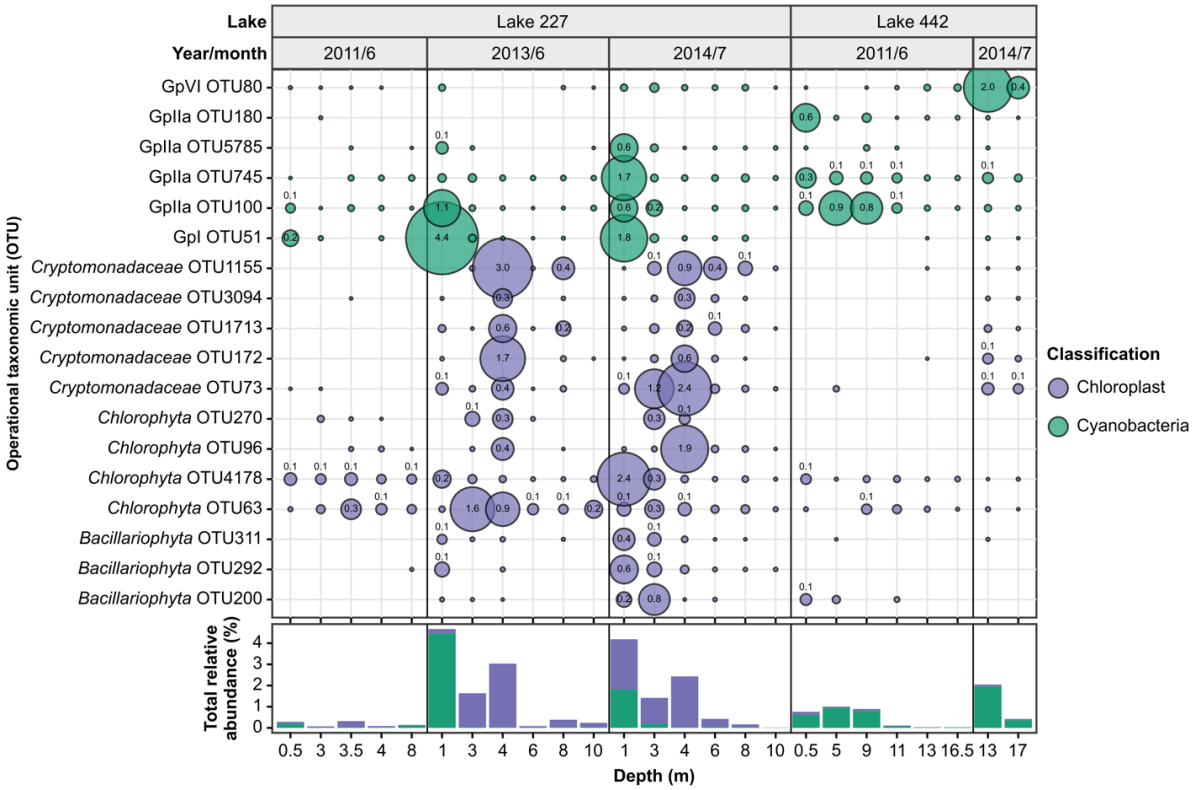


Figure 2-7 Microbial community data from the water columns of Lakes 227 and 442. The bubble plot summarizes the major operational taxonomic units (OTUs) associated with cyanobacteria and chloroplasts (e.g., of eukaryotic algae), based on previously published 16S ribosomal RNA gene sequencing data,[211] in samples from L227 and L442 from multiple years. The size of each bubble represents the percent relative abundance of an OTU compared to all 16S rRNA gene sequences from a given sample. Any bubbles without a percent relative abundance label had a relative abundance of <0.05%. Each sample, representing a depth of the lake water column, is shown along the x-axis, and all cyanobacterial/chloroplast OTUs that had ≥0.3% relative abundance in at least one sample are shown on the y-axis. The bar chart summarizes the total relative abundances of all cyanobacterial and chloroplast OTUs in each sample

Major processes that may contribute to the variation in observed epilimnetic δ^{56}Fe values in the open water season (Figure 2-8) include 1) changing δ^{56}Fe in streams with season and/or flowpath, 2) uptake by or sorption onto biomass and loss to the benthic and profundal sediments, 3) photolysis or microbial decomposition of Fe-DOC complexes, 4) coagulation and sedimentation of Fe or Fe-DOC colloids, and 5) return flux of Fe complexed to DOC from benthic sediments.

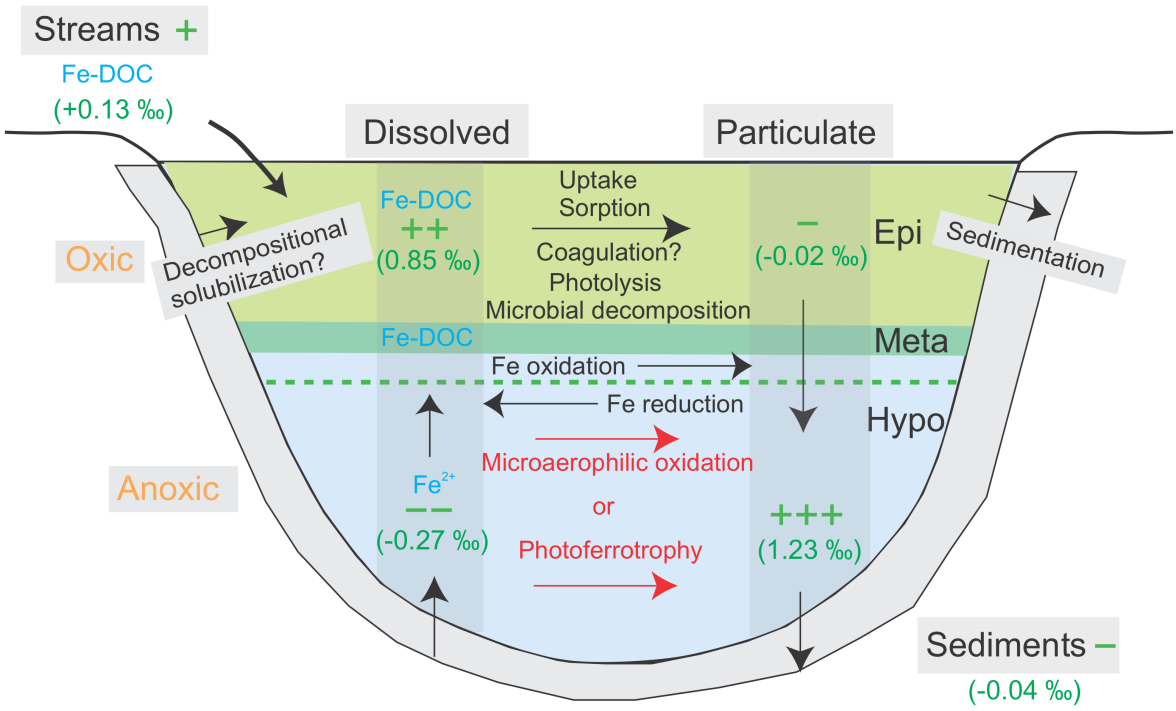


Figure 2-8 Schematic diagram showing processes operating in L227 and L442 that could impact the Fe isotope compositions of dissolved and particulate Fe.
Green positive and negative signs denote the relative magnitude of Fe isotopic values associated with each fraction. The Fe isotopic values displayed for the water column are the δ^{56}Fe of L227 measured in July 2014 (during bloom development). The values for streams and sediments are the average δ^{56}Fe of streams and sediments, respectively.

Water residence times in small headwater lakes in this portion of the Boreal Shield in Canada generally range from 4 to 26 years.[262, 263] Seasonal variability in stream inputs is muted on the annual cycle. Thus, stream Fe input with seasonal variation in δ^{56}Fe values is not the major process contributing to the variable δ^{56}Fe values in the epilimnion of the lakes.

In eutrophic L227, the development of an epilimnetic cyanobacterial bloom in summer (July 2014) led to dissolved δ^{56}Fe values in the epilimnion outside the observed range of terrestrial inputs. The isotopic fractionation ($\Delta^{56}Fe_{dis\text{-}spm}$) between dissolved and particulate Fe was 0.75 ± 0.24‰ (2σ) (Figure 2-6A,B). In the metalimnion of L227 (4 m in June 2011), the apparent $\Delta^{56}Fe_{dis\text{-}spm}$ was 0.38‰ during the bloom peak. No such values were observed in August 2011 (post bloom). Adsorption of Fe on solid surfaces can fractionate Fe isotopes, and solid surfaces are known to preferentially adsorb the heavier isotope.[183, 193, 264] One study of Fe adsorption on phytoplankton showed an apparent Fe isotope fractionation

factor $\Delta^{56}Fe_{medium\text{-}cells}$ of −0.7 to −1.8‰ between the growth medium and cells.[265] Our results that dissolved Fe is more positive by 0.4~1‰ are contrary to these experimental values, suggesting that the observed $\Delta^{56}Fe_{dis\text{-}spm}$ fractionations in the epilimnion and metalimnion of L227 are not caused by Fe adsorption. Previous studies of Fe isotope fractionation during biological uptake show contradictory results. Two studies of biological uptake of Fe by phytoplankton in the open ocean indicate a fractionation factor ($\Delta^{56}Fe_{disFe\text{-}phyto}$) of 0.2‰ between dissolved Fe and phytoplankton at the chlorophyll maximum depth and a $\Delta^{56}Fe_{disFe\text{-}phyto}$ of 0.3‰ to 1‰ in the surface mixed layer during bloom conditions.[229, 230] In contrast, two experimental studies of biological Fe uptake in growth medium shows $\Delta^{56}Fe_{medium\text{-}cells}$ of −1.1‰ for a diazotroph with Fe(III) sources and of −0.8 to −3.1‰ for a phytoplankton with Fe(II) sources.[185, 186] Our results imply that $\Delta^{56}Fe_{dis\text{-}spm}$ fractionations of 1‰ in the epilimnion (during bloom development) and 0.4‰ in the metalimnion (at peak bloom) in L227 are possibly caused by the uptake of isotopically light Fe by cyanobacteria, in contrast to observed values in laboratory cultures but similar to those of the open ocean (Figure 2-6A,B). Particulates in the epilimnion and metalimnion of L227 were almost entirely composed of cyanobacteria (peak bloom) or eukaryotic algae (development of bloom and post-bloom) based on the low C/N molar ratios of 5.8 to 7.5 (Table A1), and this observation further supports that biological uptake was the main contributor to the observed $\Delta^{56}Fe_{dis\text{-}spm}$ fractionations in L227. Particulates in oligotrophic L442 have higher C/N molar ratios (9.1 to 12.9), similar to C/N ratios in IISD-ELA stream particulates (10.4 to 14.2),[266] which may reflect allochthonous contributions (Table A1). The similarity between dissolved and particulate $\delta^{56}Fe$ in L442 suggests that biological uptake or sorption by biomass plays a minor role in affecting $\delta^{56}Fe$ of oligotrophic boreal lakes (Figure 2-6C,D).

Cyanobacteria could take up isotopically light Fe for growth and are thought to be able to migrate to acquire Fe if Fe is limiting.[210] Given the different $\Delta^{56}Fe_{dis\text{-}spm}$ fractionations in the epilimnion and metalimnion during bloom in L227, we speculate that cyanobacteria in the metalimnion may migrate to the anoxic zone and utilize Fe when bioavailable Fe is extremely limiting in the oxic zone. Distinct $\delta^{56}Fe$ of dissolved Fe in the epilimnion and metalimnion of L227 might yield clues about the source of Fe used by cyanobacteria if the fractionation factor were measured independently and is not dependant on Fe concentration.

If Fe isotope fractionations using representative eukaryotic algae and cyanobacteria in laboratory cultures are measured separately and are distinct, the δ^{56}Fe values of dissolved and particulate Fe could also potentially serve as a diagnostic tool for the amount and source of Fe uptake by cyanobacteria.

Other in-lake processes may also affect δ^{56}Fe but probably to a lesser and largely unknown degree. Photolysis of dissolved Fe complexed to DOC could enrich the dissolved phase in light Fe isotopes.[267] In contrast, microbial decomposition of DOM followed by intracellular Fe uptake could make dissolved δ^{56}Fe more positive.[267] Our observed dissolved δ^{56}Fe in the epilimnion and metalimnion of L227 is consistent with the isotopic values of microbial decomposition followed by intracellular uptake, but in contrast to the values of photolysis. However, microbial decomposition rates in boreal lakes are extremely low and biodegradation usually utilizes low molecular weight (LMW) photo-products.[268] Therefore, photolysis and microbial decomposition of DOM are unlikely the major processes contributing to the dissolved δ^{56}Fe in L227. Coagulation, sorption, and/or selective sedimentation of large terrestrial derived Fe-DOC colloids (i.e., less than 0.45 μm) could also be a fractionating process, but even the direction of isotopic fractionation of this process has not been reported previously. Returning Fe, diffusing from the epilimnetic sediments into the water column, is either all complexed with DOC to stabilize the dissolved Fe, when the epilimnetic sediment is under oxic conditions, or is composed of dissolved Fe(II) produced by dissimilatory iron reduction (DIR) when episodic anoxia in epilimnetic sediments is present at night.[269, 270] However, no measures of fractionation associated with the return flux from sediments have been reported previously.

Bulk sediments in the hypolimnion appear to provide a historical record for δ^{56}Fe of epilimnion particulates. Cores from the profundal region of L227 are laminated and have a clear demarcation of sediments deposited before and after eutrophication. The laminae become noticeably thicker in sediments layers that were deposited after eutrophication presumably began. Profundal sediments in L227, after the start of experimental nutrient additions, show a narrow range in δ^{56}Fe values (−0.09 to −0.03‰; Table A1, Figure 2-9), similar to current particulate values for the epilimnion (0.00 ± 0.14‰, 2σ). The similarity between δ^{56}Fe of epilimnetic particulate and sediment in the profundal zone reflects the high depositional flux of biomass from the epilimnion to bottom sediments that is fueled by

artificial nutrient additions (Figure 2-6, Table A1). In contrast, δ^{56}Fe of sediments at 25-26 cm, deposited approximately 50 years before the start of experimental nutrient additions, were −0.22‰ (Figure 2-9C). Sediment δ^{56}Fe values clearly record changes in lake anoxia and Fe cycling related to experimental fertilization in L227. In L442, where phytoplankton biomass is comparatively low, the surficial sediment from 17 m in the anoxic zone of the hypolimnion showed a different Fe isotopic composition (+0.28‰) compared to epilimnetic particulate Fe (+0.01‰), reflecting the combined contributions from the flux of particulate Fe settling from the overlying oxic layer and *in situ* particulate Fe formed at the bottom (Figure 2-6C, Table A1). In lakes where phytoplankton biomass is high and/or there is high Fe depositional flux, δ^{56}Fe of lake sediments may serve as an archive for past changes in lake Fe cycling.

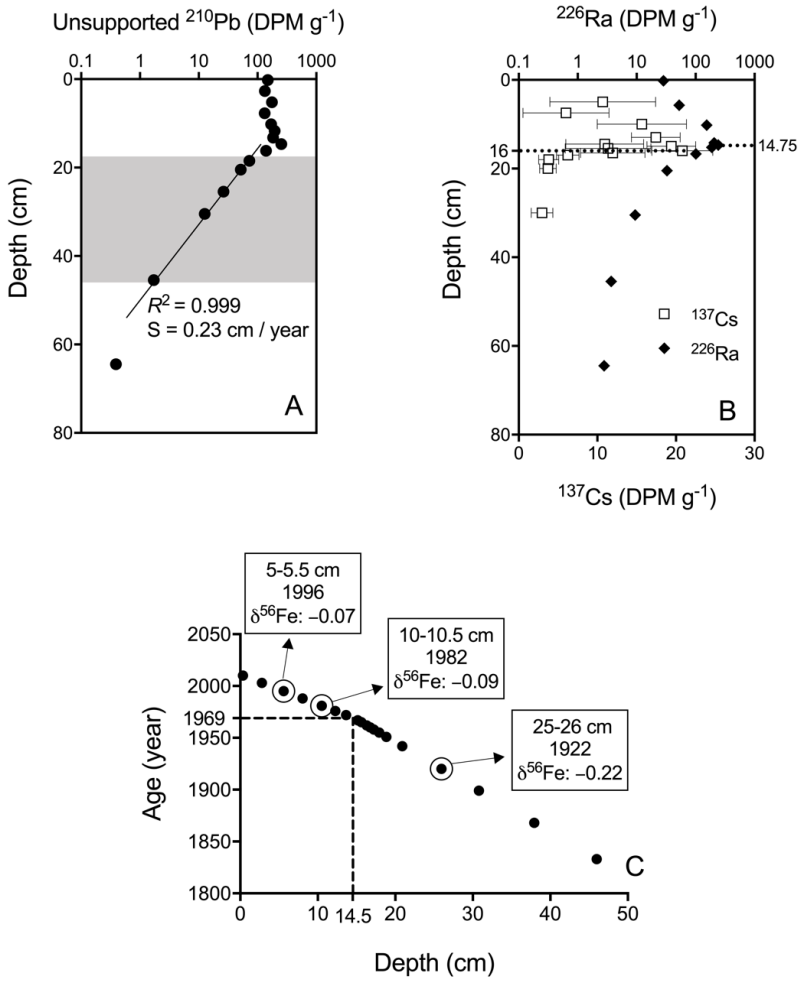


Figure 2-9 Unsupported ^{210}Pb (A), ^{226}Ra and ^{137}Cs activities (B), and age (C) versus depth profiles in a sediment core from L227 (March 2011).
Unsupported ^{210}Pb activity was calculated as total ^{210}Pb minus supported ^{210}Pb (background ^{226}Ra activity). Sedimentation rate (S) pre-eutrophication is 0.23 cm y^{-1} based on ^{210}Pb profile between 19 and 45 cm (gray zone in (A)). The alteration of ^{210}Pb profile between 0 and 18 cm is due to the addition of ^{226}Ra in 1970, making Pb-210 dating for post-eutrophication period challenging. Dotted lines in (B) show the sediment depths of maximum activities of ^{226}Ra and ^{137}Cs. Circled points in (C) are the sediment samples analyzed for δ^{56}Fe. Dashed line in (C) represents the beginning of nutrient additions in 1969, which is marked visually in the core (~14.5 cm) by the appearance of thicker laminae. Sedimentation rate of post-eutrophication is estimated as 0.35 cm y^{-1}.

Dissolved and particulate δ^{56}Fe values in oxic hypolimnion of L442

Dissolved Fe had more positive δ^{56}Fe values than particulate Fe in the oxic hypolimnion of L442, similar to the Fe isotope pattern in the epilimnion of L227 (Figure 2-6). However, we propose that $\Delta^{56}Fe_{dis\text{-}spm}$ fractionations in the oxic hypolimnion of L442 were not primarily due to the uptake of Fe by cyanobacteria. Although we detected cyanobacterial OTUs in oxic hypolimnion samples from L442 (Figure 2-7), the minimal light intensity (<2 μmol photons m^{-2} s^{-1}, which is less than 1% of the surface light intensity)[211] and low concentrations of chlorophyll *a* (<2 μg/L; Figure 2-10) in the oxic hypolimnion suggested that the photosynthetic activity of cyanobacteria in this zone would be comparatively low. The δ^{56}Fe of dissolved and particulate Fe in the oxic hypolimnion could instead be due primarily to the complexation of Fe-DOC, which makes the dissolved Fe bound to DOC more isotopically positive than inorganic Fe species.[188]

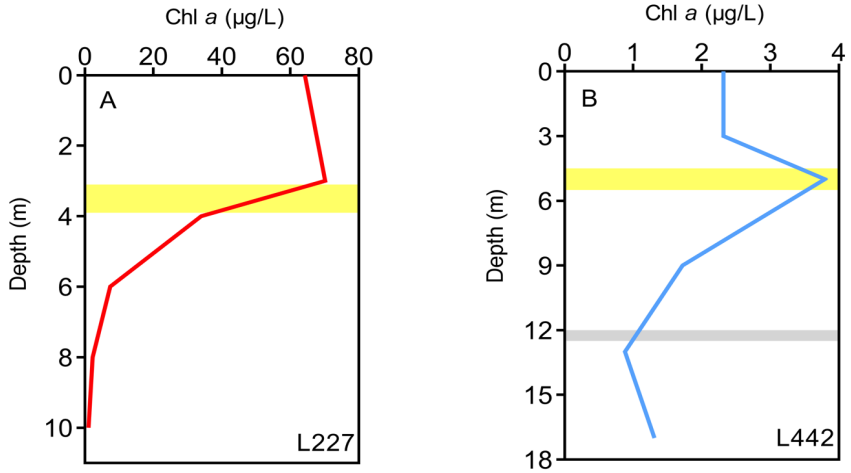


Figure 2-10 Chlorophyll *a* (chl *a*) profiles in the water column of L227 (06/28/2011) and L442 (05/30/2011).
The concentration of chlorophyll a was measured by high performance liquid chromatography (HPLC). Yellow bars indicate the approximate metalimnion depth. Gray bars indicate transition zones between oxic and anoxic hypolimnia in L442.

Dissolved and particulate δ^{56}Fe values in anoxic hypolimnia

Anoxia in the hypolimnia reversed the Fe isotope patterns in oxic waters, such that dissolved δ^{56}Fe was significantly more negative than suspended particulates (Figure 2-6, Table A1). The difference in δ^{56}Fe between dissolved and particulate Fe ($\Delta^{56}Fe_{dis\text{-}spm}$) in the anoxic zone was similar for the two lakes: −2.10 ± 0.44‰ (2σ) in L442, −1.46 ± 0.32‰ in L227 post-bloom, −1.29 ± 0.52‰ in L227 during bloom development, and −1.00 ± 0.34‰ in L227 during peak bloom.

In the anoxic hypolimnia, the main Fe inputs to the water column are commonly Fe flux from sediments and particulate Fe settling from the upper oxic layer (Figure 2-8). The Fe flux from sediment is mainly a dissolved Fe flux rather than a particulate flux by sediment remobilization, given the high dissolved Fe and low particulate Fe concentrations at the bottom of the water column (Figure 2-3, Table A1) and the high porewater Fe concentration in sediment cores at the deepest depth of L227[271] and L442 (unpublished data, average 331± 67 μM in L442). Three major redox-related processes can potentially fractionate Fe isotopes in the anoxic layers of both lakes (Figure 2-8): 1) partial oxidation of Fe(II) by O_2 at the redox boundary, 2) dissimilatory iron reduction (DIR) of either particulate Fe(III) oxyhydroxides formed *in situ*, or particulate Fe (i.e., DOC-Fe complexes or Fe(III) oxyhydroxides) originating in the overlying oxic layer or profundal sediments, and 3) oxidation of Fe(II) by photoferrotrophs or microaerophilic Fe(II)-oxidizing bacteria in the anoxic water column. Because nitrate concentrations were below detection in these lakes,[272] we predict that biological nitrate-reducing Fe(II) oxidation is not quantitatively important. The presence of Fe(II) minerals such as mackinawite (FeS) and vivianite [$Fe_3(PO_4)_2$] can be predicted by saturation index (SI) (Table 2-1). The results show that both mackinawite and vivianite are undersaturated in the hypolimnia of both lakes, indicating Fe(II) mineral formation unlikely contributes to the observed $\Delta^{56}Fe_{dis\text{-}spm}$ fractionations in the hypolimnia of the lakes.

Table 2-1 Saturation indices of Fe(II) minerals in the hypolimnia of L227 and L442

Sample name	Date	[c]IAP	[d]SI	Comment
Mackinawite (FeS) $^{a}K_{sp}=10^{-3.6}$				
Lake 227 6 m-hypo	6/28/2011	2.16E-05	-1.02	undersaturated
Lake 227 8 m-hypo	6/28/2011	1.02E-04	-0.34	undersaturated
Lake 227 10 m-hypo	6/28/2011	8.77E-05	-0.41	undersaturated
Lake 227 4 m-hypo	8/24/2011	2.44E-05	-0.96	undersaturated
Lake 227 6 m-hypo	8/24/2011	1.82E-05	-1.09	undersaturated
Lake 227 8 m-hypo	8/24/2011	5.48E-05	-0.61	undersaturated
Lake 227 10 m-hypo	8/24/2011	9.86E-05	-0.36	undersaturated
Vivianite ($Fe_3(PO_4)_2$) $^{b}K_{sp}=10^{-35.8}$				
Lake 227 6 m-hypo	6/28/2011	4.49E-42	-5.55	undersaturated
Lake 227 8 m-hypo	6/28/2011	6.36E-40	-3.40	undersaturated
Lake 227 10 m-hypo	6/28/2011	8.77E-40	-3.26	undersaturated
Lake 227 4 m-hypo	8/24/2011	4.26E-43	-6.57	undersaturated
Lake 227 6 m-hypo	8/24/2011	4.05E-41	-4.59	undersaturated
Lake 227 8 m-hypo	8/24/2011	2.09E-39	-2.88	undersaturated
Lake 227 10 m-hypo	8/24/2011	2.08E-38	-1.88	undersaturated
Lake 442 13 m-hypo	6/27/2011	7.68E-46	-9.31	undersaturated
Lake 442 16.5 m-hypo	6/27/2011	2.61E-41	-4.78	undersaturated

[a]K_{sp} and [b]K_{sp} are the solubility product constants of Mackinawite (FeS) and Vivianite ($Fe_3(PO_4)_2$) respectively.[273, 274]
[c]IAP is the ion activity product of a specific mineral.
[d]SI is the saturation index defined by SI=log [IAP/K_{sp}].

When Fe(II) diffuses upwards from sediment, partial oxidation of Fe(II) can occur by O_2, but only at the redox boundary in the water column, because vertical mixing in the hypolimnion is extremely slow and at similar rates to diffusion.[272] The overall fractionation between $Fe(II)_{aq}$ and Fe(III) oxyhydroxides caused by partial oxidation was approximately –1 to –2‰ in both laboratory experiments and field settings,[234, 275] equivalent to combining equilibrium fractionation between $Fe(II)_{aq}$ and $Fe(III)_{aq}$ and kinetic fractionation upon precipitation of Fe(III) oxyhydroxides. Our observed fractionations between dissolved and particulate Fe at the redox boundary in L227 and L442 were within the range of partial Fe(II) oxidation with O_2 as the terminal electron acceptor. However, Fe(II) oxidation by O_2 is most likely complete at the redox boundary because dissolved Fe in the water column above the

redox boundary is extremely low, much lower than in streams. Oxygenic phototrophs, including cyanobacteria and eukaryotic algae, were generally detected throughout the oxic layers of L227 and L442 according to microbial 16S rRNA gene data (Figure 2-7), and these organism could contribute to rapid O_2-mediated Fe(II) oxidation. In addition, Fe(II) oxidation by O_2 at the redox boundary is unlikely to produce the observed $\Delta^{56}Fe_{dis\text{-}spm}$ in the entire anoxic hypolimnion due to extremely low rates of physical mixing.

Dissimilatory iron reduction (DIR) is expected to produce an equilibrium fractionation $\Delta^{56}Fe$ of −3‰ between $Fe(II)_{aq}$ and Fe(III) oxyhydroxides based on studies using model microorganisms and pure Fe(III) minerals.[173, 181, 182] The particulate Fe entering the hypolimnion is comprised of (1) newly formed Fe(III) oxyhydroxides by oxidation of dissolved Fe(II) at the redox boundary when dissolved reduced Fe diffuses upward, and (2) sinking particulate Fe (as DOC-Fe complexes or Fe(III) oxyhydroxides) from the overlying oxic layer. Supported by high relative abundances of potential Fe(III)-reducing bacteria near the redox boundaries of L227 and L442,[211, 276] we hypothesize that particulate Fe entering the hypolimnion were completely reduced in the upper anoxic zone (i.e., multiple centimeters below the redox boundary) and produced no isotopic fractionation, consistent with the observed similarities between hypolimnetic dissolved $\delta^{56}Fe$ and epilimnetic particulate $\delta^{56}Fe$ in L227, and between anoxic hypolimnetic dissolved $\delta^{56}Fe$ (at 16.5 m) and oxic hypolimnetic particulate $\delta^{56}Fe$ in L442 (Figure 2-6A,C). Furthermore, the consistency between Fe isotope compositions of dissolved Fe and bulk sediments in the anoxic hypolimnia of both lakes further shows that DIR of sediments is complete and does not contribute to the observed Fe isotope discrepancy between dissolved and particulate Fe in the anoxic water column.

The observed increase in $\Delta^{56}Fe_{dis\text{-}spm}$ with depth in the hypolimnion of L227 (Figure 2-6), together with the large isotope fractionation $\Delta^{56}Fe_{dis\text{-}spm}$ in the hypolimnion of L442, suggest that additional active processes must have been operating below the redox boundary and causing the large fractionation.

Previous analysis of 16S rRNA gene sequence data derived from anoxic hypolimnetic POM samples of L227 showed the presence of green sulfur bacteria (GSB), affiliated with the *Chlorobium* genus, with high 16S rRNA gene sequence identity to the known photoferrotroph *Chlorobium ferroxidans*.[211, 277] Furthermore, genome-resolved metagenome sequence analysis was used previously for L227 samples to detect *cyc2*, a candidate gene for

photoferrotrophy, in multiple *Chlorobium*-associated genome bins, indicating the possibility of photoferrotrophy in L227, although further cultivation-based work is needed to confirm this possibility.[276] Oxidation of Fe(II) by photoferrotrophs is expected to produce a Δ^{56}Fe of +1.5 ± 0.2‰ between the oxidation product hydrous ferric oxide (HFO) and aqueous Fe(II) ($Fe(II)_{aq}$), under neutral pH conditions, based on laboratory cultures of Fe(II)-oxidizing photoautotrophic bacteria.[177] In addition, acidophilic Fe(II)-oxidizing bacteria have been shown to produce a +3.0‰ equilibrium fractionation between $Fe(III)_{aq}$ and $Fe(II)_{aq}$.[174] Kinetic fractionation upon precipitation of $Fe(III)_{aq}$ produced an overall fractionation less than +3.0‰ depending on precipitation rate and aggregate size.[174] The $\Delta^{56}Fe_{dis\text{-}spm}$ values reported in this study (+0.9 to +1.6‰) for the anoxic water column of L227 are consistent with these fractionation factors derived from laboratory cultures. Furthermore, carbon and nitrogen isotope values of POM and dissolved inorganic fractions in the hypolimnion of L227 agree well with fractionation caused by photosynthesis, despite the low but measurable light levels observed in the hypolimnion (0.01-1 μmol photons m^{-2} s^{-1}).[211] Collectively, this evidence suggests the potential for *in situ* photoferrotrophic Fe(II) oxidation in the anoxic water column of L227.

A *cyc2*-encoding genome bin classified to the *Gallionella* genus,[278, 279] which includes microaerophilic Fe(II)-oxidizing bacteria such as *Gallionella ferruginea*, was recovered from L442 metagenome data and was at high relative abundance in a L442 anoxic hypolimnion metagenome.[276] Microaerophilic Fe(II)-oxidizing bacteria are commonly associated with micro-oxic or anoxic environmental conditions[280, 281] and may outcompete abiotic oxidation and produce large isotope fractionations at 13 and 16.5 m in L442 (−2.25‰ and −1.94‰, respectively; Figure 2-6C,D). In L442, the significant offset between dissolved δ^{56}Fe at 13 m and 16.5 m is likely due to low dissolved Fe concentrations (9.8 μM at 13 m versus 102.2 μM at 16.5 m; Table A1), such that Fe cycling processes (e.g., microaerophilic Fe(II) oxidation) could cause a larger shift in $\delta^{56}Fe_{dis}$ from source material. The water column at 13 m in L442 likely developed anoxic conditions just prior to the time of sampling and was transitioning from being dominated by suboxia- to anoxia-associated biogeochemical processes.

Despite the detection of potential Fe(III)-reducing bacteria in anoxic layers of L227 and L442, the signature of partial oxidation of Fe(II) by, for example, photoferrotrophs or

microaerophilic Fe(II)-oxidizing bacteria, was still evident in the particulates. We suspect that some particulate Fe in the anoxic layer may be contained in cells or sorbed to other particulates (i.e., as biogenic iron nanoparticles or organo-mineral aggregates)[282, 283] that block access by Fe(III)-reducing bacteria.

2.3.4. Comparison of δ^{56}Fe profiles in L227 and L442 to other lakes

Studies of Fe isotopes in lakes are rare. Within the chemocline of Lake Cadagno, a permanently stratified euxinic lake with an anoxic monimolimnion,[204] dissolved δ^{56}Fe within the chemocline changed sharply from 0.75 to –0.61‰, while particulate Fe changed only slightly, from –0.18 to 0.13‰. In Lake Pavin, a permanently stratified ferruginous lake with an anoxic bottom layer, a similar sharp decrease of dissolved δ^{56}Fe was observed at the redox boundary.[200] The changes of dissolved δ^{56}Fe in both lakes were interpreted as resulting from partial oxidation of Fe(II) at the redox boundaries, although the heavier dissolved δ^{56}Fe along with a peak of cyanobacterial concentration in the lower part of oxic mixolimnion in Lake Cadagno suggested the possibility of biological uptake. In contrast, no dramatic change of dissolved δ^{56}Fe was observed at the transition layer in L227, with the exception of the peak cyanobacterial bloom period. The observed dissolved and particulate δ^{56}Fe in the anoxic layer of Lake Cadagno were also distinct from L227. The $\Delta^{56}Fe_{spm\text{-}dis}$ was small in Lake Cadagno (0.25 ± 0.10‰, 2σ). However, an increase in $\Delta^{56}Fe_{spm\text{-}dis}$ (+0.9 to +1.6‰) with depth in the hypolimnion was observed in L227, implying there are active Fe processes throughout the anoxic layer of L227. Additional distinction among the three lake systems lies in their P and S content in the water column. Dissolved Fe concentrations in Lake Cadagno were two orders of magnitude lower than in the anoxic hypolimnion of L227, while the concentration of sulfide was two orders of magnitude higher. As a result, the formation of mackinawite dominated the dissolved and particulate δ^{56}Fe in Lake Cadagno, producing a constant $\Delta^{56}Fe_{dis\text{-}spm}$ fractionation of −0.2‰ in the anoxic monimolimnion. The TDP concentrations in Lake Pavin (up to 400 μM in the monimolimnion[200]) are more than two orders of magnitude higher than that in both L227 and L442 (up to 2 μM in the hypolimnion), making Fe phosphates the predominant phase of the particulate matter in the monimolimnion[284] of Lake Pavin. Low concentrations of dissolved P and sulfide along with

the undersaturation of authigenic Fe(II) minerals in L227 and L442 imply that formation of Fe phosphates or Fe sulfide contributes negligibly to the observed $\delta^{56}Fe$ in this study. Another distinction lies in the identification of microbial communities. Microbial profile data support the existence of photoferrotrophic bacteria in Lake Cadagno[285] and L227, whereas no photoferrotrophic bacteria have been identified in the Lake Pavin.[284] The most abundant purple and green sulfur bacteria were observed in chemocline of Lake Cadagno. In contrast, potential photoferrotrophs were detected up to several meters below the top of the anoxic hypolimnion of L227,[211] associated with an increase in magnitude of fractionation $\Delta^{56}Fe_{dis\text{-}spm}$ with depth.

Chapter 3

Fe isotopes reveal distinct Fe cycling pathways during cyanobacterial blooms in Boreal Shield lakes

3.1. Introduction

Iron (Fe) redox transformations are closely linked to the biogeochemical cycles of other elements, such as carbon, nitrogen and sulfur, in aquatic ecosystems.[2] The biogeochemical cycle of Fe is mediated by abiotic and biotic processes. Abiotic processes are regulated by chemical reactions between Fe and redox species of other elements such as O_2, NO_2^-, MnO_2, various S species and organic C.[28] These abiotic processes control the mobility, solubility, and bioavailability of Fe for biotic processes.[286] The bioavailability of Fe plays a critical role in primary productivity in the oceans,[287] and the biogenic Fe products are omnipresent in natural environments.[288, 289] Fe has two main redox states in the environment: Fe(III) and Fe(II). Fe(III), the oxidized form, is insoluble at circumneutral pH in the absence of complexing organic matter, and Fe(II), the reduced form, is readily soluble in the absence of O_2.[28] Fe is intimately associated with OM by strongly binding to organic ligands in natural organic-rich environments. Organic matter forms strong complexes with ferrous[14, 290, 291] and ferric Fe.[292-294] The binding of Fe-OM increases the solubility, mobility and thus bioavailability of Fe in natural waters and wetland soils by preventing hydrolysis/oxidation.[14]

Harmful algal blooms (HABs) in freshwater are a significant environmental problem worldwide.[295-297] Cyanobacterial blooms (CyanoHABs), the most common HABs, can produce toxic compounds that can threaten the lives of animals and humans that drink contaminated water. [210, 296] Recently, Fe was suggested to play a key role in controlling harmful cyanobacterial blooms in lakes and reservoirs.[210] The competitive ability of

cyanobacteria over eukaryotic competitors may be regulated by the availability of ferrous Fe.[210]

Natural Fe isotopes are useful tracers for biogeochemical processes involving Fe. Stable Fe isotope compositions in natural environments span a range of up to 8‰ in δ^{56}Fe.[235, 236] Only a limited number of Fe isotope studies have been conducted on lakes.[200-205] One recent study on the Fe isotope compositions of dissolved and particulate phases in the water columns of two small boreal headwater lakes found that the onset of a cyanobacterial bloom affected the Fe isotope signature in the water columns (Chapter 2).[298] However, the mechanisms by which cyanobacteria blooms modify the biogeochemical cycle of Fe in freshwater lakes remain poorly understood. In this study, the seasonal variations in Fe speciation and Fe isotopic compositions of dissolved (DFe) and particulate Fe (PFe) in freshwater lakes during two annual phytoplankton blooms are reported. The study presents the concentrations of Fe(II) and Fe(III) in dissolved (DFe) and particulate Fe (PFe) along with the Fe isotope compositions of dissolved Fe, particulate Fe and total Fe in the water column of two small dimictic boreal headwater lakes: a eutrophic lake that has two blooms each summer and a reference oligotrophic lake. This study aims to (1) explore the potential biogeochemical Fe processes associated with Fe isotope fractionation during annual phytoplankton blooms; (2) use Fe isotope and speciation data to track the sources of Fe used by cyanobacteria and identify the relative importance of Fe sources; (3) assess the hypothesis that under Fe-limited conditions, cyanobacteria could migrate to anoxic zone where sufficient dissolved Fe(II) is available.

3.2. Methods

3.2.1. Study site

Lake 227 (L227) and Lake 442 (L442) are small boreal headwater lakes located in the IISD Experimental Lakes Area (IISD-ELA) in northwestern Ontario, Canada.[238, 299] L227 is a eutrophic lake that has been fertilized with nutrients for over 50 years. L227 has a surface area of 5 ha, a mean depth of 4.4 m and a maximum depth of 10 m, while L442 is an oligotrophic lake with a surface area of 16 ha, a mean depth of 9.6 m and a maximum depth of 17.8 m. No defined stream enters L227 apart from ephemeral streams that feed the lakes during snowmelt or heavy rainstorms. L227 outflow typically ceases in late spring. L442 has a lake outflow on the southeastern side and an inflowing stream in the northern basin. The ELA area lies within the Precambrian Shield on a massive batholith of pink granodiorite.[238] The surrounding watersheds are typical boreal forests, mostly jack pine and black spruce. Both lakes do not have significant groundwater recharge or discharge because of shallow soils and impermeable granitic bedrock. Data on the physico-chemical conditions of lakes, along with the hydrology and meteorology of the ELA area, have been collected for over 50 years.

L227 and L442 are dimictic lakes that are stratified in summer and winter and water column mixing occurs in spring and fall. The thermal stratification of small dimictic lakes in ELA typically occurs in early to mid May, shortly after the ice off, and lasts until late September, but sometimes as late as early November. During stratification, two distinct layers are formed within the water column: an epilimnion and a hypolimnion, separated by a narrow thermocline, metalimnion. According to the IISD-ELA procedure, the bottom of the epilimnion is defined as the depth where the water temperature changes by greater than

1°C/m and the bottom of the metalimnion is marked at the depth where 1% surface photosynthetically active radiation (PAR) is reached.

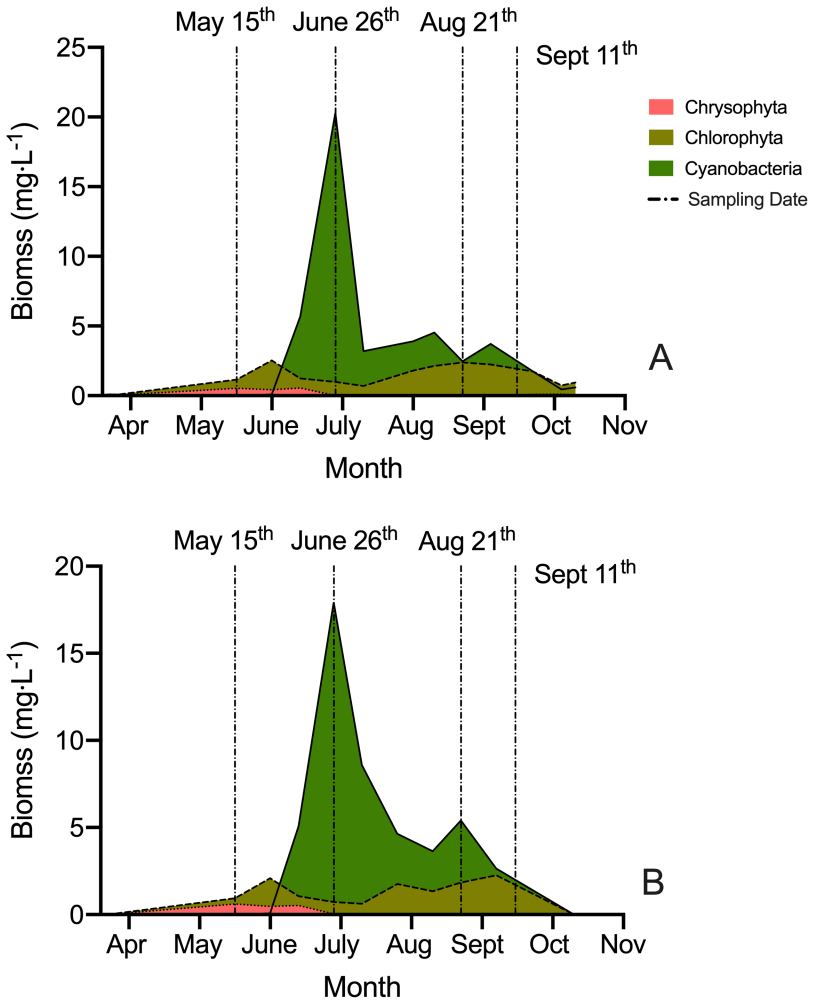


Figure 3-1 Phytoplankton biomass in the epilimnion (panel A) and metalimnion (panel B) of L227 in 2018.
Dash lines indicate 4 sampling events: May 15 was before bloom, June 26 was during the peak of the first bloom, Aug 21 was during the second bloom and Sept 11 was during the post bloom.

L227 is the site of long-term whole lake experimental eutrophication where nutrients (N, P) have been added in various ratios since 1969.[207] The regime of initial fertilization was a molar N:P ratio of 29:1 from 1969 to 1974. Then, the ratio decreased to 11:1 after 1975. In 1990, N additions were stopped, and L227 has been fertilized with P alone since then.

Oligotrophic L442 has not been manipulated in any way. L227 has two annual phytoplankton blooms in response to nutrient additions, and the bloom pattern is quite repeatable each year. The first bloom has a peak in Late June and declines sharply. The second bloom has a lower peak and a long period over late summer (late July to early September). N-fixing cyanobacteria dominate the first bloom, and the second bloom is co-dominated by cyanobacteria (ca. 60%) and chlorophytes (ca. 40%). The relationship between the timing of phytoplankton biomass bloom and sampling dates in 2018 is shown in Figure 3-1. The sampling events of May 15, June 26, August 21 and September 17 were before the bloom, during the peak of the first bloom, during the second bloom and during the post bloom, respectively.

3.2.2. Sample collection

Water column sampling campaigns were carried out in 2018. Sampling in L227 occurred on May 15, June 26, August 21 and September 17 and on June 2, July 5 and September 8 in L442. Profiles of temperature (T), dissolved oxygen (DO), pH, chlorophyll *a* (chl-*a*) and specific conductivity were collected *in situ* with a multi-parameter pre-calibrated YSI EXO2 sonde (YSI Inc., Yellow Springs, OH) at the time of sampling and every week between June and Sept. Light profiles were collected using a LI-192 underwater quantum sensor connected with a LI-250 light meter (LI-COR Biosciences, Lincoln, NE) at the time of sampling.

Lake water column samples were collected along a vertical profile from the centre of the lakes using a gear pump connected with calibrated tubing. The tubing was pre-flushed with lake water at a specific depth prior to sampling. Unfiltered water samples for dissolved inorganic carbon (DIC) and methane (CH_4) were collected without headspace in 60 mL glass

serum bottles and preserved with 300 µL of 100% $ZnCl_2$ (w/v). Dissolved samples were filtered by pumping water directly through an inline 0.45 µm filter. Filtered water samples for dissolved organic carbon (DOC), total dissolved nitrogen (TDN) and total dissolved phosphorus (TDP) were collected in 40 mL glass serum bottles and stored at 4 °C until analysis. Dissolved samples for sulfate (SO_4^{2-}), dissolved total sulfide (ΣS^{2-}) and ammonium (NH_4^+) were collected in 30 mL HDPE bottles (Nalgene) and kept frozen prior to analysis. 0.3 mL 20% zinc acetate was added to HDPE bottles prior to sampling of dissolved total sulfide. Particular attention was paid to avoiding artificial oxidation during dissolved Fe (DFe) sampling. DFe samples were collected in 160 mL glass serum bottles capped by blue butyl rubber stoppers (Bellco Glass, Vineland, NY). The empty glass serum bottles were acid-cleaned, vacuumed, and filled with N_2 gas. Before sampling, 15 mL 6 M trace-metal grade hydrochloric acid (degassed with nitrogen) was pre-injected into glass serum bottles using a needle to acidify the water samples to a final concentration of 0.5 M. Filtered water samples were injected directly into acidified glass serum bottles using a needle connected to pump tubing. Particulate Fe (PFe) samples were collected on the inline 0.45 µm membrane filters at various water depths. In addition, at the same depths, particulate organic matter (POM) for particulate organic nitrogen (PON), particulate organic carbon (POC) and suspended particulate phosphorous (SPP) samples were collected on a Whatman QM-A filters (Sigma-Aldrich, St. Louis, MI), which were pre-baked at 550 °C to remove any organic material. The PFe samples were sealed, stored on ice in the field, and frozen until analysis. Samples for microbial community analysis were collected using sterilized 0.22 µm Sterivex polyvinylidene fluoride filters, which were frozen after collection.

3.2.3. Chemical analyses

TDP concentrations were analyzed by a UV-Visible Spectrophotometer (Shimadzu, Kyoto, Japan) at the IISD-ELA Analytical Laboratory within 24 hours of sampling. DOC and TDN concentrations were measured by Total Organic Carbon (TOC-L) Analyzer (Shimadzu, Kyoto, Japan). NH_4^+ concentration analysis was performed on a Discrete Wet Chemistry Analyzer (Westco Scientific Instruments, Brookfield, CT). SO_4^{2-} concentrations were measured by Dionex ICS2100 Iron Chromatography (Thermo Fisher Scientific, Waltham, MA). DIC and CH_4 concentrations were analyzed by GC-CF-IRMS using an IsoPrime isotope ratio mass spectrometer (Elementar UK Ltd, Manchester, UK) equipped with an Agilent 6890 gas chromatograph (Thermo Fisher Scientific, Waltham, MA). Dissolved total sulfide (ΣS^{2-}) and dissolved Fe(II)/Fe(III) concentrations in the water column were measured spectrophotometrically by the methylene blue method[300] (detection limit: 0.25 μM) and the ferrozine method[240] (detection limit: 0.5 μM) respectively. The concentrations of POC and PON on the POM filters were analyzed by CE-440 Elemental Analyzer (Exeter Analytical, Coventry, UK), and SPP was analyzed by spectrophotometer (Cole-Parmer, Montreal, CA) at IISD-Experimental Lakes Area Analytical Laboratory.

The filters for PFe were cut in half in an anaerobic chamber. The first half was dissolved in 6M HCl under anoxic conditions and then preserved in 0.5 M HCl solution for Fe(II)/Fe(III) concentrations by the ferrozine method (detection limit: 0.5 μM). The second half was digested using an acid digestion protocol. Briefly, the filters were thawed, cut into pieces and placed in 22 mL Teflon vials (Savillex, Eden Prairie, MN). Then 4 mL concentrated HNO_3 and 0.8 mL concentrated HF were added to the Teflon vials. The Teflon vials were capped and heated at 110 °C for 12 hours. The mixture was evaporated to dryness.

Then 1 mL concentrated HNO_3 and 3 mL concentrated HCl were added to the vials. The vials were sealed and heated at 110 °C for 12 hours. After that, the mixture solutions were evaporated to dryness. Finally, particulate stock solutions were obtained by adding 5 mL 6 M HCl into the vials. In addition, blank filters were also digested following the same protocol. Stock solutions of particulate were diluted in 2% HNO3, and the trace element concentrations were determined by an Agilent 8800 triple quadrupole inductively coupled plasma mass spectrometer (QQQ-ICP-MS) in the Metal Isotope Geochemistry Laboratory at the University of Waterloo. The HISS-1 (National Research Council of Canada) and BHVO-2 (U.S. Geological Survey) were also digested with particulate samples to check instrument accuracy (within 10%).[301, 302] The blank filter contained 479±11 ng Fe, which is neglectable compared to the amount of Fe on the sample filters (avg. 62 μg).

3.2.4. Lake water column geochemical profiles

The geochemical profiles in L227 and L442 are generally similar from late spring to early fall.[211] In 2018, the temperature in L227 and L442 decreased from ~15-23 ºC in the epilimnion to 4 ºC in the hypolimnion during thermal stratification (Figure 3-2). The epilimnia of the two lakes were well oxygenated. Oxygen concentrations declined and became depleted ($<O_2$=0.1 mg/L) in the hypolimnia of L227 (Figure 3-2). In L442, the redox boundary (O_2=0.1 mg/L) was located between 10 and 13 m, separating the hypolimnion into oxic and anoxic zones. pH values in two lakes ranged from 6 to 9, with low pH at the bottom and high pH at the surface (Figure 3-2). In L227, the pH at the surface layer can be as high as 9 during the bloom period. In L227 and L442, SO_4^{2-} concentrations decreased from ~7-14 μM in oxic layers to ~3-5 μM in anoxic layers, accompanied by an increase in total dissolved sulfide ($\Sigma S^{2-}=H_2S+HS^-+S^{2-}$) from 1 μM in oxic layers to ~5-9 μM at the bottom of lakes

(Figure 3-2). TDP concentrations in L442 were ~1-10 µg/L, showing an increasing trend with depth. In L227, the enhanced anoxia over time significantly increased the TDP concentration (~80 µg/L) at the bottom of the lake. During the peak of the first bloom, the TDP concentration was 40 µg/L at 4 m depth, much higher than the bottom of the lake (24 µg/L). Both lakes showed increased DIC concentrations with increasing depth, ranging from 15 µM to 2000 µM (Figure 3-2). DOC, TDN and CH_4 concentrations were relatively constant in oxic layers and increased with depth in the anoxic hypolimnia of two lakes with some exceptions (Figure 3-2). The TDN concentrations were constant across all depths of L442 in July 2018. POC, PON and SPP concentrations in L442 and L227 during the pre-bloom period generally increased with depth (Figure 3-2). After the onset of bloom, both epilimnion and metalimnion samples had higher POC, PON and SPP concentrations than the hypolimnion in L227.

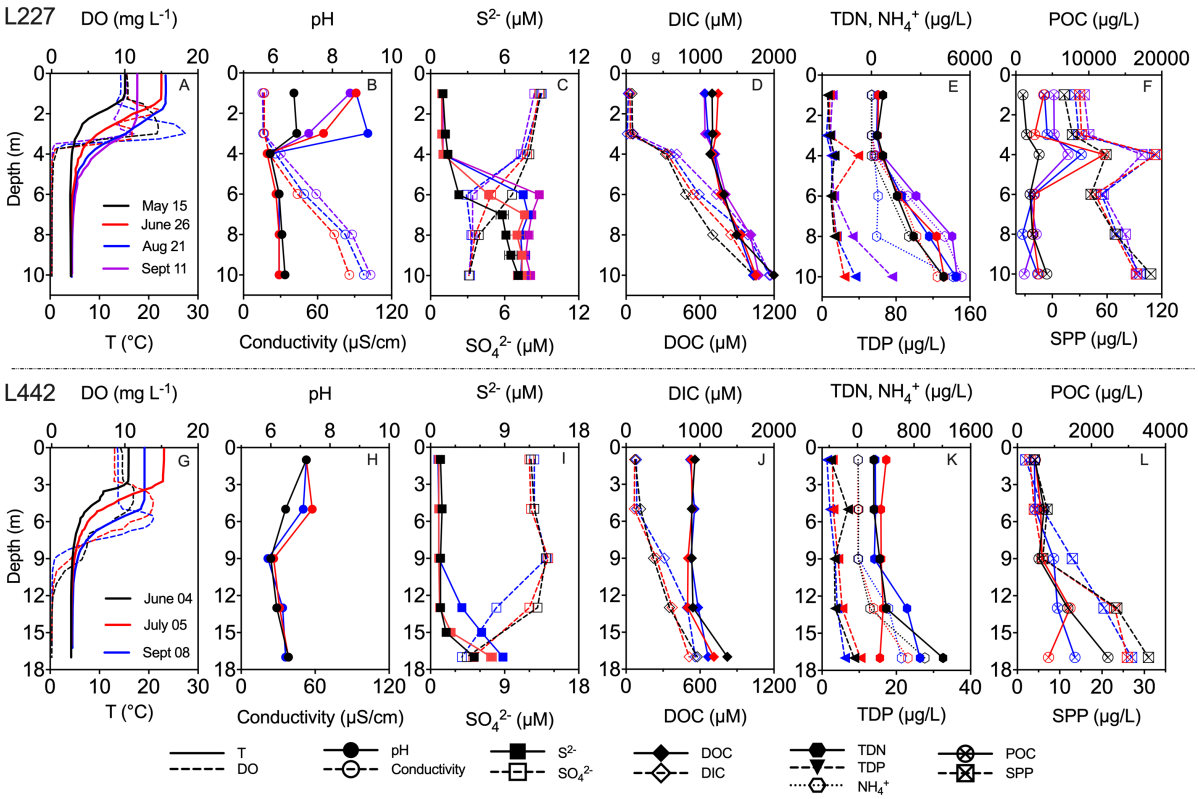


Figure 3-2 Water column depth profiles of (A, G) dissolved oxygen (DO) and temperature (T); (B, H) pH and conductivity; (C, I) total dissolved sulfide (ΣS^{2-}) and sulfate (SO_4^{2-}) (D, J) Dissolved inorganic carbon (DIC) and dissolved organic carbon (DOC); (E, K) total dissolved nitrogen (TDN), ammonium (NH_4^+) and total dissolved phosphorus (TDP); (F, L) particulate organic carbon (POC) and suspended particulate phosphorus (SPP) in L227 (upper panel) and L442 (lower panel) during 2018.

3.2.5. Iron isotope analyses

Iron isotope compositions were determined for DFe samples and PFe samples. Prior to Fe isotope analysis, Fe in the samples was quantitatively purified using anion exchange chromatography.[244] The recovery of Fe following chemical purification for all samples was 95 ± 5 %, as determined by the ferrozine method. To test the accuracy of Fe isotope analyses (e.g., matrix effect, fractionation during purification), test solutions were prepared by adding a certain amount of High Purity Standard (HPS Fe, in-house standard; Delta Scientific Laboratory Products Ltd) to synthetic samples, which contain the same concentrations of major ions (K^+, Ca^{2+}, Na^+, Mg^{2+} Cl^-, SO_4^{2-}) as DFe and PFe samples. The amount of HPS Fe added to the test solutions matched the range of Fe concentrations of the lake samples to be measured. Test solutions were passed through anion-exchange columns using the same procedure as all lake samples. In addition, five rock standards (SGR-1b, HISS-1, AGV-2, CRPG-GA, BHVO-2) representing different lithologies were carried through digestion and anion exchange chromatography to evaluate the accuracy of chemical separation and isotopic measurement. Iron isotope compositions were measured by a multi-collector, inductively coupled plasma mass spectrometer (MC-ICP-MS; Nu Plasma II) in the Metal Isotope Geochemistry Laboratory, University of Waterloo, using the standard-sample-standard bracketing technique. All Fe isotope data are reported as δ^{56}Fe values relative to the IRMM-634 (the international standard replacing IRMM-014; Institute for Reference Materials and Measurements), in units of per mil (‰):

$$\delta^{56}Fe=[(^{56}Fe/^{54}Fe_{sample})/(^{56}Fe/^{54}Fe_{IRMM634}) - 1] \times 10^3$$

The average δ^{56}Fe of test solutions was 0.15 ± 0.05‰ (2σ, n=8), which was within error of the average δ^{56}Fe of pure HPS Fe (0.15 ± 0.10‰, 2σ, n=55). The average δ^{56}Fe value of HISS-1 was reported for the first time at 0.19 ± 0.03‰ (2σ; n=6). The δ^{56}Fe value of SGR-1b, AGV-2, CRPG-GA and BHVO-2 were 0.06 ± 0.03‰ (2σ; n=3), 0.11 ± 0.01‰ (2σ, n=3), 0.11 ± 0.04‰ (2σ, n=3), 0.10 ± 0.02‰ (2σ, n=3) respectively, which were consistent with literature values for these rock standards (0.04 ± 0.02‰ for SGR-1b,[303] 0.11 ± 0.04‰ for AGV-2,[304] 0.11 ± 0.03‰ for CRPG-GA,[305] 0.11 ± 0.03‰ for BHVO-2[303]). The δ^{56}Fe values of rock standards, test solutions and lake samples were correlated to δ^{57}Fe values on a mass fractionation line with a δ^{57}Fe/δ^{56}Fe slope of 1.495± 0.022 (2σ, n=232, p<0.0001), closed to the theoretical mass-dependent fractionation slope of 1.47 (Figure 3-3).

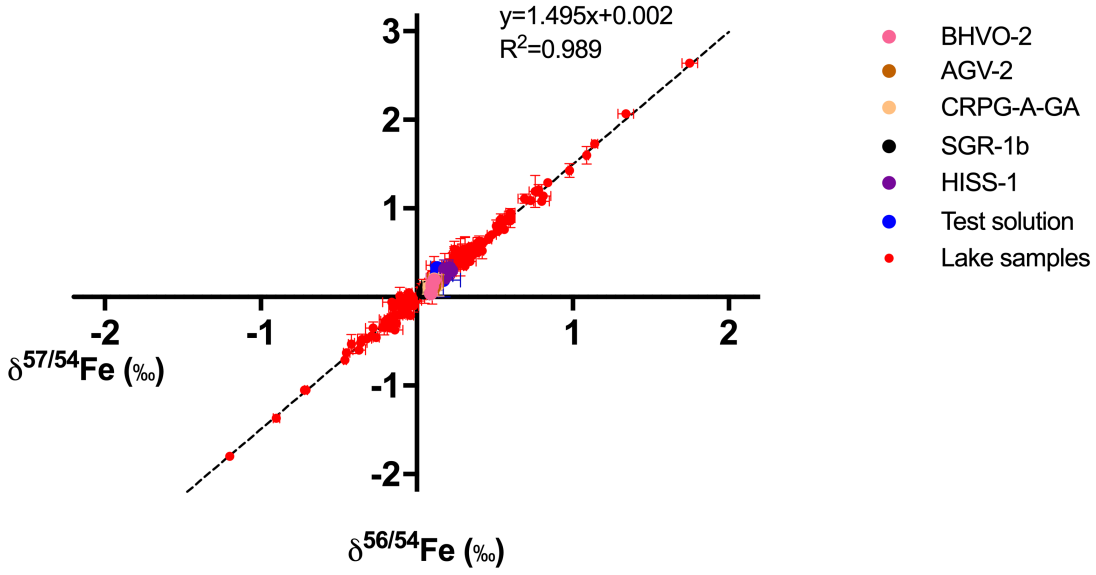


Figure 3-3 δ^{56}Fe vs δ^{57}Fe for all lake samples, together with rock standards and test solutions.

All values obtained in this study follow on a mass fractionation line with a slope close to theoretical mass-dependent fractionation value (1.47).

3.3. Results and Discussion

3.3.1. Biogeochemical cycling in the oxic layers of L227 and L442

One significant distinction between the oxic layers of the two lakes is the occurrence of phytoplankton blooms that occur twice each year during the ice-free season in L227 as a result of the nutrient addition. Four distinct stages associated with the annual phytoplankton blooms in the oxic layers of L227 are identified and compared to L442 in order to discern the effects of bloom dynamics on Fe cycling and stable Fe isotopes.

Fe redox speciation in L227 before the bloom (Stage I): The effect of photochemical reduction and abiotic precipitation

Before the bloom (May 15, Stage I), Fe speciation of DFe and PFe in the sunlit oxic layers of L227 is regulated primarily by photochemical reduction and abiotic precipitation. The phytoplankton biomass (1.6 ± 0.1 mg/L; Table 3-1) and chlorophyll *a* concentrations in the epilimnion and metalimnion of L227 (21.0 ± 17.1 μg/L; Figure 3-4) were much lower than during the bloom. DFe concentration was around 5-13 μM, and 40-90% of DFe was dissolved Fe(II) (Figure 3-5). PFe concentration was relatively constant (1-3 μM), and the particulate Fe(III) represented over 90% of PFe (Figure 3-5), suggesting that PFe is likely controlled by abiotic Fe precipitates, which comprise a mixture of lithogenic minerals and authigenic particles. Despite the fact that Fe(III) is thermodynamically favorable in oxygenated water, the relatively high dissolved Fe(II) concentrations in the oxic water column (40% to 90% of dissolved Fe) are consistent with the observations in other studies that a significant dissolved Fe(II) fraction is present in the oxic layers of circumneutral

lakes.[24, 306-308] This prevalence of dissolved Fe(II) is possibly due to the photochemical reduction of Fe(III)[30] and the complexation of dissolved Fe(II) with dissolved organic matter(DOM) in the lake.[19] Photochemical reduction of Fe(III) has been shown to produce measurable Fe(II) concentration under oxygenated circumneutral pH conditions, both in experimental studies[24, 31, 309] and natural surface aquatic systems.[310, 311] In addition to temperature and pH, the rate of photochemical reduction of Fe(III) depends on the light intensity, which generally decreases exponentially with depth due to absorption by light-absorbing components in lake water.[30] In the oxic layer of L227, the ratios of dissolved Fe(II) to DFe ($Fe(II)_{dis}$/DFe) exhibited a decreasing trend with depth (from 0.91 at 0 m to 0.40 at 4 m), reflecting a positive correlation between light intensity and $Fe(II)_{dis}$/DFe ratios. This observation further supports that the persistence of dissolved Fe(II) in oxic water could be mediated by the photochemical reduction of Fe(III). Complexation of Fe(II) with DOM following photochemical reduction of organically complexed Fe(III) could stabilize dissolved Fe(II) in the oxic layer of L227; otherwise, the photoproduced inorganic dissolved Fe(II) would have been rapidly oxidized back to dissolved Fe(III) by oxidants at the pH of L227.[312] Previous studies on the effect of Fe(II)-DOM complexation on the oxidation rates of Fe(II) showed that the presence of aromatic humic substances, tannic acids, gallic acid and pyrogallol could significantly inhibit the oxidation rate of Fe(II) and stabilize dissolved Fe(II) in oxic water.[16-18] It should be noted that Fe(II) binding to DOM also accelerates[313, 314] or has no effect[315] on the rate of Fe(II) oxidation, and the variable effects depend on the molecular composition of DOM and experimental system.[19]

While DFe and PFe concentrations in the oxic layers of L442 (0-5 μM and 0.1-1.0 μM, respectively) were generally lower than those in L227, a similar pattern of Fe speciation

was observed in the water column of L442 compared to L227 before the bloom (Figure 3-5). Particulate Fe(III) represented over 80% of PFe in the oxic layers of L442 similar to L227. Although dissolved Fe(II) represented 65-70% of DFe in the oxic epilimnion and metalimnion of L442, no dissolved Fe(II) was observed in the oxic hypolimnion of L442 (Figure 3-5), suggesting that there is a lack of photochemical reduction of Fe(III) in the hypolimnion, likely due to the limited light intensity in this zone (<2 μmol photons m^{-2} s^{-1}; 1% of the surface radiation).[211] The prevalence of dissolved Fe(II) and particulate Fe(III) in the surface oxic layers of L227 and L442 implies that photochemical reduction of Fe(III) and precipitation of Fe(III) oxyhydroxides play substantial roles in the Fe cycling in the oxic layers before the bloom.

Table 3-1 Phytoplankton biomass (mg/L) and cell density (10^6 cell/mL) in the epilimnion and metalimnion of L227 during 2018

Dates	Layers	Cyanobacteria		Chlorophyte		Chrysophyte		Total biomass	Total density
		mg/L	10^6 cell/mL	mg/L	10^6 cell/mL	mg/L	10^6 cell/mL	mg/L	10^6 cell/mL
May 15	Epi	0.01	0.04	1.16	1.42	0.54	0.54	1.71	2.01
	Meta	0.01	0.05	0.93	1.30	0.61	0.81	1.55	2.16
June 26	Epi	20.31	117.03	0.98	1.35	0.01	0.02	21.30	118.39
	Meta	17.93	114.78	0.73	1.39	0.04	0.06	18.69	116.23
Aug 21	Epi	4.53	26.06	2.13	10.33	0.00	0.00	6.67	36.39
	Meta	5.41	32.27	1.85	12.75	0.01	0.01	7.26	45.03
Sept 11	Epi	3.71	22.02	2.08	15.61	0.01	0.02	5.81	37.65
	Meta	2.65	17.02	2.25	17.30	0.03	0.04	4.93	34.37

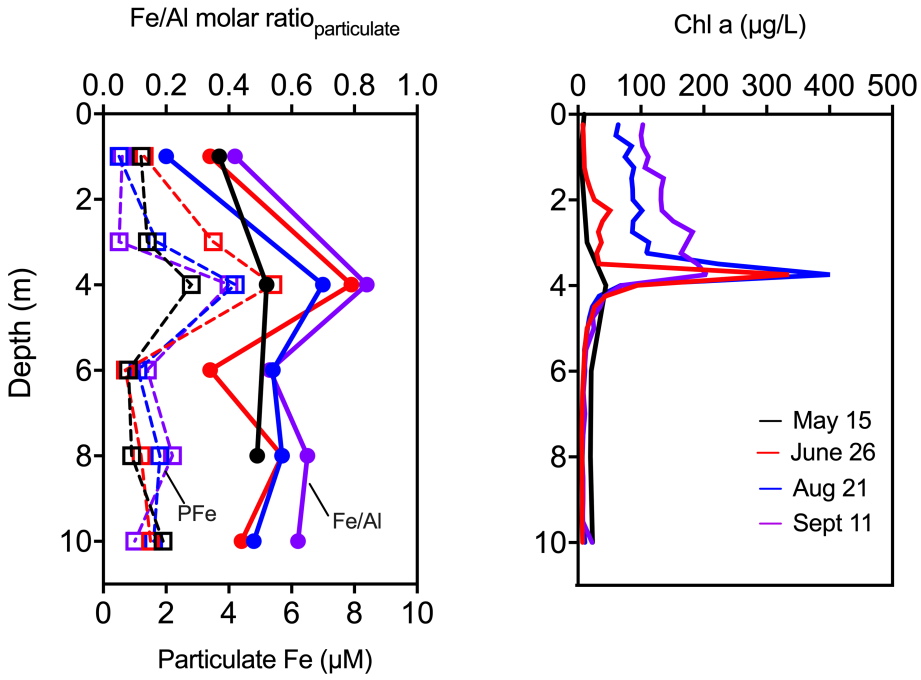


Figure 3-4 Depth profiles of (A) Fe/Al molar ratio of suspended particulates and particulate Fe concentrations, and (B) chl a concentrations in L227 during 2018.

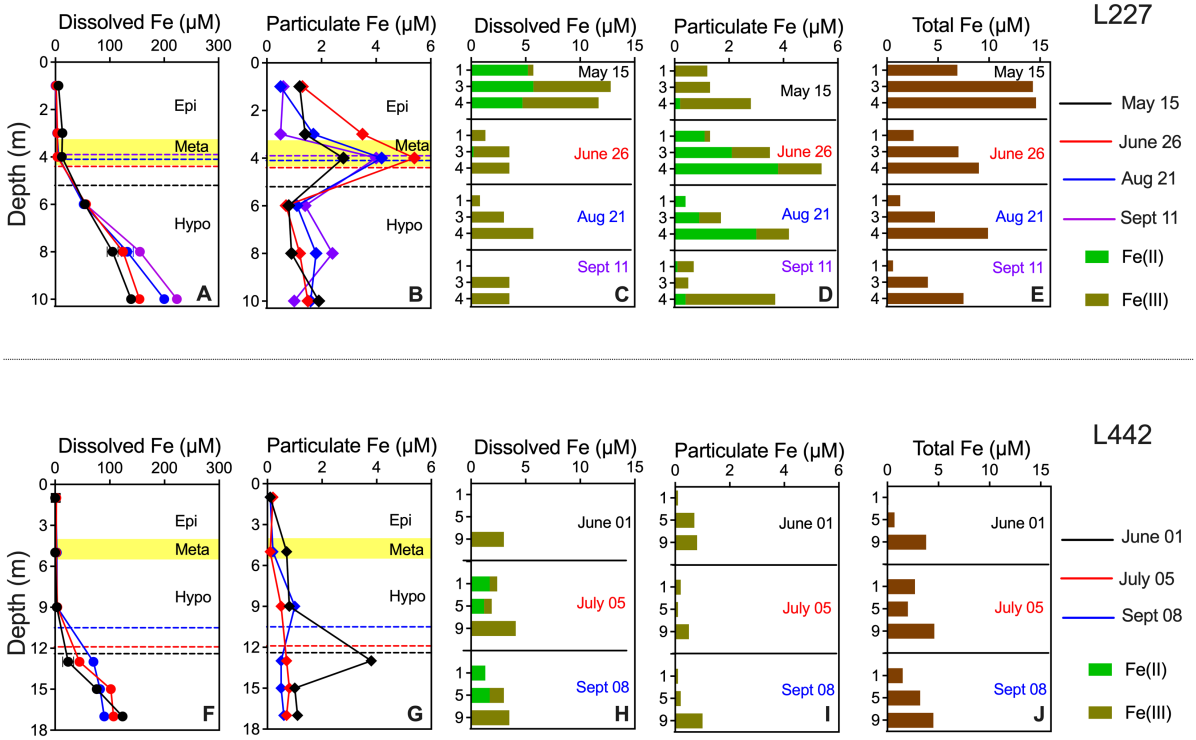


Figure 3-5 Dissolved Fe, particulate Fe, and total Fe concentrations in L227 (A-E) and L442 (F-J) during 2018.
Yellow bars indicate approximate depth of metalimnion. The thickness and depth of metalimnion may vary seasonally. Black, red, blue, purple horizontal dotted lanes represent the depth of 0.1 mg/L dissolved oxygen (redox boundaries) for May 15, June 26, August 21 and September 11, respectively, in L227. Black, red and blue horizontal dotted lanes represent the depth of 0.1 mg/L dissolved oxygen (redox boundaries) for May 01, July 05 and September 08, respectively, in L442.

Dissolved and particulate δ^{56}Fe in oxic layers of L227 before the bloom (Stage I)

During Stage I, dissolved δ^{56}Fe was slightly more positive than particulate δ^{56}Fe in the epilimnion and metalimnion of L227 given the 0.05‰ measured external precision. The isotopic fractionation between DFe and PFe ($\Delta^{56}Fe_{dis-part}$) was small (0.13 ± 0.03‰, 2σ; Figure 3-6). The δ^{56}Fe values of DFe and PFe in the epilimnion and metalimnion of L442 were similar to those observed in L227. Furthermore, the fractionation $\Delta^{56}Fe_{dis-part}$ in the epilimnion and metalimnion of L442 was 0.06 ± 0.09‰ (2σ), similar to the $\Delta^{56}Fe_{dis-part}$ observed in the oxic layers of L227 before the bloom. Collectively, this evidence indicates similar Fe processes in L442 and L227 before the bloom.

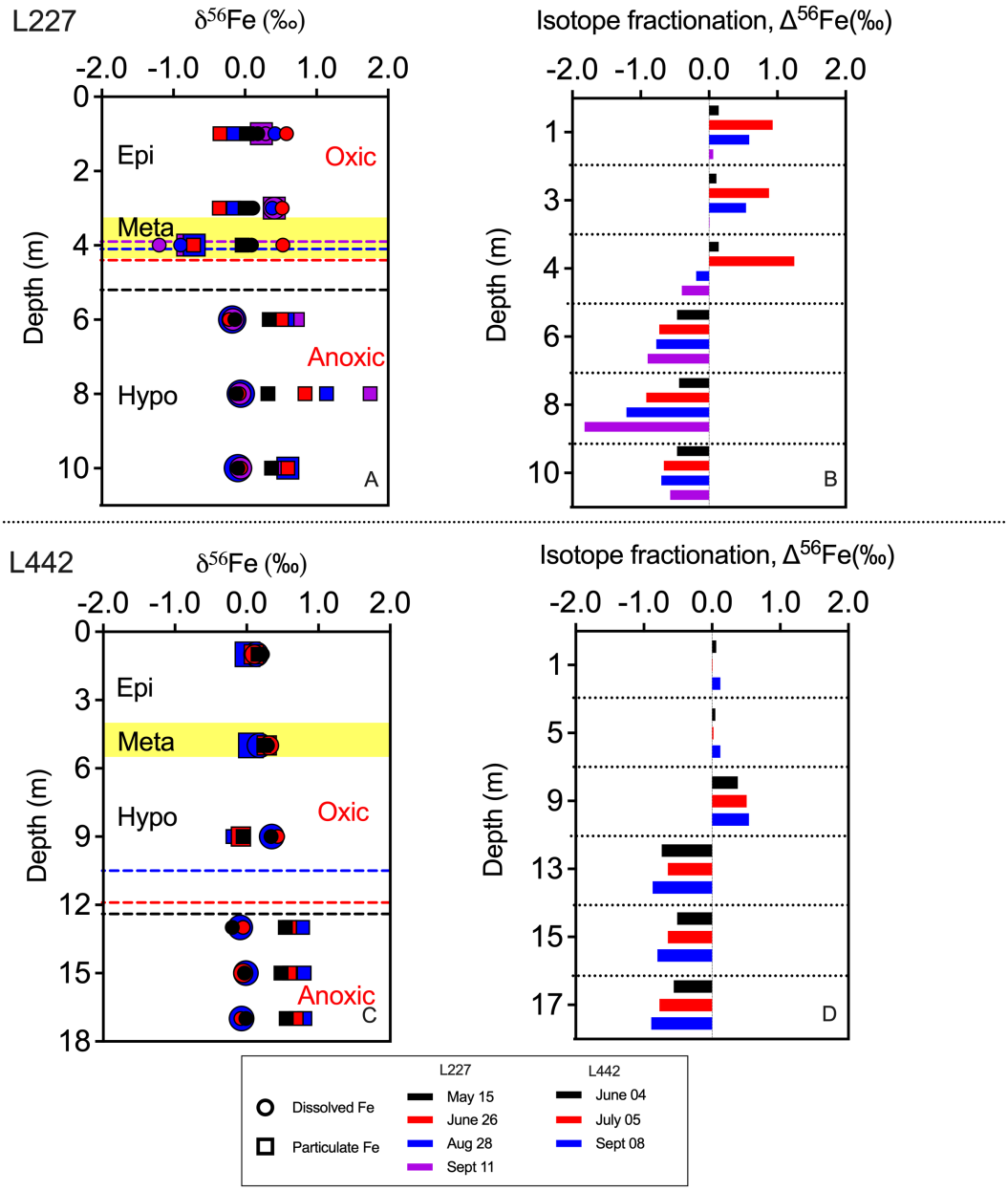


Figure 3-6 Iron isotope compositions ($\delta^{56}Fe$) of dissolved and particulate Fe in the water column of L227 (A, B) and L442 (C, D).
Yellow bars indicate approximate depth of metalimnion. The thickness and depth of metalimnion may vary seasonally due to the changing climate. Horizontal dotted lanes represent the depth of 0.1 mg/L dissolved oxygen (redox boundaries) in each lake at the time of sampling. Iron isotope fractionation, $\Delta^{56}Fe$, is defined as the difference between dissolved $\delta^{56}Fe$ and particulate $\delta^{56}Fe$.

Potential in-lake processes that could modify $\delta^{56}Fe$ in the epilimnion and metalimnion of L442 and L227 before the bloom include (1) complexation of DFe with

DOM, (2) precipitation of Fe(III) oxyhydroxides, (3) photochemical reduction of particulate Fe(III), and (4) photolysis or microbial decomposition of organic Fe complexes.

The observation that DFe is slightly enriched in heavy Fe isotopes suggests that $\delta^{56}Fe$ of DFe and PFe in the oxic layers of L442 and L227 before the bloom are likely modified by a combination of multiple processes, which counteract each other and produce the observed small $\Delta^{56}Fe_{dis-part}$ fractionations in the epilimnion and metalimnion of L442 and L227 (Figure 3-6). In oxic water, 99% or more of DFe is complexed to organic ligands.[20, 24] The complexation of DFe with DOM can make organically complexed DFe enriched in heavy isotopes. An experimental study of dissolved Fe(III) binding to siderophores showed an equilibrium fractionation $\Delta^{56}Fe$ of 0.60 ± 0.15‰ between dissolved organic Fe(III) complexes and dissolved inorganic Fe(III).[188] The latter would precipitate as Fe oxyhydroxides under circumneutral conditions and the isotope fractionation $\Delta^{56}Fe_{dis\ Fe(III)-ferric\ oxide}$ between dissolved inorganic Fe(III) and Fe oxyhydroxides tends to be 0‰ if the precipitation is rapid and complete,[316] which is likely the case in natural oxic systems considering the abundant oxygen and extremely low amount of dissolved inorganic Fe(III).[20, 24] The kinetic fractionation $\Delta^{56}Fe_{dis\ Fe(III)-ferric\ oxide}$, however, can be variable from 0.2‰ to 1.5‰ depending on the precipitation rate (moderately fast to slow).[174, 317] Furthermore, a previous study of Fe isotope fractionation between colloidal Fe and PFe in boreal organic-rich water found that $\delta^{56}Fe$ of different Fe pools increased with decreasing particle size, and the dissolved Fe-DOM complexes in the <0.4 μm fractions were enriched in heavy Fe isotopes by 0.30‰ compared to the PFe in the >0.4 μm fractions.[258] In contrast, the photochemical reduction of particulate Fe(III), producing a significant amount of dissolved Fe(II) in the oxic layers of L442 and L227 before the bloom, is known to produce dissolved

Fe(II) enriched in light Fe isotopes. One experimental study of the photochemical reduction of Fe oxides observed an apparent Fe isotope fractionation $\Delta^{56}Fe_{dis-goeth}$ of −1.7‰ between DFe and goethite.[318] Photolysis and microbial decomposition of organic Fe complexes can also fractionate Fe isotopes. Microbial decomposition of organic Fe complexes could make dissolved $\delta^{56}Fe$ more positive. A previous study on the biodegradation of DOM using boreal humic water with heterotrophic bacteria found that the DFe became isotopically heavier (~0.3‰) due to a combination of the breakdown of Fe-DOC complex, Fe adsorption and assimilation by live cells.[267] In contrast, photolysis of DFe complexed to DOM could make the dissolved phase isotopically more negative. DFe associated with DOM is isotopically more positive than inorganic Fe species[188]. A partial breakdown of the Fe-DOM complex followed by the removal of Fe by precipitation of Fe oxyhydroxides from the water column could make the dissolved phase isotopically more negative. An experimental study on the photodegradation of DOM in boreal humic water showed that the dissolved phase decreased in $\delta^{56}Fe$ during photodegradation followed by precipitation of Fe.[267] At present, given the conflicting results of various but limited studies, the relative contributions of those processes to the Fe isotope signatures of DFe and PFe cannot be disentangled. Instead, it is likely that all these processes combine to produce the observed $\Delta^{56}Fe_{dis-part}$ fractionations in the epilimnion and metalimnion of L442 and L227.

Dissolved and particulate δ^{56}Fe and relationship to Fe speciation during the peak of the first bloom (Stage II)

Both Fe speciation and isotopic values of DFe and PFe in the oxic layers of L227 are altered by the onset of the cyanobacterial bloom. The peak of the first bloom (June 26, Stage II), characterized by high phytoplankton biomass concentration (20.0 ± 1.8 mg/L; Table 3-1)

and chlorophyll *a* concentration (maximum: 336 μg/L; Figure 3-4), is dominated by diazotrophic cyanobacteria (>95% of total biomass; Figure 3-1), primarily *Aphanizomenon schindlerii*. A drawdown of DFe and an increase in PFe were observed in the oxic epilimnion and metalimnion during Stage II compared to Stage I (Figure 3-5). DFe concentration in the oxic layers of L227 during the first bloom was around 1-3 μM, much lower than DFe concentration before the bloom. In contrast, PFe concentration (1-5 μM) in the oxic layers of L227 was higher during the peak of the first bloom compared to PFe concentration before the bloom. Almost all of DFe (over 94%) was dissolved Fe(III), and particulate Fe(II) represented between 61% and 88% of PFe during the peak of the first bloom, in contrast to Fe redox speciation observed before the bloom (Figure 3-5).

Diazotrophic cyanobacteria have the potential to affect Fe cycling. These organisms, capable of N_2 fixation and oxygenic photosynthesis, have higher Fe requirements than other microorganisms such as heterotrophic bacteria and eukaryotic algae.[71, 72, 319] Excessive growth of diazotrophic cyanobacteria could cause the depletion of DFe and an increase in PFe due to intensive intracellular uptake of Fe, as well as Fe adsorption to the cell walls (further details on Fe adsorption are provided in the following paragraphs). Previous studies showed that the onset of a cyanobacterial bloom caused the drawdown of DFe in the surface layer of eutrophic lakes[320] and the open ocean.[229, 321, 322] One study on diurnal variation of DFe during summer bloom in a boreal lake found that DFe concentration decreased during daytime due to the assimilation by phytoplankton cells.[323] One recent study of Fe cycling during a phytoplankton bloom in the surface ocean showed that PFe concentrations increased in the mixed layer during the development of the bloom.[324] Furthermore, one study about the effect of fertilization with Fe on the formation of bloom in coastal waters found that PFe

concentration was higher in the bloom region than in the surrounding high-nutrient, low-chlorophyll reference seawater.[325] Moreover, PFe generally increased in the oxic layers and peaked at 7 μM at 4 m of L227 (Figure 3-4). The peak of PFe coincided with the peak of chlorophyll *a* concentration (Figure 3-4), further supporting the suggestion that uptake by cyanobacteria causes an increase in PFe and a decrease in DFe at all depths from 0 to 4 m during the peak of the first bloom in L227. Furthermore, total Fe concentrations (TFe=DFe + PFe) in the oxic layers of L227 during the first bloom also decreased compared to TFe before the bloom (Figure 3-5), suggesting a removal of Fe after onset of the cyanobacterial bloom.

DFe concentrations in the oxic layers of L442 noticeably increased from early June to early July and remained relatively constant until September (Figure 3-5). Meanwhile, PFe concentrations in the oxic layers of Lake 442 remained relatively constant from early June to early September (Figure 3-5). Collectively, these observations support the idea that the drawdown of DFe and the increase in PFe in L227 during the peak of the first bloom are likely caused by biological processes associated with cyanobacteria, possibly involving intracellular uptake of Fe by cyanobacteria. Furthermore, total Fe concentration in the oxic layers of L442 considerably increased from early June to early July (Figure 3-5), likely resulting from terrestrial Fe input; this observation supports that changes in TFe concentration in the oxic layers of L227 during the bloom are likely attributed to the removal of Fe associated with the cyanobacterial bloom, rather than abiotic aggregation and precipitation of DOC-Fe. The onset of the cyanobacterial bloom in the epilimnion and metalimnion of L227 modifies biogeochemical Fe cycling, causing changes in DFe, PFe and TFe pools.

The occurrence of diazotrophic cyanobacteria can alter Fe speciation of DFe and PFe. Phytoplankton in high density could cause elevated dissolved Fe(II) in oxygenated water, both in lakes and experimental studies.[307, 308, 326] During the cyanobacterial bloom, dissolved inorganic Fe(II) can be produced by photochemical reduction of Fe(III) and extracellular reduction of Fe(III) by cyanobacteria. Cyanobacteria reduce Fe(III) to dissolved inorganic Fe(II) on the plasma membrane (or in the periplasm) prior to transport into the cell,[85, 88, 89] or generate superoxide to reduce Fe(III) to dissolved inorganic Fe(II) extracellularly under oxic conditions.[90, 91] Furthermore, cellular secretions from phytoplankton decrease Fe(II) oxidation rates substantially.[327, 328] A recent study investigating the effect of phytoplankton on Fe reduction and oxidation rates under simulated experimental conditions showed that a high density of phytoplankton could slow Fe(II) oxidation rates, possibly due to the weak complexation between dissolved Fe(II) and organic compounds excreted by phytoplankton.[308] Nevertheless, there was no dissolved Fe(II) detected in the epilimnion and metalimnion of L227 during the bloom (Figure 3-5). The severe depletion of newly reduced dissolved Fe(II) during the peak of the first bloom is speculated to be caused by the uptake of dissolved Fe(II) by cyanobacteria.

Cyanobacteria can take up dissolved Fe(II) via porin-mediated Fe uptake and reductive Fe uptake.[79, 80, 82, 84] The newly produced dissolved inorganic Fe(II) by photochemical reduction can be transported directly through the outer membrane of cyanobacteria by porins, which are not permeable to organically complexed Fe.[83, 84] One study investigating the effect of light on Fe uptake by cyanobacteria found that dissolved inorganic Fe(II) produced by photochemical reduction dramatically promoted the uptake rate of Fe by cyanobacteria, suggesting that photochemically produced inorganic dissolved Fe(II)

is more assimilable by cyanobacteria than organically complexed Fe.[329] Furthermore, one study on the bioavailability of Fe to cyanobacteria found that dissolved inorganic Fe is the most bioavailable form in terms of Fe acquisition by cyanobacteria.[82] An alternative pathway of Fe acquisition that has been studied extensively in cyanobacteria and eukaryotic algae is reductive Fe uptake, which involves the reduction of Fe(III) before the transport of Fe into cells.[78, 80] Dissolved Fe(II) produced by extracellular reduction of Fe(III) can be subsequently transported through the plasma membrane during Fe acquisition.[82] The prevalence of Fe(II) in the particulate phase during the peak of first bloom in L227 (Figure 3-5) implies that these particulate Fe(II) particles are likely intracellular Fe(II) assimilated by cyanobacteria (and extracellular Fe(II) by adsorption; details are given below), lending support to the dominance of dissolved Fe(II) transport in Fe acquisition of cyanobacteria in L227. The dissolved Fe(III) fraction observed in the oxic layer of L227 during the bloom is possibly bound to high-molecular-weight (HMW) ligands, which cannot be readily reduced to dissolved Fe(II)[24] or directly transported into cells by siderophore mediated transport,[330] due to the low bioavailability of Fe bound to HMW ligands.[331] Another explanation for the presence of dissolved Fe(III) in the oxic layer of L227 during the bloom is that Fe is not limited in L227. As a result, siderophore mediated Fe(III) transport is not initiated in the cyanobacterial cells.

Despite the fact that siderophore mediated Fe(III) transport has been well characterized in both cyanobacteria and eukaryotic algae under Fe starvation,[85-87] this Fe-uptake mechanism is unlikely to be the dominant pathway in the cyanobacterial strains of L227, considering the prevalence of particulate Fe(II) in L227, as mentioned previously, as well as the Fe isotope results (see further details in the following paragraphs). A recent study that successfully suppressed a cyanobacterial bloom in L227 by adding oxine implied that

cyanobacterial strains in L227 mainly transport Fe(II), not Fe(III), into the cell, and the availability of dissolved Fe(II) might regulate the formation of the cyanobacterial bloom, ruling out the dominance of siderophore mediated Fe(III) transport in L227.[208] It is likely that the siderophore mediated Fe(III) transport in the cyanobacteria in L227 is either not initiated because the concentration of DFe is still "sufficient" for the growth of cyanobacteria or, if initiated, it contributes at a very low rate. Cyanobacteria can utilize siderophore mediated Fe(III) transport when subjected to extreme Fe limitation. One study on siderophore production by cyanobacteria found that siderophore was not produced until DFe concentrations drastically decreased to 10^{-19} M.[332] Furthermore, the uptake rate of siderophore mediated Fe(III) transport is 10^4 times lower than the rate of inorganic Fe transport in cyanobacteria.[82]

In the oxic epilimnion and metalimnion of L442, Fe speciation of DFe and PFe shows no seasonal variation from early June to early September, with a consistent dominance of dissolved Fe(II) and particulate Fe(III), respectively. This observation in L442 further suggests that the depletion of dissolved Fe(II) and the prevalence of particulate Fe(II) during the peak of the first bloom in L227 are likely caused by the uptake of dissolved Fe(II) by cyanobacteria. Furthermore, the interpretation that the dominance of dissolved Fe(II) transport over siderophore-mediated Fe(III) transport in cyanobacterial stains in L227 is consistent with other studies showing that non-siderophore mediated Fe uptake (i.e., porin-mediated Fe uptake and reductive Fe uptake) is dominant in Fe acquisition in freshwater cyanobacteria (e.g., *Microcystis* and *Anabaena* sp.).[331, 333, 334]

The change in Fe speciation in the epilimnion and metalimnion during the bloom in L227 was accompanied by a diagnostic change in δ^{56}Fe values of DFe and PFe. During the

peak of the first bloom, dissolved Fe was low and dissolved $\delta^{56}Fe$ was significantly more positive than particulate $\delta^{56}Fe$ in the epilimnion and metalimnion of L227 (Figure 3-6). The $\Delta^{56}Fe_{dis-part}$ in the epilimnion and metalimnion of L227 during the bloom was 1.02 ± 0.33‰ (2σ), much larger than that in L227 before the bloom (0.13 ± 0.03‰, 2σ) (Figure 3-6). Furthermore, the $\delta^{56}Fe$ values of DFe and PFe in the epilimnion and metalimnion of L442 remained constant from early June to early September, with the $\Delta^{56}Fe_{dis-part}$ of 0.06 ± 0.09‰ (2σ), much smaller than $\Delta^{56}Fe_{dis-part}$ in the epilimnion and metalimnion of L227 during the bloom. Collectively, this evidence suggests that the $\delta^{56}Fe$ values of DFe and PFe in L227 are likely modified by biological processes associated with the cyanobacterial bloom.

Uptake of isotopically light Fe by cyanobacteria during the peak bloom caused the PFe to be more isotopically negative and the remaining DFe more positive. Dissolved $\delta^{56}Fe$ is more positive than particulate $\delta^{56}Fe$ by 0.9-1.3‰ during the peak of cyanobacterial bloom (Figure 3-6), consistent with the reported values ($\Delta^{56}Fe_{dis-part}$ of 0.2 to 1‰ between dissolved Fe and particulate Fe) of biological uptake in both open ocean[229, 230] and freshwater systems.[298] Laboratory studies on the Fe isotope fractionation during biological uptake, however, yield opposite results. Uptake by a diazotroph in a culture study using Fe-citrate enriched the cells with $\Delta^{56}Fe_{cells-medium}$ of +1.1‰ compared to the growth medium.[185] The author implied that enrichment of heavy Fe isotopes in cells was possibly due to uptake of isotopically heavy siderophore Fe(III), which was produced during Fe transport and modified by the equilibrium isotope effect between siderophore bounded Fe(III) and Fe-citrate in growth medium. Another study on the biological uptake by phytoplankton using two algal species and Fe(II) sources in a culture observed a $\Delta^{56}Fe_{cells-medium}$ of 0.8 to 3.1‰ between cells and growth medium.[186] The author suggested that oxidation of adsorbed Fe(II) and

subsequent transport of adsorbed Fe(III) into cells likely led to the isotopically heavy intracellular Fe. In L227, the Fe uptake mechanism in the cyanobacteria is quite different from the proposed mechanisms of these two experimental studies. Cyanobacteria in L227 appear to mainly utilize dissolved inorganic Fe(II), which is likely produced by the photochemical reduction of Fe(III) and the extracellular reduction of Fe(III). Photochemical reduction of Fe(III) is known to produce dissolved Fe(II) enriched in light Fe isotopes.[318] Although the fractionation during extracellular reduction of Fe(III) remains unclear, this process is likely to produce isotopically light dissolved Fe(II), similar to the photochemical reduction[318] or biotic Fe(II) reductions (e.g., dissimilatory iron reduction).[181] Therefore, the uptake of bio- and photo-reduced isotopically light dissolved Fe(II) leads to the enrichment of light Fe isotopes in cells. Another explanation for the isotopically light intracellular Fe in L227 is a kinetic isotope effect whereby light Fe isotopes have relatively faster rates than heavy Fe isotopes during the biological uptake. Further isotope work is needed to constrain the isotope fractionation mechanism during the uptake of Fe by the diazotrophic cyanobacteria, *Aphanizomenon schindlerii*.

Other processes that could potentially affect Fe cycling and Fe isotopic values in the oxic layer of L227 during the peak of the first bloom include (1) Fe adsorption on cyanobacteria, (2) oxidative precipitation of Fe oxyhydroxides and formation of Fe(II) minerals and (3) hydraulic flushing via lake inflow/outflow and seasonal variation in δ^{56}Fe from stream inputs.

Adsorption of Fe on cyanobacterial biomass could cause the drawdown of DFe and an increase of PFe (Figure 3-5). Both dissolved Fe(II) and Fe(III) can adsorb on cyanobacteria, contributing to the particulate Fe(II) and Fe(III) pools. As adsorbed Fe(II) is

readily oxidized to Fe(III) under oxygenated circumneutral pH conditions,[265] the particulate Fe(II) fraction contributed from Fe(II) adsorption might be relatively small compared to the fraction from intracellular uptake of dissolved Fe(II). At this stage, the intracellular Fe(II) and extracellular Fe(II) in the particulate Fe(II) pool cannot be distinguished. The particulate Fe(II) pool is likely composed of intracellular Fe(II) and extracellular Fe(II). Fe adsorption is unlikely to dominate, however, because the presence of Fe adsorption is not supported by Fe isotope results. Sorption of Fe to a solid surface is known to favor the heavier isotope in sorbed phase, leaving DFe isotopically light, [183, 193, 264] which is in direct contradiction with the isotope results presented in this study. Two studies of Fe isotope fractionation during Fe adsorption on cyanobacteria showed that adsorbed Fe was isotopically heavier than the growth medium by >0.70‰.[176, 265] Therefore, Fe adsorption might occur in L227 and affect the observed fractionation, but it is not the major process producing the observed isotope fractionation $\Delta^{56}Fe_{dis-part}$ in the epilimnion and metalimnion of L227.

Oxidative precipitation of Fe(III) oxyhydroxides and formation of Fe(II) minerals could account for DFe loss and PFe accumulation in the epilimnion and metalimnion of L227. Specifically, Fe(II) minerals could contribute to the particulate Fe(II) pool. However, the saturation index (SI) of potential Fe(II) minerals, mackinawite (FeS) and vivianite ($Fe_3(PO_4)_2$, indicated that these Fe(II) minerals were highly undersaturated in the epilimnion and metalimnion of L227 and thus unlikely to contribute to the particulate Fe(II) pool. Therefore, precipitation of inorganic Fe minerals is likely dominated by Fe oxyhydroxides and would contribute to the particulate Fe(III) pool. Fe(II) oxidation and subsequent precipitation of Fe oxyhydroxides are known to produce isotopically heavy Fe oxides and hydroxides. The Fe isotope fractionation arising from oxidation-precipitation is thought to be

a net isotope fractionation resulting from an equilibrium fractionation between aqueous Fe(II) and aqueous Fe(III) and a kinetic fractionation between Fe(III) oxides and aqueous Fe(III).[159] Experimental studies report that the equilibrium fractionation $\Delta^{56}Fe_{Fe(II)–Fe(III)}$ between aqueous Fe(II) and aqueous Fe(III) is −3.01 ‰ at 22 °C[165] and the equilibrium fractionation $\Delta^{56}Fe_{Fe(II)–ferrihydrite}$ between aqueous Fe(II) and ferrihydrite is up to −3.2‰ reflecting differences in Fe-O bonds.[166] Recent experimental studies on the fractionation between aqueous Fe(II) and Fe(III) minerals show that the $\Delta^{56}Fe_{Fe(II)–goethite}$ fractionation of up to −1.22‰[167] and the $\Delta^{56}Fe_{Fe(II)–hematite}$ fractionation of up to −3.14‰.[169] The sign of the Fe isotope fractionations during Fe(II) oxidation and subsequent precipitation is opposite to the observed $\Delta^{56}Fe_{dis–part}$ fractionation (1.02 ± 0.33‰) (Figure 3-6), indicating that observed $\Delta^{56}Fe_{dis–part}$ fractionation cannot be produced by oxidative precipitation of Fe(III) oxyhydroxides.

Hydraulic flushing via lake inflow and outflow can dilute Fe concentrations, decreasing DFe in the surface layer of lakes. However, this process is not the major process contributing to the observed changes in DFe in the oxic layers of L227 because no such trend was observed in the nearby reference L442 during lake stratification. In addition, considering water residence times of L227 and L442 (3-4 years),[266] seasonal variation in $\delta^{56}Fe$ of stream inflow is likely muted in the lake water column, consistent with the observation that no seasonal variation in $\delta^{56}Fe$ of DFe and PFe was observed in the oxic layers of nearby reference L442 during lake stratification.

For the first time, a drawdown of DFe and an increase in PFe during a cyanobacterial bloom in the freshwater system (Figure 3-5) are reported, possibly due to the uptake of DFe by cyanobacteria. This is also the first time that *in situ* Fe speciation of both DFe and PFe

associated with cyanobacteria is determined during the bloom in freshwater. The uptake of dissolved Fe(II) by cyanobacteria is potentially facilitated through porin-mediated Fe uptake and reductive Fe uptake. Furthermore, this is the first time that Fe isotopes were analyzed in conjunction with these key measurements. One important finding is that the particulate Fe(II) pool (60-90% of PFe pool) is comprised of intracellular Fe(II) and extracellular Fe(II), which are associated with living cells, organic debris and fecal pellets. The depletion and enrichment of Fe(II) in dissolved and particulate phases, respectively, together with the large Fe isotope fractionation between DFe and PFe ($\Delta^{56}Fe_{dis-part}$) (Figures 3-5 and 3-6) clearly show that uptake of dissolved Fe(II) by cyanobacteria plays a major role in regulating the Fe cycling in the oxic layers of L227 during the peak of the first bloom. The uptake of dissolved Fe(II) that is isotopically light by cyanobacteria during the bloom led to a conversion from DFe to PFe, a shift in the speciation of PFe from particulate Fe(III) to particulate Fe(II) and a diagnostic change in the $\delta^{56}Fe$ values of both DFe and PFe.

Large shifts in dissolved and particulate $\delta^{56}Fe$ in the oxic layers of L227 during the second bloom (Stage III)

Biological uptake during the second bloom continues to further modify Fe cycling and Fe isotopes, resulting in similar Fe speciation of DFe and PFe, similar DFe concentrations but lower PFe and TFe concentrations compared to those observed during the first bloom. The second bloom was co-dominated by diazotrophic cyanobacteria (ca. 60%; A. *schindlerii*) and chlorophytes (ca. 40%; *Dictyosphaerium pulchellum* and *Spondylosium planum*). In the oxic layers of L227, Chlorophyll *a* concentration during the second bloom (August 21, Stage III) was similar to chlorophyll *a* concentration during the first bloom, with a maximum value of 400 μg/L, while the phytoplankton biomass concentration during the

second bloom was lower than the concentration during the first bloom, with a maximum of 7.3 mg/L (Table 3-1 and Figure 3-4). Lower PFe and TFe concentrations during the second bloom compared to the first bloom reflect the decreased biogenic PFe due to the decreased concentration of phytoplankton biomass. Fe(III) and Fe(II) dominated dissolved and particulate phases, respectively, in the epilimnion and metalimnion of L227 during the second bloom (Figure 3-5). The similarity in Fe speciation during the first and second blooms suggests that chlorophytes in L227 mainly transport dissolved Fe(II) into cells, similar to the Fe -uptake mechanism of diazotrophic cyanobacteria. This interpretations are consistent with other studies, which have demonstrated that reductive Fe uptake (reduction of Fe(III) prior to transporting) is a common strategy amongst eukaryotic phytoplankton.[92, 335] Collectively, the results suggested that uptake of dissolved Fe(II) by cyanobacteria and chlorophytes, along with Fe adsorption, continually regulates Fe cycling in oxic layers of L227 during the second bloom in both the epilimnion and metalimnion.

In contrast to the similarity in Fe speciation of the two blooms, dissolved $\delta^{56}Fe$ and particulate $\delta^{56}Fe$ differed between the first and second blooms (Figure 3-6). The $\Delta^{56}Fe_{dis-part}$ between DFe and PFe in the epilimnion of L227 during the second bloom was 0.56 ± 0.05‰, smaller than $\Delta^{56}Fe_{dis-part}$ during the first bloom (1.02 ± 0.33‰) (Figure 3-6). The difference between $\Delta^{56}Fe_{dis-part}$ of the first bloom and second bloom suggests that the uptake of Fe by chlorophytes might produce distinct Fe isotope fractionation compared to diazotrophic cyanobacteria. Despite the fact that both cyanobacteria and chlorophytes in L227 likely utilized dissolved Fe(II), the specific Fe-uptake mechanisms in cyanobacteria and eukaryotic algae might be different.[336] Furthermore, as mentioned previously, diazotrophic cyanobacteria have a higher Fe requirement (>10-fold higher) than eukaryotic algae.[71, 72, 319]

A recent study on the uptake rate of cyanobacteria found that the surface-area-normalized uptake rate and metabolic Fe use efficiency in picocyanobacteria (*Synechococcus*) were lower than those in diatom (Thalassiosira), suggesting that eukaryotic algae have higher Fe uptake efficiency than cyanobacteria.[336] The different uptake kinetics between cyanobacteria and eukaryotic algae might lead to different Fe isotope fractionations during biological uptake. The change in dissolved δ^{56}Fe and particulate δ^{56}Fe during phytoplankton succession from cyanobacteria dominance to co-dominance of cyanobacteria and eukaryotic algae suggests that Fe isotope fractionation produced by cyanobacteria is distinct from that produced by eukaryotic algae, likely due to the differences in their uptake kinetics, the specific Fe-uptake mechanisms and associated enzymatic processes. However, it should be noted that the difference between $\Delta^{56}Fe_{dis-part}$ of the first bloom and $\Delta^{56}Fe_{dis-part}$ of the second bloom might also result from the different balance of Fe processes between these two blooms. Further experimental studies are necessary to measure the Fe isotope fractionation during biological uptake at different uptake rates for representative cyanobacteria and eukaryotic algae separately and constrain the isotope fractionation mechanism.

Dissolved and particulate δ^{56}Fe in the oxic layers of L227 during the post bloom (Stage IV)

During the post-bloom period, the bloom collapsed gradually. The phytoplankton biomass declined during the post bloom but values were still relatively high (5.4 ± 0.6 mg/L) (Table 3-1). The chlorophyll *a* concentration decreased during the post bloom, with a maximum value of 200 μg/L (Figure 3-4). Fe concentrations and speciation are similar to those measured during the bloom period, with some exceptions (Figure 3-5). Particulate Fe(III) was the dominant species in the particulate phase during the post bloom, as opposed

to the prevalence of particulate Fe(II) during the bloom period. The dominance of particulate Fe(III) during the post bloom suggests that uptake of dissolved Fe(II) by phytoplankton no longer dominated the Fe cycling during the decline of the bloom. The particulate Fe(III) pool during the post bloom was likely composed of Fe(III) oxyhydroxides and bioaggregates.[325] During the post bloom, dissolved $\delta^{56}Fe$ and particulate $\delta^{56}Fe$ in the epilimnion of L227 were identical, with $\Delta^{56}Fe_{dis-part}$ between DFe and PFe of 0.03 ± 0.05‰ (2σ) (Figure 3-6). Adsorption of isotopically heavier Fe on bioaggregates can make the PFe pool isotopically more positive, counterbalancing the isotopic effect induced by biological uptake.[183, 193, 264] Furthermore, the degradation of organic debris and fecal pellets could release intracellular Fe(II) into the water column. Oxidation of dissolved Fe(II) followed by precipitation can produce isotopically positive Fe(III) oxyhydroxides, counterbalancing the isotopic signals produced by biological uptake.[166] The dominance of particulate Fe(III), along with the identical $\delta^{56}Fe$ of DFe and PFe, likely reflects that release of Fe from decaying cells, Fe adsorption on bioaggregates and precipitation of Fe(III) oxyhydroxide dominated the Fe cycling during the post bloom, muting the expression of the enrichment of isotopically light PFe during the biological uptake.

3.3.2. Fe isotope fractionations between dissolved and particulate Fe near the redox boundary of L227 during the second bloom (Stage III) and the post bloom (Stage IV)

The $\delta^{56}Fe$ of DFe and PFe at the redox boundary could be modified by partial oxidation and subsequent precipitation of Fe oxyhydroxides (oxidation-precipitation). During the second bloom and the post bloom, the redox boundary was located at ~ 4 m in L227. The change in dissolved $\delta^{56}Fe$ between 6 m and 4 m during the second bloom and during the post

bloom (from −0.17‰ at 6 m to −1.20‰ at 4 m and from −0.18‰ to −0.90‰, respectively; Figure 3-6) is consistent with isotope variation of dissolved δ^{56}Fe observed in the redox transition zone of Lac Pavin (−0.31‰ to −2.14‰), where such variation is interpreted to result from partial oxidation of dissolved Fe(II) diffusing upward from the anoxic layer and subsequent precipitation of Fe oxyhydroxides.[200] Coupled to the shift in dissolved δ^{56}Fe is the decrease in DFe concentrations between 6 m and 4 m in L227, suggesting that the isotopically negative dissolved δ^{56}Fe at 4 m is likely produced by partial oxidation. However, it should be noted that, in L227, partial oxidation could only occur in the uppermost part of the anoxic hypolimnion (i.e., multiple millimeters or centimeters below the redox boundary). Given the abundant oxygen above the redox boundary and high concentrations of Fe oxidizers at the redox boundary,[211] partial oxidation is likely complete above the redox boundary in L227 with the result that there would be no isotopic fractionation. The lack of fractionation effects finds support in the observation that, in L227 before the bloom, dissolved δ^{56}Fe in the anoxic hypolimnion is similar to both dissolved and particulate δ^{56}Fe in the oxic metalimnion (Figure 3-6). During the second bloom and post bloom, the water column at 4 m is likely the uppermost part of the hypolimnion under microoxic conditions, where abiotic Fe oxidation competes with dissimilatory iron reduction, resulting in partial oxidation that makes dissolved Fe at 4 m isotopically negative. Thus the difference between the early part of the season (pre-bloom and first bloom) compared to the second bloom and post-bloom are due to the fact that the same discrete depths were sampled at each sampling date whereas the precise location of the redox boundary had shifted (Figure 3-6).

Oxidation of dissolved Fe(II) followed by precipitation can make the remaining dissolved Fe(II) highly isotopically negative when the extent of oxidation is high. During the

second bloom and the post bloom, the DFe concentration at 4 m was 10 times lower than that at 6 m, suggesting that approximately 90% of DFe was oxidized, under the assumption that there were no other Fe sources contributing to the DFe pool at 4 m. Additional potential sources contributing to the DFe pool at 4 m may include the flux of Fe from sediments at this depth and the decomposition of settling particulate Fe from the epilimnion,. The input of Fe from epilimnetic sediments, consisting of the escaped porewater Fe by diffusion and newly produced dissolved Fe by reductive dissolution at the sediment-water interface (SWI), was severely retarded, considering the oxygenated overlying water in the epilimnion. Oxygen can penetrate sediments to a depth of a few millimetres to a few centimeters.[205] Porewater Fe concentration in the topmost of the epilimnetic sediment core was extremely low (3 μM), reflecting that oxygen near the sediment-water interface (SWI) acts as a barrier to prevent the diffusion of porewater Fe(II) into the overlying water. The dissolved Fe produced by the reductive dissolution at the SWI is also likely to be immobilized to Fe oxyhydroxide in the presence of oxygen. Particulate Fe settling down from the epilimnion is most likely composed of cyanobacterial biomass considering the high concentrations of phycocyanin and chl-*a* at this depth (Figure 3-9). Although the decomposition of cyanobacterial biomass could release the Fe into the dissolved phase, the highly negative δ^{56}Fe values of dissolved Fe at 4 m and the dissimilarity between dissolved δ^{56}Fe at 4 m and particulate δ^{56}Fe at 1-3 m during the second bloom and the post bloom preclude the significant contribution of decomposition of cyanobacterial biomass to the DFe pool at 4m. Collectively, this evidence suggests that dissolved Fe pool at 4 m during the second bloom and post bloom is mainly controlled by partial oxidation of dissolved Fe(II) diffusing from the anoxic hypolimnion. It should be noticed that, during the second bloom, the uptake of dissolved Fe(II) by phytoplankton

during the post bloom might also modify DFe and PFe. However, this process is unlikely to be the dominant process considering the dissimilarity in dissolved $\delta^{56}Fe$ at 4 m and 3 m, and the more negative dissolved $\delta^{56}Fe$ at 4 m compared to particulate $\delta^{56}Fe$ at 4 m.

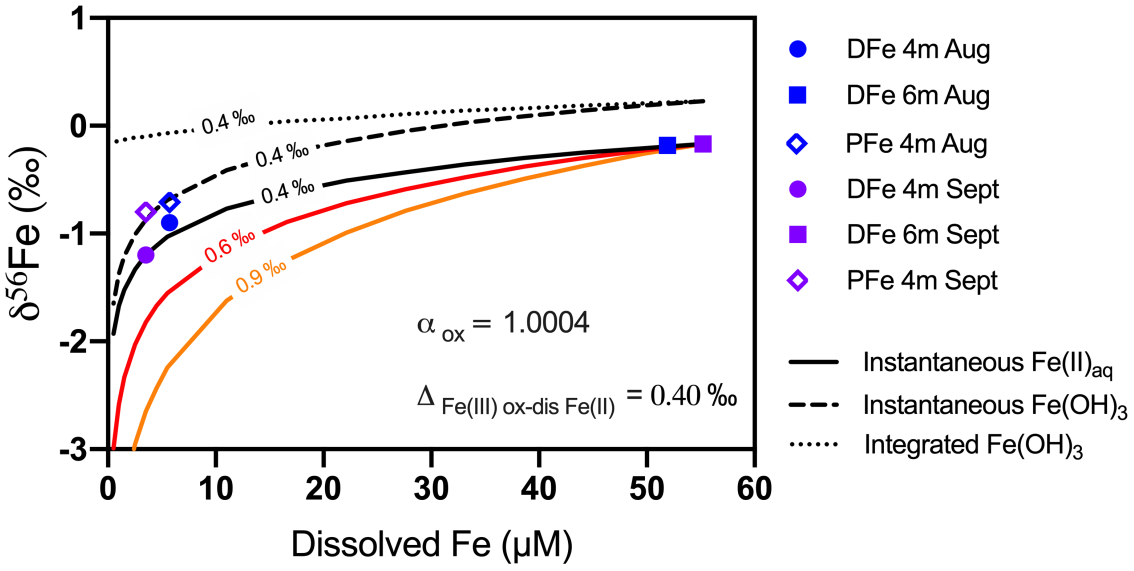


Figure 3-7 The effect of oxidation-precipitation on dissolved Fe concentration and dissolved $\delta^{56}Fe$.
Black curves shown here are the best-fit Rayleigh curves to observed data at 4m and 6m of L227 during the second bloom and the post bloom, with $\alpha_{ox} = 1.0004$ (i.e. $\Delta^{56}Fe_{Fe(III)\ ox-dis\ Fe(II)} = 0.40‰$). Red curve and orange curve are the Rayleigh curves with α_{ox} inferred from other lake studies. Model presented here is a closed system Rayleigh fractionation model using the following equations: $\delta^{56}Fe_{dissolved} = \delta^{56}Fe_{initial} + 1000 \times (\alpha_{ox} - 1) \times \ln f$; $\delta^{56}Fe_{particulate,\ instantaneous} = \delta^{56}Fe_{dissolved} + 1000 \times (\alpha_{ox} - 1)$; $\delta^{56}Fe_{particulate,\ integrated} = \delta^{56}Fe_{dissolved} - \ln(f)/(1-f) \times 1000 \times (\alpha_{ox} - 1)$.

A closed system Rayleigh fractionation model was used to fit the observed data and estimate the fractionation factor (α) between Fe(III) oxyhydroxides and dissolved Fe(II) during oxidation-precipitation. The fraction factor (α) associated with the best-fit curve is 1.004 (i.e. $\Delta^{56}Fe_{Fe(III)\ ox-dis\ Fe(II)} = 0.40‰$, Figure 3-7), compatible but smaller than the fractionation factors of oxidation-precipitation deduced in Lac Pavin and Lake Cadagno (1.009 and 1.006, respectively).[204, 337] It should be noted that the fractionation factor deduced

by the Rayleigh fractionation model might be subject to substantial uncertainty due to the limited number of observed data (N=4). The slight offset of dissolved $\delta^{56}Fe$ at 4 m during the second bloom is possibly due to the modification by the uptake of Fe by phytoplankton. The$\Delta^{56}Fe_{dis-part}$ fractionation (0.40‰) observed at 4 m during the post bloom likely reflects a net fractionation arising from oxidation-precipitation, whereas the observed $\Delta^{56}Fe_{dis-part}$ fractionation (0.19‰) at 4 m during the second bloom is much smaller, implying that dissolved $\delta^{56}Fe$ and particulate $\delta^{56}Fe$ result from a combination of oxidation-precipitation and biological uptake during the second bloom (Figures 3-6 and 3-7).

3.3.3. Effect of phytoplankton blooms on settling flux of particulate Fe in L227

Phytoplankton blooms affect the settling flux of particulate Fe. In the water column, large particulates, a mixture of allochthonous and autochthonous particles, are constantly lost to underlying sediments through sinking. The sinking rates of particulates depend on many factors, including physico-chemical parameters of the water column, particle aggregation and disaggregation, and interaction with the microbial community.[325] Before the bloom, PFe is likely dominated by aggregates of Fe with DOM and some degree of precipitated Fe(III) oxyhydroxides, considering the high DOC concentration (Figure 3-2). During the blooms, PFe is dominated by Fe associated with cyanobacterial biomass, occurring as intracellular Fe and extracellular Fe adsorbed on organic debris.

The settling flux of particulate Fe is facilitated during the early development of the cyanobacterial bloom. TFe concentration decreased from May 15 (before the bloom) to June 26 (during the peak of the first bloom) in the oxic layers of L227 as opposed to L442, where TFe concentration increased during this period (Figure 3-5), suggesting that a significant net

settling flux of particulate Fe occurred after the onset of the cyanobacterial bloom in L227. Furthermore, the sinking rates of particulates during the early development of the cyanobacterial bloom (June 2-15) was 0.9 g m^{-2} d^{-1}, which is two times higher than the rate during the subsequent bloom period (June 28-August 9),[338] suggesting that this significant settling flux of particulate Fe occurred during early development of bloom rather than the entire bloom period. The isotopic composition of total Fe (TFe) can be calculated from the following mass balance equation (Figure 3-8):

$$\delta^{56}Fe_{TFe} = \delta^{56}Fe_{DFe} \times X_{DFe} + \delta^{56}Fe_{PFe} \times X_{PFe}$$

Where X_{DFe} and X_{PFe} represent the mole fractions of DFe and PFe, respectively. In contrast to the decrease in TFe concentration, $\delta^{56}Fe_{TFe}$ in the oxic layers of L227 remained constant from pre-bloom (May 15) to the peak of the first bloom (June 26), suggesting that the significant settling flux of particulate Fe during the early development of the cyanobacterial bloom did not affect the $\delta^{56}Fe_{TFe}$ values(Figure 3-8). Several explanations can account for this lack of change in $\delta^{56}Fe_{TFe}$ between pre-bloom and the peak of the first bloom period. The settling particulate Fe during the early development of the cyanobacterial bloom might primarily consist of aggregates of Fe-DOM, which are not isotopically fractionated upon precipitation. Additionally, the settling particulate Fe could be composed of isotopically light biomass Fe, but the adsorption of Fe on the cyanobacterial biomass may suppress the expression of isotopically light biomass Fe. An alternative explanation is that terrestrial input may counterbalance the effect of settling particulate Fe, contributing to the constant $\delta^{56}Fe_{TFe}$ in the oxic layers of L227. The observation that TFe concentration decreased and $\delta^{56}Fe_{TFe}$ remained constant in the oxic layers of L227 (Figures 3-5 and 3-8) suggests that, during the early development of the cyanobacterial bloom, there is some combination of processes to

counteract the fractionation arising from biological uptake of Fe, suppressing the effect of settling particulate Fe on the $\delta^{56}Fe_{TFe}$ in the oxic layers.

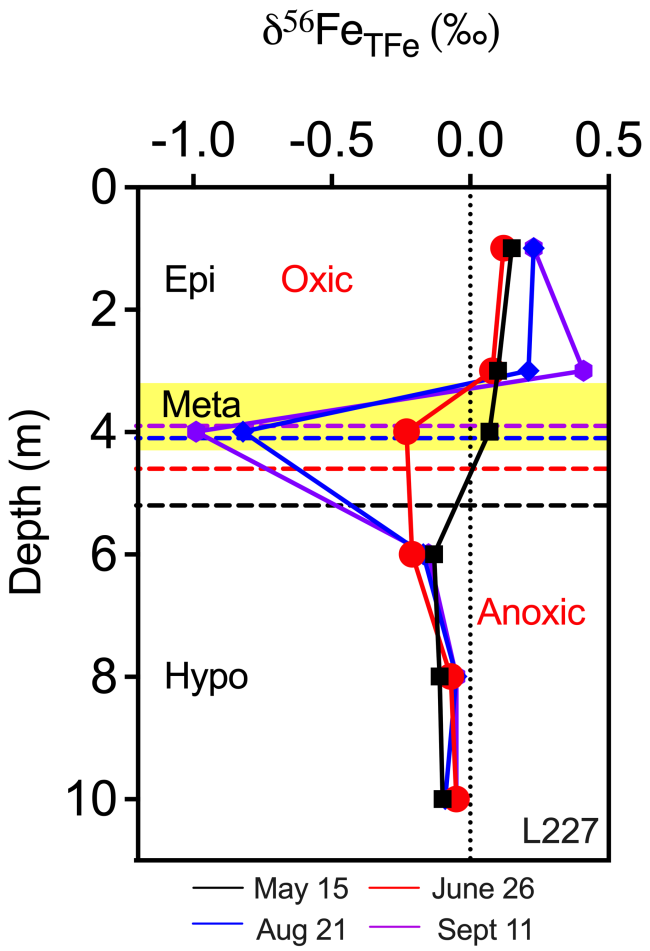


Figure 3-8 Iron isotope compositions of total Fe ($\delta^{56}Fe_{TFe}$) in the water column of L227. Yellow bars indicate approximate depth of metalimnion. The thickness and depth of metalimnion may vary seasonally due to the changing climate. Horizontal dotted lanes represent the depth of 0.1 mg/L dissolved oxygen (redox boundaries) at the time of sampling.

Despite being limited, the settling flux of particulate Fe during two blooms affects $\delta^{56}Fe_{TFe}$ in the oxic layers of L227. Lower PFe and TFe concentrations, along with lower biomass concentrations, during the second bloom compared to the peak of the first bloom suggest a considerable removal of Fe by settling biomass in the oxic layers of L227 (Figure

3-5 and Table 3-1). Furthermore, in the oxic layers, $\delta^{56}Fe_{TFe}$ during the second bloom is 0.1‰ more positive than $\delta^{56}Fe_{TFe}$ during the first bloom, indicating that isotopically light biomass Fe sinks to sediments, leaving remaining DFe isotopically more positive (Figure 3-8). However, the difference is relatively small considering the fractionation $\Delta^{56}Fe_{dis-part}$ of 0.56 ± 0.05‰ during the second bloom (Figure 3-6). The sinking rates of particulates during the first and second blooms are 0.5 g m^{-2} d^{-1}, much lower than those during the early stage, as described previously.[338] It is likely that while certain PFe particles sink to the underlying sediment, causing a shift in $\delta^{56}Fe_{TFe}$, a significant portion of PFe is either intercellular Fe retained in phytoplankton cells or bioaggregate Fe associated with organic debris, avoiding sinking out of the water column. Under Fe limited conditions, most PFe is recycled *in situ* through multiple biogeochemical processes (e.g., biological uptake vs. degradation of organic debris and fecal pellets, and biologically mediated dissolution vs. precipitation of bioaggregates)[325] during the blooms. The speculation is consistent with previous studies where the residence time of biogenic PFe during subtropical phytoplankton bloom in the ocean was >10-fold longer than lithogenic PFe, suggesting that biological uptake by phytoplankton strongly retains PFe in the water column.[324, 339, 340]

When the bloom begins to collapse, a settling flux of biomass to profundal sediment resulting from the coagulation/loss of biogenic particles (e.g., organic debris) is expected. In L227, the sinking particulate flux during the post-bloom (3.1 g m^{-2} d^{-1}) is six times higher than that during the blooms,[338, 341] suggesting that settling flux of particulate Fe may have a greater effect on $\delta^{56}Fe_{TFe}$. Indeed, the $\delta^{56}Fe_{TFe}$ in the epilimnion of L227 during the post bloom was more isotopically positive than $\delta^{56}Fe_{TFe}$ in the epilimnion during other periods (before the bloom, during two blooms), suggesting that isotopically light particulate Fe(II)

associated with biomass sinks to profundal sediment during the decline of the bloom, leaving the remaining TFe pool of the epilimnion more isotopically positive (Figure 3-8).

3.3.4. Migration of cyanobacteria for the uptake of dissolved Fe(II) during the peak of the first bloom

The vertical changes in Fe species, TFe and $\delta^{56}Fe_{TFe}$ together allow us to identify Fe sources and distribution among different pools associated with processes. Before the bloom (stage I), $\delta^{56}Fe_{TFe}$ in the epilimnion (1 and 3 m) and metalimnion (4 m) of L227 decreases slightly with depth from 0.15‰ to 0.07‰ and the average $\delta^{56}Fe_{TFe}$ is 0.11 ± 0.07‰ (2σ) (Figure 3-8). During the peak of the first bloom (stage II), $\delta^{56}Fe_{TFe}$ in the epilimnion (1 and 3 m) is 0.10 ± 0.06‰, similar to the average $\delta^{56}Fe_{TFe}$ in pre-bloom (stage I). However, $\delta^{56}Fe_{TFe}$ in the metalimnion (4 m) is −0.24‰, more isotopically negative than $\delta^{56}Fe_{TFe}$ in the epilimnion. TFe concentrationd increase with depth from 1 m to 4 m, suggesting that the more negative values of $\delta^{56}Fe_{TFe}$ observed in the metalimnion (4 m) during the peak of the first bloom (stage II) result from the contribution of an additional source of isotopically light Fe rather than the loss of isotopically heavy Fe at 4 m. Furthermore, contrasting with relatively constant dissolved $\delta^{56}Fe$ values in the epilimnion and metalimnion (0.91 ± 0.05‰, 2σ), particulate $\delta^{56}Fe$ in the metalimnion is more negative by 0.4 ‰ than particulate $\delta^{56}Fe$ in the epilimnion, resulting in considerably larger $\Delta^{56}Fe_{dis-part}$ fractionations of 1.25‰ in the metalimnion compared to the value in the epilimnion (0.91 ± 0.05‰, 2σ) (Figure 3-6). Particulate Fe increases in the metalimnion (4 m), predominantly in the form of Fe(II), while dissolved Fe remains relatively constant between 3 m and 4 m, and is only present in the form of Fe(III). These observations further suggest that this isotopically light Fe source

mainly contributes to the PFe pool rather than DFe in the metalimnion (4 m). Two potential Fe sources could contribute to the PFe pool in the metalimnion (4 m): (1) the oxidation of dissolved Fe(II) diffusing from the anoxic layer and subsequent precipitation of Fe oxyhydroxides above the redox boundary and (2) vertical migration of cyanobacteria for the uptake of dissolved Fe(II). The possibility of oxidation is ruled out since the concentrations of particulate Fe(III) at 3 and 4 m were similar, and the concentration of particulate Fe(III) at 3 m decreases during the bloom period compared to the pre-bloom period (Figure 3-5). In addition, considering that this depth is above the redox boundary during the peak of the first bloom, the oxidation of dissolved Fe(II) is likely complete at 4 m, producing no fractionation between dissolved Fe and particulate Fe. Therefore, the oxidation of dissolved Fe(II) cannot contribute to the isotopically light particulate Fe at 4 m during the peak of the first bloom.

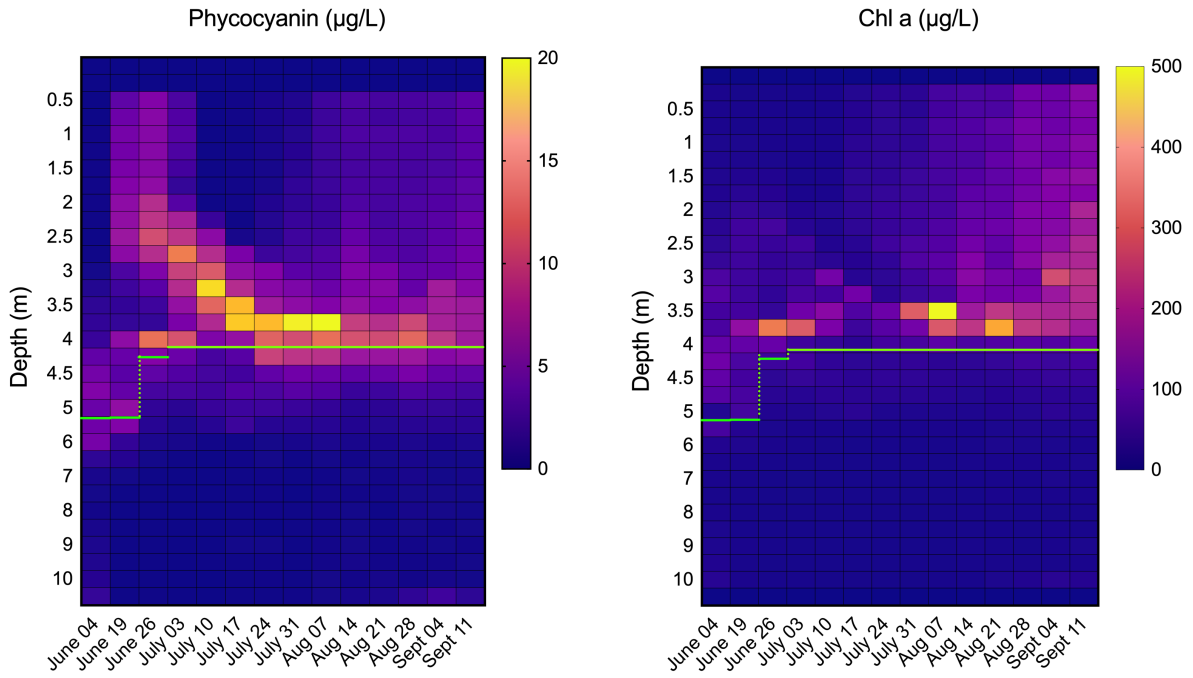


Figure 3-9 Weekly concentration profiles of phycocyanin and chlorophyll *a* in the water column of L227 during ice-free season of 2018.
Phycocyanin is a marker pigment for cyanobacteria. Chlorophyll a is a proxy for phytoplankton. The green solid line indicates depth of 0.1 mg/L dissolved oxygen (redox boundary).

Cyanobacteria can migrate vertically for optimal growth from the nutrient-exhausted epilimnion to epilimnetic sediments, metalimnion or hypolimnion, locations where nutrients have higher concentrations in stratified lakes. The concentration of phycocyanin, a pigment contained in freshwater cyanobacteria for harvesting sunlight for photosynthesis, [342, 343] is shown in Figure 3-9 as a marker for cyanobacterial biomass. An important observation is that particulate Fe(II) (biogenic Fe(II) including intracellular and extracellular Fe(II)) at 4 m was 2 times higher than those at 3 m even though the concentrations of phycocyanin (as well as cyanobacteria cell density) at 3 and 4 m were almost the same (Figures 3-5 and 3-9; Table 3-1). The Fe adsorption unlikely contributed to particulate Fe(II) elevation at 4 m because DFe concentrations, DOC concentration, the cyanobacteria cell densities and other water column chemistry (e.g., pH, T) at 3 and 4 m remained relatively constant (Figures 3-2 and 3-5 and Table 3-1). Therefore, individual cyanobacteria cells at 4 m had higher intracellular Fe content than cells at 3 m, possibly due to different Fe limitations during Fe acquisition. It is important to note that the dominant cyanobacterial species at 3 m and 4 m arre the same (*Aphanizomenon skujae*), precluding the possibility of contributions from different species. One recent experimental study on the effect of Fe limitation on the uptake by cyanobacteria has shown that Fe-limited cyanobacteria cells have lower Fe content than Fe-replete cells.[344] Cyanobacteria at 4 m can upregulate Fe acquisition to alleviate Fe-limited conditions and facilitate dissolved Fe(II) uptake compared to cyanobacteria at 3 m. There are two potential strategies for the upregulation of Fe acquisitions: (1) increasing the rate of *in situ* Fe uptake by resident cyanobacteria and (2) use of alternative Fe sources via vertical migration. Cyanobacteria have been shown to increase the uptake rate to meet the Fe requirement under

Fe-limited conditions.[345, 346] If this is the case, the enhanced rate of Fe uptake at 4 m should cause more depletion of DFe at 4 m compared to DFe at 3 m. However, DFe concentration remained relatively constant with depths in the oxic layers of L227 during the bloom and dissolved Fe(II), the required form of Fe for cyanobacteria, is below the detection limit, suggesting that *in situ* enhanced Fe uptake unlikely contributed to the elevated intracellular Fe content in the metalimnion of L227 (Figure 3-5). Given the isotopically lighter PFe pool and total Fe pool, larger $\Delta^{56}Fe_{dis-part}$ fractionation and elevated intracellular Fe content in the metalimnion (4 m) compared to epilimnion (Figures 3-5, 3-6 and 3-8), it is postulated that cyanobacteria at 4 m could potentially further migrate to the top of the anoxic zone to take up abundant dissolved Fe(II) and then rise through buoyancy regulation.

A simple isotopic mass balance modeling can be used to explore the effect of vertical migration of cyanobacteria on the Fe isotope composition of PFe in the metalimnion of L227 and identify the potential depth in the hypolimnion where cyanobacteria migrate to uptake Fe. The particulate $\delta^{56}Fe$ at 4 m is the net isotopic composition of migrating cyanobacteria and non-migrating cyanobacteria, using the following mass balance equation:

$$\delta^{56}Fe_{PFe\ 4m} = \delta^{56}Fe_{\ PFe\ migration} \times X_{PFe\ migration} + \delta^{56}Fe_{\ PFe\ non\text{-}migration} \times X_{PFe\ non\text{-}migration}$$

where $X_{PFe\ migration}$ and $X_{PFe\ non\text{-}migration}$ represent the mole fractions of intracellular Fe in migrating cyanobacteria and non-migrating cyanobacteria at 4 m, respectively; $\delta^{56}Fe_{PFe\ migration}$ and $\delta^{56}Fe_{PFe\ non\text{-}migration}$ are the Fe isotope compositions of non-migrating cyanobacteria and migrating cyanobacteria particles at 4 m, respectively. For simplicity, all PFe in the epilimnion and metalimnion is assumed to be intracellular Fe. This assumption excludes the effect of adsorbed Fe, and abiotic Fe precipitates on the Fe isotope composition of PFe in the oxic layers of L227 (See Appendix A for justification).

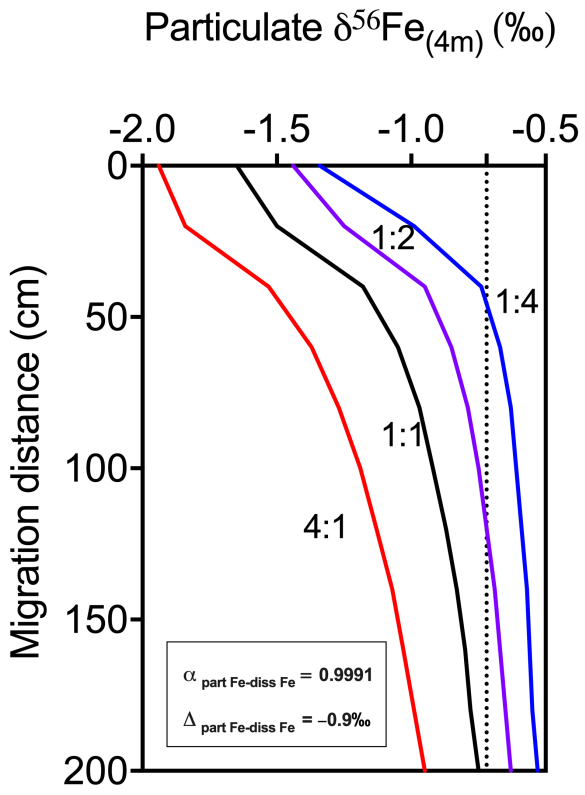


Figure 3-10 Modelling of integrated intracellular particulate $\delta^{56}Fe$ at 4m contributed from non-migrating cyanobacteria and migrating cyanobacteria.
The y-axis is traveling distance between the original depth (4 m) and the depth where cyanobacteria migrate to utilize Fe. We assume that migrating cyanobacteria return to 4 m after the uptake. Different model curves were computed using different ratios of *in situ* intracellular Fe to migrating intracellular Fe at 4 m, indicated by the values beside each curve. The vertical dashed line is the observed particulate $\delta^{56}Fe$ (−0.72 ‰) at 4m. See Appendix A for model details.

The calculated particulate $\delta^{56}Fe$ at 4 m, contributed from both non-migrating and migrating cyanobacteria, ranges from −0.54 ‰ to −1.96 ‰, depending on the specific depth where cyanobacteria migrate to utilize Fe and the relative proportion of non-migrating and migrating cyanobacteria at 4 m (Figure 3-10). DFe concentration and dissolved $\delta^{56}Fe$ in the upper anoxic zone of hypolimnion (i.e., multiple centimeters below redox boundary) are likely modified by partial oxidation, as suggested by the profiles of Fe concentration and Fe isotope compositions during the post bloom (Sept 2018; Figures 3-5 and 3-6). Therefore, the

uptake of Fe in this upper anoxic zone tends to produce more negative particulate δ^{56}Fe. The observed particulate δ^{56}Fe at 4 m is −0.72‰ (Figure 3-6), within the range of calculated particulate δ^{56}Fe. Although the specific depth where cyanobacteria migrated to utilize Fe during the peak of the first bloom cannot be identified due to the unknown relative proportion of non-migrating and migrating cyanobacteria at 4 m, the modeling results suggested that a smaller proportion of migrating cyanobacteria at 4 m would require cyanobacteria to have migrated to deeper depths to produce the observed particulate δ^{56}Fe at 4 m (−0.72‰) (Figure 3-10). Assuming that the excess of PFe at 4 m compared to 3 m comes from migrating cyanobacteria, the ratio of non-migrating to migrating cyanobacteria at 4 m is around 1:1 (Figure 3-5). With this assumption, the modeling results suggest that cyanobacteria may migrate down to 6 m for the uptake of Fe (Figure 3-10). Depending on the proportion of migrating cyanobacteria and how far cyanobacteria can migrate downward in anoxic water column, the Fe isotope composition of particulate Fe in the metalimnion would yield a range of values that are likely more negative than particulate δ^{56}Fe in the epilimnion (Figure 3-10). Distinct particulate δ^{56}Fe in the epilimnion and metalimnion of L227 can be used to probe the source of Fe used by cyanobacteria if the isotope fractionation factor of uptake can be measured under controlled laboratory conditions and the dependence on the Fe concentration is known.

δ^{56}Fe of DFe and PFe, along with Fe speciation, was used to track the vertical migration of cyanobacteria. The results presented in this study clearly demonstrate that isotopically light PFe and total Fe measured in the metalimnion during the peak of the first bloom are best explained by the migration of cyanobacteria below the redox boundary for the uptake of dissolved Fe(II).

3.4. Conclusion

Phytoplankton blooms alter the cycling of Fe and the Fe isotope signatures in the oxic epilimnion and metalimnion of L227. The cycling of Fe before the bloom is likely modified by a combination of multiple processes, including the complexation of DFe with DOM, precipitation of Fe(III), photochemical reduction of particulate Fe(III), photolysis and microbial decomposition of organic Fe complexes, resulting in the prevalence of Fe(II) in dissolved Fe, the dominance of Fe(III) in particulate Fe and a relatively small positive fractionation $\Delta^{56}Fe_{dis\text{-}part}$ between dissolved and particulate Fe. The onset of cyanobacteria bloom leads to a conversion from DFe to PFe, a shift in Fe speciation from dissolved Fe(II) to particulate Fe(II) and an increase in the magnitude of the $\Delta^{56}Fe_{dis\text{-}part}$ fractionation. This is the first time that changes in Fe concentration, Fe speciation and conjunction Fe isotope compositions associated with the progression of phytoplankton blooms are reported in a freshwater system. The most plausible explanation for the depletion of dissolved Fe(II), the enrichment of particulate Fe(II) and the more negative $\delta^{56}Fe$ values of particulate Fe compared to dissolved Fe is the uptake of isotopically light dissolved Fe(II) by cyanobacteria. This is the first time that the uptake of dissolved Fe(II) by cyanobacteria has been proposed in natural environments, which was previously confirmed only in experimental studies. The similar Fe speciation, Fe concentrations, but distinct $\Delta^{56}Fe_{dis\text{-}part}$ fractionation between the first bloom and second bloom indicate that while both cyanobacteria and chlorophytes utilize the dissolved Fe(II), they might produce distinct Fe isotope fractionation, likely due to differences in uptake kinetics. During the first bloom, a larger $\Delta^{56}Fe_{dis\text{-}part}$ fractionation in the metalimnion compared to that in the epilimnion is most

plausibly explained by the migration of metalimnetic cyanobacteria below the redox boundary for Fe acquisition.

Chapter 4

Fe isotopes track microbial Fe cycling in the water column and sediments of Boreal Shield lakes

4.1. Introduction

Biogeochemical cycling of Fe plays diverse and essential roles in freshwater environments. Fe redox transformations are tightly coupled to other biogeochemical cycles such as C, N, O and S[347, 348] and can influence the fate and biological availability of many nutrients (e.g., P) and contaminants (e.g., As and Cd) by changing the mobility of these substances.[9, 10, 349]

Fe redox transformations can be mediated by both iron-reducing and iron-oxidizing bacteria, especially in redox transition and anoxic zones,[28, 32, 33] but abiotic reactions are also important. Dissimilatory iron-reducing bacteria (DIRB) can combine the oxidation of H_2 or organic matter (OM) with the reduction of Fe(III) oxyhydroxides and use the energy produced during this process to maintain cellular activities.[52] Conversely, photoferrotrophs can oxidize Fe(II) and use light energy to fix bicarbonate into organic carbon.[40] Microaerophilic iron-oxidizing bacteria can harvest energy from chemical reactions when utilizing Fe(II) as an electron donor and a trace level of O_2 as an electron acceptor.[34] Similarly, nitrate-reducing iron-oxidizing bacteria can couple the oxidation of Fe(II) with the reduction of nitrate in the presence of organic co-substrate.[44] Finally, oxidation of Fe(II) in oxic waters is relatively fast in the pH range of most freshwater aquatic environments.

Fe cycling plays a crucial role in regulating microbial and chemical evolution of the ocean throughout Earth's history.[94, 148] The chemistry of the Archaean ocean (3.8-2.5 billion years ago, Ga) is commonly thought to have been anoxic and ferruginous, with abundant

dissolved Fe(II) and exceptionally low concentrations of sulfate.[93, 94, 138] It is generally agreed that the Great Oxidation Event (GOE) occurred between 2.4 and 2.2 Ga, transferring the atmosphere from almost no oxygen to oxygenated.[97, 350] Banded iron formations (BIFs) are layered chemical sedimentary rocks that contain Fe oxide, Fe carbonate and Fe silicate minerals. The deposition of BIF extends over a long geologic time (3.8 to 0.55 Ga), with the majority of BIF in the Archean and early Paleoproterozoic successions, where the ocean was under anoxic and ferruginous conditions.[119, 161] It is generally accepted that there are four Fe oxidation mechanisms involved in the deposition of BIF in anoxic and ferruginous seawater: (1) biotic (microaerophilic iron oxidation) or abiotic oxidation by O_2 that is produced by oxygenic photosynthesis, (2) abiotic photo-oxidation by UV, (3) photoferrotrophy, and (4) nitrate-dependent Fe oxidation. Although there is still debate about the relative contribution of these proposed mechanisms, many studies suggest that photoferrotrophy may have played a paramount role in the deposition of BIF in anoxic and ferruginous Archaean oceans.[143, 144, 146, 148]

Fe isotopes can help to elucidate biogeochemical Fe processes in a variety of environments, including marine, soils, riverine and groundwater settings.[159] Large variations in the Fe isotope composition of BIF are also reported in many studies and used to infer the unique Fe cycling in early Earth. In contrast, there is limited Fe isotope work on lake systems. Most of them are carried out in low sulfate meromictic lakes, which are commonly considered to be scarce globally.[200-205] This study presents the seasonal variations in Fe isotope fractionation between dissolved Fe and particulate Fe in the anoxic hypolimnia of four Boreal Shield lakes and the Fe isotope compositions of porewater Fe and bulk sediment Fe in sediment cores collected from the bottom of three lakes. This study aims to (1) use Fe

isotopes and associated Fe isotope fractionations to determine the contribution of biogeochemical Fe processes to Fe cycling in the anoxic water column and investigate the occurrence of microbial Fe oxidation, especially photoferrotrophy, in this zone; (2) evaluate predominant processes responsible for sediment Fe release; (3) use Fe isotope data to constrain diagenetic processes in sediments; (4) estimate the role of sediment in supplying Fe to the overlying hypolimnetic water column.

4.2. Methods

4.2.1. Study site

Lake 221 (L221), Lake 227 (L227), Lake 304 (L304) and Lake 442 (L442) are small boreal headwater lakes located in the IISD Experimental Lakes Area (IISD-ELA) in northwestern Ontario, Canada (Figure 4-1).[238, 299] L221, L304 and L442 are oligotrophic lakes, while L227 is an experimentally eutrophic lake. The morphometric characteristics of each lake are presented in Table 4-1. While L221 and L442 have both an inflow stream and an outlet, L227 and L304 have only outflows that typically cease in late spring (Figure 4-1). There was no significant groundwater recharge or discharge due to the underlying impermeable Precambrian granodiorite.[238] Whole-lake experiments were manipulated in some ELA lakes over the last 40 years. L221 had a biomanipulation experiment by introducing piscivores in 1987 to study the effect of top predators on water chemistry and phytoplankton. However, no nutrients or other substances have been added to the lake.[351] Since 1969, L227 has been subject to ongoing whole lake experimental eutrophication through nutrient additions (N and P or only P), resulting in annual summer phytoplankton blooms.[207] L304 was fertilized (N, P and C) from 1971-1976 for the experimental study of

lake eutrophication and acidification, and the lake recovered rapidly after nutrient addition was stopped.[352, 353] Oligotrophic L442 has not been manipulated in any way.

Table 4-1 Morphological characteristics and trophic state of ELA lakes

Lake	Surface area (ha)	Mean depth (m)	Max depth (m)	Trophic state	Hydrological flow
L221	9.0	2.1	5.7	oligotrophic	one inflow stream; one outflow stream
L227	5.0	4.4	10.0	eutrophic	no inflow stream; one outflow ceases in late spring
L304	3.6	3.2	6.7	oligotrophic	no inflow stream; one outflow stream
L442	16.0	9.0	17.8	oligotrophic	one inflow stream and one outflow stream

L221, L227, L304 and L442 are small dimictic lakes that undergo turnover in spring and fall. Typically beginning in early to mid-May, dimictic lakes in ELA develop two distinct layers until late September-late October: an upper well-mixed epilimnion and a deeper hypolimnion, separated by a thermocline known as metalimnion. The boundaries of epilimnion and hypolimnion in this chapter follow the IISD-ELA procedure, whereby the bottom of the epilimnion is defined as the depth at which the water temperature changes by more than 1°C/m and the bottom of the metalimnion is determined at the depth where 1% surface photosynthetically active radiation (PAR) is attained. These four small dimictic headwater lakes are ideal modern natural laboratories to study internal Fe cycling associated with microbial metabolic processes of boreal lakes underlain by Precambrian Shield geology.

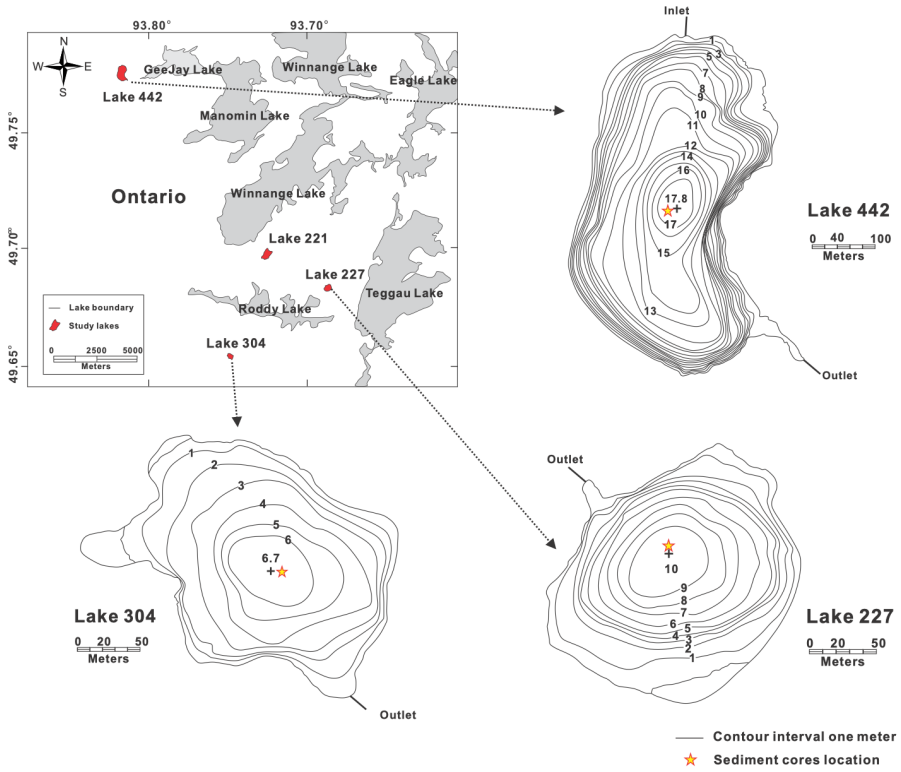


Figure 4-1 Location of the study lakes in the Sustainable Development - Experimental Lake Area (IISD-ELA) and the bathymetry of Lake 227, L304 and L442.
Yellow stars indicate the locations of sediment cores.

4.2.2. Water sample collection

Water samples were collected during summer stratification in 2018. Sampling in L227 occurred on May 15, June 26, August 21 and September 11 and on June 2, July 5 and September 8 in L442. Sampling in L221 and L304 occurred on July 30 and 26, respectively. Water sample collection was previously described in Chapter 3. In brief, physicochemical profiles and light profiles were collected *in situ* using a multi-parameter YSI EXO2 sonde (YSI Inc., Yellow Springs, OH) and a LI-192 underwater quantum sensor connected with a LI-250 light meter (LI-COR Biosciences, Lincoln, NE), respectively. Water samples were taken from various depths at the centre of the lakes. Unfiltered water samples were collected for dissolved inorganic carbon (DIC) and methane (CH_4). Filtered water samples were

obtained through an inline filter (0.45 μm membrane filter; Advantec, Dublin, CA) for dissolved organic carbon (DOC), total dissolved nitrogen (TDN) and total dissolved phosphorus (TDP), sulfate (SO_4^{2-}), dissolved total sulfide (ΣS^{2-}), ammonium (NH_4^+) and dissolved Fe (DFe). The inline 0.45 μm membrane filters were collected for particulate Fe (PFe). Particular attention was given to avoiding artificial oxidation during the collection of dissolved Fe and particulate Fe samples. Particulate organic matter (POM) was collected on Whatman QM-A filters (Sigma-Aldrich, St. Louis, MI) for particulate organic nitrogen (PON), particulate organic carbon (POC) and suspended particulate phosphorus (SPP). Sterivex filters (0.22 μm polyvinylidene fluoride filters) were also collected for microbial community analysis.

4.2.3. Sediment cores and porewater collection

Lake sediment cores were collected from two sampling campaigns. Two sediment cores were collected by a freeze corer from the deepest depth of L227 and L442 (10.6 m and 17.8 m, respectively) during the ice cover period in March 2018 following a modified procedure (Figure 4-1).[239] The L227 sediment core was then sectioned while frozen into 0.5 cm (to a depth of 3cm) or 1 cm slices (after the depth of 3 cm) using a band saw. The L442 sediment core was sectioned into 1 cm slices. The sectioned sediment samples were sealed in Whirl-Pak bags and frozen until analysis. Porewater samples were obtained by centrifugation (5000 rpm, 20 mins) and filtration (0.2 μm syringe filter; Whatman) under anoxic conditions. The porewater samples were immediately acidified with trace-metal grade HCl (degassed with N_2) in an anaerobic chamber. The sediment samples were freeze-dried and stored under anoxic conditions until analysis. During the second campaign in July 2018, one sediment core was collected by gravity corers at the deepest depth of L304 (6.3m) (Figure 4-1). One

sediment core collected by the Uwitec corer was dedicated to porewater sampling, and another was collected by the NLA corer for sediment samples. The porewater samples were obtained by Rhizon samplers (Rhizosphere RP, Wageningen, Netherlands) on shore immediately after collection to avoid any disturbances. An aliquot (1 mL) of porewater was collected directly into HDPE bottles pre-filled with zinc acetate for sulfide measurement. The rest of the porewater was collected in vacuum glass serum bottles capped with blue butyl rubber stoppers. The vacuum glass serum glass bottles were pre-acidified with degassed trace-metal grade HCl prior to sampling to preserve porewater in 0.5M HCl. The sediment cores collected by NLA corer were transferred into the glove bag under 100% N_2 condition within two hours after collection. It was sectioned into 0.5 cm scale fractions to a depth of 3 cm and then at 1 cm interval after the depth of 3 cm in the glove bag. Porewater samples for sulfide measurement were frozen prior to analysis. Porewater samples for Fe measurement were stored at 4 °C until analysis. The sediment samples were sealed in Whirl-Pak bags and frozen until freeze-drying.

4.2.4. Chemical analysis

Chemical analysis procedures for water column samples were previously described in Chapter 3. Importantly, particulate Fe on the 0.45 μm filters was dissolved in 6M HCl and preserved in 0.5 M HCl under anoxic conditions. Fe concentrations (Fe(II) and Fe(III)) for dissolved Fe, particulate Fe and porewater Fe samples were determined spectrophotometrically using the ferrozine method (detection limit: 0.5 μM).[240] Dissolved total sulfide (ΣS^{2-}) concentrations for water samples and porewater samples were measured spectrophotometrically by the methylene blue method (detection limit: 0.25 μM).[300]

Sediment samples were digested using an acid digestion protocol.[354, 355] Briefly, 100 mg of freeze-dried sediment was placed in a 550 °C oven for 24 hours to remove organic matter. Then, the samples were dissolved by concentrated HF-HNO_3-HCl, with the final sediment stock solutions preserved in 6M HCl. The concentrations of various trace elements were measured by an Agilent 8800 triple quadrupole inductively coupled plasma mass spectrometer (QQQ-ICP-MS) in the Metal Isotope Geochemistry Laboratory at the University of Waterloo. Two rock standards (HISS-1 from the National Research Council of Canada and BHVO-2 from the U.S. Geological Survey) was used as secondary reference standards to test the accuracy (within 10%).[301, 302]

4.2.5. Iron isotope analyses

Iron isotope compositions were determined on water column samples (dissolved and particulate Fe), porewater and bulk sediments. Fe was purified using ion-exchange chromatography before Fe isotope analysis.[244] Iron isotope compositions of dissolved Fe, particulate Fe, porewater Fe and sediment Fe were measured by a multi-collector, inductively coupled plasma mass spectrometer (MC-ICP-MS; Nu Plasma II) in the Metal Isotope Geochemistry Laboratory, University of Waterloo, using the standard-sample-standard bracketing technique. All Fe isotope data are reported as $\delta^{56}Fe$ values relative to the IRMM-634 (the international standard replacing IRMM-014; Institute for Reference Materials and Measurements), in units of per mil (‰):

$$\delta^{56}Fe=[(^{56}Fe/^{54}Fe_{sample})/(^{56}Fe/^{54}Fe_{IRMM634}) - 1] \times 10^3$$

Test solutions and five rock standards were used to test the precision and accuracy of Fe isotope analysis. The detailed protocol and results are given in Chapter 3.

4.2.6. Lake water column geochemical profiles

The temperature remained relatively constant in the epilimnia of all four lakes, then decreased to 4 ºC in the hypolimnia of L227 and L442 and 7 ºC in the hypolimnia of L221 and L304 (Figure 4-2). In L221, L227 and L304, oxygen concentrations declined sharply in the metalimnion and were below the detection limit (O_2=0.1 mg/L) in the hypolimnion, while in L442, the metalimnion and the upper part of hypolimnion remained well oxygenated with the depletion of oxygen occurring between 10m and 13m (Figure 4-2). pH values in four lakes ranged from 6 to 9, indicating the prevalence of circumneutral conditions. In L227, L304 and L442, a decrease in SO_4^{2-} concentrations with depth (from 7-14 μM to 3-5 μM) was coupled with an increase in dissolved total sulfide (1 μM to 5-9 μM), indicating sulfate reduction in the hypolimnia (Figure 4-2). In contrast, SO_4^{2-} concentrations and ΣS^2 concentrations remained relatively constant with depth in L221 (average of SO_4^{2-}: 12.5 ± 0.9 μM; average of ΣS^{2-}: 1.7 ± 0.5 μM). TDP concentrations showed an increase with depth, with maximum values of 10 μg/L in L304 and L442 and 70 μg/L in L227 (Figure 4-2). In addition, an increase in SPP concentrations was observed with depth, with maximum values of 30 μg/L in L304 and L442 and 108 μg/L in L227 (Figure 4-2). It should be noted that a second peak of SPP concentrations was observed at 4 m in L227, possibly due to the contribution of phytoplankton biomass during the blooms. NH_4^+ concentrations remained relatively constant in the oxic layers and increased abruptly in anoxic hypolimnia, with maximum values of 1391 μg/L in 221, 5509 μg/L in L227, 604 μg/L in L304 and 623 μg/L in L442 (Figure 4-2). DOC concentrations were high in all lakes, with average values of 912, 810, 720 and 570 μM in L221, L227, L304 and L442, respectively (Figure 4-2). A significant increase in DIC concentrations was observed with depth, with maximum values of 620 μM in 221, 1950 μM in L227, 750 μM in L304 and 960 μM in L442 (Figure 4-2).

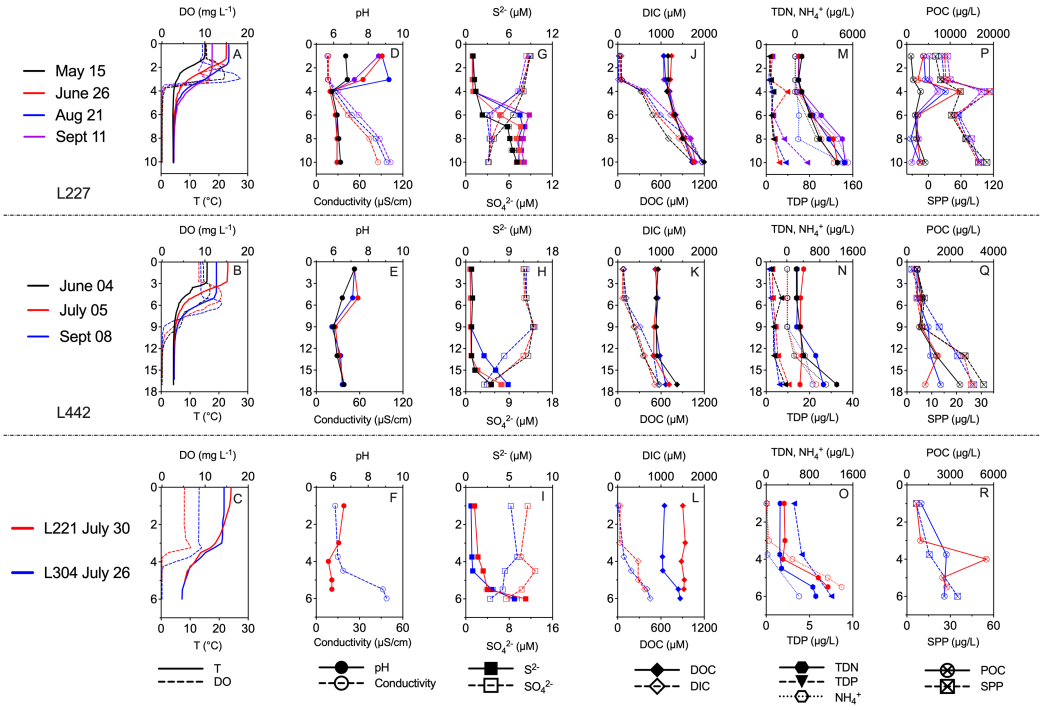


Figure 4-2 Water column depth profiles of (A-C) dissolved oxygen (DO) and temperature (T); (D-F) pH and conductivity; (G-I) total dissolved sulfide (ΣS^{2-}) and sulfate (SO_4^{2-}); (J-L) Dissolved inorganic carbon (DIC) and dissolved organic carbon (DOC); (M-O) total dissolved nitrogen (TDN), ammonium (NH_4^+) and total dissolved phosphorus (TDP); (P-R) particulate organic carbon (POC) and suspended particulate phosphorus (SPP) in L227 (upper panel), L442 (middle panel) and L221& L304 (lower panel) during 2018.

4.3. Results and Discussion

Dissolved Fe and particulate Fe in the water column of four lakes have δ^{56}Fe values that range from −1.2 to 1.8‰ (Figure 4-4), spanning nearly half of the total known range of aquatic environments worldwide. The largest difference between dissolved Fe and particulate Fe was observed in eutrophic lake 227, which likely indicates increased aquatic biological cycling in this lake as discussed in Chapters 2 and 3. Furthermore, for each lake, distinctive dissolved δ^{56}Fe and particulate δ^{56}Fe were exhibited in different layers and patterns in Fe

isotopes were similarly reversed from oxic epilimnia to anoxic hypolimnia (Figure 4-4), suggesting that different Fe processes occur between the oxic and anoxic layers.

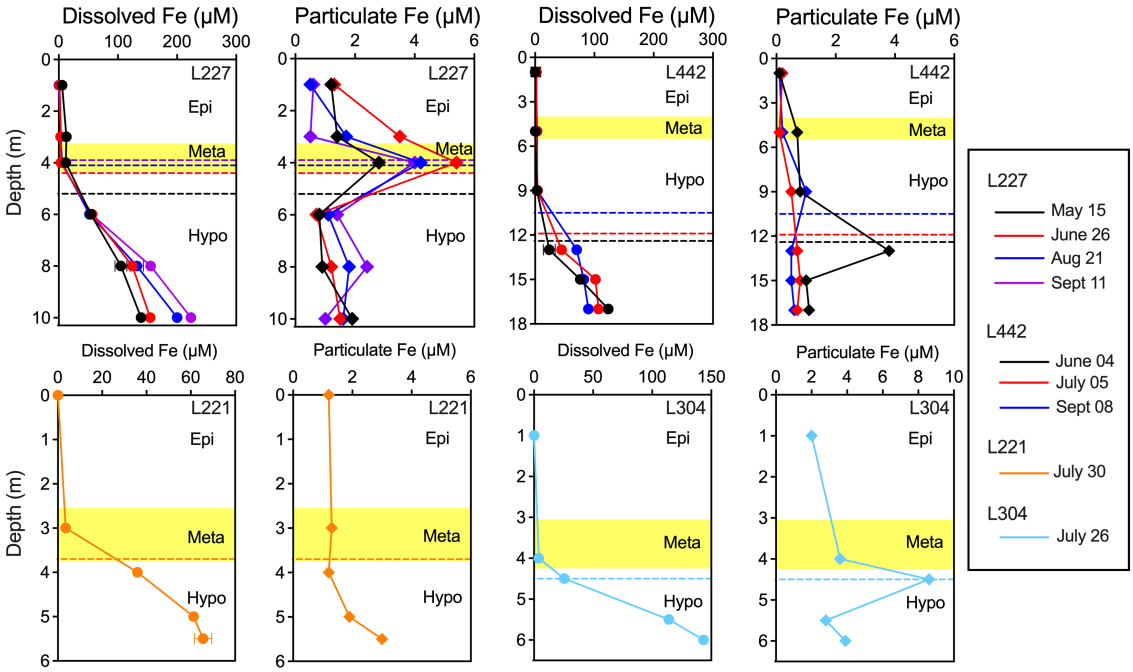


Figure 4-3 Profiles of dissolved Fe and particulate Fe in L227 (a, b), L442 (c, d), L221 (e, f) and L304 (g, h) during 2018.
Yellow bars indicate approximate depth of metalimnion. The thickness and depth of metalimnion may vary seasonally due to the changing climate. Horizontal dotted lanes represent the depth of 0.1 mg/L dissolved oxygen (redox boundaries) in each lake at the time of sampling. Error bars represent 1-standard deviation for duplicate samples. Error bars not visible are contained within the symbols. Note that, in anoxic hypolimnion, most of dissolved Fe (>92%) and particulate Fe (>90%) are Fe(II) and Fe(III), respectively.

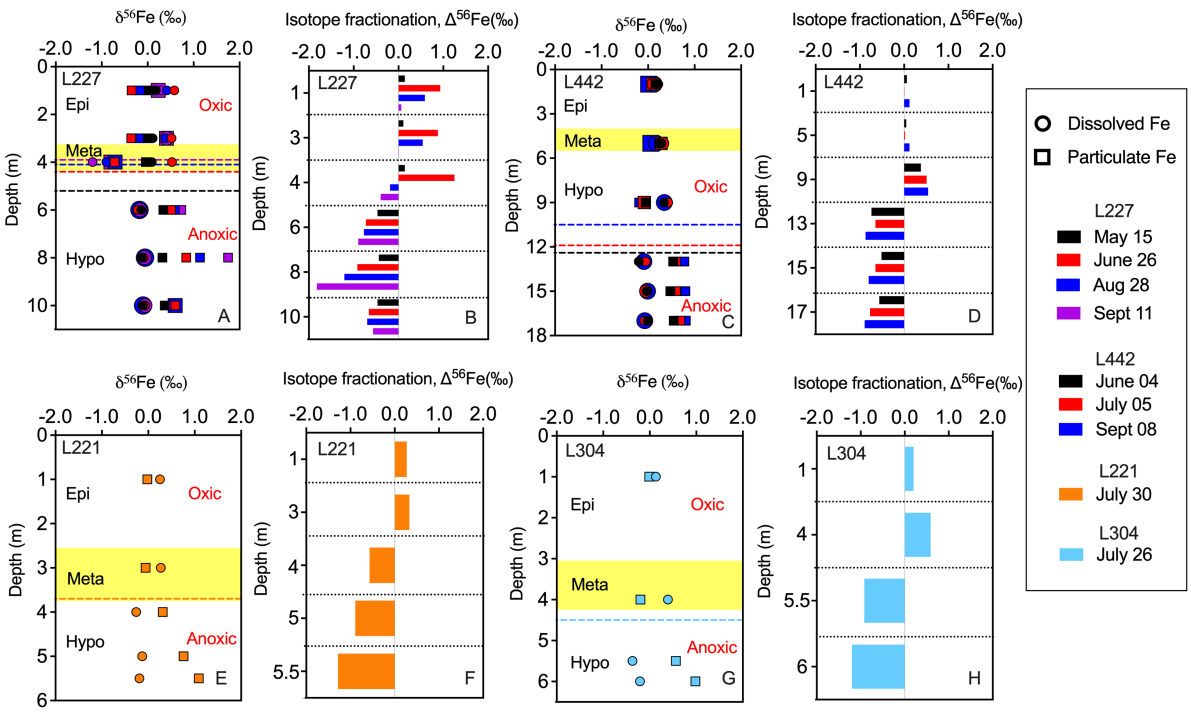


Figure 4-4 Iron isotope compositions ($\delta^{56}Fe$) of dissolved and particulate Fe in water column of L227 (A, B), L442 (D, D), L221 (E, F) and L304 (G, H).
Yellow bars indicate approximate depth of metalimnion. The thickness and depth of metalimnion may vary seasonally due to the changing climate. Horizontal dashed lanes represent the depth of 0.1 mg/L dissolved oxygen (redox boundaries) in each lake at the time of sampling. Iron isotope fractionation, $\Delta^{56}Fe_{dis\text{-}part}$, is defined as the difference between dissolved $\delta^{56}Fe$ and particulate $\delta^{56}Fe$.

4.3.1. Fe concentrations in the water column

The water column profiles of Fe concentrations exhibited similar patterns in all lakes, reflecting large semi-annual fluxes in the internal Fe cycle. Dissolved Fe concentrations were relatively low and constant in the oxic layers (2.6 ± 3.5 μM) of all lakes (Figure 4-3). For each lake, a substantial fraction of Fe(II) was observed in dissolved Fe, with a higher fraction (70-100% of dissolved Fe) observed in the sunlit surface oxic water and a lower fraction (30-60%) in deeper oxic water. The prevalence of dissolved Fe(II) in the sunlit oxic water of these DOC-rich boreal lakes likely results from the photochemical reduction of Fe(III) and the complexation of Fe(II)-DOM, as inferred in one recent study (Chapter 3). In the anoxic

layers, dissolved Fe increased significantly with depth, with the highest values at the bottom of lakes (179 ± 39 μM for L227, 107 ± 17 μM for L442, 71 μM for L221 and 143 μM for L304; Figure 4-3), reflecting the intensive Fe internal loading from anoxic sediment. Most of the dissolved Fe (>96%) was Fe(II) in the anoxic layers of all lakes. The increase in dissolved Fe concentrations with depth in the anoxic layers of four lakes is similar to what is observed in other lakes.[200, 201] In the anoxic layers of Lake Nyos[201] and Lac Pavin,[200] an increase in Fe concentrations is coupled with an increase in dissolved δ^{56}Fe, indicating that the variation of dissolved Fe concentration with depth results from either partial oxidation of upward diffusing dissolved Fe or microbial reduction of settling particulate Fe. However, dissolved δ^{56}Fe is relatively constant in the anoxic layers of lakes (Figure 4-4), suggesting that this increase in dissolved Fe concentration with depth in anoxic layers is due to the more accumulation of dissolved Fe(II) fuelled by a high flux of Fe(II) from the sediments, supported by the observation that there is much more sediment in contact with deep water column than shallow water column.[238] Particulate Fe concentrations were relatively constant through the water column, with a distinct localized peak occurring near the redox boundary in all lakes (Figure 4-3). Fe(III) dominated particulate Fe (over 95% of particulate Fe) in the oxic layers of all lakes, with some exceptions in L227, where the onset of bloom led to the dominance of particulate Fe(II). Therefore, in L221, L442 and L227 before the bloom, the peak of particulate Fe near the redox boundary and the dominance of particulate Fe(III) suggest that dissolved Fe(II) in the anoxic layer diffuses upwards to the redox boundary, rapidly oxidizing to form Fe oxyhydroxides (Figure 4-3). In contrast, in L227 during the blooms, the peak of particulate Fe mainly derived from intracellular Fe(II) uptake (Chapter 3). Furthermore, in all lakes, dissolved Fe(II) concentrations at the redox boundary were

extremely low (a few μM), comparable to dissolved Fe concentrations in the epilimnia, suggesting that diffusing dissolved Fe(II) is completely oxidized at and above the redox boundary (Figure 4-3). The strong concentration gradients of dissolved Fe between the oxic layers and anoxic layers, along with the peak of particulate Fe near the redox boundary, reflect that in these boreal lakes, sediments supply dissolved Fe(II) to the anoxic water column, whereby the dissolved Fe(II) diffuses upwards and is almost quantitatively oxidized at the redox boundary.

4.3.2. Fe isotopic compositions and associated Fe isotope fractionations in the oxic layers

Dissolved $\delta^{56}Fe$ was generally more positive than particulate $\delta^{56}Fe$ in the oxic epilimnia and metalimnia of four lakes, with some exceptions in the metalimnion of L227 (Figure 4-4). In the epilimnia and metalimnia of L442 and L221, and in the epilimnia of L304, the $\Delta^{56}Fe_{dis\text{-}part}$ fractionations were relatively small, with the values of 0.06 ± 0.09‰ (2σ), 0.30 ± 0.08‰ (2σ), 0.14 ± 0.08‰ (2σ), respectively. The dissolved and particulate $\delta^{56}Fe$ in the epilimnia and metalimnia of L442, L221, and in the epilimnion of L304 is likely governed by a combination of multiple processes, including photochemical reduction of particulate Fe(III), complexation of dissolved Fe-DOM, photolysis and microbial decomposition whereby the isotopic effects induced by each process may be opposite and counteracting with each other, as inferred in one recent study (Chapter 3). In contrast, dissolved and particulate $\delta^{56}Fe$ in the epilimnion and metalimnion of L227 showed more variations, corresponding to the progression of bloom over the open water season (Figure 4-4). While $\Delta^{56}Fe_{dis\text{-}part}$ fractionation in the epilimnion and metalimnion of L227 before the bloom was relatively small (0.13 ± 0.04‰ (2σ)), biological uptake of isotopically light Fe(II)

during the blooms fractionated Fe isotopes, resulting in $\Delta^{56}Fe_{dis\text{-}part}$ fractionations of 1.02 ± 0.33‰(2σ) in the epilimnion and metalimnion during the first bloom and 0.56 ± 0.07‰(2σ) in the epilimnion during the second bloom. It should be noted that the $\Delta^{56}Fe_{dis\text{-}part}$ fractionation of 0.59± 0.02‰(2σ) in the metalimnion of L304 (Figure 4-4) is also likely produced by biological uptake by phytoplankton, supported by the observation that chlorophyll *a* concentrations peak at 50 µg/L at 4 m (Figure 4-5). Moreover, the opposite sign of $\Delta^{56}Fe_{dis\text{-}part}$ fractionations at 4 m depth in L227 during the second bloom and the post-bloom period, compared to $\Delta^{56}Fe_{dis\text{-}part}$ fractionations observed in the metalimnia of L442, L221, L304 and L227 before the bloom and during the peak of the first bloom (Figure 4-4), was likely modified by partial oxidation within the microoxic zone of hypolimnion, as redox boundary was located at ~4 m in L227 at the time of sampling (Chapter 3).

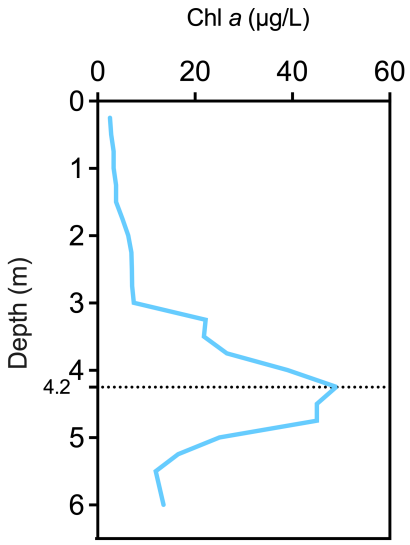


Figure 4-5 Depth profile of chlorophyll *a* (chl *a*) concentrations in L304 on July 26 2018. The horizontal dashed line indicates the depth of the maximum chl *a* concentration.

In the oxic hypolimnion of L442, dissolved $\delta^{56}Fe$ was more positive than particulate $\delta^{56}Fe$, consistent with the trend in the epilimnion and metalimnion of L442, despite the lack

of vertical mixing within the layer (Figure 4-4). However, isotope fractionation $\Delta^{56}Fe_{dis\text{-}part}$ in the oxic hypolimnion was 0.48 ± 0.17‰ (2σ), much larger than $\Delta^{56}Fe_{dis\text{-}part}$ (0.06 ± 0.09‰, 2σ) in the epilimnion and metalimnion, possibly reflecting the expression of the isotope fractionation arising from complexation of dissolved Fe-DOM due to the absence of photolysis in the oxic hypolimnion. The complexation of dissolved Fe-DOM accompanied by rapid precipitation of dissolved inorganic Fe can lead to the enrichment of heavier isotopes in dissolved organic Fe relative to particulate Fe in the organic-rich oxic water column (Chapter 3).[188, 258] Conversely, the photolysis of Fe-DOC complexes could make dissolved Fe isotopically light by breaking Fe-DOM complexes and removing the isotopically heavy Fe from water column via precipitation.[267] In the epilimnion and metalimnion of L442, the expression of the isotope fractionation arising from complexation of dissolved Fe-DOM is probably suppressed by the photolysis, resulting in relatively small $\Delta^{56}Fe_{dis\text{-}part}$ (0.06 ± 0.09‰, 2σ; Figure 4-4). In contrast, in the oxic hypolimnion where the photolysis is likely inhibited due to the very low light intensities (~<1 μmol photons m^{-2} s^{-1}),[356] the complexation of dissolved Fe-DOM could cause dissolved Fe more positive, resulting in $\Delta^{56}Fe_{dis\text{-}part}$ of 0.48 ± 0.17‰. It should be noted that biological uptake by phytoplankton could also contributed to the fractionation $\Delta^{56}Fe_{dis\text{-}part}$ in the oxic hypolimnion. Deep chlorophyll maximum (DCM), which is an indicator for phytoplankton in deep water column, have been observed in oligotrophic boreal lakes.[357, 358] Chlorophyll *a* profile in L442 exhibit a peak concentration of 3.7 μg/L at 8m within the oxic hypolimnion,[357] suggesting that Fe acquisition by phytoplankton might contribute to the observed $\Delta^{56}Fe_{dis\text{-}part}$ in the oxic hypolimnion.

In the oxic layers of four lakes, biological uptake, photochemical reduction, complexation of dissolved Fe-DOM, photolysis and microbial decomposition combine to

modify the $\delta^{56}Fe$ of dissolved and particulate Fe, producing systematically positive $\Delta^{56}Fe_{dis\text{-}part}$ in all lakes. The large $\Delta^{56}Fe_{dis\text{-}part}$ observed in the oxic layers is attributed to biological uptake, whereas small $\Delta^{56}Fe_{dis\text{-}part}$ is observed in surface sunlit water when biological uptake is absent.

4.3.3. Fe isotopic compositions and associated Fe isotope fractionations in anoxic hypolimnia

In contrast to the trend observed in the epilimnia and metalimnia, dissolved $\delta^{56}Fe$ was more negative than the particulate $\delta^{56}Fe$ in the anoxic hypolimnia of all four lakes with $\Delta^{56}Fe_{dis\text{-}part}$ fractionations of $-0.91 \pm 0.58‰$ (2σ) in L221, $-0.87 \pm 0.81‰$ (2σ) in L227, $-1.06 \pm 0.26‰$ (2σ) in L304 and $-0.72 \pm 0.25‰$ (2σ) in L442 (Figure 4-4). Furthermore, particulate $\delta^{56}Fe$ in the anoxic hypolimnia differed from particulate $\delta^{56}Fe$ in the oxic layers by > 0.3‰ in all lakes (Figure 4-4). Similarly, $\delta^{56}Fe$ of dissolved Fe in the anoxic hypolimnia differed from $\delta^{56}Fe$ of dissolved Fe in the oxic layers by >0.2‰. Thus, neither the particulate $\delta^{56}Fe$ nor dissolved $\delta^{56}Fe$ nor the sign of the isotope fractionation is the same between the oxic layers and anoxic hypolimnion. Fe isotopes elucidate the importance of novel Fe cycling pathways in the hypolimnia of small boreal lakes.

Fe redox processes near redox boundaries

Particulate Fe is lost from the overlying oxic layers to the anoxic hypolimnia and this input could modify the dissolved and particulate $\delta^{56}Fe$ in the anoxic hypolimnia. Particulate Fe originating from overlying oxic layers comprises biogenic Fe, flocculating DOM-Fe complexes, authigenic Fe minerals ($68 \pm 11\%$, see Appendix A) and some degree of lithogenic minerals. Biogenic Fe likely dominates the particulate phase in eutrophic L227

(see further details in the following paragraphs) while authigenic Fe minerals and flocculating DOM-Fe complexes could predominantly contribute to particulate phase in oligotrophic L221, L304 and L442. In these oligotrophic lakes, the sinking particulate Fe could be later reduced by a combination of diagenesis and dissimilatory iron reduction (DIR) in the anoxic hypolimnion after sinking through the redox boundary. Experimental studies using microorganisms and different ferric substances (ferrihydrite, hematite or goethite) found that the equilibrium fractionation $\Delta^{56}Fe$ of ~−3‰ between enzymatically-produced $Fe(II)_{aq}$ and Fe(III) oxyhydroxides can be produced by dissimilatory iron reduction.[173, 181, 182] Considering the abundant Fe reducers detected in the upper anoxic hypolimnion,[211, 276] these sinking inorganic Fe particulates or flocculating Fe-DOM complexes that are not protected by organic coatings are speculated to be completely reduced to dissolved Fe(II) in the uppermost part of the anoxic hypolimnion (i.e., multiple centimeters below the redox boundary). This process produces no isotopic fractionation, supported by the observation that particulate $\delta^{56}Fe$ in the overlying oxic layers was similar to the dissolved $\delta^{56}Fe$ in the anoxic layers of four lakes except for L227 during the blooms and post-bloom periods (Figure 4-4).

Contrasting with the dominance of authigenic Fe(III) oxyhydroxides and flocculating DOM-Fe complexes in the oxic layers of other lakes, the particulate Fe in the oxic layers of L227 during the blooms and post-bloom periods is mainly of biogenic origin, as most of PFe is either intracellular Fe retained in cells or extracellular Fe associated with organic debris (Chapter 3). Particulate Fe pool, dominated by Fe(II) fraction (60%~90%), shows enrichment in light isotopes in the oxic layers of L227 during the bloom, possibly due to the uptake of isotopically light Fe(II) by cyanobacteria. A settling flux of biomass associated with isotopically light particulate Fe(II) is expected to settle down from an oxic to anoxic layer

during the bloom, and in particular, during the post bloom where bloom collapsed gradually, modifying the particulate $\delta^{56}Fe$ in the anoxic hypolimnion. However, there was no significant Fe(II) fraction (<10%) observed in particulate Fe in the anoxic hypolimnion during the bloom and post-bloom periods, suggesting that particulate Fe measured in the anoxic hypolimnion is more likely to be suspended particulate Fe formed *in situ* rather than sinking bioaggregates originating from oxic layers. As a result, the sinking biogenic particulate Fe originating from the overlying oxic layers during the bloom and post-bloom periods is unlikely to affect particulate $\delta^{56}Fe$ measured in the anoxic hypolimnion. This is consistent with the observation that the $\delta^{13}C$ and $\delta^{15}N$ of the particulate matter in the hypolimnion differs substantially from the biogenic particulates in the epilimnion.[211]

Dissolved Fe(II) in the anoxic hypolimnia can diffuse upwards and be oxidized by oxygen at the redox boundaries. The net fractionation between aqueous Fe(II) and Fe(III) oxyhydroxides during partial oxidation has been reported to be –1 to –2‰, arising from the combination of an equilibrium fractionation between aqueous Fe(II) and Fe(III) and a kinetic fractionation between aqueous Fe(III) and Fe(III) oxyhydroxides, in both experimental studies and natural aquatic systems.[234, 275, 359] The isotope fractionation $\Delta^{56}Fe_{dis\text{-}part}$ between dissolved Fe and particulate Fe at 4m in L227 during the second bloom and the post bloom (Figure 4-4) likely resulted from partial oxidation within the uppermost microoxic zone of hypolimnion, as described previously. However, the signal of dissolved $\delta^{56}Fe$ and particulate $\delta^{56}Fe$ produced by partial oxidation was unlikely carried into the anoxic hypolimnion as these freshly *in situ* formed Fe(III) oxyhydroxides were likely reduced completely by DIR near the redox boundary (i.e., multiple centimeters below redox boundary) due to extremely low mixing rate and abundant Fe reducers in the anoxic hypolimnion.[211, 276] Therefore, partial

oxidation is unlikely to result in the observed fractionation in the anoxic hypolimnia or contribute to the $\delta^{56}Fe$ of the dissolved and particulate Fe in the epilimnia.

Water column biogeochemical Fe processes throughout anoxic hypolimnia

Particulate Fe originating from the epilimnia can be dissolved completely through reductive dissolution, contributing to the $\delta^{56}Fe$ of dissolved Fe in the hypolimnion as the particulate $\delta^{56}Fe$ in the epilimnion and dissolved $\delta^{56}Fe$ in the hypolimnion is similar (Figure 4-4). However, in the anoxic hypolimnia of all sampled lakes, the highly positive $\delta^{56}Fe$ values of particulate Fe and the distinct difference between dissolved $\delta^{56}Fe$ and particulate $\delta^{56}Fe$ cannot be supported by any input of Fe from the epilimnia or Fe processes near the redox boundaries of these lakes (Figure 4-4). The large isotope fractionation between dissolved and particulate Fe in the anoxic hypolimnia indicates active Fe cycling in the anoxic hypolimnia of four lakes where dissolved Fe concentrations are high. We hypothesize that the observed magnitude of Fe isotope fractionation in the anoxic hypolimnion results from the Fe processes occurring *in situ* throughout the anoxic hypolimnion. Possible *in situ* processes that could modify the dissolved and particulate $\delta^{56}Fe$ include (1) Fe adsorption, (2) formation of Fe(II) minerals and (3) microbial Fe oxidation.

Sorption of Fe(II) on Fe oxides is known to favor heavy isotopes on the solid surface and produce ~–0.9‰ of $\Delta^{56}Fe_{Fe(II)aq\text{-}Fe(II)sorb}$ fractionation between aqueous Fe(II) and sorbed Fe(II).[168, 181, 187, 264] Sorption of dissolved Fe(II) onto particulate Fe could occur *in situ* considering the range of pH (5.7 to 6.6) in anoxic hypolimnia of four lakes [360] and the $\Delta^{56}Fe_{Fe(II)aq\text{-}Fe(II)sorb}$ fractionation is similar to the observed $\Delta^{56}Fe_{dis\text{-}part}$ fractionation (Figure 4-4). However, considering the very low fraction of Fe(II) in particulate Fe in the anoxic

hypolimnion, the extent of Fe adsorption is likely limited, and this process cannot produce the observed $\Delta^{56}Fe_{dis\text{-}part}$ fractionation (Figure 4-4).

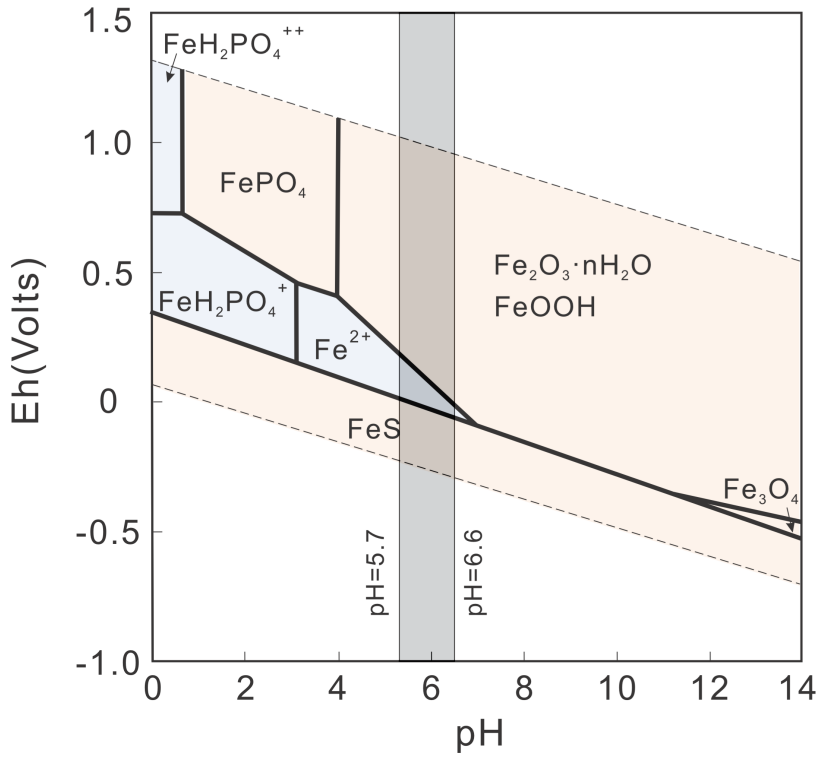


Figure 4-6 Eh versus pH diagram for species of Fe at 4.5°C.
The pressure was set at 1 bar. The Fe concentration was set at 150 µM, phosphate was set at 0.2 µM, sulfate/sulfide was set at 0.1 µM and bicarbonate was set at 0.8 mM. These values are representative of physico chemical parameters in the hypolimnia of four lakes. The grey zone represent the pH range in anoxic hypolimnia of four lakes.

Precipitation of Fe(II) minerals can fractionate Fe isotopes in anoxic hypolimnia. The possible common Fe(II) minerals in the water column of lakes are Fe sulfides (e.g., mackinawite), siderite ($FeCO_3$) and vivianite ($Fe_3(PO_4)_2$). Despite the fact that dissolved Fe concentrations are much higher than dissolved sulfide concentrations, an increase in dissolved sulfide concentrations with depth coupled with a decrease in dissolved sulfate highlights that Fe sulfide formation may have a strong effect on $\delta^{56}Fe$ of dissolved and particulate Fe, as inferred by other studies.[200, 204] Experimental studies have shown that

mackinawite is the dominant Fe sulfide in the presence of sulfate reducing bacteria, which are abundant in the anoxic hypolimnia of four lakes.[276] The $\Delta^{56}Fe_{Fe(II)aq\text{-}mackinawite}$ fractionation between aqueous Fe(II) and mackinawite could be driven by kinetic isotope effects with variable values of 0.34~0.85‰ at low pH (pH=4),[191, 192] but at near-neutral pH, the $\Delta^{56}Fe_{Fe(II)aq\text{-}mackinawite}$ fractionation yields an equilibrium value of –0.32±0.29 ‰ (at 20 °C).[190] Given the fact that dissolved Fe(II) concentration is two orders of magnitude higher than dissolved sulfide concentration in the anoxic hypolimnia under circumneutral pH conditions, the mackinawite, if it is being formed, is probably in isotopic equilibrium with dissolved Fe(II) in the anoxic hypolimnia of four lakes, leading to negative $\Delta^{56}Fe_{Fe(II)aq\text{-}mackinawite}$ fractionations. Based on the Eh-pH diagram, Fe sulfide minerals are the stable solid inorganic phase in the anoxic hypolimnia of four lakes considering the pH range (5.7~6.6) (Figure 4-6). Furthermore, the presence of Fe sulfide minerals can be assessed by saturation indices (SI) given by

$$SI = \log\left[\frac{IAP}{K_{sp}}\right]$$

where IAP is the observed ion activity product and Ksp is the solubility product of Fe sulfide (Table A2). Based on these calculations, Fe sulfide is undersaturated and unlikely formed in the anoxic hypolimnia of four lakes. Despite current limited knowledge of Fe isotope fractionation $\Delta^{56}Fe_{Fe(II)aq\text{-}vivianite}$ between aqueous Fe(II) and vivianite (~–0.3‰), the formation of vivianite is thought to cause the enrichment of heavy isotopes in the solid phase,[177] consistent with the sign of observed $\Delta^{56}Fe_{dis\text{-}part}$ in the anoxic hypolimnia (Figure 4-4). However, calculation of saturation indices for vivianite formation shows that vivianite is undersaturated and unlikely formed in the anoxic hypolimnia of four lakes (Table A2). One experimental study has reported that Fe isotope fractionation $\Delta^{56}Fe_{Fe(II)aq\text{-}siderite}$ between

aqueous Fe and siderite under equilibrium control is +0.48 ± 0.22‰,[189] which is opposite of the observed $\Delta^{56}Fe_{dis\text{-}part}$ in the anoxic hypolimnia of four lakes (Figure 4-4). Therefore, formation of Fe(II) minerals unlikely contribute to the observed $\Delta^{56}Fe_{dis\text{-}part}$ in the anoxic hypolimnia of four lakes.

It is now well established that microbial Fe oxidation could cause the enrichment of heavy isotopes in Fe(III) oxides relative to aqueous Fe(II). Acidophilic iron-oxidizing bacteria are known to produce higher $\delta^{56}Fe$ of oxidized Fe (mainly aqueous Fe(III) at acidic pH) compared to co-existing aqueous Fe(II) under oxic conditions and at low pH (<3), with an equilibrium $\Delta^{56}Fe_{aq\ Fe(II)\text{-}aq\ Fe(III)}$ fractionation of ~–3‰ between aqueous Fe(II) and aqueous Fe(III)[174] but this process is ruled out based on the pH range of 5.9-6.4 and lack of oxygen in the anoxic hypolimnia. Moreover, one experimental study using nitrate-reducing Fe(II) oxidizing bacteria, *Acidovorax* sp. strain BoFeN1, has shown that biological nitrate-reducing Fe(II) oxidation at circumneutral pH can produce an apparent $\Delta^{56}Fe_{Fe(II)aq\text{-}Fe(III)\ oxide}$ fractionation of 2-3‰ between aqueous Fe(II) and Fe(III) oxides, which is in agreement with observed $\Delta^{56}Fe_{dis\text{-}part}$ in the anoxic hypolimnion (Figure 4-4). However, biological nitrate-reducing Fe(II) oxidation is unlikely to contribute the observed$\Delta^{56}Fe_{dis\text{-}part}$ in the anoxic hypolimnion, considering that the concentration of nitrate was very low (i.e., on the order of <1 uM) and the nitrate-reducing Fe(II) oxidizing bacteria (e.g., *Acidovorax*, *Thiobacillus denitrificans* and *Pseudogulbenkiania*) have not been identified in the hypolimnion.[276, 361]

Experimental studies on photoferrotrophy using anoxygenic photosynthetic microorganisms (both freshwater strains and marine strains) show that photoferrotrophy can produce a $\Delta^{56}Fe_{Fe(II)aq\text{-}Fe(III)\ oxide}$ fractionation of –1 to –3‰ between aqueous Fe(II) and Fe(III) oxides.[177-180] The observed $\Delta^{56}Fe_{dis\text{-}part}$ in the anoxic hypolimnia is consistent with

those $\Delta^{56}Fe_{Fe(II)aq\text{-}Fe(III)\ oxide}$ values deduced from photoferrotrophy experiments (Figure 4-4). Furthermore, 16S rRNA gene sequence data confirmed the presence of *Chlorobi,* which is close to the known photoferrotroph *Chlorobium ferroxidans,* among the most abundant operational taxonomic units in the anoxic zones of L221, L304 and L227.[276] The following genome-resolved metagenome sequence data showed that the *cyc2* gene, a candidate gene for photoferrotrophy, was detected in the *chlorobi* genome bins,[276] highlighting the possibility of photoferrotrophy in the anoxic zones of L221, L304 and L227. Moreover, photoferrotrophy can adapt to very low light intensities, and light saturation observed in photoferrotrophy incubation experiments using freshwater *Chlorobium ferrooxidans* strain KoFox was less than 50 lux (~1.2μmol photons m^{-2} s^{-1}).[42] The light intensities exceed 0.4 μmol photons m^{-2} s^{-1} at the bottom of L221 and L304 and 8m of L227 (Figure 4-7), comparable to light intensities (0.2-1.0 μmol photons m^{-2} s^{-1}) observed at the certain depth of other lakes where green sulfur bacteria (GSB) that potentially regulate anoxygenic photosynthesis were detected [152, 153] and rates of photoferrotrophy were measured.[151, 155] Collectively, this evidence suggests that the photoferrotrophy might occur in the anoxic hypolimnia of L221, L304 and L227, producing the observed $\Delta^{56}Fe_{dis\text{-}part}$. However, it should be noted that *Chlorobi* were not detected at the bottom of L227 (10 m),[361] where light intensities were very low (~0.02 μmol photons m^{-2} s^{-1}; Figure 4-7). A decrease in $\Delta^{56}Fe_{dis\text{-}part}$ fractionation coupled with the disappearance of *Chlorobi* at 10 m of L227 suggested the lack of photoferrotrophy, precluding the contribution of photoferrotrophy to the $\Delta^{56}Fe_{dis\text{-}part}$ at 10m (Figure 4-4). Rather, the observed $\Delta^{56}Fe_{dis\text{-}part}$ at 10 m probably results from the formation of FeS and the abiotic oxidation by O_2 produced by phytoplankton. The calculation of SI for FeS shows that FeS is near saturated at 10 m (Table A2), possibly contributing to the observed $\Delta^{56}Fe_{dis\text{-}part}$.

Furthermore, 16S rRNA gene sequence data and microscopy image analysis show that three genera of cyanobacteria (*Dolichospermum* sp., *Planktothrix* sp. and *Phormidium* sp.) were the most abundant organisms detected on the surface sediments at 10 m (Figure 4-8). Despite the very low light intensities at this depth (0.02 µmol photons m^{-2} s^{-1}; Figure 4-7), cyanobacteria could be producing minimal amounts of O_2. This cryptic O_2 cycling has the potential to abiotically oxidize Fe(II), contributing to the observed $\Delta^{56}Fe_{dis\text{-}part}$ at 10m in the water column of L227 (Figure 4-4).

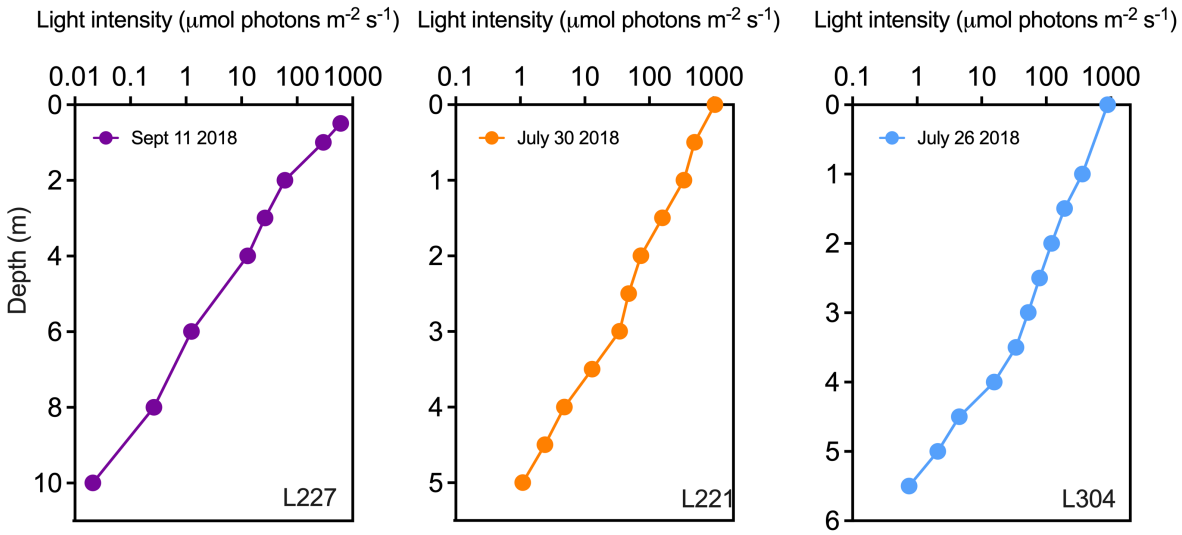


Figure 4-7 Light profiles of the water column of L227, L221 and L304 in 2018. Detection limit is 0.01 µmol photons m^{-2} s^{-1}.

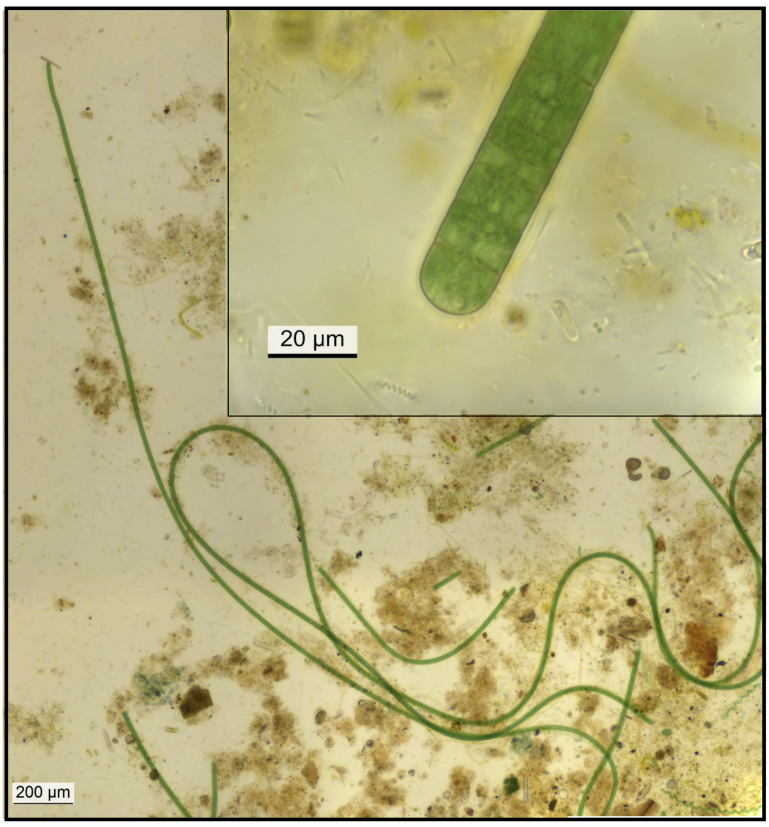


Figure 4-8 Microscopy images showing longitudinal sections of cyanobacterial cells in the surface sediment of one sediment core collected at the bottom of L227.

An increase in the magnitude of $\Delta^{56}Fe_{dis\text{-}part}$ fractionation with depth was observed in the anoxic hypolimnia of L221, L227 and L304, with the maximum value observed at the bottoms of L221 and L304 and 8 m of L227 (Figure 4-4). The increase in the magnitude of $\Delta^{56}Fe_{dis\text{-}part}$ fractionation with depth is speculated to reflects different *in situ* oxidation rates of photoferrotrophy at different depths. Dissolved Fe concentrations increased with depth and were two orders of magnitude higher than particulate Fe concentrations in the anoxic hypolimnia (Figure 4-3), suggesting a significant Fe input flux from the sediments. The constancy of the dissolved $\delta^{56}Fe$ with depth further supports that there is substantial accumulating dissolved Fe compared to *in situ* precipitated particulate Fe (Figure 4-4). Particulate Fe concentration also increased with depth in the anoxic hypolimnia (Figure 4-3).

The increasing $\delta^{56}Fe$ values of particulate Fe with depth concurrently with the increase in particulate Fe concentrations indicate that biological Fe oxidation, likely photoferrotrophy, contributes to the variation in particulate $\delta^{56}Fe$ (Figure 4-4). Collectively, this evidence suggests that anoxic hypolimnion is an open system for Fe behavior where dissolved Fe is dominated by Fe input from sediments and particulate Fe is modified by *in situ* processes. Fractionation factors $\Delta^{56}Fe_{Fe(II)aq\text{-}Fe(III)\ oxide}$ deduced from different photoferrotrophy experiments in a recent study study[159] showed a variation corresponding to the oxidation rate, with a smaller $\Delta^{56}Fe_{Fe(II)aq\text{-}Fe(III)\ oxide}$ value of –1.5‰ for the slower oxidation rate and a larger value of –2.5‰ for the rapid oxidation rate. $\Delta^{56}Fe_{Fe(II)aq\text{-}Fe(III)\ oxide}$ fractionation during photoferrotrophy is thought to reflect an initial 3‰ equilibrium fractionation between aqueous Fe(III) and aqueous Fe(II) overprinted by a kinetic fractionation during the precipitation.[177-179] Higher oxidation rates of photoferrotrophy tend to induce smaller kinetic fractionation during precipitation and thus result in an overall larger $\Delta^{56}Fe_{Fe(II)aq\text{-}Fe(III)\ oxide}$ fractionation.[159] In the anoxic hypolimnia of L221, L304 and L227, particulate Fe concentrations were relatively higher at deeper depth compared to shallow depth, suggesting that photoferrotrophy has a larger oxidation rate than shallow depth (Figure 4-3). If this is the case, then larger $\Delta^{56}Fe_{dis\text{-}part}$ fractionation should be observed at deeper depths of anoxic hypolimnia, which is consistent with the observation that an increase in the magnitude of $\Delta^{56}Fe_{dis\text{-}part}$ fractionation with depth was observed, further supporting that spatial variation of $\Delta^{56}Fe_{dis\text{-}part}$ fractionation in the anoxic hypolimnia is likely due to the increased oxidation rates of photoferrotrophy with depth (Figure 4-4).

It has been demonstrated that the oxidation rate of photoferrotrophy is dependent on Fe concentration, light intensity, temperature and pH.[362-365] The narrow range of pH and

temperature in the anoxic hypolimnia of L221, L304 and L227 preclude their influence on differences in the oxidation rate of photoferrotrophy (Figure 4-2). One study on the Fe oxidation rate mediated by freshwater photoferrotrophs found that both the increased dissolved Fe(II) concentration (up to ~15 mM) and the increased light intensity (~light saturation< 1.2μmol photons m^{-2} s^{-1}) can facilitate Fe oxidation rate under anaerobic conditions.[42] In the anoxic hypolimnia of L221, L304 and L227, a substantial increase in dissolved Fe(II) concentration (40-220 μM) with depth might result in a higher Fe oxidation rate at deeper depth compared to shallower depth while a decrease in light intensities with depth likely lead to lower Fe oxidation rate at deeper depth (Figure 4-3). The higher oxidation rate at deeper depths inferred from the Fe concentration and isotope data suggests that photoferrotrophs are able to live deeper in the anoxic hypolimnia with higher Fe concentration and lower light intensity and still sustain a relatively high level of metabolic activity by lowering their requirements for light, which is proposed as an adaptation mechanism of photoferrotrophs to optimize metabolic activities in recent studies.[42, 43]

Time-dependent variations in $\Delta^{56}Fe_{dis\text{-}part}$ fractionations were also observed in the anoxic hypolimnion of L227, whereby an increase in $\Delta^{56}Fe_{dis\text{-}part}$ fractionation was observed at 6 m and 8 m throughout the stratification period (Figure 4-4). Dissolved Fe(II) concentration at the same depth in anoxic layers increased over the May to September period due to the accumulation of dissolved Fe(II) fueled by a high flux of Fe(II) from the sediment (Figure 4-3). Increased Fe concentrations can facilitate the Fe oxidation rate over the stratified time. This is further supported by the observation that particulate Fe concentration at 6 m and 8 m increased over the stratification period (Figure 4-3). Therefore, seasonal variation in $\Delta^{56}Fe_{dis\text{-}part}$ fractionations observed in the anoxic hypolimnion of L227 over

stratified time is likely caused by the increased Fe oxidation rate of photoferrotrophy (Figure 4-4).

Spatial and temporal variations in $\Delta^{56}Fe_{dis\text{-}part}$ fractionations were observed in the anoxic hypolimnia of Boreal Shield lakes where *Chlorobi* were found among the most abundant operational taxonomic units with cyc2 genes is detected. These $\Delta^{56}Fe_{dis\text{-}part}$ fractionations are likely produced by photoferrotrophy, and variations in $\Delta^{56}Fe_{dis\text{-}part}$ fractionations were possibly due to different oxidation rates of photoferrotrophy. The $\Delta^{56}Fe_{dis\text{-}part}$ fractionations under varying environmental conditions help better understand Fe cycling under anoxic conditions in modern and ancient settings. If inferences that the observed $\Delta^{56}Fe_{dis\text{-}part}$ fractionation is related to photoferrotrophy are correct, then the wide range of $\Delta^{56}Fe_{dis\text{-}part}$ fractionation might suggest that, in natural environments, photoferrotrophs must cope with environmental conditions that change spatially or temporally, thus producing distinct $\Delta^{56}Fe_{dis\text{-}part}$ fractionation patterns. Furthermore, photoferrotrophs are thought to live under strictly anoxic and phototrophic conditions, whereby the former requires them to live deep in the water column and the latter requires them to stay close to the surface. The larger oxidation rate inferred at deeper depths where higher Fe concentrations but lower light intensities are observed suggests that photoferrotrophy can live deeper to meet the strictly anoxic conditions and still sustain a relatively high oxidation rate, probably by lowering their requirement for light. This is in good agreement with the general observation that green-sulfur bacteria have a very low light requirement compared to purple sulfur bacteria.[42, 43] Moreover, the large Fe isotope fractionation observed in the anoxic hypolimnion, possibly arising from photoferrotrophy, suggests that photoferrotrophs could thrive in the ferruginous deep water with limited light

intensity, lending support to the possibility of active photoferrotrophy occurring in deep layers of the Precambrian ocean.[144] Highly variable and positive Fe isotope composition of Fe oxyhydroxides that range from 0.3‰ to 1.8‰ in the anoxic hypolimnia is in good agreement with Fe isotope variations of Fe oxides minerals in BIF that deposited between 3.0-3.8 Ga,[146, 366, 367] supporting the hypothesis that photoferrotrophy plays a substantial role in the production of ferric Fe during the formation of BIF in the Archean ocean.[40, 118, 144, 368]

4.3.4. Fe cycling pathways in the profundal sediments at the bottom of lakes

In L227, newly deposited Fe in the profundal sediments includes biomass Fe(II) associated with phytoplankton, aggregates of Fe(III) and DOM, terrestrial inorganic Fe particles and autochthonous Fe(III) oxyhydroxides. The sediments in L227 are highly enriched in organic matter, with an average organic matter content of 62 ± 7 dwt.%. The Fe concentrations in bulk sediments in L227 are 3.6 ± 0.5 dwt.%. Mössbauer and XANES spectroscopies on a sediment core from the bottom of L227 have implied that over 76% of sediment Fe is organic complexed Fe(III) (in the form of ferrihydrite associated with organic matter and organic complexed Fe(III)) and 24% of sediment Fe is low-spin Fe(II),[369] which was inferred as pyrite but could also be some organic Fe(II) complexes. During the bloom and post bloom periods, the phytoplankton biomass associated with Fe(II) and the aggregates of Fe(III) and DOM, originating from the epilimnion and metalimnion, can sink to profundal sediments. During the fall and spring overturn, some terrestrial inorganic Fe particles likely composed of Fe(III) oxyhydroxides and other crystalline Fe minerals can transit through the entire water column without being reduced. Fe(III) oxyhydroxides in the overlying water column that precipitates due to the oxidation of dissolved Fe(II) during the overturn can also sink to the profundal sediments.

In L227, most newly deposited Fe is recycled back to the water column at the sediment-water interface (SWI). Much of newly deposited phytoplankton biomass Fe(II) is quickly decomposed at SWI and recycled back to the water column, supported by the observation that 95% of the C and N in settling phytoplankton biomass is released back to the hypolimnion through decomposition in the sediment within one year after settling down. Fe(III) oxyhydroxides generated at overturn are also likely reduced to Fe(II) very quickly at the SWI by reductive dissolution as the dissolved Fe concentration quickly builds up in the anoxic hypolimnion of L227 in May shortly after spring overturn (Figure 4-3). Some phytoplankton biomass Fe(II) and organic Fe(III) complexes are buried annually in the sediments as the sedimentation rate in the profundal sediment doubles after fertilization.[298] This buried organic bound Fe (both Fe(II) and Fe(III)) can be released to porewater in the form of Fe(II) by decomposition and subsequent dissimilatory iron reduction. Excess Fe(III) oxyhydroxides that cannot be reduced at the SWI could also be buried in the sediment and later reduced to porewater Fe(II) by dissimilatory iron reduction.

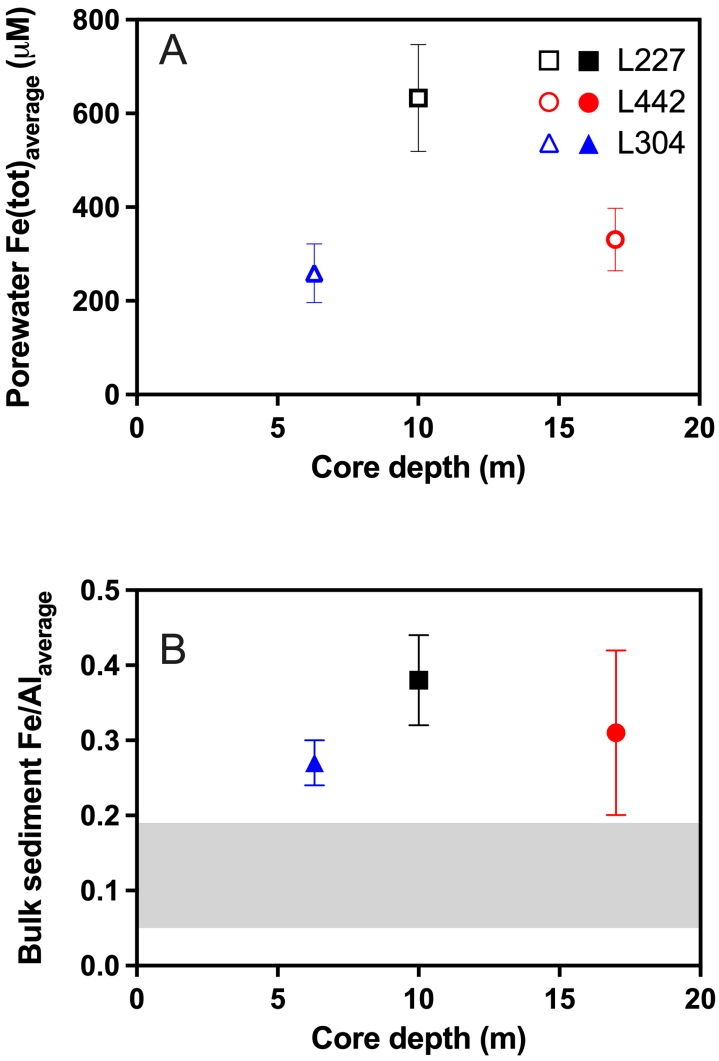


Figure 4-9 Average Fe concentrations of porewater (A) and average Fe/Al molar ratios of bulk sediment (B) in each sediment core versus the depth of the sediment core in L227, L304 and L442.

Error bas represent 1-standard deviation for each sediment core. Error bars not visible are contained within the symbols. In panel (B), the grey zone represents the range of Fe/Al ratios (0.05 to 0.19) for Canadian Precambrian Shield (the bedrock of ELA).

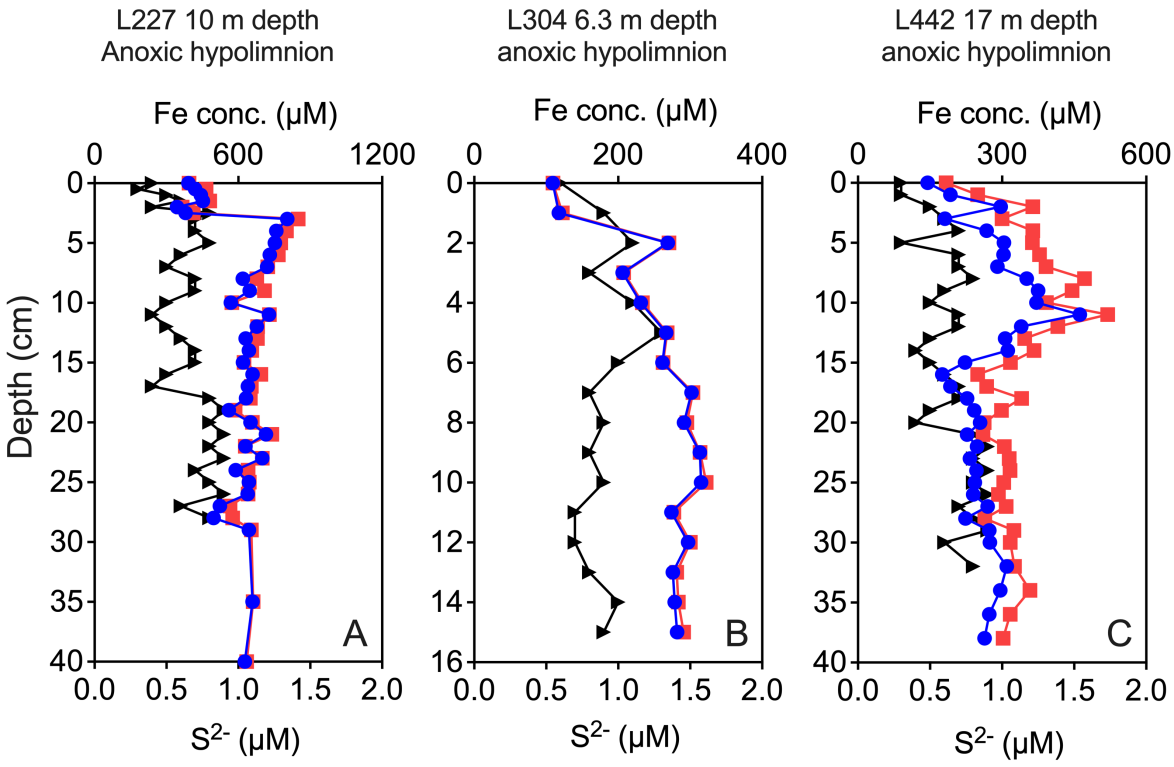


Figure 4-10 Fe concentrations of porewater and bulk sediments in the sediment core of L227 (A), L304 (B) and L442 (C).
Error bars represent 2-SD errors of all replicates and duplicates. Error bars not visible are contained within the symbols.

The high porewater Fe concentration observed in L227 was generated by a combination of dissimilatory iron reduction and the decomposition of organic Fe complexes. Porewater Fe concentrations in the sediment core of L227 steadily increased within the uppermost sediments (~0-3 cm) and remained constant in the sediments below, with average values of 633 ± 114 μM (Figures 4-9 and 4-10). Almost all porewater Fe in the L227 is Fe(II) (98±2%; Figure 4-10). Dissimilatory iron reduction (DIR) is one of the most important anaerobic pathways for the oxidation of organic carbon in sediments,[193, 370] and it can generate high Fe(II) concentrations (several mM) in the porewater of freshwater lakes.[200, 371] As ferrihydrite and organic matter serve as an electron acceptor and an electron donor for DIR respectively,[52] the high ferrihydrite abundances[369] and the significant organic matter

content in the profundal sediments of L227 probably offer a continuous supply of substrates for DIR in the sediment of L227, in agreement with earlier findings that active DIR is observed in the organic- and Fe oxides-rich sediments.[372-374] Furthermore, a previous study on the sediment Fe speciation of one sediment core from the bottom of L227 using sequential chemical extraction demonstrates that carbonate-associated minerals, likely siderite or ankerite, made up 20% of total reactive Fe in the sediments.[369] As the formation of siderite in the overlying water column has been ruled out, as described previously, the siderite present in the sediment likely formed *in situ* during the early diagenesis. The relatively high abundance of siderite, which is the common end product of DIR when reduction of poorly crystalline Fe(III) oxide is coupled with oxidation of organic carbon,[56, 173, 375] further suggests that DIR is active in the sediment of L227. However, previous experimental studies on cultivating iron-reducing bacteria with ferrihydrite have demonstrated the anticipated formation of goethite or magnetite, depending on whether the flux of Fe(II) is low or high, respectively.[55-57, 376]. Given the high concentration of porewater Fe(II) (Figures 4-9 and 4-10) and high abundance of ferrihydrite,[369] the presence of magnetite would be expected in the sediments of L227. However, previous investigation by spectroscopic techniques ((Mössbauer and XANES) showed that crystalline Fe minerals such as hematite, goethite and magnetite are not detected in the sediment core,[369] suggesting a lack of diagenetic reactions between porewater Fe(II) and ferrihydrite. The porewater Fe(II) cannot react with the ferrihydrite, possibly due to the adsorption of organic matter on the surface of ferrihydrite or aggregation of ferrihydrite and OM, supported by the observation that almost all ferrihydrite is associated with OM.[369] The coating of OM on ferrihydrite could prevent the ferrihydrite from reacting readily with aqueous Fe(II) (e.g., inhibit the adsorption of aqueous Fe(II)). It

should be noted that the release of Fe(II) by the decomposition of buried organic Fe(II) complexes also significantly contributes to the porewater Fe(II), considering the high settling flux of phytoplankton biomass associated with Fe(II) (Chapter 3) and elevated sedimentation rate caused by the bloom.[298] The higher porewater Fe concentration in L227 compared to L304 and L442 (Figure 4-10) further supports the significant contribution from the decomposition of buried organic Fe(II) complexes in L227 (see the detail in the following paragraph).

Fe cycling in the sediments of L304 and L442 are different from L227. Organic matter content is 59 ± 8 dwt.% and 39 ± 5 dwt.%, and the concentrations of bulk Fe are 3.8 ± 1.1 dwt.% and 2.7 ± 0.3 in the sediment cores of L30 and L442, respectively, similar to what was observed in the sediment core of L227. However, in L304 and L442, no significant flux of settling biomass Fe(II) was observed in the water column. As a result, newly deposited Fe in the profundal sediments of L304 and L442 were likely dominated by Fe(III) oxyhydroxides and aggregates of Fe(III) and organic matter. High porewater Fe concentrations were observed in the sediment cores of L304 and L442, with average values of 259 ± 63 and 331 ± 67 μM, respectively (Figures 4-9 and 4-10). Fe(II) makes up over 98% of porewater Fe in the sediment core of L304, whereas porewater Fe(II) represents between 70 and 97% of porewater Fe in the L442 sediment core (Figure 4-10). The relatively high concentrations of porewater Fe(III) (9 to 120 μM, Figure 4-10) in L442 were likely due to oxidation artifacts during the sediment collection, despite the fact that a small fraction of porewater Fe(III) may reflect true dissolved Fe(III) resulting from the dissolution of Fe(III) oxidation followed by the complexation of Fe(III)-DOM.[377, 378] The high porewater Fe(II) concentrations in L304 and L442 were likely dominated by extensive DIR in the sediments.

Dissimilatory sulfate reduction (DSR) could also play an important role in the degradation of organic carbon in sediments.[370] Porewater H_2S generated by DSR could react with both aqueous Fe and solid phase Fe to form a variety of Fe sulfide minerals, reducing the availability of Fe for DIR.[193] However, given the fact that porewater sulfide concentrations are two orders of magnitude lower as compared to porewater Fe concentration in L227, 304 and L442 (Figure 4-10), decomposition of organic Fe(II) complexes and DIR combine to dominate over DSR throughout the sediment cores of L227 and DIR dominated in L304 and L442 in terms of Fe diagenesis, consistent with the observations in other freshwater sediments[372, 379, 380] and microcosm studies.[51, 381] The extremely low concentration of porewater sulfide indicates that the DSR-produced sulfide is consumed due to the quantitative titration by a large flux of porewater Fe(II).

Dissimilatory sulfate reduction can lead to the formation of Fe sulfides (FeS and pyrite) through diagenetic processes. The porewater sulfate concentration profile of one hypolimnetic sediment core of L227 measured in the previous study showed that sulfate concentrations were relatively constant around 25-35 μM in the upper 8 cm but decreased progressively to a minimum of 5 μM at a depth of 20 cm.[369] Consistent with this trend, pyrite, whose formation in sediments requires a supply of reactive Fe and sulfide,[382] was absent in the upper 4 cm of sediment core in L227, while it made up a maximum of 20% of total reactive Fe in the 5-17 cm depth intervals of the sediment core.[369] These multiple lines of evidence suggest that DSR is absent in the first few cm of the sediment core in L227 and occurs only in the deeper portion of the sediment, producing sulfide that reacts with reactive Fe to form pyrite.

In the seasonally stratified L227, L304 and L442, the Fe cycle in the anoxic hypolimnion is driven by the "ferrous wheel".[247, 337] Fe(III) oxyhydroxides and aggregates of Fe(III) and DOM, originating from terrestrial input and overlying water column, transit through the entire water column and deposit in the anoxic sediments at the bottom of lakes, especially during spring and fall overturn. When anoxia prevails in the deep layers of the water column during the stratification, much of the newly deposited Fe(III) is reduced at SWI and released back to the water column, while some Fe is lost to the sediment by burial and undergoes diagenesis. In the sediment, DIR can slowly reduce Fe(III) and release Fe(II) into porewater, leading to high porewater Fe(II) concentrations. Secondary minerals such as siderite could be produced during DIR. Some porewater Fe(II) and solid Fe(II) phases can react with other elements, such as sulfide produced by DSR, to form other Fe compounds (e.g., FeS and pyrite). In eutrophic L227, blooms also deliver significant phytoplankton biomass flux containing biogenic Fe(II) particles. Much of biogenic Fe(II) newly deposited phytoplankton biomass Fe(II) is quickly decomposed at the sediment-water interface (SWI) and recycled back to the water column. Some biogenic Fe(II) can be buried in the sediment and subjected to diagenesis, which can decompose the organic matter and release Fe(II) into the porewater, producing higher porewater Fe(II) concentrations compared to L304 and L442. In L227, L304 and L442, the Fe flux from sediment is composed of the diffusion of porewater Fe(II) and the release of dissolved Fe produced by reductive dissolution or decomposition at SWI, the latter of which likely dominated the Fe flux. The dissolved Fe accumulated in the hypolimnion is largely supplied by the bi-annual return of recently deposited Fe in the "ferrous wheel" rather than by porewater diffusion. This ferrous wheel plays an important role in regulating microbial activities related to Fe redox transformation.

4.3.5. Fe isotope compositions of porewater Fe and bulk sediment Fe reflect early diagenetic processes

Sediment δ^{56}Fe remains relatively constant throughout the sediment core while porewater δ^{56}Fe varies with depth in both L227 and L304. A narrow range of δ^{56}Fe values was observed for the bulk sediment Fe of L304 from the top of the core to the bottom at 12cm, with an average value of 0.13±0.15‰ (2σ) (Figure 4-11). Although δ^{56}Fe values of bulk sediment Fe in L227 were distinctly different between the 0-10 cm depth interval and the 11-35cm depth interval, the δ^{56}Fe values of bulk sediment Fe for each interval was homogeneous, with average values of 0.14±0.13‰(2σ) and –0.17±0.09‰(2σ) respectively (Figure 4-11). This distinctive pattern in bulk sediment δ^{56}Fe between 0-10 cm depth interval and 11-35 cm depth interval corresponds to the onset of the experimental fertilization in L227 whereby Fe deposited after eutrophication is isotopically more positive than that deposited before eutrophication.[298] The average δ^{56}Fe values of bulk sediments in L227 and L304 are in agreement with those measured for other lake sediments that range from –0.10±0.11‰ to 0.11±0.20‰.[200, 372] In contrast to the isotopic homogeneity of bulk sediment Fe, δ^{56}Fe values of porewater Fe(II) in both L227 and L304 increased progressively with depth, from –0.47‰ to 0.24‰ and –0.45‰ to 0.39‰, respectively (Figure 4-11). The variation in porewater δ^{56}Fe in the sediment cores of L227 and L304 is probably due to the diagenetic effect associated with organic matter diagenesis and Fe burial in lake sediments.

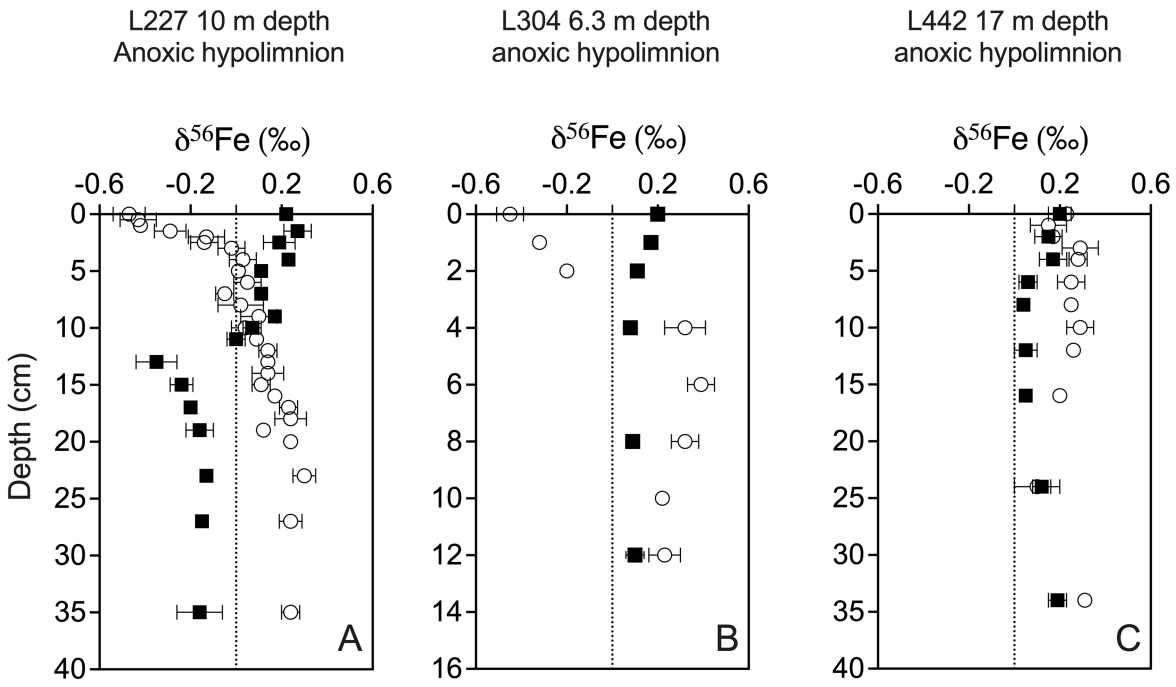


Figure 4-11 Iron isotope composition of porewater and bulk sediments in the sediment core of L227 (A), L304 (B) and L442 (C).
Error bars represent 2-SD errors. Error bars not visible are contained within the symbols.

In the upper section of sediment cores in L227 and L304, porewater $\delta^{56}Fe$ was more negative than sediment $\delta^{56}Fe$, possibly modified by initial DIR followed by the formation of siderite (Figure 4-11). DIR is known to produce aqueous Fe(II) that is enriched in light isotopes by 1-3‰ relative to the ferric substrate.[173, 181, 182] The most negative $\delta^{56}Fe$ values of porewater Fe(II) were observed in the uppermost sediments associated with high concentrations of porewater Fe(II) (Figures 4-10 and 4-11), suggesting that the isotopically light porewater Fe(II) was produced by DIR, consistent with the observations in freshwater sediments[205, 373] and marine sediments.[374, 383, 384] Partial oxidation in the near-surface sediments can also produce isotopically light porewater Fe(II). However, it appears unlikely that partial oxidation occurs in the sediment of L227 and L304 given the fact that the hypolimnia of L227 and L304 are anoxic and the concentration of porewater NO_3^- is very

low (<10 μM).[369] The most negative $\delta^{56}Fe$ values of porewater Fe(II) in L227 and L304 (−0.5 ‰ and −0.4‰ respectively, Figure 4-11) are comparable but less negative than those measured in DIR-dominated freshwater sediment (−1.1‰)[373] or DIR-dominated marine sediment (−3‰),[374] although in the latter case, the most negative values (−3‰) is likely due to the combination of DIR and partial oxidation in the surface sediments. The $\delta^{56}Fe$ values of porewater Fe(II) in L227 and L304 are plausibly explained by either smaller fractionation factors during DIR attributed to differences in Fe bonding or the combined effect of DIR and the formation of siderite (Figure 4-11). Sequential chemical extraction on the sediment core from the bottom of L227 has shown that approximately 20% of the total reactive Fe is composed of carbonate-associated minerals, most likely siderite or ankerite.[369] One experimental study on Fe isotope fractionation during siderite precipitation has estimated an equilibrium fractionation $\Delta^{56}Fe_{Fe(II)aq\text{-}siderite}$ between aqueous Fe(II) and siderite of +0.48 ± 0.22‰, at 20 °C.[189] In addition, one experimental study on the Fe isotope fractionation during the formation of siderite coupled with the microbial reduction of ferrihydrite estimated an equilibrium fractionation of 0.9% between aqueous Fe(II) and Ca-substituted siderite.[173] The formation of siderite that is enriched in light isotopes can affect $\delta^{56}Fe$ values of porewater Fe(II) in a direction opposite to the effect of DIR, driving the $\delta^{56}Fe$ of porewater Fe(II) towards less negative values (Figure 4-11).

In L227, the decomposition of biomass Fe(II) also significantly contributes to porewater Fe(II). The Fe(II) released from the decomposition should have similar $\delta^{56}Fe$ values as the particulate Fe(II) in the epilimnion and metalimnion during the bloom, ranging from −0.16‰ to −0.72‰. Therefore, the isotopically light porewater $\delta^{56}Fe$ in the upper

section of sediment cores in L227 is likely modified by the combination of DIR and the decomposition of buried biomass Fe(II).

In the deeper portion of sediments in L227 (11-35 cm) and L304 (4-12 cm), porewater Fe(II) had positive δ^{56}Fe values of 0.17±0.13‰(2σ) and 0.23±0.13‰(2σ) respectively, isotopically heavier than corresponding bulk sediment Fe by 0.1~0.5‰ (Figure 4-11). The positive δ^{56}Fe values of porewater Fe(II) are probably caused by the precipitation of Fe sulfides (FeS and pyrite), as observed in other organic-rich lake sediments where δ^{56}Fe values of 0.2~1‰ in porewater Fe are attributed to the formation of Fe sulfides.[61, 200] The formation of FeS such as mackinawite cannot explain the positive δ^{56}Fe values of porewater Fe(II) in L227 and L304, as this process leads to the enrichment of light isotopes in aqueous Fe(II) relative to FeS at near-neutral pH [190] and multiple spectroscopic techniques did not identify the presence of FeS in the sediment core of L227.[369] As mentioned previously, pyrite represented up to 20% of total reactive Fe in the deeper portion (5-17 cm) of sediment core in L227. The formation of pyrite could lead to the enrichment of heavy isotopes in aqueous Fe(II) relative to pyrite. Experimental studies on the Fe isotope fractionation during the formation of pyrite at low temperatures demonstrate that the kinetically controlled fractionation $\Delta^{56}Fe_{Fe(II)aq\text{-}pyrite}$ between aqueous Fe(II) and pyrite varies from 0.5 to 2.2‰, in which the magnitude of $\Delta^{56}Fe_{Fe(II)aq\text{-}pyrite}$ depends on the precipitation rates and the extent of isotope exchange.[385, 386] One recent study on the formation of pyrite in the euxinic water column of the Black Sea estimate an Fe isotope fractionation factor $\Delta^{56}Fe_{Fe(II)aq\text{-}pyrite}$ between aqueous Fe(II) and pyrite of 2.75±0.02‰.[386] Furthermore, another study on the marine sulfide-rich sediment observed that the apparent fractionation between porewater Fe(II) and

pyrite was up to 1.5‰.[374] Therefore, the positive δ^{56}Fe values of porewater Fe(II) in the deeper portion of sediment in L227 and L304 are likely caused by the precipitation of pyrite.

In L442, porewater Fe and bulk sediment Fe both displayed similar Fe isotope patterns, with average values of 0.23±0.13‰(2σ) and 0.12±0.10‰(2σ), respectively (Figure 4-11). This similarity in δ^{56}Fe between porewater Fe and bulk sediment Fe suggests that extensive DIR in L442 is near-complete, producing no change in δ^{56}Fe values of porewater Fe, similar to what has been observed in other lake sediments.[200, 372] Despite the lack of knowledge regarding sediment Fe speciation in L442, the slightly more positive δ^{56}Fe values of porewater Fe compared to bulk sediment Fe are probably due to the formation of siderite or pyrite, which could make aqueous Fe(II) isotopically more positive.

4.3.6. The flux of Fe from sediments in the hypolimnion of L227

The total flux of Fe from sediments is composed of the diffusion of porewater Fe(II) and the release of dissolved Fe produced by the decomposition of biomass Fe(II) and reductive dissolution of Fe(III) oxyhydroxides at sediment-water interface. The high porewater Fe(II) concentrations and the steep concentration gradient in the uppermost zone of the sediment cores collected at the bottom of L227 (Figure 4-10) indicate a substantial Fe flux through the diffusion of porewater. However, the diffusion flux is expected to be much lower than Fe flux produced at SWI. Total sediment Fe flux is retarded during the turnover in spring and fall, as the introduction of oxygen provides a barrier near the sediment-water interface. Chemical oxidation rates of diffusing Fe(II) is fast at the pH of these lakes, preventing porewater Fe from diffusing into the water column. During stratification, the

onset of anoxia releases this constraint on the upward Fe flux from the sediments, leading to accumulation of dissolved Fe in the hypolimnion of L227 (Figure 4-3).

Fe/Al molar ratio in sediments are commonly used to investigate authigenic Fe enrichment. The Fe/Al molar ratio of the sediment core collected from the bottom of L227 is 0.38±0.06, lower than the Fe/Al molar ratio in particulate Fe in the water column (0.54±0.15). The lower Fe/Al molar ratio in the sediments suggests that a significant portion of newly deposited particulate Fe, including settling biogenic Fe (biomass and Fe-DOM aggregates) and precipitated Fe(III) oxyhydroxides resulting from the oxidation of dissolved Fe(II) during the fall and spring overturn, is subsequently released back into the hypolimnion during stratification. Furthermore, this indicates that the sediments are effectively mined for Fe by the Fe cycling processes in the lakes. This idea finds further support in the observation that there is considerable sediment contact area between sediment and the hypolimnetic water column (Figure 4-1).

Porewater $\delta^{56}Fe$ at 0-1 cm of sediment core was more negative by 0.4‰ as compared to dissolved $\delta^{56}Fe$ at 10 m (Figures 4-4 and 4-11), suggesting that dissolved $\delta^{56}Fe$ produced at the sediment-water interface produce dissolved Fe that is more positive than porewater $\delta^{56}Fe$ at the top of sediment core. The total flux of Fe from sediments could be estimated by the accumulation of dissolved Fe mass in the hypolimnion during the stratification and the contact area between sediment and hypolimnetic water column. The flux of porewater Fe diffusion could be calculated by the concentration gradient of porewater Fe in the uppermost sediment section. Additionally, the flux of dissolved Fe resulting from Fe released at sediment-water interface could be estimate by the difference between total flux and the

diffusing flux. The calculation of Fe flux from sediment will be the subject of further research.

4.4. Conclusion

Fe isotopes provide valuable insights into the Fe cycling in the seasonally anoxic Boreal Shield lakes. The Fe cycling in the oxic layers of four lakes is regulated by a combination of multiple processes, including biological uptake, photochemical reduction of particulate Fe(III), complexation of dissolved Fe and dissolved organic matter, photolysis and microbial decomposition, which together produce systematically positive $\Delta^{56}Fe_{dis\text{-}part}$ between dissolved Fe and particulate Fe. In the anoxic layers of four lakes, microbial Fe oxidation, probably photoferrotrophy, modifies the $\delta^{56}Fe$ of particulate Fe, inducing large negative $\Delta^{56}Fe_{dis\text{-}part}$. Spatial and temporal changes in $\Delta^{56}Fe_{dis\text{-}part}$ were observed in the anoxic hypolimnion, likely caused by variations in the oxidation rate of photoferrotrophy. The dissolved Fe pool in the anoxic hypolimnion is governed by the flux of Fe from sediments, where DIR produces significant quantities of porewater Fe(II). During the water mixing in spring and fall, Fe(III) oxyhydroxides precipitate from the oxidation of dissolved Fe(II) in the water column and sink to underlying sediments. These newly deposited Fe(III) oxyhydroxides are reduced by DIR in the presence of abundant organic matter, leading to high porewater Fe(II) in the sediment. During the stratification, anoxia prevails in the hypolimnion, allowing a large portion of Fe in the sediment to escape into the anoxic hypolimnion through the diffusion of porewater Fe and the release of dissolved Fe via reductive dissolution at the sediment-water interface.

Chapter 5
Conclusions and recommendations

5.1. Major conclusions with implications

The overall goal of this thesis research was to evaluate the use of Fe isotopes to track the source of Fe for cyanobacteria and to investigate the Fe processes in water column and sediments of stratified boreal lakes, providing valuable new insights into the Fe cycling in modern and ancient environments. The key findings and their implications of each research chapter are described below.

In Chapter 2, the first comprehensive data on Fe isotopes of stream inflows, dissolved and particulate phases in the water column and bulk sediments of any freshwater lakes is presented. There was a positive correlation between dissolved Fe concentrations and DOC concentrations in boreal streams, implying a strong binding of Fe by DOC. Dissolved Fe in boreal streams exhibit a larger range of δ^{56}Fe (–0.2 to +0.6‰), with the positive values reflecting the net effect of processes involved in DOM mobilization of Fe in these boreal streams. Large variations of δ^{56}Fe observed in IISD-ELA among boreal streams and with season demonstrate the strong potential for Fe isotopic techniques to decipher sources of Fe and seasonally variable Fe-DOC complexation in streams in order to understand the coupled contributions of DOC and Fe to brownification of water in northern catchments worldwide.

A wide range in δ^{56}Fe (–0.9 to +1.8‰) is observed in the water column of two small Boreal Shield lakes, spanning more than half the entire range of natural samples. Such variation is likely induced by Fe isotope fractionation arising from Fe cycling processes, reflecting the potential of Fe isotopes to track biogeochemical processes in Boreal Shield

lakes. One of the novel and notable findings is that two water column layers with distinctive and contrasting isotope fractionations between dissolved and particulate Fe were observed in two boreal lakes despite large differences in their trophic states. Uptake of isotopically light Fe by cyanobacteria likely fractionates Fe, leading to fractionation $\Delta^{56}Fe_{dis\text{-}spm}$ of 1‰ between dissolved and particulate Fe in the epilimnion. This is the first time that Fe isotope fractionation arising from cyanobacterial uptake is observed in freshwater, which can be used to understand the sources of reduced Fe that fuel harmful cyanobacterial blooms and further aid the management of waters affected by these blooms.

Patterns in Fe isotopes are similarly reversed from epilimnia to anoxic hypolimnia in both lakes. The large isotope fractionation in the anoxic hypolimnion indicated that there must be some fractionating mechanism involving Fe cycling between Fe(II) and Fe(III) within the water column, likely photoferrotrophy or microaerophilic Fe(II) oxidation, in the hypolimnia that were previously thought to be quiescent. This important Fe cycling is active enough to change the isotopic signature of Fe (and C and N) in the hypolimnia even by early summer, suggesting robust activity of Fe oxidizers and reducers that live in the water columns in these small headwater lakes. This is the first time large Fe isotope fractionation in the anoxic zone is possibly associated with photoferrotrophy, providing insights into the deposition of banded iron formations and biogeochemical processes of Fe cycling in early Earth history. The biogeochemical processes suggested by distinctive Fe isotope signatures, along with the low sulfate and high Fe conditions in the water column, show the potential of Boreal Shield lakes to serve as Archean ocean analogues.

All the particulate samples in the epilimnia of both lakes have $\delta^{56}Fe$ values almost identical to those of the epilimnetic surficial sediments, both in L227, where algal biomass is

high and in L442, where it is very low, suggesting that in the epilimnia of both lakes, particulates are deposited as surficial sediments without significant diagenetic effects on the Fe isotope signals. Therefore, the $\delta^{56}Fe$ of lake sediments may serve as an archive that records past changes in the Fe cycling of lakes.

The large fractionations observed as a result of Fe cycling in these small boreal lakes demonstrate that stable Fe isotopes are a powerful new tool to understand biogeochemical Fe cycling, the role of Fe metabolism in lakes and the sources of reduced Fe that fuels cyanobacterial blooms.

In Chapter 3, the first comprehensive data on Fe speciation and Fe isotopes associated with cyanobacterial bloom in freshwater ecosystems is presented. Fe concentration, speciation, and isotope compositions all exhibit seasonal variations corresponding to the progression of two annual blooms in L227, a small experimentally eutrophic Boreal Shield lake.

The onset of cyanobacterial bloom leads to a drawdown of dissolved Fe and an increase in particulate Fe in the oxic layers of L227, possibly due to the intracellular uptake of Fe. Furthermore, the depletion of Fe(II) in the dissolved phase and the prevalence of Fe(II) in the particulate phase are observed during the cyanobacterial bloom, likely resulting from the uptake of Fe(II) by cyanobacteria. This is the first time that changes in dissolved and particulate Fe concentrations, along with Fe speciation during a cyanobacterial bloom, are reported in the freshwater system. This study highlights the importance of Fe(II) in the dominance of cyanobacteria. Fe speciation of DFe and PFe during the cyanobacterial bloom might provide useful insights to explore the uptake mechanism utilized by cyanobacteria.

During the peak of the first cyanobacterial bloom, $\Delta^{56}Fe_{dis\text{-}part}$ fractionation in the metalimnion was considerably larger than $\Delta^{56}Fe_{dis\text{-}part}$ in the epilimnion (1.3‰ vs 0.9‰). Likewise, the particulate $\delta^{56}Fe$ is more negative by 0.4‰ in the metalimnion than in the epilimnion. Particulate Fe(II) in the metalimnion is two times higher than particulate Fe(II) in the epilimnion. Collectively, this evidence suggests that under Fe-limited conditions, cyanobacteria could further migrate to an anoxic zone to take up Fe and then rise to more favourable light conditions through buoyancy regulation. A simple isotopic mass balance modelling was used to test the migration of cyanobacteria from the oxic layer to the anoxic layer in L227. This study is the first time that Fe speciation and Fe isotope composition were used to track the vertical migration of cyanobacteria. The results demonstrate that the most plausible explanation for both isotopically light particulate Fe and total Fe (sums of dissolved Fe and particulate Fe) is the migration of cyanobacteria below the redox boundary for the uptake of dissolved Fe(II). Distinct $\delta^{56}Fe$ of dissolved and particulate Fe in the epilimnion and metalimnion could provide valuable sights for the source of Fe used by cyanobacteria if the Fe isotope fractionation factor can be measured under controlled laboratory conditions and it is independent of Fe concentrations.

Dissolved $\delta^{56}Fe$ differs from particulate $\delta^{56}Fe$ in the oxic layers of L227 after the onset of the cyanobacterial bloom and both change seasonally during phytoplankton succession from cyanobacteria dominance to co-dominance of cyanobacteria and eukaryotic algae. The $\Delta^{56}Fe_{dis\text{-}part}$ fractionation during the second bloom is much smaller than $\Delta^{56}Fe_{dis\text{-}part}$ during the first bloom, suggesting that chlorophytes might produce distinct Fe isotope fractionation during Fe acquisition compared to diazotrophic cyanobacteria. This study represents the first field evidence demonstrating that Fe isotope fractionation may vary

among phytoplankton species during Fe acquisition. The specific transport pathways and enzymatic processes employed by phytoplankton during Fe acquisition might influence Fe isotope fractionation. Different species, in this particular case cyanobacteria and chlorophytes, may produce distinct Fe isotope fractionation patterns during biological uptake. If this is the case, then δ^{56}Fe of dissolved Fe and particulate Fe could potentially serve as a diagnostic tool for investigating the source of Fe for cyanobacteria and eukaryotic algae, and evaluating the role of Fe in the competition between cyanobacteria and eukaryotic algae.

Stable Fe isotopes show great potential in deciphering the source of Fe for cyanobacterial blooms. The isotope results suggest that cyanobacteria could access abundant Fe by migrating to an anoxic zone. The internal Fe loading from the sediment after the onset of anoxia could continually support the activity of cyanobacteria during the bloom despite extremely low concentrations of dissolved Fe in the oxic layers. As a result, Fe availability is unlikely a limiting factor for cyanobacteria in L227. Furthermore, onset of the first cyanobacterial bloom occurs shortly after the stratification of L227, suggesting that internal Fe loading from sediment could be an important Fe source for the formation of cyanobacterial bloom, consistent with the observation that sediment anoxia and internal Fe loading are identified as precursor factors for cyanobacterial bloom in several lakes. Understanding the role of Fe in the formation of cyanobacterial bloom and determining the availability and source of Fe for cyanobacterial uptake are crucial for assessing triggers for the onset of cyanobacterial bloom and evaluating corresponding management options.

Chapter 4 presents temporal and spatial variations in Fe isotope fractionation between dissolved Fe and particulate Fe in the anoxic hypolimnia of Boreal Shield lakes, along with

the Fe isotope compositions of porewater and sediment in sediment cores collected from the lake bottoms.

Contrary to the traditional limnological paradigm, where hypolimnia of small lakes simply accumulate products of sediment and water column diagenesis of surface derived material during the stratified period, Fe isotopes elucidate the importance of novel Fe cycling pathways in the hypolimnia of small boreal lakes. For the first time, spatial and temporal variations in $\Delta^{56}Fe_{dis\text{-}part}$ fractionations were observed in the anoxic hypolimnia of Boreal Shield lakes, likely due to active microbial Fe oxidation occurring *in situ* throughout the anoxic hypolimnion rather than *in situ* abiotic Fe processes and settling of particulate Fe from the oxic layers or the redox boundary. The wide range of $\Delta^{56}Fe_{dis\text{-}part}$ fractionations observed in this study suggested that microbial Fe oxidation might produce distinct $\Delta^{56}Fe_{dis\text{-}part}$ fractionation patterns corresponding to the change in environmental conditions. Supported by 16S rRNA gene sequence data and metagenome sequence data, the observed $\Delta^{56}Fe_{dis\text{-}part}$ fractionations in the anoxic hypolimnion are probably produced by photoferrotrophy, and the variations in $\Delta^{56}Fe_{dis\text{-}part}$ fractionations are likely due to the different oxidation rates of photoferrotrophy which was affected by the change of Fe concentrations or light intensities. The large Fe isotope fractionation in the anoxic hypolimnion, likely due to photoferrotrophy, suggests that photoferrotrophs could thrive in the low-light conditions of anoxic ferruginous deep water, lending the idea that photoferrotrophy may have played a substantial role in the deep layer of the Precambrian ocean. Highly variable and positive $\delta^{56}Fe$ of particulate Fe, likely produced by *in situ* photoferrotrophy, is within the range of $\delta^{56}Fe$ observed in the Fe oxides minerals in BIF. This observation supports the idea that photoferrotrophy could have

played a substantial role in the production of ferric Fe during the formation of BIF, where the produced Fe(III) oxyhydroxides are the precursor of Fe oxide minerals in the BIF.

DIR dominates organic mineralization pathways in anoxic sediments. A consistently high porewater Fe concentration (primarily Fe(II)) throughout the sediment core (mainly Fe(II)), along with a steep gradient in the uppermost zone, demonstrated that the source of Fe in the hypolimnion during stratification results from an intensive Fe flux from anoxic sediment, which is generated by DIR in the presence of abundant organic carbon. This intensive internal Fe cycling is remarkable, considering the entire water column undergoes mixing twice a year. The lower Fe_T/Al ratio in the sediments of L227, compared to that in the particulate Fe in the water column of L227, suggests that most of the newly deposited Fe is progressively released back into the hypolimnion through diffusion and reductive dissolution by DIR in the sediment during the stratification. The negative $\delta^{56}Fe$ values of porewater Fe(II) in the upper portion of sediments likely result from the initial DIR and the subsequent precipitation of siderite. The dissimilarity in $\delta^{56}Fe$ values between dissolved Fe(II) in the anoxic hypolimnion and porewater Fe(II) near the SWI suggest that the flux of Fe from sediments to the water column is composed of diffusing porewater Fe(II) and dissolved Fe produced by reductive dissolution at SWI. The less negative $\delta^{56}Fe$ of dissolved Fe in the hypolimnion compared to $\delta^{56}Fe$ of porewater suggests that reductive dissolution at SWI is likely near complete, producing isotopically heavy dissolved Fe that is equal to $\delta^{56}Fe$ in bulk sediments. This is consistent with the similarity of the $\delta^{56}Fe$ of dissolved Fe in the hypolimnion and the $\delta^{56}Fe$ of particulate Fe in the epilimnion.

Combining oxygenic photosynthesis facilitated by cyanobacteria in the oxic surface layers, photoferrotrophy inferred in the anoxic bottom layers, and DIR in the organic

sediment, these active Fe processes in L227 collectively show the potential of seasonally anoxic Boreal Shield lakes as an analog of late Archean ocean and the use of Fe isotopes to unravel the Fe cycle in freshwater lakes.

5.2. Recommendations for Future Research

The key findings in this thesis suggest several avenues for future research in the field of Fe isotope and Fe geochemistry, both in laboratory studies and natural settings.This research shows that cyanobacteria in the water column of L227 likely preferential use Fe(II) rather than Fe(III). Fe-uptake mechanisms of cyanobacteria could be further examined in the enrichment cultures using oxic water samples from L227. Further experimental studies may be required to measure Fe isotope fractionation during biological uptake using representative cyanobacteria and eukaryotic algae under different N and P conditions. The source of Fe for cyanobacterial blooms could differ among ecosystems. Therefore, the pattern in δ^{56}Fe and associated fractionation need to be examined systematically among lakes where variation in organic matter supply, geology and lake characteristics may influence the Fe isotope signals. If patterns and behaviors of δ^{56}Fe related to cyanobacterial blooms are exhibited, then Fe isotopes hold great promise to track Fe sources and related processes for the formation of cyanobacterial blooms and to investigate the relative importance of different Fe sources in reservoirs and lakes worldwide. Integrative modelling work, which incorporates cycling of C, N and Fe with their stable isotopes, could be utilized to predict the occurrence of cyanobacterial bloom and develop management approaches. Moreover, Fe is not the sole essential micronutrient for cyanobacteria. Future lake studies with improved spatial and

temporal resolutions could be used to track the progression of blooms in the context of the uptake of other micronutrients (e.g., Mn and Mo).

Confirmation of photoferrotrophy in the anoxic hypolimnia of L221, L227 and L304 requires further investigation. Photoferrotrophic activity needs to be demonstrated in field incubations or enrichment cultures in the laboratory for L221, L227 and L304. Active Fe cycling, including the potential occurrence of photoferrotroph and microaerophilic Fe(II) oxidation inferred in the anoxic layers of Boreal Shield lakes, highlights the potential of Boreal Shield lakes as Archean ocean analogues. Other processes such as nitrate-reducing Fe(II) oxidation, Fe(II) oxidation by O_2 produced by cyanobacteria, Fe-ammox, Fe(III)-dependent anaerobic methane oxidation and sulfur redox reactions can be examined in these lakes in the context of early Earth research, shedding light on the relative importance of these processes in modern and ancient environments.

References

(1) Taylor, S. R.; McLennan, S. M.; Armstrong, R. L.; Tarney, J. The Composition and Evolution of the Continental Crust: Rare Earth Element Evidence from Sedimentary Rocks [and Discussion]. *Philosophical Transactions of the Royal Society of London. Series A, Mathematical and Physical Sciences* **1981**, *301* (1461), 381-399. (acccessed 2023/08/02/).JSTOR.
(2) Kendall, B.; Anbar, A. D.; Kappler, A.; Konhauser, K. The global iron cycle. In *Fundamentals of Geobiology*, Knoll, A. H., Canfield, D. E., Konhauser, K. Eds.; Wiley-Blackwell, 2012.
(3) Knoll, A. H.; Canfield, D. E.; Konhauser, K. Fundamentals of Geobiology. Wiley-Blackwell: Hoboken, NY, 2012.
(4) Buerge, I. J.; Hug, S. J. Influence of mineral surfaces on chromium (VI) reduction by iron(II). *Environ Sci Technol* **1999**, *1999*, 4285-4291.
(5) Chen, W.; Parette, R.; Zou, J.; Cannon, F. S.; Dempsey, B. A. Arsenic removal by iron-modified activated carbon. *Water Res* **2007**, *41* (9), 1851-1858. DOI: 10.1016/j.watres.2007.01.052.
(6) Liger, E.; Charlet, L.; Cappellen, P. V. Surface catalysis of uranium(VI) reduction by iron(II). *Geochim Cosmochim Acta* **1999**, *63* (19/20), 2939-2955.
(7) Elsner, M.; Schwarzenbach, R. P.; Haderlein, S. B. Reactivity of Fe(II)-bearing minerals toward reductive transformation of organic contaminants. *Environ Sci Technol* **2004**, *38*, 799-807.
(8) Strathmann, T. J.; Stone, A. T. Mineral surface catalysis of reactions between FeII and oxime carbamate pesticides. *Geochim. Cosmochim. Acta.* **2003**, *67* (15), 2775-2791. DOI: 10.1016/s0016-7037(03)00088-7.
(9) Muehe, E. M.; Obst, M.; Hitchcock, A.; Tyliszczak, T.; Behrens, S.; Schroder, C.; Byrne, J. M.; Michel, F. M.; Kramer, U.; Kappler, A. Fate of Cd during microbial Fe(III) mineral reduction by a novel and Cd-tolerant Geobacter species. *Environ Sci Technol* **2013**, *47* (24), 14099-14109. DOI: 10.1021/es403365w.
(10) Glodowska, M.; Stopelli, E.; Schneider, M.; Lightfoot, A.; Rathi, B.; Straub, D.; Patzner, M.; Duyen, V. T.; AdvectAs Team, M.; Berg, M.; et al. Role of in Situ Natural Organic Matter in Mobilizing As during Microbial Reduction of Fe(III)-Mineral-Bearing Aquifer Sediments from Hanoi (Vietnam). *Environ Sci Technol* **2020**, *54* (7), 4149-4159. DOI: 10.1021/acs.est.9b07183.
(11) Borch, T.; Kretzschmar, R.; Kappler, A.; Cappellen, P. V.; Ginder-Vogel, M.; Voegelin, A. R.; Campbell, K. Biogeochemical redox processes and their impact on contaminant dynamics. *Environ Sci Technol* **2010**, *44*, 15-23.
(12) Stumm, W.; Morgan, J. J. *Aquatic Chemistry: Chemical Equilibria and Rates in Natural Waters*; John Wiley & Sons, 1996.
(13) Rose, A. L.; Waite, T. D. Kinetics of iron complexation by dissolved natural organic matter in coastal waters. *Mar. Chem.* **2003**, *84* (1-2), 85-103. DOI: 10.1016/s0304-4203(03)00113-0.
(14) Catrouillet, C.; Davranche, M.; Dia, A.; Bouhnik-Le Coz, M.; Marsac, R.; Pourret, O.; Gruau, G. Geochemical modeling of Fe(II) binding to humic and fulvic acids. *Chem. Geol.* **2014**, *372*, 109-118. DOI: 10.1016/j.chemgeo.2014.02.019.

(15) Weber, T.; Allard, T.; Tipping, E.; Benedetti, M. F. Modeling Iron Binding to Organic Matter. *Environmental Science & Technology* **2006**, *40* (24), 7488-7493. DOI: 10.1021/es0607077.
(16) Lee, Y. P.; Fujii, M.; Kikuchi, T.; Terao, K.; Yoshimura, C. Variation of iron redox kinetics and its relation with molecular composition of standard humic substances at circumneutral pH. *PLoS One* **2017**, *12* (4), e0176484. DOI: 10.1371/journal.pone.0176484.
(17) Theis, T. L.; Singer, P., C. Complexation of Iron(ll) by Organic Matter and Its Effect on Iron(ll) Oxygenation. *Environ Sci Technol* **1974**, *8* (6).
(18) Jobin, R.; Ghosh, i. M. Effect of Buffer Intensity and Organic Matter on the Oxygenation of Ferrous Iron. *J. Am. Water Works Assoc* **1972**, *64* (9), 590-595. DOI: 10.1002/j.1551-8833.1972.tb02752.x.
(19) Daugherty, E. E.; Gilbert, B.; Nico, P. S.; Borch, T. Complexation and Redox Buffering of Iron(II) by Dissolved Organic Matter. *Environ Sci Technol* **2017**, *51* (19), 11096-11104. DOI: 10.1021/acs.est.7b03152.
(20) Powell, R. T.; Donat, J. R. Organic complexation and speciation of iron in the South and Equatorial Atlantic. *Deep-Sea Research II* **2001**, *48*, 2877-2893.
(21) Rue, E. L.; Bruland, K. W. The role of organic complexation on ambient iron chemistry in the equatorial Pacific Ocean and the response of a mesoscale iron addition experiment. *Limnol. Oceanogr.* **1997**, *42* (5), 901-910. DOI: 10.4319/lo.1997.42.5.0901.
(22) Van den Berg, C. M. G. Evidence for organic complexation of iron in seawater. *Mar. Chem.* **1995**, *50* (139-157).
(23) Gledhill, M.; Van den Berg, C. M. G. Determination of complexation of iron(III) with natural organic complexing ligands in seawater using cathodic stripping voltammetry. *Mar. Chem.* **1994**, *47*, 41-54.
(24) Meunier, L.; Laubscher, H.; Hug, S. J.; Sulzberger, B. Effects of size and origin of natural dissolved organic matter compounds on the redox cycling of iron in sunlit surface waters. *Aquat. Sci.* **2005**, *67* (3), 292-307. DOI: 10.1007/s00027-005-0779-0.
(25) Davison, W.; Seed, G. The kinetics of the oxidation of ferrous iron in synthetic and natural waters. *Geochim Cosmochim Acta* **1982**, *47*, 67-69.
(26) Madison, A. S.; Tebo, B. M.; Mucci, A.; Sundby, B.; Luther III, G. W. Abundant oorewater Mn(III) is a major component of the sedimentary redox system. *Science.* **2013**, *341*, 875-878.
(27) Sørensen, J.; Thorling, L. Stimulation by lepidocrocite (7-FeOOH) of Fe(II)-dependent nitrite reduction. *Geochim. Cosmochim. Acta.* **1991**, *55* (5), 1289-1294. DOI: https://doi.org/10.1016/0016-7037(91)90307-Q.
(28) Melton, E. D.; Swanner, E. D.; Behrens, S.; Schmidt, C.; Kappler, A. The interplay of microbially mediated and abiotic reactions in the biogeochemical Fe cycle. *Nat Rev Microbiol* **2014**, *12* (12), 797-808. DOI: 10.1038/nrmicro3347.
(29) Yao, W.; Millero, F. J. Oxidation of hydrogen sulfide by hydrous Fe(III) oxides in seawater *Mar. Chem.* **1996**, *52*, 1-16.
(30) Lueder, U.; Jorgensen, B. B.; Kappler, A.; Schmidt, C. Photochemistry of iron in aquatic environments. *Environ Sci Process Impacts* **2020**, *22* (1), 12-24. DOI: 10.1039/c9em00415g.
(31) Barbeau, K.; Rue, E. L.; Bruland, K. W.; A., B. Photochemical cycling of iron in the surface ocean mediated by microbial iron(III)-binding ligands. *Nature* **2001**, *413*, 409-413.

(32) Weber, K. A.; Achenbach, L. A.; Coates, J. D. Microorganisms pumping iron: anaerobic microbial iron oxidation and reduction. *Nat Rev Microbiol* **2006**, *4* (10), 752-764. DOI: 10.1038/nrmicro1490.
(33) Kappler, A.; Bryce, C.; Mansor, M.; Lueder, U.; Byrne, J. M.; Swanner, E. D. An evolving view on biogeochemical cycling of iron. *Nat Rev Microbiol* **2021**, *19* (6), 360-374. DOI: 10.1038/s41579-020-00502-7.
(34) Emerson, D.; Moyer, C. Isolation and characterization of novel iron-oxidizing bacteria that grow at circumneutral pH. *Appl. Environ. Microbiol.* **1997**, *63* (12), 4784-4792.
(35) Emerson, D.; Fleming, E. J.; McBeth, J. M. Iron-oxidizing bacteria: an environmental and genomic perspective. *Annu Rev Microbiol* **2010**, *64*, 561-583. DOI: 10.1146/annurev.micro.112408.134208.
(36) Druschel, G. K.; Emerson, D.; Sutka, R.; Suchecki, P.; Luther, G. W. Low-oxygen and chemical kinetic constraints on the geochemical niche of neutrophilic iron(II) oxidizing microorganisms. *Geochim. Cosmochim. Acta.* **2008**, *72* (14), 3358-3370. DOI: 10.1016/j.gca.2008.04.035.
(37) Chiu, B. K.; Kato, S.; McAllister, S. M.; Field, E. K.; Chan, C. S. Novel Pelagic Iron-Oxidizing Zetaproteobacteria from the Chesapeake Bay Oxic-Anoxic Transition Zone. *Front Microbiol* **2017**, *8*, 1280. DOI: 10.3389/fmicb.2017.01280.
(38) McAllister, S. M.; Moore, R. M.; Gartman, A.; Luther, G. W.; Emerson, D.; Chan, C. S. The Fe(II)-oxidizing Zetaproteobacteria: historical, ecological and genomic perspectives. *FEMS Microbiol Ecol* **2019**, *95* (4). DOI: 10.1093/femsec/fiz015.
(39) Maisch, M.; Lueder, U.; Laufer, K.; Scholze, C.; Kappler, A.; Schmidt, C. Contribution of Microaerophilic Iron(II)-Oxidizers to Iron(III) Mineral Formation. *Environ Sci Technol* **2019**, *53* (14), 8197-8204. DOI: 10.1021/acs.est.9b01531.
(40) Widdel, F.; Schnell, S.; Heising, S.; Ehrenreich, A.; Assmus, B.; Schink, B. Ferrous iron oxidation by anoxygenic phototrophic bacteria. *Nature* **1993**, *362* (6423), 834-836.
(41) Kuhl, M.; Lassen, C.; Jorgensen, B. B. Light penetration and light intensity in sandy marine sediments measured with irradiance and scalar irradiance fiber-optic microprobes. *Mar. Ecol. Prog. Ser.* **1994**, *105*, 139-148.
(42) Hegler, F.; Posth, N. R.; Jiang, J.; Kappler, A. Physiology of phototrophic iron(II)-oxidizing bacteria: implications for modern and ancient environments. *FEMS Microbiol Ecol* **2008**, *66* (2), 250-260. DOI: 10.1111/j.1574-6941.2008.00592.x.
(43) Overmann, J.; Garcia-Pichel, F. *The phototrophic way of life*; Springer, 2000.
(44) Straub, K. L.; Benz, M.; Schink, B.; Widdel, F. Anaerobic, nitrate-dependent microbial oxidation of ferrous iron. *Appl. Environ. Microbiol.* **1996**, *62* (4), 1458-1460.
(45) Blothe, M.; Roden, E. E. Composition and activity of an autotrophic Fe(II)-oxidizing, nitrate-reducing enrichment culture. *Appl Environ Microbiol* **2009**, *75* (21), 6937-6940. DOI: 10.1128/AEM.01742-09.
(46) Laufer, K.; Roy, H.; Jorgensen, B. B.; Kappler, A. Evidence for the Existence of Autotrophic Nitrate-Reducing Fe(II)-Oxidizing Bacteria in Marine Coastal Sediment. *Appl Environ Microbiol* **2016**, *82* (20), 6120-6131. DOI: 10.1128/AEM.01570-16.
(47) Muehe, E. M.; Gerhardt, S.; Schink, B.; Kappler, A. Ecophysiology and the energetic benefit of mixotrophic Fe(II) oxidation by various strains of nitrate-reducing bacteria. *FEMS Microbiol Ecol* **2009**, *70* (3), 335-343. DOI: 10.1111/j.1574-6941.2009.00755.x.
(48) Straub, K. L.; Schönhuber, W. A.; Buchholz-Cleven, B. E. E.; Schink, B. Diversity of Ferrous Iron-Oxidizing, Nitrate-Reducing Bacteria and their Involvement in Oxygen-

Independent Iron Cycling. *Geomicrobiol. J.* **2004**, *21* (6), 371-378. DOI: 10.1080/01490450490485854.
(49) Carlson, H. K.; Clark, I. C.; Melnyk, R. A.; Coates, J. D. Toward a mechanistic understanding of anaerobic nitrate-dependent iron oxidation: balancing electron uptake and detoxification. *Front Microbiol* **2012**, *3*, 57. DOI: 10.3389/fmicb.2012.00057.
(50) Klueglein, N.; Kappler, A. Abiotic oxidation of Fe(II) by reactive nitrogen species in cultures of the nitrate-reducing Fe(II) oxidizer Acidovorax sp. BoFeN1 - questioning the existence of enzymatic Fe(II) oxidation. *Geobiology.* **2013**, *11* (2), 180-190. DOI: 10.1111/gbi.12019.
(51) Lovley, D. R.; Phillips, E. J. P. Competitive mechanisms for inhibition of sulfate reduction and methane production in the zone of ferric iron reduction in sediments. *Appl Environ Microbiol* **1987**, 2636-2641.
(52) Lovley, D. R. Dissimilatory Fe(III) and Mn(IV) reduction. *Microbiological Reviews* **1991**, *55* (2), 259-287.
(53) Roden, E. E.; Zachara, J. M. Microbial reduction of crystalline iron(III) oxides: influence of oxide surface area and potential for cell growth. *Environ Sci Technol* **1996**, *30*, 1618-1628.
(54) Kostka, J. E.; Dalton, D. D.; Skelton, H.; Dollhopf, S.; Stucki, J. W. Growth of iron(III)-reducing bacteria on clay minerals as the sole electron acceptor and comparison of growth yields on a variety of oxidized iron forms. *Appl Environ Microbiol* **2002**, *68* (12), 6256-6262. DOI: 10.1128/AEM.68.12.6256-6262.2002.
(55) Salas, E. C.; Berelson, W. M.; Hammond, D. E.; Kampf, A. R.; Nealson, K. H. The Impact of Bacterial Strain on the Products of Dissimilatory Iron Reduction. *Geochim Cosmochim Acta* **2010**, *74* (2), 574-583. DOI: 10.1016/j.gca.2009.10.039.
(56) Zachara, J. M.; Kukkadapu, R. K.; Fredrickson, J. K.; Gorby, Y. A.; Smith, S. C. Biomineralization of poorly crystalline Fe(III) oxides by dissimilatory metal reducing bacteria (DMRB). *Geomicrobiol. J.* **2002**, *19*, 179-207.
(57) Fredrickson, J. K.; Zachara, J. M.; Kenney, D. W.; Dong, H.; Onstott, T. C.; Hinman, N. W.; Li, S. Biogenic iron mineralization accompanying the dissimilatory reduction of hydrous ferric oxide by a groundwater bacterium. *Geochim Cosmochim Acta* **1998**, *62* (19/20), 3239-3257.
(58) Huang, S.; Jaffe, P. R. Isolation and characterization of an ammonium-oxidizing iron reducer: Acidimicrobiaceae sp. A6. *PLoS One* **2018**, *13* (4), e0194007. DOI: 10.1371/journal.pone.0194007.
(59) Clement, J.; Shrestha, J.; Ehrenfeld, J.; Jaffe, P. Ammonium oxidation coupled to dissimilatory reduction of iron under anaerobic conditions in wetland soils. *Soil Biology and Biochemistry* **2005**, *37* (12), 2323-2328. DOI: 10.1016/j.soilbio.2005.03.027.
(60) Huang, S.; Jaffé, P. R. Characterization of incubation experiments and development of an enrichment culture capable of ammonium oxidation under iron-reducing conditions. *Biogeosciences* **2015**, *12* (3), 769-779. DOI: 10.5194/bg-12-769-2015.
(61) Sivan, O.; Adler, M.; Pearson, A.; Gelman, F.; Bar-Or, I.; John, S. G.; Eckert, W. Geochemical evidence for iron-mediated anaerobic oxidation of methane. *Limnol. Oceanogr.* **2011**, *56* (4), 1536-1544. DOI: 10.4319/lo.2011.56.4.1536.
(62) Crowe, S. A.; Katsev, S.; Leslie, K.; Sturm, A.; Magen, C.; Nomosatryo, S.; Pack, M. A.; Kessler, J. D.; Reeburgh, W. S.; Roberts, J. A.; et al. The methane cycle in ferruginous Lake Matano. *Geobiology.* **2011**, *9* (1), 61-78. DOI: 10.1111/j.1472-4669.2010.00257.x.

(63) Amos, R. T.; Bekins, B. A.; Cozzarelli, I. M.; Voytek, M. A.; Kirshtein, J. D.; Jones, E. J.; Blowes, D. W. Evidence for iron-mediated anaerobic methane oxidation in a crude oil-contaminated aquifer. *Geobiology.* **2012**, *10* (6), 506-517. DOI: 10.1111/j.1472-4669.2012.00341.x.
(64) Dong, Y.; Shan, Y.; Xia, K.; Shi, L. The Proposed Molecular Mechanisms Used by Archaea for Fe(III) Reduction and Fe(II) Oxidation. *Front Microbiol* **2021**, *12*, 690918. DOI: 10.3389/fmicb.2021.690918 From NLM PubMed-not-MEDLINE.
(65) Kozubal, M.; Macur, R. E.; Korf, S.; Taylor, W. P.; Ackerman, G. G.; Nagy, A.; Inskeep, W. P. Isolation and Distribution of a Novel Iron-Oxidizing Crenarchaeon from Acidic Geothermal Springs in Yellowstone National Park. *Appl. Environ. Microbiol.* **2008**, *74* (4), 942-949. DOI: doi:10.1128/AEM.01200-07.
(66) Slobodkina, G. B.; Kolganova, T. V.; Querellou, J.; Bonch-Osmolovskaya, E. A.; Slobodkin, A. I. Geoglobus acetivorans sp. nov., an iron(III)-reducing archaeon from a deep-sea hydrothermal vent. *Int J Syst Evol Microbiol* **2009**, *59* (Pt 11), 2880-2883. DOI: 10.1099/ijs.0.011080-0 From NLM Medline.
(67) Beal, E. J.; House, C. H.; Orphan, V. J. Manganese- and Iron-Dependent Marine Methane Oxidation. *Science.* **2009**, *325* (5937), 184-187. DOI: doi:10.1126/science.1169984.
(68) Sunda, W. G.; Swift, D. G.; Huntsman, S. A. Low iron requirement for growth in oceanic phytoplankton. *Nature* **1991**, *351*, 55-57.
(69) Kasting, J. F.; Siefert, J. L. Life and the evolution of Earth's atmosphere. *Science.* **2002**, *296* (5570), 1066-1068. DOI: 10.1126/science.1071184 From NLM.
(70) Keren, N.; Aurora, R.; Pakrasi, H. B. Critical roles of bacterioferritins in iron storage and proliferation of cyanobacteria. *Plant Physiol* **2004**, *135* (3), 1666-1673. DOI: 10.1104/pp.104.042770.
(71) Schoffman, H.; Lis, H.; Shaked, Y.; Keren, N. Iron-Nutrient Interactions within Phytoplankton. *Front Plant Sci* **2016**, *7*, 1223. DOI: 10.3389/fpls.2016.01223.
(72) Whittaker, S.; Bidle, K. D.; Kustka, A. B.; Falkowski, P. G. Quantification of nitrogenase in Trichodesmium IMS 101: implications for iron limitation of nitrogen fixation in the ocean. *Environ Microbiol Rep* **2011**, *3* (1), 54-58. DOI: 10.1111/j.1758-2229.2010.00187.x.
(73) Martin, J. H.; Fitzwater, S. E. Iron deficiency limits phytoplankton growth in the north-east Pacific subarctic. *Nature* **1988**, *331*, 341-343.
(74) de Baar, H. J. W.; de Jong, J. T. M.; Bakker, D. C. E.; Loscher, B. M.; Veth, C.; Bathmann, U.; Smetacek, V. Importance of iron for plankton blooms and carbon dioxide drawdown in the Southern Ocean. *Nature* **1995**, *373*, 412-415.
(75) Kolber, Z. S.; Barber, R. T.; Coale, K. H.; Fitzwater, S. E.; Greene, R. M.; Johnson, K. S.; Lindley, S.; Falkowski, P. G. Iron limitation of phytoplankton photosynthesis in the equatorial Pacific Ocean. *Nature* **1994**, *371*, 145-149.
(76) Vrede, T.; Tranvik, L. J. Iron Constraints on Planktonic Primary Production in Oligotrophic Lakes. *Ecosystems.* **2006**, *9* (7), 1094-1105. DOI: 10.1007/s10021-006-0167-1.
(77) North, R. L.; Guildford, S. J.; Smith, R. E. H.; Havens, S. M.; Twiss, M. R. Evidence for phosphorus, nitrogen, and iron colimitation of phytoplankton communities in Lake Erie. *Limnol. Oceanogr.* **2007**, *52* (1), 315-328. DOI: 10.4319/lo.2007.52.1.0315.
(78) Lis, H.; Shaked, Y.; Kranzler, C.; Keren, N.; Morel, F. M. Iron bioavailability to phytoplankton: an empirical approach. *ISME J* **2015**, *9* (4), 1003-1013. DOI: 10.1038/ismej.2014.199.

(79) Kranzler, C.; Rudolf, M.; Keren, N.; Schleiff, E. Iron in Cyanobacteria. In *Genomics of Cyanobacteria*, Advances in Botanical Research, 2013; pp 57-105.
(80) Qiu, G. W.; Koedooder, C.; Qiu, B. S.; Shaked, Y.; Keren, N. Iron transport in cyanobacteria - from molecules to communities. *Trends Microbiol* **2022**, *30* (3), 229-240. DOI: 10.1016/j.tim.2021.06.001.
(81) Jiang, H. B.; Lou, W. J.; Ke, W. T.; Song, W. Y.; Price, N. M.; Qiu, B. S. New insights into iron acquisition by cyanobacteria: an essential role for ExbB-ExbD complex in inorganic iron uptake. *ISME J* **2015**, *9* (2), 297-309. DOI: 10.1038/ismej.2014.123.
(82) Lis, H.; Kranzler, C.; Keren, N.; Shaked, Y. A Comparative Study of Iron Uptake Rates and Mechanisms amongst Marine and Fresh Water Cyanobacteria: Prevalence of Reductive Iron Uptake. *Life (Basel)* **2015**, *5* (1), 841-860. DOI: 10.3390/life5010841.
(83) Kowata, H.; Tochigi, S.; Takahashi, H.; Kojima, S. Outer Membrane Permeability of Cyanobacterium Synechocystis sp. Strain PCC 6803: Studies of Passive Diffusion of Small Organic Nutrients Reveal the Absence of Classical Porins and Intrinsically Low Permeability. *J Bacteriol* **2017**, *199* (19). DOI: 10.1128/JB.00371-17.
(84) Qiu, G. W.; Jiang, H. B.; Lis, H.; Li, Z. K.; Deng, B.; Shang, J. L.; Sun, C. Y.; Keren, N.; Qiu, B. S. A unique porin meditates iron-selective transport through cyanobacterial outer membranes. *Environ Microbiol* **2021**, *23* (1), 376-390. DOI: 10.1111/1462-2920.15324.
(85) Hopkinson, B. M.; Morel, F. M. The role of siderophores in iron acquisition by photosynthetic marine microorganisms. *Biometals* **2009**, *22* (4), 659-669. DOI: 10.1007/s10534-009-9235-2.
(86) Boiteau, R. M.; Mende, D. R.; Hawco, N. J.; McIlvin, M. R.; Fitzsimmons, J. N.; Saito, M. A.; Sedwick, P. N.; DeLong, E. F.; Repeta, D. J. Siderophore-based microbial adaptations to iron scarcity across the eastern Pacific Ocean. *Proc Natl Acad Sci U S A* **2016**, *113* (50), 14237-14242. DOI: 10.1073/pnas.1608594113.
(87) Wilhelm, S. W.; Trick, C. G. Iron-limited growth of cyanobacteria: Multiple siderophore production is a common response. *Limnol. Oceanogr.* **1994**, *39* (8), 1979-1984. DOI: 10.4319/lo.1994.39.8.1979.
(88) Kranzler, C.; Lis, H.; Shaked, Y.; Keren, N. The role of reduction in iron uptake processes in a unicellular, planktonic cyanobacterium. *Environ Microbiol* **2011**, *13* (11), 2990-2999. DOI: 10.1111/j.1462-2920.2011.02572.x.
(89) Dang, T. C.; Fujii, M.; Rose, A. L.; Bligh, M.; Waite, T. D. Characteristics of the freshwater cyanobacterium Microcystis aeruginosa grown in iron-limited continuous culture. *Appl Environ Microbiol* **2012**, *78* (5), 1574-1583. DOI: 10.1128/AEM.06908-11.
(90) Salmon, T. P.; Rose, A. L.; Neilan, B. A.; Waite, T. D. The FeL model of iron acquisition: Nondissociative reduction of ferric complexes in the marine environment. *Limnol. Oceanogr.* **2006**, *51* (4), 1744-1754. DOI: 10.4319/lo.2006.51.4.1744.
(91) Rose, A. L.; Salmon, T. P.; Lukondeh, T.; Neilan, B. A.; Waite, T. D. Use of superoxide as an electron shuttle for iron acquisition by the marine cyanobacterium Lyngbya majuscula. *Environ Sci Technol* **2005**, *39*, 3708-3715.
(92) Maldonado, M. T.; Price, N. M. Reduction and Transport of Organically Bound Iron Bythalassiosira Oceanica(Bacillariophyceae). *Journal of Phycology* **2001**, *37* (2), 298-310. DOI: 10.1046/j.1529-8817.2001.037002298.x.
(93) Canfield, D. E. THE EARLY HISTORY OF ATMOSPHERIC OXYGEN: Homage to Robert M. Garrels. *Annu. Rev. Earth Planet. Sci.* **2005**, *33* (1), 1-36. DOI: 10.1146/annurev.earth.33.092203.122711.

(94) Poulton, S. W.; Canfield, D. E. Ferruginous Conditions: A Dominant Feature of the Ocean through Earth's History. *Elements* **2011**, *7* (2), 107-112. DOI: 10.2113/gselements.7.2.107.
(95) Habicht, K. S.; Gade, M.; Thamdrup, B.; Berg, P.; Canfield, D. E. Calibration of sulfate levels in the Archean ocean. *Science.* **2002**, *298*, 2372-2374.
(96) Crowe, S. A.; Paris, G.; Katsev, S.; Jones, C.; Kim, S.-T.; Zerkle, A.; Nomosatryo, S.; Fowle, D. A.; Adkins, J. F.; Sessions, A. L.; et al. Sulfate was a trace constituent of Archean seawater. *Science.* **2014**, *346*, 735-739.
(97) Holland, H. D. *The Chemical Evolution of the Atmosphere and Oceans*; Princeton University Press, 1984. DOI: 10.2307/j.ctv15r58kg.
(98) Kendall, B.; Reinhard, C. T.; Lyons, T. W.; Kaufman, A. J.; Poulton, S. W.; Anbar, A. D. Pervasive oxygenation along late Archaean ocean margins. *Nature Geoscience* **2010**, *3* (9), 647-652. DOI: 10.1038/ngeo942.
(99) Reinhard, C. T.; Raiswell, R.; Scott, C.; Anbar, A. D.; Lyons, T. W. A late Archean sulfidic sea stimulated by early oxidative weathering of the continents. *Science.* **2009**, *326*, 713-716.
(100) Czaja, A. D.; Johnson, C. M.; Roden, E. E.; Beard, B. L.; Voegelin, A. R.; Nägler, T. F.; Beukes, N. J.; Wille, M. Evidence for free oxygen in the Neoarchean ocean based on coupled iron–molybdenum isotope fractionation. *Geochim. Cosmochim. Acta.* **2012**, *86*, 118-137. DOI: 10.1016/j.gca.2012.03.007.
(101) Planavsky, N. J.; Asael, D.; Hofmann, A.; Reinhard, C. T.; Lalonde, S. V.; Knudsen, A.; Wang, X.; Ossa Ossa, F.; Pecoits, E.; Smith, A. J. B.; et al. Evidence for oxygenic photosynthesis half a billion years before the Great Oxidation Event. *Nature Geoscience* **2014**, *7* (4), 283-286. DOI: 10.1038/ngeo2122.
(102) Farquhar, J.; Bao, H.; Thiemens, M. Atmospheric influence of Earth's earliest sulfur cycle. *Science.* **2000**, *289*, 756-758.
(103) Canfield, D. E.; Poulton, S. W.; Narbonne, G. M. Late-Neoproterozoic deep-ocean oxygenation and the rise of animal life. *Science.* **2007**, *315*, 92-95.
(104) Canfield, D. E.; Poulton, S. W.; Knoll, A. H.; Narbonne, G. M.; Ross, G.; Goldberg, T.; Strauss, H. Ferruginous conditions dominated later Neoproterozoic deep-water chemistry. *Science.* **2008**, *321*, 949-950.
(105) Fakhraee, M.; Hancisse, O.; Canfield, D. E.; Crowe, S. A.; Katsev, S. Proterozoic seawater sulfate scarcity and the evolution of ocean–atmosphere chemistry. *Nature Geoscience* **2019**, *12* (5), 375-380. DOI: 10.1038/s41561-019-0351-5.
(106) Och, L. M.; Shields-Zhou, G. A. The Neoproterozoic oxygenation event: Environmental perturbations and biogeochemical cycling. *Earth-Sci. Rev.* **2012**, *110* (1-4), 26-57. DOI: 10.1016/j.earscirev.2011.09.004.
(107) Poulton, S. W.; Fralick, P. W.; Canfield, D. E. Spatial variability in oceanic redox structure 1.8 billion years ago. *Nature Geoscience* **2010**, *3* (7), 486-490. DOI: 10.1038/ngeo889.
(108) Li, C.; Love, G. D.; Lyons, T. W.; Fike, D. A.; Sessions, A. L.; Chu, X. A stratified redox model for the Ediacaran ocean. *Science.* **2010**, *328*, 80-83.
(109) Song, H.; Jiang, G.; Poulton, S. W.; Wignall, P. B.; Tong, J.; Song, H.; An, Z.; Chu, D.; Tian, L.; She, Z.; et al. The onset of widespread marine red beds and the evolution of ferruginous oceans. *Nat Commun* **2017**, *8* (1), 399. DOI: 10.1038/s41467-017-00502-x.

(110) Anbar, A. D.; Knoll, A. H. Proterozoic Ocean chemistry and evolution: a bioinorganic bridge? *Science.* **2002**, *297*, 1137-1142.
(111) Kharecha, P.; Kasting, J.; Siefert, J. A coupled atmosphere-ecosystem model of the early Archean Earth. *Geobiology.* **2005**, *3* (2), 53-76. DOI: 10.1111/j.1472-4669.2005.00049.x.
(112) Xiong, J.; Fischer, W. M.; Inoue, K.; Nakahara, M.; Bauer, C. E. Molecular evidence for the early evolution of photosynthesis. *Science.* **2000**, *289*, 1724-1730.
(113) Xiong, J. Photosynthesis: what color was its origin? *Genome Biol* **2006**, *7* (12), 245. DOI: 10.1186/gb-2006-7-12-245.
(114) Gupta, R. S. Chapter Two - Molecular Markers for Photosynthetic Bacteria and Insights into the Origin and Spread of Photosynthesis. In *Advances in Botanical Research*, Beatty, J. T. Ed.; Vol. 66; Academic Press, 2013; pp 37-66.
(115) Johnston, D. T.; Wolfe-Simon, F.; Pearson, A.; Knoll, A. H. Anoxygenic photosynthesis modulated Proterozoic oxygen and sustained Earth's middle age. *Proc Natl Acad Sci U S A* **2009**, *106* (40), 16925-16929. DOI: 10.1073/pnas.0909248106.
(116) Konhauser, K. O.; Newman, D. K.; Kappler, A. The potential significance of microbial Fe(III) reduction during deposition of Precambrian banded iron formations. *Geobiology.* **2005**, *3* (3), 167-177. DOI: 10.1111/j.1472-4669.2005.00055.x.
(117) Canfield, D. E.; Rosing, M. T.; Bjerrum, C. J. Early anaerobic metabolisms. *Phil. Trans. R. Soc. B* **2006**, *361*, 1819-1836.
(118) Bekker, A.; Slack, J. F.; Planavsky, N. J.; Krapež, B.; Hofmann, A.; Konhauser, K. O.; Rouxel, O. J. Iron formation: the sedimentary product of a complex interplay among mantle, tectonic, oceanic, and biospheric processes. *Econ. Geol.* **2010**, *105* (3), 467-508.
(119) Konhauser, K. O.; Planavsky, N. J.; Hardisty, D. S.; Robbins, L. J.; Warchola, T. J.; Haugaard, R.; Lalonde, S. V.; Partin, C. A.; Oonk, P. B. H.; Tsikos, H.; et al. Iron formations: a global record of Neoarchaean to Palaeoproterozoic environmental history. *Earth-Sci. Rev.* **2017**, *172*, 140-177. DOI: 10.1016/j.earscirev.2017.06.012.
(120) Isley, A. E.; Abbott, D. H. Plume-related mafic volcanism and the deposition of banded iron formation. *Journal of Geophysical Research: Solid Earth* **1999**, *104* (B7), 15461-15477. DOI: 10.1029/1999jb900066.
(121) Canfield, D. E.; Zhang, S.; Wang, H.; Wang, X.; Zhao, W.; Su, J.; Bjerrum, C. J.; Haxen, E. R.; Hammarlund, E. U. A Mesoproterozoic iron formation. *Proc Natl Acad Sci U S A* **2018**, *115* (17), E3895-E3904. DOI: 10.1073/pnas.1720529115.
(122) Li, Z. Q.; Zhang, L. C.; Xue, C. J.; Zheng, M. T.; Zhu, M. T.; Robbins, L. J.; Slack, J. F.; Planavsky, N. J.; Konhauser, K. O. Earth's youngest banded iron formation implies ferruginous conditions in the Early Cambrian ocean. *Sci Rep* **2018**, *8* (1), 9970. DOI: 10.1038/s41598-018-28187-2.
(123) Sun, J.; Zhu, X.; Li, Z. Confirmation and global significance of a large-scale early Neoproterozoic banded iron formation on Hainan Island, China. *Precambrian Research* **2018**, *307*, 82-92. DOI: 10.1016/j.precamres.2018.01.005.
(124) Slack, J. F.; Grenne, T.; Bekker, A.; Rouxel, O.; Lindberg, P. A. Suboxic deep seawater in the late Paleoproterozoic: Evidence from hematitic chert and iron formation related to seafloor-hydrothermal sulfide deposits, central Arizona, USA. *Earth Planet. Sci. Lett.* **2007**, *255*, 243-256.
(125) Holland, H. D. The oxygenation of the atmosphere and oceans. *Philos Trans R Soc Lond B Biol Sci* **2006**, *361* (1470), 903-915. DOI: 10.1098/rstb.2006.1838.

(126) Poulton, S. W.; Fralick, P. W.; Canfield, D. E. The transition to a sulphidic ocean ~ 1.84 billion years ago. *Nature* **2004**, *431*, 173-177. DOI: 10.1038/nature02863.
(127) Canfield, D. E. A new model for Proterozoic ocean chemistry. *Nature* **1998**, *396*, 450-453.
(128) Alibert, C.; McCulloch, M. T. Rare earth element and neodymium isotopic compositions of the banded iron-formations and associated shales from Hamersley, western Australia. *Geochim Cosmochim Acta* **1993**, *57*, 187-204.
(129) Derry, L. A.; Jacobsen, S. B. The chemical evolution of Precambrian seawater: Evidence from REEs in banded iron formations. *Geochim Cosmochim Acta* **1990**, *54*, 2965-2977.
(130) Bau, M.; Moller, P. Rare earth element systematics of the chemically precipitated component in Early Precambrian iron formations and the evolution of the terrestrial atmosphere-hydrosphere-lithosphere system. *Geochim Cosmochim Acta* **1993**, *57*, 2239-2249.
(131) Klein, C. Some Precambrian banded iron-formations (BIFs) from around the world: Their age, geologic setting, mineralogy, metamorphism, geochemistry, and origins. *American Mineralogist* **2005**, *90* (10), 1473-1499. DOI: 10.2138/am.2005.1871 (acccessed 7/31/2023).
(132) Heck, P. R.; Huberty, J. M.; Kita, N. T.; Ushikubo, T.; Kozdon, R.; Valley, J. W. SIMS analyses of silicon and oxygen isotope ratios for quartz from Archean and Paleoproterozoic banded iron formations. *Geochim. Cosmochim. Acta.* **2011**, *75* (20), 5879-5891. DOI: 10.1016/j.gca.2011.07.023.
(133) Andre, L.; Cardinal, D.; Alleman, L.; Moorbath, S. Silicon isotopes in ~3.8 Ga West Greenland rocks as clues to the Eoarchaean supracrustal Si cycle. *Earth Planet. Sci. Lett.* **2006**, *245* (1-2), 162-173. DOI: 10.1016/j.epsl.2006.02.046.
(134) Li, W.; Beard, B. L.; Johnson, C. M. Biologically recycled continental iron is a major component in banded iron formations. *Proc Natl Acad Sci U S A* **2015**, *112* (27), 8193-8198. DOI: 10.1073/pnas.1505515112.
(135) Raiswell, R.; Kesler, S. E.; Ohmoto, H. An evaluation of diagenetic recycling as a source of iron for banded iron formations. In *Evolution of Early Earth's Atmosphere, Hydrosphere, and Biosphere - Constraints from Ore Deposits*, Vol. 198; Geological Society of America, 2006; p 0.
(136) Holland, H. D. The Oceans; A Possible Source of Iron in Iron-Formations. *Econ. Geol.* **1973**, *68* (7), 1169-1172. DOI: 10.2113/gsecongeo.68.7.1169 (acccessed 7/31/2023).
(137) Klein, C. Presidential Address To The Mineralogical Society Of Amrica, Boston, November 6, 2001: Some Precambrian Banded Iron-Formations (BiIFs) From Around The World: Their Age, Geologic Setting, Mineralogy, Metamorphism, Geochemistry, And Origin. *American Mineralogist* **2005**, *90* (10), 1473-1499. DOI: doi:10.2138/am.2005.1871 (acccessed 2023-08-01).
(138) Tosca, N. J.; Guggenheim, S.; Pufahl, P. K. An authigenic origin for Precambrian greenalite: implications for iron formation and the chemistry of ancient seawater. *Geol. Soc. Am. Bull.* **2016**, *128* (3-4), 511-530. DOI: 10.1130/B31339.1.
(139) Johnson, J. E.; Muhling, J. R.; Cosmidis, J.; Rasmussen, B.; Templeton, A. S. Low-Fe(III) Greenalite Was a Primary Mineral From Neoarchean Oceans. *Geophysical Research Letters* **2018**, *45* (7), 3182-3192. DOI: 10.1002/2017gl076311.

(140) Muhling, J. R.; Rasmussen, B. Widespread deposition of greenalite to form Banded Iron Formations before the Great Oxidation Event. *Precambrian Research* **2020**, *339*, 105619. DOI: https://doi.org/10.1016/j.precamres.2020.105619.
(141) Cloud, P. E. Atmospheric and Hydrospheric Evolution on the Primitive Earth. *Science.* **1968**, *160* (3829), 729-736. DOI: doi:10.1126/science.160.3829.729.
(142) Cairns-Smith, A. G. Precambrian solution photochemistry, inverse segregation, and banded iron formations. *Nature* **1978**, *276* (5690), 807-808. DOI: 10.1038/276807a0.
(143) Konhauser, K.; Hamade, T.; Raiswell, R.; Morris, R. C.; Ferris, F. G.; Southam, G.; Canfield, D. E. Could bacteria have formed the Precambrian banded iron formations? *Geology.* **2002**, *30* (12), 1079-1082.
(144) Kappler, A.; Pasquero, C.; Konhauser, K. O.; Newman, D. K. Deposition of banded iron formations by anoxygenic phototrophic Fe(II)-oxidizing bacteria. *Geology.* **2005**, *33* (11). DOI: 10.1130/g21658.1.
(145) Gauger, T.; Byrne, J. M.; Konhauser, K. O.; Obst, M.; Crowe, S.; Kappler, A. Influence of organics and silica on Fe(II) oxidation rates and cell–mineral aggregate formation by the green-sulfur Fe(II)-oxidizing bacterium *Chlorobium ferrooxidans* KoFox – Implications for Fe(II) oxidation in ancient oceans. *Earth Planet. Sci. Lett.* **2016**, *443*, 81-89. DOI: 10.1016/j.epsl.2016.03.022.
(146) Czaja, A. D.; Johnson, C. M.; Beard, B. L.; Roden, E. E.; Li, W.; Moorbath, S. Biological Fe oxidation controlled deposition of banded iron formation in the ca. 3770Ma Isua Supracrustal Belt (West Greenland). *Earth Planet. Sci. Lett.* **2013**, *363*, 192-203. DOI: 10.1016/j.epsl.2012.12.025.
(147) Koeksoy, E.; Halama, M.; Konhauser, K. O.; Kappler, A. Using modern ferruginous habitats to interpret Precambrian banded iron formation deposition. *International Journal of Astrobiology* **2015**, *15* (3), 205-217. DOI: 10.1017/s1473550415000373.
(148) Swanner, E. D.; Lambrecht, N.; Wittkop, C.; Harding, C.; Katsev, S.; Torgeson, J.; Poulton, S. W. The biogeochemistry of ferruginous lakes and past ferruginous oceans. *Earth-Sci. Rev.* **2020**, *211*, 103430. DOI: 10.1016/j.earscirev.2020.103430.
(149) Hutchinson, G. E. *A Treatise on Limnology. I. Geography, Physics, and Chemistry.*; John Wiley & Sons, 1957.
(150) Lambrecht, N. Insights into early Earth ocean biogeochemistry from intensive monitoring of two ferruginous meromictic lakes. phD thesis, Iowa State University, Iowa, USA, 2019.
(151) Lliros, M.; Garcia-Armisen, T.; Darchambeau, F.; Morana, C.; Triado-Margarit, X.; Inceoglu, O.; Borrego, C. M.; Bouillon, S.; Servais, P.; Borges, A. V.; et al. Pelagic photoferrotrophy and iron cycling in a modern ferruginous basin. *Sci. Rep.* **2015**, *5*, 13803. DOI: 10.1038/srep13803.
(152) Crowe, S. A.; Jones, C.; Katsev, S.; Magen, C.; O'Neill, A. H.; Sturm, A.; Canfield, D. E.; Haffner, G. D.; Mucci, A.; Sundby, B.; et al. Photoferrotrophs thrive in an Archean Ocean analogue. *Proc Natl Acad Sci U S A* **2008**, *105* (41), 15938-15943. DOI: 10.1073/pnas.0805313105.
(153) Crowe, S. A.; Maresca, J. A.; Jones, C.; Sturm, A.; Henny, C.; Fowle, D. A.; Cox, R. P.; Delong, E. F.; Canfield, D. E. Deep-water anoxygenic photosythesis in a ferruginous chemocline. *Geobiology.* **2014**, *12* (4), 322-339. DOI: 10.1111/gbi.12089.
(154) Savvichev, A. S.; Kokryatskaya, N. M.; Zabelina, S. A.; Rusanov, II; Zakharova, E. E.; Veslopolova, E. F.; Lunina, O. N.; Patutina, E. O.; Bumazhkin, B. K.; Gruzdev, D. S.; et al.

Microbial processes of the carbon and sulfur cycles in an ice-covered, iron-rich meromictic lake Svetloe (Arkhangelsk region, Russia). *Environ Microbiol* **2017**, *19* (2), 659-672. DOI: 10.1111/1462-2920.13591.
(155) Walter, X. A.; Picazo, A.; Miracle, M. R.; Vicente, E.; Camacho, A.; Aragno, M.; Zopfi, J. Phototrophic Fe(II)-oxidation in the chemocline of a ferruginous meromictic lake. *Front. Microbiol.* **2014**, *5*, 713. DOI: 10.3389/fmicb.2014.00713.
(156) Camacho, A.; Walter, X. A.; Picazo, A.; Zopfi, J. Photoferrotrophy: remains of an ancient photosynthesis in modern environments. *Front. Microbiol.* **2017**, *8*, 323. DOI: 10.3389/fmicb.2017.00323.
(157) Morana, C.; Roland, F. A. E.; Crowe, S. A.; Llirós, M.; Borges, A. V.; Darchambeau, F.; Bouillon, S. Chemoautotrophy and anoxygenic photosynthesis within the water column of a large meromictic tropical lake (Lake Kivu, East Africa). *Limnol. Oceanogr.* **2016**, *61* (4), 1424-1437. DOI: 10.1002/lno.10304.
(158) Crowe, S. A.; Hahn, A. S.; Morgan-Lang, C.; Thompson, K. J.; Simister, R. L.; Lliros, M.; Hirst, M.; Hallam, S. J. Draft Genome Sequence of the Pelagic Photoferrotroph Chlorobium phaeoferrooxidans. *Genome Announc* **2017**, *5* (13). DOI: 10.1128/genomeA.01584-16.
(159) Johnson, C. M.; Beard, B. L.; Weyer, S. *Iron geochemistry: an isotopic perspective*; Springer, 2020.
(160) Dauphas, N.; Rouxel, O. Mass spectrometry and natural variations of iron isotopes. *Mass Spectrom Rev* **2006**, *25* (4), 515-550. DOI: 10.1002/mas.20078.
(161) Dauphas, N.; John, S. G.; Rouxel, O. Iron Isotope Systematics. *Rev. Mineral. Geochem.* **2017**, *82* (1), 415-510. DOI: 10.2138/rmg.2017.82.11.
(162) Wu, B.; Amelung, W.; Xing, Y.; Bol, R.; Berns, A. E. Iron cycling and isotope fractionation in terrestrial ecosystems. *Earth-Sci. Rev.* **2019**, *190*, 323-352. DOI: 10.1016/j.earscirev.2018.12.012.
(163) Yin, N. H.; Louvat, P.; Thibault, D. E. C. A.; Sebilo, M.; Amouroux, D. Iron isotopic fractionation driven by low-temperature biogeochemical processes. *Chemosphere.* **2023**, *316*, 137802. DOI: 10.1016/j.chemosphere.2023.137802.
(164) Vanhaecke, F.; Degryse, P. *Isotopic analysis: fundamentals and applications using ICP-MS*; Wiley-VCH, 2012.
(165) Welch, S. A.; Beard, B. L.; Johnson, C. M.; Braterman, P. S. Kinetic and equilibrium Fe isotope fractionation between aqueous Fe(II) and Fe(III). *Geochim. Cosmochim. Acta.* **2003**, *67* (22), 4231-4250. DOI: 10.1016/s0016-7037(03)00266-7.
(166) Wu, L.; Beard, B. L.; Roden, E. E.; Johnson, C. M. Stable iron isotope fractionation between aqueous Fe(II) and hydrous ferric oxide. *Environ Sci Technol* **2011**, *45* (5), 1847-1852. DOI: 10.1021/es103171x.
(167) Frierdich, A. J.; Beard, B. L.; Reddy, T. R.; Scherer, M. M.; Johnson, C. M. Iron isotope fractionation between aqueous Fe(II) and goethite revisited: New insights based on a multi-direction approach to equilibrium and isotopic exchange rate modification. *Geochim. Cosmochim. Acta.* **2014**, *139*, 383-398. DOI: 10.1016/j.gca.2014.05.001.
(168) Beard, B. L.; Handler, R. M.; Scherer, M. M.; Wu, L.; Czaja, A. D.; Heimann, A.; Johnson, C. M. Iron isotope fractionation between aqueous ferrous iron and goethite. *Earth Planet. Sci. Lett.* **2010**, *295* (1-2), 241-250. DOI: 10.1016/j.epsl.2010.04.006.
(169) Frierdich, A. J.; Nebel, O.; Beard, B. L.; Johnson, C. M. Iron isotope exchange and fractionation between hematite (α-Fe2O3) and aqueous Fe(II): A combined three-isotope and

reversal-approach to equilibrium study. *Geochim. Cosmochim. Acta.* **2019**, *245*, 207-221. DOI: 10.1016/j.gca.2018.10.033.
(170) Saunier, G.; Pokrovski, G. S.; Poitrasson, F. First experimental determination of iron isotope fractionation between hematite and aqueous solution at hydrothermal conditions. *Geochim. Cosmochim. Acta.* **2011**, *75* (21), 6629-6654. DOI: 10.1016/j.gca.2011.08.028.
(171) Wu, L.; Beard, B. L.; Roden, E. E.; Kennedy, C. B.; Johnson, C. M. Stable Fe isotope fractionations produced by aqueous Fe(II)-hematite surface interactions. *Geochim. Cosmochim. Acta.* **2010**, *74* (15), 4249-4265. DOI: 10.1016/j.gca.2010.04.060.
(172) Frierdich, A. J.; Beard, B. L.; Scherer, M. M.; Johnson, C. M. Determination of the Fe(II)aq–magnetite equilibrium iron isotope fractionation factor using the three-isotope method and a multi-direction approach to equilibrium. *Earth Planet. Sci. Lett.* **2014**, *391*, 77-86. DOI: 10.1016/j.epsl.2014.01.032.
(173) Johnson, C. M.; Roden, E. E.; Welch, S. A.; Beard, B. L. Experimental constraints on Fe isotope fractionation during magnetite and Fe carbonate formation coupled to dissimilatory hydrous ferric oxide reduction. *Geochim. Cosmochim. Acta.* **2005**, *69* (4), 963-993. DOI: 10.1016/j.gca.2004.06.043.
(174) Balci, N.; Bullen, T. D.; Witte-Lien, K.; Shanks, W. C.; Motelica, M.; Mandernack, K. W. Iron isotope fractionation during microbially stimulated Fe(II) oxidation and Fe(III) precipitation. *Geochim. Cosmochim. Acta.* **2006**, *70* (3), 622-639. DOI: 10.1016/j.gca.2005.09.025.
(175) Kappler, A.; Johnson, C. M.; Crosby, H. A.; Beard, B. L.; Newman, D. K. Evidence for equilibrium iron isotope fractionation by nitrate-reducing iron(II)-oxidizing bacteria. *Geochim Cosmochim Acta* **2010**, *74* (10), 2826-2842. DOI: 10.1016/j.gca.2010.02.017.
(176) Swanner, E. D.; Bayer, T.; Wu, W.; Hao, L.; Obst, M.; Sundman, A.; Byrne, J. M.; Michel, F. M.; Kleinhanns, I. C.; Kappler, A.; et al. Iron Isotope Fractionation during Fe(II) Oxidation Mediated by the Oxygen-Producing Marine Cyanobacterium Synechococcus PCC 7002. *Environ Sci Technol* **2017**, *51* (9), 4897-4906. DOI: 10.1021/acs.est.6b05833.
(177) Croal, L. R.; Johnson, C. M.; Beard, B. L.; Newman, D. K. Iron isotope fractionation by Fe(II)-oxidizing photoautotrophic bacteria *Geochim. Cosmochim. Acta.* **2004**, *68* (6), 1227-1242. DOI: 10.1016/j.gca.2003.09.011.
(178) Swanner, E. D.; Wu, W.; Schoenberg, R.; Byrne, J.; Michel, F. M.; Pan, Y.; Kappler, A. Fractionation of Fe isotopes during Fe(II) oxidation by a marine photoferrotroph is controlled by the formation of organic Fe-complexes and colloidal Fe fractions. *Geochim. Cosmochim. Acta.* **2015**, *165*, 44-61. DOI: 10.1016/j.gca.2015.05.024.
(179) Wu, W.; Swanner, E. D.; Kleinhanns, I. C.; Schoenberg, R.; Pan, Y.; Kappler, A. Fe isotope fractionation during Fe(II) oxidation by the marine photoferrotroph Rhodovulum iodosum in the presence of Si – Implications for Precambrian iron formation deposition. *Geochim. Cosmochim. Acta.* **2017**, *211*, 307-321. DOI: 10.1016/j.gca.2017.05.033.
(180) Han, X.; He, Y.; Li, J.; Kappler, A.; Pan, Y. Iron isotope fractionation in anoxygenic phototrophic Fe(II) oxidation by Rhodobacter ferrooxidans SW2. *Geochim. Cosmochim. Acta.* **2022**, *332*, 355-368. DOI: 10.1016/j.gca.2022.06.034.
(181) Crosby, H. A.; Johnson, C. M.; Roden, E. E.; Beard, B. L. Coupled Fe(II)-Fe(III) electron and atom exchange as a mechanism for Fe isotope fractionation during dissimilatory iron oxide reduction. *Environ. Sci. Technol.* **2005**, *39*, 6698-6704.

(182) Wu, L.; Beard, B. L.; Roden, E. E.; Johnson, C. M. Influence of pH and dissolved Si on Fe isotope fractionation during dissimilatory microbial reduction of hematite. *Geochim. Cosmochim. Acta.* **2009**, *73* (19), 5584-5599. DOI: 10.1016/j.gca.2009.06.026.
(183) Crosby, H. A.; Roden, E. E.; Johnson, C. M.; Beard, B. L. The mechanisms of iron isotope fractionation produced during dissimilatory Fe(III) reduction by *Shewanella putrefaciens* and *Geobacter sulfurreducens*. *Geobiology.* **2007**, *5* (2), 169-189. DOI: 10.1111/j.1472-4669.2007.00103.x.
(184) Brantley, S. L.; Liermann, L. J.; Guynn, R. L.; Anbar, A.; Icopini, G. A.; Barling, J. Fe isotopic fractionation during mineral dissolution with and without bacteria. *Geochim. Cosmochim. Acta.* **2004**, *68* (15), 3189-3204. DOI: 10.1016/j.gca.2004.01.023.
(185) Wasylenki, L. E.; Anbar, A. D.; Liermann, L. J.; Mathur, R.; Gordon, G. W.; Brantley, S. L. Isotope fractionation during microbial metal uptake measured by MC-ICP-MS. *J. Anal. At. Spectrom.* **2007**, *22* (8), 905-910. DOI: 10.1039/b705476a.
(186) Sun, R.; Wang, B. Iron isotope fractionation during uptake of ferrous ion by phytoplankton. *Chem. Geol.* **2018**, *481*, 65-73. DOI: 10.1016/j.chemgeo.2018.01.031.
(187) Mikutta, C.; Wiederhold, J. G.; Cirpka, O. A.; Hofstetter, T. B.; Bourdon, B.; Gunten, U. V. Iron isotope fractionation and atom exchange during sorption of ferrous iron to mineral surfaces. *Geochim. Cosmochim. Acta.* **2009**, *73* (7), 1795-1812. DOI: 10.1016/j.gca.2009.01.014.
(188) Dideriksen, K.; Baker, J. A.; Stipp, S. L. S. Equilibrium Fe isotope fractionation between inorganic aqueous Fe(III) and the siderophore complex, Fe(III)-desferrioxamine B. *Earth Planet. Sci. Lett.* **2008**, *269* (1-2), 280-290. DOI: 10.1016/j.epsl.2008.02.022.
(189) Wiesli, R. A.; Beard, B. L.; Johnson, C. M. Experimental determination of Fe isotope fractionation between aqueous Fe(II), siderite and "green rust" in abiotic systems. *Chem. Geol.* **2004**, *211* (3-4), 343-362. DOI: 10.1016/j.chemgeo.2004.07.002.
(190) Wu, L.; Druschel, G.; Findlay, A.; Beard, B. L.; Johnson, C. M. Experimental determination of iron isotope fractionations among Feaq2+–FeSaq–Mackinawite at low temperatures: Implications for the rock record. *Geochim. Cosmochim. Acta.* **2012**, *89*, 46-61. DOI: 10.1016/j.gca.2012.04.047.
(191) Butler, I. B.; Archer, C.; Vance, D.; Oldroyd, A.; Rickard, D. Fe isotope fractionation on FeS formation in ambient aqueous solution. *Earth Planet. Sci. Lett.* **2005**, *236* (1-2), 430-442. DOI: 10.1016/j.epsl.2005.05.022.
(192) Guilbaud, R.; Butler, I. B.; Ellam, R. M.; Rickard, D. Fe isotope exchange between Fe(II)aq and nanoparticulate mackinawite (FeSm) during nanoparticle growth. *Earth Planet. Sci. Lett.* **2010**, *300* (1-2), 174-183. DOI: 10.1016/j.epsl.2010.10.004.
(193) Johnson, C. M.; Beard, B. L.; Roden, E. E. The iron isotope fingerprints of redox and biogeochemical cycling in modern and ancient earth. *Annu. Rev. Earth Planet. Sci.* **2008**, *36* (1), 457-493. DOI: 10.1146/annurev.earth.36.031207.124139.
(194) Planavsky, N.; Rouxel, O. J.; Bekker, A.; Hofmann, A.; Little, C. T. S.; Lyons, T. W. Iron isotope composition of some Archean and Proterozoic iron formations. *Geochim. Cosmochim. Acta.* **2012**, *80*, 158-169. DOI: 10.1016/j.gca.2011.12.001.
(195) Rouxel, O.; Bekker, A.; Edwards, K. J. Iron isotope constraints on the archean and paleoproterozoic ocean redox state. *Science.* **2005**, *307*, 1088-1091.
(196) Tsikos, H.; Matthews, A.; Erel, Y.; Moore, J. M. Iron isotopes constrain biogeochemical redox cycling of iron and manganese in a Palaeoproterozoic stratified basin. *Earth Planet. Sci. Lett.* **2010**, *298* (1-2), 125-134. DOI: 10.1016/j.epsl.2010.07.032.

(197) Heimann, A.; Johnson, C. M.; Beard, B. L.; Valley, J. W.; Roden, E. E.; Spicuzza, M. J.; Beukes, N. J. Fe, C, and O isotope compositions of banded iron formation carbonates demonstrate a major role for dissimilatory iron reduction in ~2.5Ga marine environments. *Earth Planet. Sci. Lett.* **2010**, *294* (1-2), 8-18. DOI: 10.1016/j.epsl.2010.02.015.
(198) Johnson, C. M.; Ludois, J. M.; Beard, B. L.; Beukes, N. J.; Heimann, A. Iron formation carbonates: Paleoceanographic proxy or recorder of microbial diagenesis? *Geology.* **2013**, *41* (11), 1147-1150. DOI: 10.1130/g34698.1.
(199) Johnson, C. M.; Beard, B. L.; Klein, C.; Beukes, N. J.; Roden, E. E. Iron isotopes constrain biologic and abiologic processes in banded iron formation genesis. *Geochim. Cosmochim. Acta.* **2008**, *72* (1), 151-169. DOI: 10.1016/j.gca.2007.10.013.
(200) Busigny, V.; Planavsky, N. J.; Jézéquel, D.; Crowe, S.; Louvat, P.; Moureau, J.; Viollier, E.; Lyons, T. W. Iron isotopes in an Archean ocean analogue. *Geochim. Cosmochim. Acta.* **2014**, *133*, 443-462. DOI: 10.1016/j.gca.2014.03.004.
(201) Teutsch, N.; Schmid, M.; Müller, B.; Halliday, A. N.; Bürgmann, H.; Wehrli, B. Large iron isotope fractionation at the oxic–anoxic boundary in Lake Nyos. *Earth Planet. Sci. Lett.* **2009**, *285* (1-2), 52-60. DOI: 10.1016/j.epsl.2009.05.044.
(202) Malinovsky, D. N.; Rodyushkin, I. V.; Shcherbakova, E. P.; Ponter, C.; Öhlander, B.; Ingri, J. Fractionation of Fe isotopes as a result of redox processes in a basin. *Geochem. Int.* **2005**, *43* (8), 797-803.
(203) Song, L.; Liu, C.-Q.; Wang, Z.-L.; Zhu, X.; Teng, Y.; Liang, L.; Tang, S.; Li, J. Iron isotope fractionation during biogeochemical cycle: information from suspended particulate matter (SPM) in Aha Lake and its tributaries, Guizhou, China. *Chem. Geol.* **2011**, *280* (1-2), 170-179. DOI: 10.1016/j.chemgeo.2010.11.006.
(204) Ellwood, M. J.; Hassler, C.; Moisset, S.; Pascal, L.; Danza, F.; Peduzzi, S.; Tonolla, M.; Vance, D. Iron isotope transformations in the meromictic Lake Cadagno. *Geochim. Cosmochim. Acta.* **2019**, *255*, 205-221. DOI: 10.1016/j.gca.2019.04.007.
(205) Liu, K.; Wu, L.; Couture, R.-M.; Li, W.; Van Cappellen, P. Iron isotope fractionation in sediments of an oligotrophic freshwater lake. *Earth Planet. Sci. Lett.* **2015**, *423*, 164-172. DOI: 10.1016/j.epsl.2015.05.010.
(206) Lewis, W. M.; Wurtsbaugh, W. A.; Paerl, H. W. Rationale for control of anthropogenic nitrogen and phosphorus to reduce eutrophication of inland waters. *Environ. Sci. Technol.* **2011**, *45* (24), 10300-10305. DOI: 10.1021/es202401p.
(207) Schindler, D. W.; Hecky, R. E.; Findlay, D. L.; Stainton, M. P.; Parker, B. R.; Paterson, M. J.; Beaty, K. G.; Lyng, M.; Kasian, S. E. M. Eutrophication of lakes cannot be controlled by reducing nitrogen input: results of a 37-year whole-ecosystem experiment. *Proc. Natl. Acad. Sci. U.S.A.* **2008**, *105* (32), 11254-11258.
(208) Molot, L. A.; Li, G.; Findlay, D. L.; Watson, S. B. Iron-mediated suppression of bloom-forming cyanobacteria by oxine in a eutrophic lake. *Freshw. Biol.* **2010**, *55* (5), 1102-1117. DOI: 10.1111/j.1365-2427.2009.02384.x.
(209) Molot, L. A.; Schiff, S. L.; Venkiteswaran, J. J.; Baulch, H. M.; Higgins, S. N.; Zastepa, A.; Verschoor, M. J.; Walters, D. Low sediment redox promotes cyanobacteria blooms across a trophic range: implications for management. *Lake Reserv. Manag.* **2021**, *37* (2), 120-142. DOI: 10.1080/10402381.2020.1854400.
(210) Molot, L. A.; Watson, S. B.; Creed, I. F.; Trick, C. G.; McCabe, S. K.; Verschoor, M. J.; Sorichetti, R. J.; Powe, C.; Venkiteswaran, J. J.; Schiff, S. L. A novel model for

cyanobacteria bloom formation: the critical role of anoxia and ferrous iron. *Freshw. Biol.* **2014**, *59* (6), 1323-1340. DOI: 10.1111/fwb.12334.
(211) Schiff, S. L.; Tsuji, J. M.; Wu, L.; Venkiteswaran, J. J.; Molot, L. A.; Elgood, R. J.; Paterson, M. J.; Neufeld, J. D. Millions of boreal shield lakes can be used to probe Archaean Ocean biogeochemistry. *Sci. Rep.* **2017**, *7*, 46708. DOI: 10.1038/srep46708.
(212) Wetzel, R. G. *Limnology: Lake and River Ecosystems.*; Academic Press, 2001.
(213) Murphy, T. P.; Lean, D. R.; Nalewajko, C. Blue-green algae: their excretion of iron-selective chelators enables them to dominate other algae. *Science.* **1976**, *192* (4242), 900-902.
(214) Brown, C. M.; Trick, C. G. Response of the cyanobacterium, *Oscillatoria tenuis*, to low iron environments: the effect on growth rate and evidence for siderophore production. *Arch. Microbiol.* **1992**, *157*, 349-354.
(215) Wilhelm, S. W.; Maxwell, D. P.; Trick, C. G. Growth, iron requirements, and siderophore production in iron-limited *Synechococcus* PCC 7002. *Limnol. Oceanogr.* **1996**, *41* (1), 89-97.
(216) Nikeleit, V.; Mellage, A.; Bianchini, G.; Sauter, L.; Buessecker, S.; Gotterbarm, S.; Schad, M.; Konhauser, K.; Zerkle, A.; Sánchez-Baracaldo, P.; et al. Inhibition of photoferrotrophy by nitric oxide in ferruginous environments. *EarthArXiv. Preprint* **2021**. DOI: https://doi.org/10.31223/X5XS60.
(217) Chan, C. S.; Emerson, D.; Luther, G. W., 3rd. The role of microaerophilic Fe-oxidizing micro-organisms in producing banded iron formations. *Geobiology.* **2016**, *14* (5), 509-528. DOI: 10.1111/gbi.12192.
(218) Crowe, S. A.; Jones, C.; Katsev, S.; Magen, C.; O'Neill, A. H.; Sturm, A.; Canfield, D. E.; Haffner, G. D.; Mucci, A.; Sundby, B.; et al. Photoferrotrophs thrive in an Archean Ocean analogue. *Proc. Natl. Acad. Sci. U.S.A.* **2008**, *105* (41), 15938-15943.
(219) Lehours, A. C.; Evans, P.; Bardot, C.; Joblin, K.; Gerard, F. Phylogenetic diversity of archaea and bacteria in the anoxic zone of a meromictic lake (Lake Pavin, France). *Appl. Environ. Microbiol.* **2007**, *73* (6), 2016-2019. DOI: 10.1128/AEM.01490-06.
(220) Wiederhold, J. G.; Teutsch, N.; Kraemer, S. M.; Halliday, A. N.; Kretzschmar, R. Iron isotope fractionation in oxic soils by mineral weathering and podzolization. *Geochim. Cosmochim. Acta.* **2007**, *71* (23), 5821-5833. DOI: 10.1016/j.gca.2007.07.023.
(221) Lemanceau, P.; Bauer, P.; Kraemer, S.; Briat, J.-F. Iron dynamics in the rhizosphere as a case study for analyzing interactions between soils, plants and microbes. *Plant Soil.* **2009**, *321* (1-2), 513-535. DOI: 10.1007/s11104-009-0039-5.
(222) Mansfeldt, T.; Schuth, S.; Häusler, W.; Wagner, F. E.; Kaufhold, S.; Overesch, M. Iron oxide mineralogy and stable iron isotope composition in a Gleysol with petrogleyic properties. *J. Soils Sediments.* **2011**, *12* (1), 97-114. DOI: 10.1007/s11368-011-0402-z.
(223) Teutsch, N.; von Gunten, U.; Porcelli, D.; Cirpka, O. A.; Halliday, A. N. Adsorption as a cause for iron isotope fractionation in reduced groundwater. *Geochim. Cosmochim. Acta.* **2005**, *69* (17), 4175-4185. DOI: 10.1016/j.gca.2005.04.007.
(224) Xie, X.; Johnson, T. M.; Wang, Y.; Lundstrom, C. C.; Ellis, A.; Wang, X.; Duan, M. Mobilization of arsenic in aquifers from the Datong Basin, China: evidence from geochemical and iron isotopic data. *Chemosphere.* **2013**, *90* (6), 1878-1884. DOI: 10.1016/j.chemosphere.2012.10.012.
(225) Guo, H.; Liu, C.; Lu, H.; Wanty, R. B.; Wang, J.; Zhou, Y. Pathways of coupled arsenic and iron cycling in high arsenic groundwater of the Hetao basin, Inner Mongolia,

China: an iron isotope approach. *Geochim. Cosmochim. Acta.* **2013**, *112*, 130-145. DOI: 10.1016/j.gca.2013.02.031.
(226) Bergquist, B. A.; Boyle, E. A. Iron isotopes in the Amazon River system: weathering and transport signatures. *Earth Planet. Sci. Lett.* **2006**, *248* (1-2), 54-68. DOI: 10.1016/j.epsl.2006.05.004.
(227) Fantle, M. S.; DePaolo, D. J. Iron isotopic fractionation during continental weathering. *Earth Planet. Sci. Lett.* **2004**, *228* (3-4), 547-562. DOI: 10.1016/j.epsl.2004.10.013.
(228) Poitrasson, F.; Cruz Vieira, L.; Seyler, P.; Márcia dos Santos Pinheiro, G.; Santos Mulholland, D.; Bonnet, M.-P.; Martinez, J.-M.; Alcantara Lima, B.; Resende Boaventura, G.; Chmeleff, J.; et al. Iron isotope composition of the bulk waters and sediments from the Amazon River Basin. *Chem. Geol.* **2014**, *377*, 1-11. DOI: 10.1016/j.chemgeo.2014.03.019.
(229) Ellwood, M. J.; Hutchins, D. A.; Lohan, M. C.; Milne, A.; Nasemann, P.; Nodder, S. D.; Sander, S. G.; Strzepek, R.; Wilhelm, S. W.; Boyd, P. W. Iron stable isotopes track pelagic iron cycling during a subtropical phytoplankton bloom. *Proc. Natl. Acad. Sci. U.S.A.* **2015**, *112* (1), E15-20. DOI: 10.1073/pnas.1421576112.
(230) Radic, A.; Lacan, F.; Murray, J. W. Iron isotopes in the seawater of the equatorial Pacific Ocean: new constraints for the oceanic iron cycle. *Earth Planet. Sci. Lett.* **2011**, *306* (1-2), 1-10. DOI: 10.1016/j.epsl.2011.03.015.
(231) Severmann, S.; Lyons, T. W.; Anbar, A.; McManus, J.; Gordon, G. Modern iron isotope perspective on the benthic iron shuttle and the redox evolution of ancient oceans. *Geology.* **2008**, *36* (6), 487-490. DOI: 10.1130/g24670a.1.
(232) Sharma, M.; Polizzotto, M.; Anbar, A. D. Iron isotopes in hot springs along the Juan de Fuca Ridge. *Earth Planet. Sci. Lett.* **2001**, *194* (1-2), 39-51.
(233) Bennett, S. A.; Rouxel, O.; Schmidt, K.; Garbe-Schönberg, D.; Statham, P. J.; German, C. R. Iron isotope fractionation in a buoyant hydrothermal plume, 5°S Mid-Atlantic Ridge. *Geochim. Cosmochim. Acta.* **2009**, *73* (19), 5619-5634. DOI: 10.1016/j.gca.2009.06.027.
(234) Wu, L.; Brucker, R. P.; Beard, B. L.; Roden, E. E.; Johnson, C. M. Iron isotope characteristics of hot springs at Chocolate Pots, Yellowstone National Park. *Astrobiology.* **2013**, *13* (11), 1091-1101. DOI: 10.1089/ast.2013.0996.
(235) Hofmann, A.; Bekker, A.; Rouxel, O.; Rumble, D.; Master, S. Multiple sulphur and iron isotope composition of detrital pyrite in Archaean sedimentary rocks: a new tool for provenance analysis. *Earth Planet. Sci. Lett.* **2009**, *286* (3-4), 436-445. DOI: 10.1016/j.epsl.2009.07.008.
(236) Nishizawa, M.; Yamamoto, H.; Ueno, Y.; Tsuruoka, S.; Shibuya, T.; Sawaki, Y.; Yamamoto, S.; Kon, Y.; Kitajima, K.; Komiya, T.; et al. Grain-scale iron isotopic distribution of pyrite from Precambrian shallow marine carbonate revealed by a femtosecond laser ablation multicollector ICP-MS technique: Possible proxy for the redox state of ancient seawater. *Geochim. Cosmochim. Acta.* **2010**, *74* (9), 2760-2778. DOI: 10.1016/j.gca.2010.02.014.
(237) Ruttner, F. *Fundamentals of Limnology*; University of Toronto Press, 1963.
(238) Brunskill, G. J.; Schindler, D. W. Geography and bathymetry of selected lake basins, experimental lakes area, northwestern Ontario. *J. Fish. Res. Board C.* **1971**, (28), 139-155.
(239) Huttunen, P.; Merilaninen, J. New Freezing Device Providing Large Unmixed Sediment Samples from Lakes. *Ann. Bot. Fenn.* **1978**, *15*, 128-130.
(240) Stookey, L. L. Ferrozine-a new spectrophotometric reagent for iron. *Anal. Chem.* **1970**, *42* (7), 779-781.

(241) Viollier, E.; Inglett, P. W.; Hunter, K.; Roychoudhury, A. N.; Van Cappellen, P. The ferrozine method revisited: Fe(II)/Fe(III) determination in natural waters. *Appl. Geochem.* **2000**, *15*, 785-790.
(242) Heyes, A.; Bell, J. T. Sulfide analysis using ion specific electrode (with preservation in sulfide anti-oxidant buffer) Appendix D. In *Standard Operating Procedures*, Academy of Natural Sciences, 1999.
(243) Stainton, M. P.; Capel, M. J.; Armstrong, F. A. J. The chemical analysis of freshwater, 2nd ed. *Can. Fish. Mar. Serv. Misc. Spec. Publ.* **1977**, *25*, 180.
(244) Beard, B. L.; Johnson, C. M.; Skulan, J. L.; Nealson, K. H.; Cox, L.; Sun, H. Application of Fe isotopes to tracing the geochemical and biological cycling of Fe. *Chem. Geol.* **2003**, *195* (1-4), 87-117. DOI: 10.1016/s0009-2541(02)00390-x.
(245) Luther, G. W.; Rozan, T. F.; Taillefert, M.; Nuzzio, D. B.; Meo, C. D.; Shank, T. M.; Lutz, R. A.; Cary, S. C. Chemical speciation drives hydrothermal vent ecology. *Nature* **2001**, *410*, 813-816.
(246) Stephenson, M.; Schwartz, W. J.; Melnyk, T. W.; Motycka, M. F. Measurement of advective water velocity in lake sediment using natural helium gradients. *J. Hydrol.* **1994**, *154*, 63-84.
(247) Campbell, P.; Torgeson, T. Maintenance of iron meromixis by iron redeposition in a rapidly flushed monimolimnion. *Can. J. Fish. Aquat. Sci.* **1980**, *37*, 1303-1313.
(248) Chan, W. H.; Tang, A. J. S.; Chung, D. H. S.; Lusis, M. A. Concentration and deposition of trace metals in Ontario-1982. *Wat. Air and Soil Poll.* **1986**, *29*, 373-389.
(249) Barrie, L. A. Aspects of atmospheric pollutant origin and deposition revealed by multielemental observations at a rural location in eastern Canada. *J. Geophys. Res.* **1988**, *93*, 3773-3788.
(250) Laudon, H.; Berggren, M.; Ågren, A.; Buffam, I.; Bishop, K.; Grabs, T.; Jansson, M.; Köhler, S. Patterns and dynamics of dissolved organic carbon (DOC) in boreal streams: the role of processes, connectivity, and scaling. *Ecosystems.* **2011**, *14* (6), 880-893. DOI: 10.1007/s10021-011-9452-8.
(251) Buffam, I.; Laudon, H.; Temnerud, J.; Mörth, C.-M.; Bishop, K. Landscape-scale variability of acidity and dissolved organic carbon during spring flood in a boreal stream network. *J. Geophys. Res.* **2007**, *112*, G01022. DOI: 10.1029/2006jg000218.
(252) Ågren, A.; Buffam, I.; Berggren, M.; Bishop, K.; Jansson, M.; Laudon, H. Dissolved organic carbon characteristics in boreal streams in a forest-wetland gradient during the transition between winter and summer. *J. Geophys. Res.* **2008**, *113*, G03031. DOI: 10.1029/2007jg000674.
(253) Pokrovsky, O. S.; Schott, J. Iron colloids/organic matter associated transport of major and trace elements in small boreal rivers and their estuaries (NW Russia). *Chem. Geol.* **2002**, *190*, 141-179.
(254) Ingri, J.; Malinovsky, D.; Rodushkin, I.; Baxter, D. C.; Widerlund, A.; Andersson, P.; Gustafsson, Ö.; Forsling, W.; Öhlander, B. Iron isotope fractionation in river colloidal matter. *Earth Planet. Sci. Lett.* **2006**, *245* (3-4), 792-798. DOI: 10.1016/j.epsl.2006.03.031.
(255) Mead, J. The control of Fe and pH on the photodegradation and characterization of dissolved organic matter in small, oligotrophic Canadian Shield freshwaters. Master's thesis, University of Waterloo, Waterloo, Canada, 2017.

(256) Escoube, R.; Rouxel, O. J.; Sholkovitz, E.; Donard, O. F. X. Iron isotope systematics in estuaries: the case of North River, Massachusetts (USA). *Geochim. Cosmochim. Acta.* **2009**, *73* (14), 4045-4059. DOI: 10.1016/j.gca.2009.04.026.
(257) dos Santos Pinheiro, G. M.; Poitrasson, F.; Sondag, F.; Cochonneau, G.; Vieira, L. C. Contrasting iron isotopic compositions in river suspended particulate matter: the Negro and the Amazon annual river cycles. *Earth Planet. Sci. Lett.* **2014**, *394*, 168-178. DOI: 10.1016/j.epsl.2014.03.006.
(258) Ilina, S. M.; Poitrasson, F.; Lapitskiy, S. A.; Alekhin, Y. V.; Viers, J.; Pokrovsky, O. S. Extreme iron isotope fractionation between colloids and particles of boreal and temperate organic-rich waters. *Geochim. Cosmochim. Acta.* **2013**, *101*, 96-111. DOI: 10.1016/j.gca.2012.10.023.
(259) Lotfi-Kalahroodi, E.; Pierson-Wickmann, A. C.; Rouxel, O.; Marsac, R.; Bouhnik-Le Coz, M.; Hanna, K.; Davranche, M. More than redox, biological organic ligands control iron isotope fractionation in the riparian wetland. *Sci. Rep.* **2021**, *11* (1), 1933. DOI: 10.1038/s41598-021-81494-z.
(260) Wiederhold, J. G.; Teutsch, N.; Kraemer, S. M.; Halliday, A. N.; Kretzschmar, R. Iron Isotope Fractionation during Pedogenesis in Redoximorphic Soils. *Soil Science Society of America Journal* **2007**, *71* (6), 1840-1850. DOI: 10.2136/sssaj2006.0379.
(261) Brantley, S. L.; Liermann, L. J.; Bullen, T. D. Fractionation of Fe isotopes by soil microbes and organic acids. *Geology.* **2001**, *29* (6), 535-538.
(262) Schindler, D. W.; Bayley, S. E.; Parker, B. R. The effects of climatic warming on the properties of boreal lakes and streams at the Experimental Lakes Area, northwestern Ontario. *Limnol. Oceanogr.* **1996**, *41* (5), 1004-1017.
(263) Schindler, D. W.; Curtis, P. J.; Bayley, S. E.; Parker, B. R.; Beaty, K. G.; Stainton, M. P. Climate-induced changes in the dissolved organic carbon budgets of boreal lakes. *Biogeochemistry.* **1997**, *36*, 9-28.
(264) Icopini, G. A.; Anbar, A. D.; Ruebush, S. S.; Tien, M.; Brantley, S. L. Iron isotope fractionation during microbial reduction of iron: the importance of adsorption. *Geology.* **2004**, *32* (3). DOI: 10.1130/g20184.1.
(265) Mulholland, D. S.; Poitrasson, F.; Shirokova, L. S.; González, A. G.; Pokrovsky, O. S.; Boaventura, G. R.; Vieira, L. C. Iron isotope fractionation during Fe(II) and Fe(III) adsorption on cyanobacteria. *Chem. Geol.* **2015**, *400*, 24-33. DOI: 10.1016/j.chemgeo.2015.01.017.
(266) Hecky, R. E.; Campbell, P.; Hendzel, L. L. The stoichiometry of carbon, nitrogen, and phosphorus in particulate matter of lakes and oceans. *Limnol. Oceanogr.* **1993**, *38* (4), 709-724.
(267) Oleinikova, O. V.; Poitrasson, F.; Drozdova, O. Y.; Shirokova, L. S.; Lapitskiy, S. A.; Pokrovsky, O. S. Iron isotope fractionation during bio- and photodegradation of organoferric colloids in boreal humic waters. *Environ. Sci. Technol.* **2019**, *53* (19), 11183-11194. DOI: 10.1021/acs.est.9b02797.
(268) Gennings, C.; Molot, L. A.; Dillon, P. J. Enhanced photochemical loss of organic carbon in acidic waters. *Biogeochemistry.* **2001**, *52*, 339-354.
(269) Tammeorg, O.; Nürnberg, G.; Niemistö, J.; Haldna, M.; Horppila, J. Internal phosphorus loading due to sediment anoxia in shallow areas: implications for lake aeration treatments. *Aquat. Sci.* **2020**, *82* (3), 54. DOI: 10.1007/s00027-020-00724-0.

(270) Andersen, M. R.; Kragh, T.; Sand-Jensen, K. Extreme diel dissolved oxygen and carbon cycles in shallow vegetated lakes. *Proc. Royal Soc. B.* **2017**, *284*, 20171427. DOI: 10.1098/rspb.2017.1427.
(271) Cook, R. B. Distributions of ferrous iron and sulfide in an anoxic hypolimnion. *Can. J. Fish. Aquat. Sci* **1984**, *41*, 286-293.
(272) Quay, P. D.; Broecker, W. S.; Hesslein, R. H.; Schindler, D. W. Vertical diffusion rates determined by tritium tracer experiments in the thermocline and hypolimnion of two lakes. *Limnol. Oceanogr.* **1980**, *25* (2), 201-218.
(273) Davison, W. The solubility of iron sulphides in synthetic and natural waters at ambient temperature. *Aquat. Sci.* **1991**, *53* (4), 309-329.
(274) Al-Borno, A.; Tomson, M. B. The temperature dependence of the solubility product constant of vivianite. *Geochim. Cosmochim. Acta.* **1994**, *58* (24), 5373-5378.
(275) Beard, B. L.; Johnson, C. M. Fe isotope variations in the modern and ancient earth and other planetary bodies. *Rev. Mineral. Geochem.* **2004**, *55* (1), 319-357.
(276) Tsuji, J. M.; Tran, N.; Schiff, S. L.; Venkiteswaran, J. J.; Molot, L. A.; Tank, M.; Hanada, S.; Neufeld, J. D. Anoxygenic photosynthesis and iron-sulfur metabolic potential of *Chlorobia* populations from seasonally anoxic Boreal Shield lakes. *ISME J.* **2020**, *14*, 2732-2747. DOI: 10.1038/s41396-020-0725-0.
(277) Heising, S.; Richter, L.; Ludwig, W.; Schink, B. *Chlorobium ferrooxidans* sp. nov., a phototrophic green sulfur bacterium that oxidizes ferrous iron in coculture with a "*Geospirillum*" sp. strain. *Arch. Microbiol.* **1999**, *172*, 116-124.
(278) Hanert, H. H. The Genus *Gallionella*. In *The Prokaryotes*, Balows, A., Trüper, H. G., Dworkin, M., Harder, W., Schleifer, K. H. Eds.; Springer, 1992; p 4082.
(279) McAllister, S. M.; Polson, S. W.; Butterfield, D. A.; Glazer, B. T.; Sylvan, J. B.; Chan, C. S. Validating the cyc2 neutrophilic iron oxidation pathway using meta-omics of *Zetaproteobacteria* iron mats at marine hydrothermal vents. *mSystems* **2020**, *5* (1). DOI: 10.1128/mSystems.00553-19.
(280) Jin, L.; Lee, C. S.; Ahn, C. Y.; Lee, H. G.; Lee, S.; Shin, H. H.; Lim, D.; Oh, H. M. Abundant iron and sulfur oxidizers in the stratified sediment of a eutrophic freshwater reservoir with annual cyanobacterial blooms. *Sci. Rep.* **2017**, *7*, 43814. DOI: 10.1038/srep43814.
(281) Fabisch, M.; Beulig, F.; Akob, D. M.; Kusel, K. Surprising abundance of *Gallionella*-related iron oxidizers in creek sediments at pH 4.4 or at high heavy metal concentrations. *Front Microbiol* **2013**, *4*, 390. DOI: 10.3389/fmicb.2013.00390.
(282) Posth, N. R.; Huelin, S.; Konhauser, K. O.; Kappler, A. Size, density and composition of cell–mineral aggregates formed during anoxygenic phototrophic Fe(II) oxidation: Impact on modern and ancient environments. *Geochim. Cosmochim. Acta.* **2010**, *74* (12), 3476-3493. DOI: 10.1016/j.gca.2010.02.036.
(283) Schädler, S.; Burkhardt, C.; Hegler, F.; Straub, K. L.; Miot, J.; Benzerara, K.; Kappler, A. Formation of cell-iron-mineral aggregates by phototrophic and nitrate-reducing anaerobic Fe(II)-oxidizing bacteria. *Geomicrobiol. J.* **2009**, *26* (2), 93-103. DOI: 10.1080/01490450802660573.
(284) Miot, J.; Jézéquel, D.; Benzerara, K.; Cordier, L.; Rivas-Lamelo, S.; Skouri-Panet, F.; Férard, C.; Poinsot, M.; Duprat, E. Mineralogical diversity in lake Pavin: connections with water column chemistry and biomineralization processes. *Minerals.* **2016**, *6* (2), 24. DOI: 10.3390/min6020024.

(285) Berg, J. S.; Michellod, D.; Pjevac, P.; Martinez-Perez, C.; Buckner, C. R.; Hach, P. F.; Schubert, C. J.; Milucka, J.; Kuypers, M. M. Intensive cryptic microbial iron cycling in the low iron water column of the meromictic Lake Cadagno. *Environ. Microbiol.* **2016**, *18* (12), 5288-5302. DOI: 10.1111/1462-2920.13587.
(286) Garg, S.; Jiang, C.; Miller, C. J.; Rose, A. L.; Waite, T. D. Iron redox transformations in continuously photolyzed acidic solutions containing natural organic matter: kinetic and mechanistic insights. *Environmental science & technology* **2013**, *47* (16), 9190-9197, Research Support, Non-U.S. Gov't. DOI: 10.1021/es401087q.
(287) Martin, J. H.; Fitzwater, S. E. Iron deficiency limits phytoplankton growth in the north-east Pacific subarctic. *Nature* **1988**, *353* (331), 341-343.
(288) Frankel, R. B. Iron biominerals: an overview. In *Iron biominerals*, Frankel, R. B., Blakemore, R. P. Eds.; Plenum Press, 1991.
(289) Lowenstam, H. A. Mineral formed by organisms. *Science* **1981**, *211*, 1126-1131. DOI: 10.1007/s00216-015-9025-3.
(290) Rose, A. L.; Waite, T. D. Kinetics of Iron Complexation by Dissolved Natural Organic Matter in Coastal Waters. *Marine Chemistry* **2003**, *84*, 85-103. DOI: 10.1016/j.gca.2004.04.023.
(291) Yamamoto, M.; Nishida, A.; Otsuka, K.; Komai, T.; Fukushima, M. Evaluation of the Binding of Iron(II) to Humic Substances Derived from a Compost Sample by Colorimetric Method Using Ferrozine. *Bioresour. Technol.* **2010**, *101*, 4456-4460. DOI: 10.1016/j.gca.2004.04.023.
(292) Weber, T.; Allard, T.; Tipping, E.; Benedetti, M. F. Modeling Iron Binding to Organic Matter. *Environmental science & technology* **2006**, *40*, 7488-7493.
(293) Van Schaik, J. W.; Persson, I.; Kleja, D. B.; Gustafsson, J. P. EXAFS Study on the Reaction between Iron and Fulvic Acid in Acid Aqueous Solutions. *Environmental science & technology* **2008**, *42*, 2367-2373.
(294) Morris, A. J.; Hesterberg, D. L. Iron(III) Coordination and Phosphate Sorption in Peat Reacted with Ferric or Ferrous Iron. *Soil Science Society of America Journal* **2012**, *76* (1), 101. DOI: 10.2136/sssaj2011.0097.
(295) Anderson, D. M.; Glibert, P. M.; Burkholder, J. M. Harmful Algal and Blooms and Eutrophication Nutrient Sources, Composition, and Consequences. *Estuaries* **2002**, *25* (4b), 704-726.
(296) Backer, L.; McGillicuddy, D. Harmful Algal Blooms at the Interface Between Coastal Oceanography and Human Health. *Oceanography* **2006**, *19* (2), 94-106. DOI: 10.5670/oceanog.2006.72.
(297) Glibert, P. M.; Anderson, D. M.; Gentien, P.; Graneli, E.; Sellner, K. G. The Global Complex Phenomena of Harmful Algal Blooms. *Oceanography* **2005**, *18* (2), 136-147.
(298) Liu, K.; Schiff, S. L.; Wu, L.; Molot, L. A.; Venkiteswaran, J. J.; Paterson, M. J.; Elgood, R. J.; Tsuji, J. M.; Neufeld, J. D. Large Fractionation in Iron Isotopes Implicates Metabolic Pathways for Iron Cycling in Boreal Shield Lakes. *Environ Sci Technol* **2022**, *56* (20), 14840-14851. DOI: 10.1021/acs.est.2c04247.
(299) McCullough, G. K.; Campbell, P. Lake Variation and Climate Change Study: ELA Lakes, 1986-1990. II. Watershed Geography and Lake Morphology. *Can. Tech. Rep. Fish. Aquat. Sci* **1993**, (1898), iv + 29 p.
(300) Cline, J. D. Spectrophotometric Determination of Hydrogen Sulfide in Natural Waters. *Limnol. Oceanogr.* **1969**, *14* (3), 454-458.

(301) Raczek, I.; Stoll, B.; Hofmann, A. W.; Peter Jochum, K. High-Precision Trace Element Data for the USGS Reference Materials BCR-1, BCR-2, BHVO-1, BHVO-2, AGV-1, AGV-2, DTS-1, DTS-2, GSP-1 and GSP-2 by ID-TIMS and MIC-SSMS. *Geostandards Newsletter* **2007**, *25* (1), 77-86. DOI: 10.1111/j.1751-908X.2001.tb00789.x.
(302) Waheed, S.; Rahman, A.; Siddique, N.; Ahmad, S. Rare earth and other trace element content of NRCC HISS-1 sandy marine sediment reference material. *Geostandards and Geoanalytical Research* **2007**, *31* (2), 133-141.
(303) Craddock, P. R.; Dauphas, N. Iron Isotopic Compositions of Geological Reference Materials and Chondrites. *Geostandards and Geoanalytical Research* **2011**, *35* (1), 101-123. DOI: 10.1111/j.1751-908X.2010.00085.x.
(304) Liu, S.-A.; Li, D.; Li, S.; Teng, F.-Z.; Ke, S.; He, Y.; Lu, Y. High-precision copper and iron isotope analysis of igneous rock standards by MC-ICP-MS. *J. Anal. At. Spectrom.* **2014**, *29* (1), 122-133. DOI: 10.1039/c3ja50232e.
(305) Poitrasson, F.; Freydier, R. Heavy iron isotope composition of granites determined by high resolution MC-ICP-MS. *Chem. Geol.* **2005**, *222* (1-2), 132-147. DOI: 10.1016/j.chemgeo.2005.07.005.
(306) Sivan, O.; Erel, Y.; Mandler, D.; Nishri, A. The Dynamic Redox Chemistry of Iron in the Epilimnion of Lake Kinneret (Sea of Galilee). *Geochim. Cosmochim. Acta.* **1998**, *62* (4), 565-576. DOI: 10.1016/s0016-7037(97)00376-1.
(307) Emmenegger, L.; Schönenberger, R.; Sigg, L.; Sulzberger, B. Light-induced redox cycling of iron in circumneutral lakes. *Limnol. Oceanogr.* **2001**, *46* (1), 49-61. DOI: 10.4319/lo.2001.46.1.0049.
(308) Shaked, Y.; Erel, Y.; Sukenik, A. Phytoplankton-mediated redox cycle of iron in the epilimnion of lake Kinneret. *Environmental Science & Technology* **2002**, *36*, 460-467.
(309) Voelker, B. M.; Morel, F. M. M.; Sulzberger, B. Iron redox cycling in surface waters: effects of humic substances and light. *Environ Sci Technol* **1997**, *31*, 1004-1011.
(310) Croot, P. L.; Bowie, A. R.; Frew, R. D.; Maldonado, M. T.; Hall, J. A.; Safi, K. A.; La Roche, J.; Boyd, P. W.; Law, C. S. Retention of dissolved iron and FeIIin an iron induced Southern Ocean phytoplankton bloom. *Geophysical Research Letters* **2001**, *28* (18), 3425-3428. DOI: 10.1029/2001gl013023.
(311) Roy, E. G.; Wells, M. L. Persistence of iron(II) in surface waters of the western subarctic Pacific. *Limnol. Oceanogr.* **2008**, *53* (1), 89-98.
(312) Emmenegger, L.; King, D. W.; Sigg, L.; Sulzberger, B. Oxidation kinetics of Fe(II) in a eutrophic swiss lake. *Environ Sci Technol* **1998**, *32*, 2990-2996.
(313) Pham, A. N.; Waite, T. D. Modeling the kinetics of Fe(II) oxidation in the presence of citrate and salicylate in aqueous solutions at pH 6.0-8.0 and 25 °C. *The Journal of Physical Chemistry A* **2008**, *112*, 5395-5405.
(314) Rose, A. L.; Waite, T. D. Effect of dissolved natural organic matter on the kinetics of ferrous iron oxygenation in seawater. *Environ. Sci. Technol.* **2003**, *37*, 4877-4886.
(315) Santana-Casiano, J. M.; González-Dávila, M.; Rodrígueza, M. J.; JMillerob, F. The effect of organic compounds in the oxidation kinetics of Fe(II). *Mar. Chem.* **2000**, *70*, 211-222.
(316) Johnson, C. M.; Skulan, J. L.; Beard, B. L.; Sun, H.; Nealson, K. H.; Braterman, P. S. Isotopic fractionation between Fe(III) and Fe(II) in aqueous solutions. *Earth Planet. Sci. Lett.* **2002**, *195*, 141-153.

(317) Skulan, J. L.; Beard, B. L.; Johnson, C. M. Kinetic and equilibrium Fe isotope fractionation between aqueous Fe(III) and hematite. *Geochim. Cosmochim. Acta.* **2002**, *66* (17), 2995-3015.
(318) Wiederhold, J. G.; Kraemer, S.; Teutsch, N.; Borer, P. M.; Halliday, A. N.; Kretzschmar, R. Iron isotope fractionation during proton-promoted, ligand-controlled, and reductive dissolution of goethite. *Environ. Sci. Technol.* **2006**, *40*, 3787-3793.
(319) Brand, L. E. Minimum iron requirements of marine phytoplankton and the implications for the biogeochemical control of new production. *Limnol. Oceanogr.* **1991**, *36* (8), 1756-1771. DOI: 10.4319/lo.1991.36.8.1756.
(320) Leung, T.; Wilkinson, G. M.; Swanner, E. D. Iron availability allows sustained cyanobacterial blooms: a dual-lake case study. *Inland Waters* **2021**, *11* (3), 417-429. DOI: 10.1080/20442041.2021.1904762.
(321) Schoemann, V.; de Baar, H. J. W.; de Jong, J. T. M.; Lancelot, C. Effects of phytoplankton blooms on the cycling of manganese and iron in coastal waters. *Limnol. Oceanogr.* **1998**, *43* (7), 1427-1441. DOI: 10.4319/lo.1998.43.7.1427.
(322) Gobler, C.; Donat, J. R.; Consolvo III, J. A.; Sañudo-Wilhelmy, S. A. Physicochemical speciation of iron during coastal algal blooms. *Mar. Chem.* **2002**, *77*, 71-89.
(323) Pokrovsky, O. S.; Shirokova, L. S. Diurnal variations of dissolved and colloidal organic carbon and trace metals in a boreal lake during summer bloom. *Water Res* **2013**, *47* (2), 922-932. DOI: 10.1016/j.watres.2012.11.017.
(324) Ellwood, M. J.; Nodder, S. D.; King, A. L.; Hutchins, D. A.; Wilhelm, S. W.; Boyd, P. W. Pelagic iron cycling during the subtropical spring bloom, east of New Zealand. *Mar. Chem.* **2014**, *160*, 18-33. DOI: 10.1016/j.marchem.2014.01.004.
(325) van der Merwe, P.; Bowie, A. R.; Quéroué, F.; Armand, L.; Blain, S.; Chever, F.; Davies, D.; Dehairs, F.; Planchon, F.; Sarthou, G.; et al. Sourcing the iron in the naturally fertilised bloom around the Kerguelen Plateau: particulate trace metal dynamics. *Biogeosciences* **2015**, *12* (3), 739-755. DOI: 10.5194/bg-12-739-2015.
(326) Swanner, E. D.; Maisch, M.; Wu, W.; Kappler, A. Oxic Fe(III) reduction could have generated Fe(II) in the photic zone of Precambrian seawater. *Sci Rep* **2018**, *8* (1), 4238. DOI: 10.1038/s41598-018-22694-y.
(327) Lee, Y. P.; Fujii, M.; Kikuchi, T.; Natsuike, M.; Ito, H.; Watanabe, T.; Yoshimura, C. Importance of allochthonous and autochthonous dissolved organic matter in Fe(II) oxidation: A case study in Shizugawa Bay watershed, Japan. *Chemosphere.* **2017**, *180*, 221-228. DOI: 10.1016/j.chemosphere.2017.04.008.
(328) Gonzalez, A. G.; Santana-Casiano, J. M.; Gonzalez-Davila, M.; Perez-Almeida, N.; Suarez de Tangil, M. Effect of Dunaliella tertiolecta organic exudates on the Fe(II) oxidation kinetics in seawater. *Environ Sci Technol* **2014**, *48* (14), 7933-7941. DOI: 10.1021/es5013092.
(329) Fujii, M.; Dang, T. C.; Rose, A. L.; Omura, T.; Waite, T. D. Effect of light on iron uptake by the freshwater cyanobacterium Microcystis aeruginosa. *Environ Sci Technol* **2011**, *45* (4), 1391-1398. DOI: 10.1021/es103311h.
(330) Hasegawa, H.; Tate, Y.; Ogino, M.; Maki, T.; Begum, Z. A.; Ichijo, T.; Rahman, I. M. M. Laboratory culture experiments to study the effect of lignite humic acid fractions on iron solubility and iron uptake rates in phytoplankton. *Journal of Applied Phycology* **2016**, *29* (2), 903-915. DOI: 10.1007/s10811-016-0982-5.

(331) Fujii, M.; Dang, T. C.; Bligh, M. W.; Rose, A. L.; Waite, T. D. Effect of natural organic matter on iron uptake by the freshwater cyanobacterium Microcystis aeruginosa. *Environ Sci Technol* **2014**, *48* (1), 365-374. DOI: 10.1021/es404090h.
(332) Kerry, A.; Laudenbach, D. E.; Trick, C. G. Influence of Iron Limitation and Nitrogen Source on Growth and Siderophore Production by Cyanobacteria. *Journal of Phycology* **1988**, *24* (4), 566-571. DOI: 10.1111/j.1529-8817.1988.tb00107.x.
(333) Fujii, M.; Rose, A. L.; Omura, T.; Waite, T. D. Effect of Fe(II) and Fe(III) transformation kinetics on iron acquisition by a toxic strain of *Microcystis aeruginosa*. *Environ Sci Technol* **2010**, *44*, 1980-1986.
(334) Wirtz, N. L.; Treble, R. G.; Weger, H. G. Siderophore-Independent Iron Uptake by Iron-Limited Cells of the Cyanobacterium Anabaena Flos-Aquae1. *Journal of Phycology* **2010**, *46* (5), 947-957. DOI: 10.1111/j.1529-8817.2010.00881.x.
(335) Shaked, Y.; Kustka, A. B.; Morel, F. M. M. A general kinetic model for iron acquisition by eukaryotic phytoplankton. *Limnol. Oceanogr.* **2005**, *50* (3), 872-882. DOI: 10.4319/lo.2005.50.3.0872.
(336) Sunda, W. G.; Huntsman, S. A. High iron requirement for growth, photosynthesis, and low-light acclimation in the coastal cyanobacterium Synechococcus bacillaris. *Front Microbiol* **2015**, *6*, 561. DOI: 10.3389/fmicb.2015.00561.
(337) Busigny, V.; Je´ze´quel, D.; Cosmidis, J.; Viollier, E.; Benzerara, K.; Planavsky, N. J.; Albe´ric, P.; Lebeau, O.; Sarazin, G.; Michard, G. The iron wheel in Lac Pavin: interaction with phosphorus cycle. In *Lake Pavin: History, Geology, Biogeochemistry, and Sedimentology of a Deep Meromictic Maar Lake*, Sime-Ngando, T., Boivin, P., Chapron, E., Jezequel, D., Meybeck, M. Eds.; Springer International Publishing, 2016; pp 205-220.
(338) Dachs, J.; Eisenreich, S.; Baker, J. E.; Ko, F.; Jeremiason, J. D. Coupling of phytoplankton uptake and air-water exchange of persistent organic pollutants. *Environ Sci Technol* **1999**, *33*, 3653-3366
.
(339) Planquette, H.; Sanders, R. R.; Statham, P. J.; Morris, P. J.; Fones, G. R. Fluxes of particulate iron from the upper ocean around the Crozet Islands: A naturally iron-fertilized environment in the Southern Ocean. *Global Biogeochemical Cycles* **2011**, *25* (2), n/a-n/a. DOI: 10.1029/2010gb003789.
(340) Lamborg, C. H.; Buesseler, K. O.; Lam, P. J. Sinking fluxes of minor and trace elements in the North Pacific Ocean measured during the VERTIGO program. *Deep Sea Research Part II: Topical Studies in Oceanography* **2008**, *55* (14-15), 1564-1577. DOI: 10.1016/j.dsr2.2008.04.012.
(341) Jeremiason, J. D.; Eisenreich, S. J.; Paterson, M. J.; Beaty, K. G.; Hecky, R.; Elser, J. J. Biogeochemical cycling of PCBs in lakes of variable trophic status: A paired-lake experiment. *Limnol. Oceanogr.* **1999**, *44* (3part2), 889-902. DOI: 10.4319/lo.1999.44.3_part_2.0889.
(342) Kasinak, J.-M. E.; Holt, B. M.; Chislock, M. F.; Wilson, A. E. Benchtop fluorometry of phycocyanin as a rapid approach for estimating cyanobacterial biovolume. *Journal of Plankton Research* **2015**, *37* (1), 248-257. DOI: 10.1093/plankt/fbu096.
(343) Woźniak, M.; Bradtke, K.; Darecki, M.; Krężel, A. Empirical Model for Phycocyanin Concentration Estimation as an Indicator of Cyanobacterial Bloom in the Optically Complex Coastal Waters of the Baltic Sea. *Remote Sensing* **2016**, *8* (3). DOI: 10.3390/rs8030212.

(344) Cunningham, B. R.; John, S. G. The effect of iron limitation on cyanobacteria major nutrient and trace element stoichiometry. *Limnol. Oceanogr.* **2017**, *62* (2), 846-858. DOI: 10.1002/lno.10484.
(345) Harrison, G. I.; Morel, F. M. M. Response of the marine diatom Thalassiosira weissflogii
to iron stress1. *Limnol. Oceanogr.* **1986**, *31* (5), 989-997. DOI: 10.4319/lo.1986.31.5.0989.
(346) Ellwood, M. J.; Strzepek, R. F.; Strutton, P. G.; Trull, T. W.; Fourquez, M.; Boyd, P. W. Distinct iron cycling in a Southern Ocean eddy. *Nat Commun* **2020**, *11* (1), 825. DOI: 10.1038/s41467-020-14464-0.
(347) Michiels, C. C.; Darchambeau, F.; Roland, F. A. E.; Morana, C.; Llirós, M.; García-Armisen, T.; Thamdrup, B.; Borges, A. V.; Canfield, D. E.; Servais, P.; et al. Iron-dependent nitrogen cycling in a ferruginous lake and the nutrient status of Proterozoic oceans. *Nature Geoscience* **2017**, *10* (3), 217-221. DOI: 10.1038/ngeo2886.
(348) Ayala-Munoz, D.; Macalady, J. L.; Sanchez-Espana, J.; Falagan, C.; Couradeau, E.; Burgos, W. D. Microbial carbon, sulfur, iron, and nitrogen cycling linked to the potential remediation of a meromictic acidic pit lake. *ISME J* **2022**, *16* (12), 2666-2679. DOI: 10.1038/s41396-022-01320-w.
(349) Orihel, D. M.; Schindler, D. W.; Ballard, N. C.; Graham, M. D.; O'Connell, D. W.; Wilson, L. R.; Vinebrooke, R. D. The “nutrient pump:” Iron-poor sediments fuel low nitrogen-to-phosphorus ratios and cyanobacterial blooms in polymictic lakes. *Limnol. Oceanogr.* **2015**, *60* (3), 856-871. DOI: 10.1002/lno.10076.
(350) Gumsley, A. P.; Chamberlain, K. R.; Bleeker, W.; Soderlund, U.; de Kock, M. O.; Larsson, E. R.; Bekker, A. Timing and tempo of the Great Oxidation Event. *Proc Natl Acad Sci U S A* **2017**, *114* (8), 1811-1816. DOI: 10.1073/pnas.1608824114.
(351) Findlay, D. L.; Vanni, M. J.; Paterson, M.; Mills, K. H.; Kasian, S. E. M.; Findlay, W. J.; Salki, A. G. Dynamics of a Boreal Lake Ecosystem during a Long-Term Manipulation of Top Predators. *Ecosystems.* **2005**, *8* (6), 603-618. DOI: 10.1007/s10021-005-1221-0.
(352) Schindler, D. W.; Fee, E. J. Experimental Lakes Area: Whole-Lake Experiments in Eutrophication. *J. Fish. Res. Bd. Canada* **1974**, *31*, 937-953.
(353) Schindler, D. W. The dilemma of controlling cultural eutrophication of lakes. *Proc Biol Sci* **2012**, *279* (1746), 4322-4333. DOI: 10.1098/rspb.2012.1032.
(354) Kendall, B.; Brennecka, G. A.; Weyer, S.; Anbar, A. D. Uranium isotope fractionation suggests oxidative uranium mobilization at 2.50 Ga. *Chem. Geol.* **2013**, *362*, 105-114. DOI: 10.1016/j.chemgeo.2013.08.010.
(355) Weyer, S.; Anbar, A. D.; Gerdes, A.; Gordon, G. W.; Algeo, T. J.; Boyle, E. A. Natural fractionation of 238U/235U. *Geochim. Cosmochim. Acta.* **2008**, *72* (2), 345-359. DOI: 10.1016/j.gca.2007.11.012.
(356) Schiff, S. L.; Tsuji, J. M.; Wu, L.; Venkiteswaran, J. J.; Molot, L. A.; Elgood, R. J.; Paterson, M. J.; Neufeld, J. D. Millions of Boreal Shield Lakes can be used to Probe Archaean Ocean Biogeochemistry. *Scientific reports* **2017**, *7*, 46708. DOI: 10.1038/srep46708.
(357) Tonin, J.; Sherbo, B.; Higgins, S. N.; Schiff, S. L.; Paterson, M. J. Dissolved organic carbon affects the occurrence of deep chlorophyll peaks and zooplankton resource use and biomass. *Freshw. Biol.* **2022**, *67* (8), 1357-1369. DOI: 10.1111/fwb.13922.

(358) Fee, E. J. The vertical and seasonal distribution of chlorophyll in lakes of the Experimental Lakes Area, northwestern Ontario: Implications for primary production estimates. *Limnol. Oceanogr.* **2003**, *21* (6), 767-783. DOI: 10.4319/lo.1976.21.6.0767.
(359) Bullen, T. D.; White, A. F.; Childs, C. W.; Vivit, D. V.; Schulz, M. S. Demonstration of significant abiotic iron isotope fractionation in nature. *Geology.* **2001**, *29*, 699-702.
(360) Jeon, B.; Dempsey, B. A.; Burgos, W. D. Kinetics and mechanisms for reactions of Fe(II) with iron(III) oxides. *Environmental Science & Technology* **2003**, *37*, 3309-3315.
(361) Tsuji, J. M. Microbial ecology of phototrophs in iron-rich Boreal Shield lakes. University of Waterloo, Waterloo, Canada, 2020.
(362) Han, X.; Tomaszewski, E. J.; Sorwat, J.; Pan, Y.; Kappler, A.; Byrne, J. M. Oxidation of green rust by anoxygenic phototrophic Fe(II)-oxidising bacteria. *Geochemical Perspectives Letters* **2020**, 52-57. DOI: 10.7185/geochemlet.2004.
(363) Kappler, A.; Newman, D. K. Formation of Fe(III)-minerals by Fe(II)-oxidizing photoautotrophic bacteria 1 1Associate editor: L. G. Benning. *Geochim. Cosmochim. Acta.* **2004**, *68* (6), 1217-1226. DOI: 10.1016/j.gca.2003.09.006.
(364) Laufer, K.; Niemeyer, A.; Nikeleit, V.; Halama, M.; Byrne, J. M.; Kappler, A. Physiological characterization of a halotolerant anoxygenic phototrophic Fe(II)-oxidizing green-sulfur bacterium isolated from a marine sediment. *FEMS Microbiol Ecol* **2017**, *93* (5). DOI: 10.1093/femsec/fix054.
(365) Wu, W.; Swanner, E. D.; Hao, L.; Zeitvogel, F.; Obst, M.; Pan, Y.; Kappler, A. Characterization of the physiology and cell-mineral interactions of the marine anoxygenic phototrophic Fe(II) oxidizer Rhodovulum iodosum--implications for Precambrian Fe(II) oxidation. *FEMS Microbiol Ecol* **2014**, *88* (3), 503-515. DOI: 10.1111/1574-6941.12315.
(366) Li, W.; Czaja, A. D.; Kranendonk, M. J. V.; Beard, B. L.; Roden, E. E.; Johnson, C. M. An anoxic, Fe(II)-rich, U-poor ocean 3.46 billion years ago. *Geochim. Cosmochim. Acta.* **2013**, *120*, 65-79. DOI: 10.1016/j.gca.2013.06.033.
(367) Busigny, V.; Marin-Carbonne, J.; Muller, E.; Cartigny, P.; Rollion-Bard, C.; Assayag, N.; Philippot, P. Iron and sulfur isotope constraints on redox conditions associated with the 3.2 Ga barite deposits of the Mapepe Formation (Barberton Greenstone Belt, South Africa). *Geochim. Cosmochim. Acta.* **2017**, *210*, 247-266. DOI: 10.1016/j.gca.2017.05.002.
(368) Pecoits, E.; Smith, M. L.; Catling, D. C.; Philippot, P.; Kappler, A.; Konhauser, K. O. Atmospheric hydrogen peroxide and Eoarchean iron formations. *Geobiology.* **2015**, *13* (1), 1-14. DOI: 10.1111/gbi.12116.
(369) O'Connell, D. W.; Ansems, N.; Kukkadapu, R. K.; Jaisi, D.; Orihel, D. M.; Cade-Menun, B. J.; Hu, Y.; Wiklund, J.; Hall, R. I.; Chessell, H.; et al. Changes in Sedimentary Phosphorus Burial Following Artificial Eutrophication of Lake 227, Experimental Lakes Area, Ontario, Canada. *Journal of Geophysical Research: Biogeosciences* **2020**, *125* (8). DOI: 10.1029/2020jg005713.
(370) Canfield, D. E.; Jorgensen, B. B.; Fossing, H.; Glud, R.; Gundersen, J.; Ramsing, N. B.; Thamdrup, B.; Hansen, J. W.; Nielsen, L. P.; hALL, P. O. J. Pathways of organic carbon oxidation in three continental margin sediments. *Marine Geology* **1993**, *113*, 27-40.
(371) Cummings, D. E.; March, A. W.; Bostick, B.; Spring, S.; Caccavo, F. J.; Fendorf, S.; Rosenzweig, R. F. Evidence for microbial Fe(III) reduction in anoxic, mining-impacted lake sediments (Lake Coeur d'Alene, Idaho). *Appl. Environ. Microbiol.* **2000**, *66* (1), 154-162.

(372) Percak-Dennett, E. M.; Loizeau, J.-L.; Beard, B. L.; Johnson, C. M.; Roden, E. E. Iron isotope geochemistry of biogenic magnetite-bearing sediments from the Bay of Vidy, Lake Geneva. *Chem. Geol.* **2013**, *360-361*, 32-40. DOI: 10.1016/j.chemgeo.2013.10.008.
(373) Tangalos, G. E.; Beard, B. L.; Johnson, C. M.; Alpers, C. N.; Shelobolina, E. S.; Xu, H.; Konishi, H.; Roden, E. E. Microbial production of isotopically light iron(II) in a modern chemically precipitated sediment and implications for isotopic variations in ancient rocks. *Geobiology.* **2010**, *8* (3), 197-208. DOI: 10.1111/j.1472-4669.2010.00237.x.
(374) Severmann, S.; Johnson, C. M.; Beard, B. L.; McManus, J. The effect of early diagenesis on the Fe isotope compositions of porewaters and authigenic minerals in continental margin sediments. *Geochim. Cosmochim. Acta.* **2006**, *70* (8), 2006-2022. DOI: 10.1016/j.gca.2006.01.007.
(375) Salas, E. C.; Berelson, W. M.; Hammond, D. E.; Kampf, A. R.; Nealson, K. H. The Influence of Carbon Source on the Products of Dissimilatory Iron Reduction. *Geomicrobiol. J.* **2009**, *26* (7), 451-462. DOI: 10.1080/01490450903060806.
(376) Lovley, D. R.; Stolz, J. F.; Nord, G. J.; Phillips, E. J. P. Anaerobic production of magnetite by a dissimilatory iron-reducing microorganism. *Science.* **1987**, *330*, 252-254.
(377) Taillefert, M.; Hover, V. C.; Rozan, T. F.; Theberge, S. M.; Luther, G. W. The influence of sulfides on soluble organic-Fe(III) in anoxic sediment porewaters. *Estuarine* **2002**, *25* (6A), 1088-1096.
(378) Beckler, J. S.; Jones, M. E.; Taillefert, M. The origin, composition, and reactivity of dissolved iron(III) complexes in coastal organic- and iron-rich sediments. *Geochim. Cosmochim. Acta.* **2015**, *152*, 72-88. DOI: 10.1016/j.gca.2014.12.017.
(379) Thomsen, U.; Thamdrup, B.; Stahl, D. A.; Canfield, D. E. Pathways of organic carbon oxidation in a deep lacustrine sediment, Lake Michigan. *Limnol. Oceanogr.* **2004**, *49* (6), 2046-2057. DOI: 10.4319/lo.2004.49.6.2046.
(380) Roden, E. E.; Wetzel, R. G. Organic carbon oxidation and suppression of methane production by microbial Fe(III) oxide reduction in vegetated and unvegetated freshwater wetland sediments. *Limnol. Oceanogr.* **1996**, *41* (8), 1733-1748. DOI: 10.4319/lo.1996.41.8.1733.
(381) Chapelle, F. H.; Lovley, D. R. Competitive Exclusion of Sulfate Reduction by Fe(lll)-Reducing Bacteria: A Mechanism for Producing Discrete Zones of High-Iron Ground Water. *Ground Water* **1992**, *30* (1), 29-36. DOI: 10.1111/j.1745-6584.1992.tb00808.x.
(382) Thiel, J.; Byrne, J. M.; Kappler, A.; Schink, B.; Pester, M. Pyrite formation from FeS and H(2)S is mediated through microbial redox activity. *Proc Natl Acad Sci U S A* **2019**, *116* (14), 6897-6902. DOI: 10.1073/pnas.1814412116.
(383) Homoky, W. B.; John, S. G.; Conway, T. M.; Mills, R. A. Distinct iron isotopic signatures and supply from marine sediment dissolution. *Nat Commun* **2013**, *4*, 2143. DOI: 10.1038/ncomms3143.
(384) Klar, J. K.; Homoky, W. B.; Statham, P. J.; Birchill, A. J.; Harris, E. L.; Woodward, E. M. S.; Silburn, B.; Cooper, M. J.; James, R. H.; Connelly, D. P.; et al. Stability of dissolved and soluble Fe(II) in shelf sediment pore waters and release to an oxic water column. *Biogeochemistry.* **2017**, *135* (1), 49-67. DOI: 10.1007/s10533-017-0309-x.
(385) Guilbaud, R.; Butler, I. B.; Ellam, R. M. Abiotic pyrite formation produces a large Fe isotope fractionation. *Science.* **2011**, *332*, 1548-1551.

(386) Rolison, J. M.; Stirling, C. H.; Middag, R.; Gault-Ringold, M.; George, E.; Rijkenberg, M. J. A. Iron isotope fractionation during pyrite formation in a sulfidic Precambrian ocean analogue. *Earth Planet. Sci. Lett.* **2018**, *488*, 1-13. DOI: 10.1016/j.epsl.2018.02.006.
(387) Planquette, H.; Sherrell, R. M.; Stammerjohn, S.; Field, M. P. Particulate iron delivery to the water column of the Amundsen Sea, Antarctica. *Mar. Chem.* **2013**, *153*, 15-30. DOI: 10.1016/j.marchem.2013.04.006.
(388) Barrett, P. M.; Resing, J. A.; Buck, N. J.; Buck, C. S.; Landing, W. M.; Measures, C. I. The trace element composition of suspended particulate matter in the upper 1000m of the eastern North Atlantic Ocean: A16N. *Mar. Chem.* **2012**, *142-144*, 41-53. DOI: 10.1016/j.marchem.2012.07.006.
(389) Mito, S.; Kawashina, M.; Sohrin, Y. Characterization of Suspended Solids in Lake Biwa by Measuring Their Elemental Composition of Al, Si, P, S, K, Ca, Ti, Mn, and Fe. *Limnology* **2002**, *3*, 11-19.
(390) Brunskill, G. J.; Povoledo, D.; Graham, B. W.; Stainton, M. P. Chemistry of Surface Sediments of Sixteen Lakes in the Experimental Lakes Area, Northwestern Ontario. *J. Fish. Res. Bd. Canada* **1971**, *28*, 277-294.
(391) Teng, F.-Z.; Dauphas, N.; Watkins, J. M. Non-Traditional Stable Isotopes: Retrospective and Prospective. *Reviews in Mineralogy and Geochemistry* **2017a**, *82* (1), 1-26. DOI: 10.2138/rmg.2017.82.1.
(392) Wunder, B.; Meixner, A.; Romer, R. L.; Feenstra, A.; Schettler, G.; Heinrich, W. Lithium isotope fractionation between Li-bearing staurolite, Li-mica and aqueous fluids: An experimental study. *Chemical Geology* **2007**, *238* (3-4), 277-290. DOI: 10.1016/j.chemgeo.2006.12.001.
(393) Burton, K. W.; Vigier, N. Lithium Isotopes as Tracers in Marine and Terrestrial Environments. In *Handbook of Enviromental Isotope Geochemistry*, Baskaran, M. Ed.; Vol. 1; Springer.
(394) Teng, F.-Z. Magnesium Isotope Geochemistry. *Reviews in Mineralogy and Geochemistry* **2017b**, *82* (1), 219-287. DOI: 10.2138/rmg.2017.82.1.
(395) Wombacher, F.; Eisenhauer, A.; Böhm, F.; Gussone, N.; Regenberg, M.; Dullo, W. C.; Rüggeberg, A. Magnesium stable isotope fractionation in marine biogenic calcite and aragonite. *Geochimica et Cosmochimica Acta* **2011**, *75* (19), 5797-5818. DOI: 10.1016/j.gca.2011.07.017.
(396) Li, W.-Y.; Teng, F.-Z.; Ke, S.; Rudnick, R. L.; Gao, S.; Wu, F.-Y.; Chappell, B. W. Heterogeneous magnesium isotopic composition of the upper continental crust. *Geochimica et Cosmochimica Acta* **2010**, *74* (23), 6867-6884. DOI: 10.1016/j.gca.2010.08.030.
(397) Teng, F.-Z.; Li, W.-Y.; Rudnick, R. L.; Gardner, L. R. Contrasting lithium and magnesium isotope fractionation during continental weathering. *Earth and Planetary Science Letters* **2010**, *300* (1-2), 63-71. DOI: 10.1016/j.epsl.2010.09.036.
(398) Moynier, F.; Vance, D.; Fujii, T.; Savage, P. The Isotope Geochemistry of Zinc and Copper. *Reviews in Mineralogy and Geochemistry* **2017**, *82* (1), 543-600. DOI: 10.2138/rmg.2017.82.13.
(399) Cloquet, C.; Carignan, J.; Lehmann, M. F.; Vanhaecke, F. Variation in the isotopic composition of zinc in the natural environment and the use of zinc isotopes in biogeosciences: a review. *Analytical and bioanalytical chemistry* **2008**, *390*, 451-463. DOI: 10.2138/rmg.2017.82.1.

(400) Savage, P.; Moynier, F.; Harvey, J.; Burton, K. The behavior of copper isotopes during igneous processes. *AGU conference, San Francisco* **2015**, *390* (2), 451-463. DOI: 10.1007/s00216-007-1635-y.
(401) Sossi, P. A.; Nebel, O.; O'Neill, H. S. C.; Moynier, F. Zinc isotope composition of the Earth and its behaviour during planetary accretion. *Chemical Geology* **2018**, *477*, 73-84. DOI: 10.1016/j.chemgeo.2017.12.006.
(402) Kendall, B.; Dahl, T. W.; Anbar, A. D. The Stable Isotope Geochemistry of Molybdenum. *Reviews in Mineralogy and Geochemistry* **2017**, *82* (1), 683-732. DOI: 10.2138/rmg.2017.82.16.
(403) Wasylenki, L. E.; Rolfe, B. A.; Weeks, C. L.; Spiro, T. G.; Anbar, A. D. Experimental investigation of the effects of temperature and ionic strength on Mo isotope fractionation during adsorption to manganese oxides. *Geochimica et Cosmochimica Acta* **2008**, *72* (24), 5997-6005. DOI: 10.1016/j.gca.2008.08.027.
(404) Barling, J.; Anbar, A. D. Molybdenum isotope fractionation during adsorption by manganese oxides. *Earth and Planetary Science Letters* **2004**, *217* (3-4), 315-329. DOI: 10.1016/s0012-821x(03)00608-3.
(405) Glass, J. B.; Wolfe-Simon, F.; Anbar, A. D. Coevolution of metal availability and nitrogen assimilation in cyanobacteria and algae. *Geobiology* **2009**, *7* (2), 100-123. DOI: 10.1111/j.1472-4669.2009.00190.x.
(406) Lovley, D. R. Dissimilatory Metal Reduction. *Annual review of microbiology* **1993**, *47*, 263-290.
(407) Albarède, F.; Beard, B. L. Analytical methods for non-traditional isotopes. In *Geochemistry of Non-traditional Stable Isotopes*, Johnson, C. M., Beard, B. L., Albarede, F. Eds.; Reviews in Mineralogy & Geochemistry, The Mineralogical Society of America, 2004; pp 113-152.
(408) Coyle, D.; Stanley, M. *Thermo Electron Manufacturing Limited and GV Instruments Limited merger inquiry: a report on the completed acquisition of GV Instruments Limited by Thermo Electron Manufacturing Limited*; Commission, G. B. C., Ed.; The stationery Office, 2007.
(409) Becker, J. S. *Inorganic mass spectrometry: principles and applications*; Wiley, 2007.
(410) Wieser, M.; Schwieters, J.; Douthitt, C. Multi-collector inductively coupled plasma mass spectrometry. In *Isotopic analysis:fundamentals and applications using ICP-MS*, Vanhaecke, F., Degryse, P. Eds.; Wiley-VCH, 2012.
(411) Beard, B. L.; Johnson, C. M. High precision iron isotope measurements of terrestrial and lunar materials. *Geochim Cosmochim Acta* **1999**, *63*, 1653-1660.
(412) Beard, B. L.; Johnson, C. M.; Cox, L.; Sun, H.; Nealson, K. H.; Aguilar, C. Iron isotope biosignatures. *Science* **1999**, *285*, 1889-1892.
(413) Johnson, C. M.; Beard, B. L. Correction of instrumentally produced mass fractionation during isotopic analysis of Fe by thermal ionization mass spectrometry. *Int J Mass Spectrom* **1999**, *193*, 87-99.
(414) Dodson, M. H. A theoretical study of the use of internal standards for precise isotopic analysis by the surface ionization technique: Part I - General first-order algebraic solutions. *Journal of Scientific Instruments* **1963**, *40*, 289-295.
(415) Fantle, M. S.; Bullen, T. D. Essentials of iron, chromium and calcium isotope analysis of natural materials by thermal ionization mass spectrometry. *Chem. Geol.* **2009**, *258*, 50-64.

(416) Anbar, A. D.; Roe, J. E.; Barling, J.; Nealson, K. H. Nonbiological Fractionation of Iron Isotopes. *Science* **2000**, *288* (5463), 126-128. DOI: 10.1126/science.288.5463.126.
(417) Belshaw, N. S.; Zhu, X.; Guo, Y.; O'Nions, R. K. High precision measurement of iron isotopes by plasma source mass spectrometry. *Int J Mass Spectrom* **2000**, *197*, 191-195.
(418) Vanhaecke, F. Single-collector inductively coupled plasma mass spectrometry. In *Isotopic analysis: fundamentals and applications using ICP-MS*, Vanhaecke, F., Degryse, P. Eds.; Wiley-VCH, 2012.
(419) Strelow, F. W. E. Improved separation of iron from copper and other elements by anion-exchange chromatography on a 4% cross-linked resin with high concentrations of hydrochloric acid. *Tatlanta* **1980**, *27*, 727-732.
(420) Cullum, D. C. Introdyction to surfactant analysis. Chapman & Hall: Madras, India, 1994; pp 81-83.
(421) Borrok, D. M.; Wanty, R. B.; Ridley, W. I.; Wolf, R.; Lamothe, P. J.; Adams, M. Separation of copper, iron, and zinc from complex aqueous solutions for isotopic measurement. *Chemical Geology* **2007**, *242* (3-4), 400-414. DOI: 10.1016/j.chemgeo.2007.04.004.
(422) Marechal, C. N.; Telouk, P.; Albarede, F. Precise analysis of copper and zinc isotopic compositions by plasma-source mass spectrometry. *Chem. Geol.* **1999**, *156*, 251-273.
(423) Malinovsky, D.; Stenberg, A.; Rodushkin, I.; Andren, H.; Ingri, J.; Öhlander, B.; Baxter, D. C. Performance of high resolution MC-ICP-MS for Fe isotope ratio measurements in sedimentary geological materials. *J. Anal. At. Spectrom.* **2003**, *18* (7), 687-695. DOI: 10.1039/b302312e.
(424) Skulan, J. L.; Beard, B. L.; Johnson, C. M. Kinetic and equilibrium Fe isotope fractionation between aqueous Fe(III) and hematite. *Geochim Cosmochim Acta* **2002**, *66* (17), 2995-3015.
(425) Meija, J.; Yang, L.; Mester, Z.; Sturgeon, R. E. Correction of instrumental mass discrimination for isotope ratio determination with multi-collector inductively coupled plasma mass spectrometry. In *Isotopic analysis: fundamentals and applications using ICP-MS*, Vanhaecke, F., Degryse, P. Eds.; WILEY-VCH, 2012.
(426) Rehkamper, M.; Schonbachler, M.; Andreasen, R. Application of multiple-collector inductively coupled plasma mass spectrometry to isotopic analysis in cosmochemistry. In *Isotopic analysis: fundamentals and applications using ICP-MS*; Vanhaecke, F., Degryse, P., Eds.; Wiley-VCH, 2012; pp 275-315.
(427) Matthews, A.; Zhu, X.; O'Nions, R. K. Kinetic iron stable isotope fractionation between iron (-II) and (-III) complexes in solution. *Earth and Planetary Science Letters* **2001**, *192*, 81-92.
(428) Anbar, A. D. Iron stable isotopes: beyond biosignatures. *Earth and Planetary Science Letters* **2004**, *217* (3-4), 223-236. DOI: 10.1016/s0012-821x(03)00572-7.
(429) Azrieli-Tal, I.; Matthews, A.; Bar-Matthews, M.; Almogi-Labin, A.; Vance, D.; Archer, C.; Teutsch, N. Evidence from molybdenum and iron isotopes and molybdenum–uranium covariation for sulphidic bottom waters during Eastern Mediterranean sapropel S1 formation. *Earth and Planetary Science Letters* **2014**, *393*, 231-242. DOI: 10.1016/j.epsl.2014.02.054.
(430) Xie, X.; Johnson, T. M.; Wang, Y.; Lundstrom, C. C.; Ellis, A.; Wang, X.; Duan, M.; Li, J. Pathways of arsenic from sediments to groundwater in the hyporheic zone: Evidence

from an iron isotope study. *Journal of Hydrology* **2014**, *511*, 509-517. DOI: 10.1016/j.jhydrol.2014.02.006.
(431) Dekov, V. M.; Vanlierde, E.; Billström, K.; Garbe-Schönberg, C. D.; Weiss, D. J.; Gatto Rotondo, G.; Van Meel, K.; Kuzmann, E.; Fortin, D.; Darchuk, L.; et al. Ferrihydrite precipitation in groundwater-fed river systems (Nete and Demer river basins, Belgium): Insights from a combined Fe-Zn-Sr-Nd-Pb-isotope study. *Chemical Geology* **2014**, *386*, 1-15. DOI: 10.1016/j.chemgeo.2014.07.023.
(432) Malinovsky, D.; Rodyushkin, L. V.; Shcherbakova, E. P.; Ponter, C.; Ohlander , B.; Ingri, J. Frationation of Fe Isotopes as a Result of Redox Processes in a Basin. *Geochemistry International* **2005**, *43* (8), 797-803.
(433) Homoky, W. B.; Severmann, S.; Mills, R. A.; Statham, P. J.; Fones, G. R. Pore-fluid Fe isotopes reflect the extent of benthic Fe redox recycling: Evidence from continental shelf and deep-sea sediments. *Geology* **2009**, *37* (8), 751-754. DOI: 10.1130/g25731a.1.
(434) Severmann, S.; Lyons, T. W.; Anbar, A.; McManus, J.; Gordon, G. Modern iron isotope perspective on the benthic iron shuttle and the redox evolution of ancient oceans. *Geology* **2008**, *36* (6), 487. DOI: 10.1130/g24670a.1.
(435) Severmann, S.; McManus, J.; Berelson, W. M.; Hammond, D. E. The continental shelf benthic iron flux and its isotope composition. *Geochimica et Cosmochimica Acta* **2010**, *74* (14), 3984-4004. DOI: 10.1016/j.gca.2010.04.022.
(436) John, S. G.; Mendez, J.; Moffett, J.; Adkins, J. The flux of iron and iron isotopes from San Pedro Basin sediments. *Geochimica et Cosmochimica Acta* **2012**, *93*, 14-29. DOI: 10.1016/j.gca.2012.06.003.
(437) Scholz, F.; Severmann, S.; McManus, J.; Hensen, C. Beyond the Black Sea paradigm: The sedimentary fingerprint of an open-marine iron shuttle. *Geochimica et Cosmochimica Acta* **2014**, *127*, 368-380. DOI: 10.1016/j.gca.2013.11.041.
(438) Staubwasser, M.; Blanckenburg, F.; Schoenberg, R. Iron Isotopes in the Early Marine Diagenetic Iron Cycle. *Geology* **2006**, *34* (8), 629-632. DOI: 10.1130/622647.1.
(439) Chever, F.; Rouxel, O. J.; Croot, P. L.; Ponzevera, E.; Wuttig, K.; Auro, M. Total dissolvable and dissolved iron isotopes in the water column of the Peru upwelling regime. *Geochimica et Cosmochimica Acta* **2015**, *162*, 66-82. DOI: 10.1016/j.gca.2015.04.031.
(440) Labatut, M.; Lacan, F.; Pradoux, C.; Chmeleff, J.; Radic, A.; Murray, J. W.; Poitrasson, F.; Johansen, A. M.; Thil, F. Iron Sources and Dissolved-particulate Interactionsin the Seawater of the Western Equatorial Pacific,Iron Isotope Perspectives. *Global Biogeochemical Cycles* **2014**, *28* (10), 1044-1065. DOI: 10.1002/.
(441) Gelting, J.; Breitbarth, E.; Stolpe, B.; Hassellöv, M.; Ingri, J. Fractionation of iron species and iron isotopes in the Baltic Sea euphotic zone. *Biogeosciences* **2010**, *7* (8), 2489-2508. DOI: 10.5194/bg-7-2489-2010.
(442) Rouxel, O.; Auro, M. Iron Isotope Variations in Coastal Seawater Determined by Multicollector ICP-MS. *Geostandards and Geoanalytical Research* **2010**, *34* (2), 135-144.
(443) Guelke, M.; von Blanckenburg, F.; Schoenberg, R.; Staubwasser, M.; Stuetzel, H. Determining the stable Fe isotope signature of plant-available iron in soils. *Chemical Geology* **2010**, *277* (3-4), 269-280. DOI: 10.1016/j.chemgeo.2010.08.010.
(444) Buss, H. L.; Mathur, R.; White, A. F.; Brantley, S. L. Phosphorus and iron cycling in deep saprolite, Luquillo Mountains, Puerto Rico. *Chemical Geology* **2010**, *269* (1-2), 52-61. DOI: 10.1016/j.chemgeo.2009.08.001.

(445) Collins, R. N.; Waite, T. D. Isotopically Exchangeable Concentrations of Elements Having Multiple Oxidation States: The Case of Fe(II)/Fe(III) Isotope Self-Exchange in Coastal Lowland Acid Sulfate Soils. *Environmental science & technology* **2009**, *43*, 5365-5370.
(446) Pinheiro, G. M. S.; Poitrasson, F.; Sondag, F.; Cochonneau, G.; Vieiraa, L. C. Contrasting Iron Isotopic Compositions in River Suspended Particulate Matter:the Negro and the Amazon Annual River Cycles. *Earth and Planetary Science Letters* **2014**, *394*, 168-178. DOI: 10.1016/j.epsl.2014.03.006
10.1016/j.epsl.2014.03.008.
(447) Poitrasson, F.; Viers, J.; Martin, F.; Braun, J.-J. Limited iron isotope variations in recent lateritic soils from Nsimi, Cameroon: Implications for the global Fe geochemical cycle. *Chemical Geology* **2008**, *253* (1-2), 54-63. DOI: 10.1016/j.chemgeo.2008.04.011.
(448) Wiederhold, J. G.; Kraemer, S. M.; Teutsch, N.; Borer, P. M.; Halliday, A. N.; Kretzschmar, R. Iron Isotope Fractionation during Proton-Promoted, Ligand-Controlled, and Reductive Dissolution of Goethite. *Environmental science & technology* **2006**, *40* (12), 3787-3793. DOI: 10.1021/es052228y.
(449) Chen, J.-B.; Busigny, V.; Gaillardet, J.; Louvat, P.; Wang, Y.-N. Iron isotopes in the Seine River (France): Natural versus anthropogenic sources. *Geochimica et Cosmochimica Acta* **2014**, *128*, 128-143. DOI: 10.1016/j.gca.2013.12.017.
(450) Hotz, K.; Walczyk, T. Natural iron isotopic composition of blood is an indicator of dietary iron absorption efficiency in humans. *Journal of biological inorganic chemistry : JBIC : a publication of the Society of Biological Inorganic Chemistry* **2013**, *18* (1), 1-7. DOI: 10.1007/s00775-012-0943-7.
(451) Walczyk, T.; Blanckenburg, F. Natural Iron Isotope Variations in Human Blood. *Science* **2002**, *295*, 2065-2066.
(452) Van Heghe, L.; Delanghe, J.; Van Vlierberghe, H.; Vanhaecke, F. The relationship between the iron isotopic composition of human whole blood and iron status parameters. *Metallomics : integrated biometal science* **2013**, *5* (11), 1503-1509. DOI: 10.1039/c3mt00054k.

Appendix A.

A.1 Modelling of migration of cyanobacteria

$\delta^{56}Fe_{PFe\ 4m} = \delta^{56}Fe_{\ PFe\ migration} \times X_{PFe\ migration} + \delta^{56}Fe_{\ PFe\ non\text{-}migration} \times X_{PFe\ non\text{-}migration}$

$\delta^{56}Fe_{PFe\ non\text{-}migration} = \delta^{56}Fe_{\ DFe\ 4m} - \varepsilon_{\ uptake}$

$\delta^{56}Fe_{\ PFe\ migration} = \delta^{56}Fe_{\ DFe,z} - \varepsilon_{\ uptake}$

$\delta^{56}Fe_{\ DFe,z} = \delta^{56}Fe_{\ DFe,z\ (initial)} + \varepsilon_{\ uptake} \times \ln(f)$; this equation assume the reaction products are effectively removed and isolated from the reactant pool during Fe assimilation.

Where

$\varepsilon_{\ uptake}$ is Fe isotope fractionation factor during biological uptake of Fe by cyanobacteria.

$\varepsilon_{\ uptake} = \Delta^{56}Fe_{dis\text{-}part\ (1m,\ 3m)}$ equals to the average isotope fractionation between dissolved Fe and particulate Fe at 1 and 3 m during the peak of the first bloom.

$X_{PFe\ migration}$ and $X_{PFe\ non\text{-}migration}$ represent the mole fractions of intracellular Fe in migrating cyanobacteria and non-migrating cyanobacteria at 4m, respectively.

$\delta^{56}Fe_{PFe\ non\text{-}migration}$ and $\delta^{56}Fe_{PFe\ migration}$ are the Fe isotope composition of non-migrating cyanobacteria and migrating cyanobacteria particles at 4m, respectively.

$\delta^{56}Fe_{\ DFe\ 4m}$ is the Fe isotope composition of dissolved Fe at 4m

$\delta^{56}Fe_{\ DFe\ z}$ is the Fe isotope composition of remaining dissolved Fe at z (m) depth after uptake by migrating cyanobacteria.

$\delta^{56}Fe_{\ DFe,z\ (initial)}$ is the Fe isotope composition of initial dissolved Fe at z (m) depth before uptake by migrating cyanobacteria.

f is the proportion of remaining DFe after uptake relative to the initial dissolved Fe before uptake at z (m)]

A.2 Contribution of lithogenic and non-lithogenic Fe in particulate Fe pool

The Fe to Al ratio of suspended particulates can be used to examine the relative contribution of lithogenic and non-lithogenic (biogenic (e.g., phytoplankton) or abiotically-derived authigenic (e.g., hydrous Fe oxides)) material in marine[387, 388] and freshwater systems[203, 389]. Assuming that all particulate Al reflects lithogenic origin, the fraction of particulate Fe derived from non-lithogenic materials was calculated using the following equation:

$$\text{Non-lithogenic Fe } (\mu M) = Fe_{meas} - (Fe/Al)_{litho} \times Al_{meas}$$

where Fe_{meas} and Al_{meas} are the measured concentrations of Fe and Al, respectively, and $(Fe/Al)_{litho}$ is the average Fe/Al ratio (=0.18[390]) in Canadian Precambrian Shield bedrock in Ontario. The non-lithogenic Fe composed 68 ± 11% of total particulate Fe in all lakes, indicating that the particulate Fe phase is dominated by non-lithogenic materials.

Table A1 Summary of geochemical data in streams, L227 and L442

Sample name	[b]Date	O_2	T	[a]DOC	[a]POC	SO_4^{2-}	S^{2-}	[a]PON	[a]TDP	[a]SPP	[a]C/N POM	N/P POM	C/P POM	[a]DFe	δ^{56}Fe DFe (2-SD)	[a]PFe	δ^{56}Fe PFe (2-SD)
	(m/d/y)	(mg/L)	(°C)	(μM)	(μM)	(μM)	(μM)	(μM)	(μM)	(μM)				(μM)	(‰)	(μM)	(‰)
Streams																	
L239EIF	06/22/11	NA	NA	1758	NA	NA	NA	NA	NA	NA	NA	NA	NA	14.63	0.62±0.02	NA	NA
L239EIF	06/22/16	7.0	15.4	2087	NA	7.2	NA	NA	NA	NA	NA	NA	NA	14.20	0.01±0.10	NA	NA
L239EIF	09/19/16	7.5	13.2	2829	NA	6.5	NA	NA	NA	NA	NA	NA	NA	15.58	0.41±0.08	2.30	NA
L239EIF	06/06/17	NA	NA	1530	NA	NA	NA	NA	NA	NA	NA	NA	NA	12.44	NA	NA	NA
L239EIF	07/05/17	NA	NA	2174	NA	NA	NA	NA	NA	NA	NA	NA	NA	14.92	NA	NA	NA
L239NEIF	06/22/11	NA	NA	3042	NA	NA	NA	NA	NA	NA	NA	NA	NA	12.43	-0.01±0.04	NA	NA
L239NEIF	07/10/14	NA	9.8	3483	NA	8.9	NA	NA	NA	NA	NA	NA	NA	13.03	0.07±0.02	NA	NA
L239NEIF	06/22/16	7.1	8.8	3785	NA	2.0	NA	NA	NA	NA	NA	NA	NA	15.50	-0.13±0.02	NA	NA
L239NEIF	09/19/16	4.3	NA	5301	NA	2.6	NA	NA	NA	NA	NA	NA	NA	20.18	0.05±0.06	0.09	NA
L239NEIF	06/06/17	NA	NA	2908	NA	NA	NA	NA	NA	NA	NA	NA	NA	11.33	NA	NA	NA
L239NEIF	06/20/17	NA	NA	3357	NA	NA	NA	NA	NA	NA	NA	NA	NA	12.07	NA	NA	NA
L239NEIF	07/05/17	NA	NA	3657	NA	NA	NA	NA	NA	NA	NA	NA	NA	12.99	NA	NA	NA
L239NWIF	06/22/11	NA	NA	1733	NA	NA	NA	NA	NA	NA	NA	NA	NA	8.97	-0.07±0.02	NA	NA
L239NWIF	07/10/14	NA	15.0	1883	NA	23.9	NA	NA	NA	NA	NA	NA	NA	9.13	0.21±0.02	NA	NA
L239NWIF	06/23/16	6.7	15.8	1862	NA	9.9	NA	NA	NA	NA	NA	NA	NA	8.85	-0.09±0.02	NA	NA
L239NWIF	09/19/16	3.7	12.9	2565	NA	4.1	NA	NA	NA	NA	NA	NA	NA	10.61	0.08±0.04	0.14	NA
U8	07/07/14	NA	11.0	1375	NA	10.4	NA	NA	NA	NA	NA	NA	NA	6.37	0.39±0.02	NA	NA
U8	06/21/16	NA	9.3	1346	NA	8.4	NA	NA	NA	NA	NA	NA	NA	6.21	-0.19±0.08	NA	NA
U8	09/19/16	NA	12.1	1660	NA	11.8	NA	NA	NA	NA	NA	NA	NA	8.07	0.34±0.04	0.05	NA
U1	07/07/14	NA	NA	1183	NA	6.6	NA	NA	NA	NA	NA	NA	NA	6.38	0.16±0.02	NA	NA
L114 IF	07/08/14	NA	12.0	1100	NA	13.8	NA	NA	NA	NA	NA	NA	NA	6.09	0.28±0.02	NA	NA
L661 IF	06/22/16	NA	NA	NA	NA	NA	NA	NA	NA	NA	NA	NA	NA	6.91	0.15±0.02	NA	NA

Sample name	[b]Date	O_2	T	[a]DOC	[a]POC	SO_4^{2-}	S^{2-}	[a]PON	[a]TDP	[a]SPP	[a]C/N POM	N/P POM	C/P POM	[a]DFe	δ^{56}Fe DFe (2-SD)	[a]PFe	δ^{56}Fe PFe (2-SD)
	(m/d/y)	(mg/L)	(°C)	(µM)	(µM)	(µM)	(µM)	(µM)	(µM)	(µM)				(µM)	(‰)	(µM)	(‰)
BO	09/19/16	NA	NA	1542	NA	4.6	NA	NA	NA	NA	NA	NA	NA	7.57	0.02±0.10	0.01	NA
ELA Lake 227 / Water Column																	
1 m-epi	07/09/14	9.2	20.6	899	259	16.3	NA	43	0.26	1.13	6.0	17.3	88.9	0.80	0.72±0.02	1.35	0.09±0.00
3 m-epi	07/09/14	10.5	12.0	766	230	12.9	NA	38	0.26	1.19	6.0	14.5	74.6	0.80	0.85±0.02	0.97	-0.02±0.02
4 m-meta	07/09/14	0.5	NA	NA	198	13.2	NA	27	0.32	1.58	7.5	7.6	48.6	1.90	NA	NA	NA
6 m-hypo	07/09/14	0.0	4.9	808	154	5.1	NA	22	0.42	1.90	7.0	5.2	31.4	21.94	-0.25±0.02	13.93	0.77±0.02
8 m-hypo	07/09/14	0.0	4.3	908	252	7.0	NA	39	0.68	3.77	6.4	4.7	25.8	83.00	-0.27±0.02	10.08	1.27±0.02
10 m-hypo	07/09/14	0.0	4.3	1157	373	6.6	NA	60	1.35	5.29	6.2	5.1	27.3	110.24	-0.26±0.02	6.56	1.05±0.02
1 m-epi	06/28/11	10.0	19.4	767	318	14.3	[c]bdl	55	0.19	1.13	5.8	21.8	108.9	0.69	-0.26±0.10	NA	NA
4 m-meta	06/28/11	0.3	6.4	703	184	14.7	0.3	25	0.26	1.52	7.4	7.4	47	2.64	-0.09±0.00	0.56	-0.47±0.02
6 m-hypo	06/28/11	0.0	4.3	811	128	5.3	6.3	18	0.32	1.58	7.2	5.1	31.4	29.49	-0.36±0.00	2.24	0.48±0.02
8 m-hypo	06/28/11	0.0	4.3	1071	255	4.1	8.2	39	0.55	4.58	6.5	3.9	21.5	107.12	-0.20±0.00	2.55	0.78±0.02
10 m-hypo	06/28/11	0.0	4.3	1189	305	4.0	7.0	49	0.61	5.71	6.2	3.9	20.7	118.29	-0.18±0.08	3.05	1.00±0.02
1 m-epi	08/24/11	8.0	21.3	769	254	12.4	[c]bdl	32	0.23	0.94	6.5	11.4	63.0	0.84	0.03±0.14	0.29	-0.08±0.02
4 m-hypo	08/24/11	0.1	8.7	865	352	7.1	2.2	54	0.29	2.16	NA	NA	NA	17.80	-0.28±0.06	0.56	1.04±0.02
6 m-hypo	08/24/11	0.0	4.9	960	161	4.2	2.8	22	0.35	2.26	7.3	4.4	27.6	61.46	-0.09±0.00	0.25	1.32±0.02
8 m-hypo	08/24/11	0.0	4.5	1159	268	4.1	3.9	42	0.87	4.81	6.4	3.9	21.5	110.36	-0.12±0.02	0.66	1.52±0.02
10 m-hypo	08/24/11	0.0	4.4	1193	317	4.5	5.5	52	1.90	5.81	6.1	4.1	21.1	140.87	NA	NA	NA

Sample name	[b]Date (m/d/y)	O_2 (mg/L)	T (°C)	[a]DOC (µM)	[a]POC (µM)	SO_4^{2-} (µM)	S^{2-} (µM)	[a]PON (µM)	[a]TDP (µM)	[a]SPP (µM)	[a]C/N POM	N/P POM	C/P POM	[a]DFe (µM)	δ^{56}Fe DFe (2-SD) (‰)	[a]PFe (µM)	δ^{56}Fe PFe (2-SD) (‰)
ELA Lake 442 / Water Column																	
0.5 m-epi	06/27/11	7.0	19.8	555	29	19.0	NA	3	0.06	0.19	9.1	NA	NA	0.87	0.10±0.04	0.21	0.01±0.04
5 m-meta	06/27/11	10.6	9.5	562	43	19.5	NA	3	0.06	0.23	12.9	NA	NA	0.74	0.30±0.04	0.20	0.33±0.00
9 m-hypo	06/27/11	4.0	5.0	530	36	21.5	NA	3	0.10	0.26	12.5	NA	NA	1.20	0.46±0.04	0.38	-0.03±0.04
11 m-hypo	06/27/11	NA	4.5	538	NA	NA	NA	NA	NA	NA	NA	NA	NA	1.39	0.44±0.04	0.70	-0.01±0.04
13 m-hypo	06/27/11	0.0	4.4	529	77	20.8	NA	9	0.03	0.03	8.6	NA	NA	9.83	-0.91±0.04	1.22	1.34±0.00
16.5 m-hypo	06/27/11	0.0	4.4	677	94	18.4	NA	13	0.03	0.03	9.7	NA	NA	102.18	-0.11±0.02	0.97	1.83±0.04
ELA Lake 227 Sediments																	Bulk sediment δ^{56}Fe (‰)
Epi Surficial 1.0m	07/24/10	NA	NA	NA	NA	NA	NA	NA	NA	NA	NA	NA	NA	NA	NA	NA	-0.04±0.02
Profundal Surficial 10m	07/24/10	NA	NA	NA	NA	NA	NA	NA	NA	NA	NA	NA	NA	NA	NA	NA	-0.03±0.02
Profundal 10m Core 2 5-5.5cm	03/01/11	NA	NA	NA	NA	NA	NA	NA	NA	NA	NA	NA	NA	NA	NA	NA	-0.07±0.02
Profundal 10m Core 2	03/01/11	NA	NA	NA	NA	NA	NA	NA	NA	NA	NA	NA	NA	NA	NA	NA	-0.09±0.07

Sample name	[b]Date	O_2	T	[a]DOC	[a]POC	SO_4^{2-}	S^{2-}	[a]PON	[a]TDP	[a]SPP	[a]C/N POM	N/P POM	C/P POM	[a]DFe	δ^{56}Fe DFe (2-SD)	[a]PFe	δ^{56}Fe PFe (2-SD)
	(m/d/y)	(mg/L)	(°C)	(µM)	(µM)	(µM)	(µM)	(µM)	(µM)	(µM)				(µM)	(‰)	(µM)	(‰)
10-10.5cm Profundal 10m Core 2 25-26 cm	03/01/11	NA	NA	NA	NA	NA	NA	NA	NA	NA	NA	NA	NA	NA	NA	NA	-0.22±0.01
ELA Lake 442/ Sediments																	
Epi Surficial 1m	07/23/10	NA	NA	NA	NA	NA	NA	NA	NA	NA	NA	NA	NA	NA	NA	NA	-0.05±0.05
Epi Surficial 2.9 m	07/23/10	NA	NA	NA	NA	NA	NA	NA	NA	NA	NA	NA	NA	NA	NA	NA	-0.06±0.00
Profundal Surficial 17 m	07/23/10	NA	NA	NA	NA	NA	NA	NA	NA	NA	NA	NA	NA	NA	NA	NA	0.28±0.02

[a]DOC denotes dissolved organic carbon, POC is particulate organic carbon, PON is particulate organic nitrogen, TDP is total dissolved phosphorus, SPP is suspended particulate phosphorus, C/N POM is C/N molar ratio of particulate organic matter, DFe is dissolved Fe, PFe is particulate Fe.

[b]For Lake 227, 07/09/2014 was during development of bloom, 06/28/2011 was during peak bloom, 08/24/2011 was during post bloom.

[c]bdl means "below detection limit".

Table A2 Saturation indices of Fe(II) minerals in the anoxic hypolimnia of L221, L227, L304 and L442

Lake	Date	Depth (m)	Mackinawite (FeS) $^{a}K_{sp}=10^{-3.5}$			Vivianite ($Fe_3(PO_4)_2$) $^{b}K_{sp}=10^{-35.8}$		
			^{c}IAP	^{d}SI	Comment	^{c}IAP	^{d}SI	Comment
L227	15-May-18	6	1.44E-05	-1.34	undersaturated	2.5E-42	-5.80	undersaturated
		8	1.16E-04	-0.43	undersaturated	8.9E-41	-4.25	undersaturated
		10	2.85E-04	-0.04	near saturated	-	-	undersaturated
	26-Jun-18	4	1.30E-07	-3.39	undersaturated	2.7E-45	-8.76	undersaturated
		6	2.23E-05	-1.15	undersaturated	1.7E-42	-5.96	undersaturated
		8	1.02E-04	-0.49	undersaturated	7.7E-41	-4.31	undersaturated
		10	1.31E-04	-0.18	undersaturated	3.7E-40	-3.63	undersaturated
	21-Aug-18	4	2.57E-07	-3.09	undersaturated	7.4E-46	-9.33	undersaturated
		6	4.51E-05	-0.85	undersaturated	2.7E-42	-5.76	undersaturated
		8	1.04E-04	-0.48	undersaturated	7.9E-41	-4.30	undersaturated
		10	1.68E-04	-0.07	near saturated	1.8E-39	-2.94	undersaturated
	11-Sep-18	4	4.15E-07	-2.88	undersaturated	2.3E-45	-8.84	undersaturated
		6	5.60E-05	-0.75	undersaturated	5.0E-42	-5.50	undersaturated
		8	1.33E-04	-0.37	undersaturated	5.9E-40	-3.43	undersaturated
		10	2.45E-04	0.02	near saturated	1.5E-38	-2.01	undersaturated
L442	02-Jun-18	13	1.39E-06	-2.26	undersaturated	2.1E-45	-8.89	undersaturated
		15	2.48E-05	-1.01	undersaturated	-	-	
		17	1.85E-04	-0.13	undersaturated	1.4E-40	-4.05	undersaturated
	05-Jul-18	13	8.50E-06	-1.47	undersaturated	1.1E-42	-6.16	undersaturated
		15	4.53E-05	-0.74	undersaturated	-	-	
		17	2.40E-04	-0.02	near saturated	1.6E-40	-3.99	undersaturated
	08-Sep-18	13	8.70E-05	-0.46	undersaturated	8.1E-42	-5.29	undersaturated
		15	1.48E-04	-0.23	undersaturated	-	-	

		17	3.47E-04	-0.02	near saturated	7.2E-41	-4.34	undersaturated
		4	9.68E-07	-2.41	undersaturated	-	-	
L221	30-Jul-18	5	5.54E-06	-1.66	undersaturated	-	-	
		5.5	1.56E-05	-1.21	undersaturated	-	-	
		4.5	1.38E-06	-2.26	undersaturated	3.0E-44	-7.72	undersaturated
L304	26-Jul-18	5.5	1.49E-05	-1.23	undersaturated	-	-	
		6	3.57E-05	-0.85	undersaturated	4.1E-42	-5.58	undersaturated

[a]K_{sp} and [b]K_{sp} are the solubility product constants of Mackinawite (FeS) and Vivianite ($Fe_3(PO_4)_2$) respectively.[273, 274]
[c]IAP is the ion activity product of a specific mineral.
[d]SI is the saturation index defined by SI=log [IAP/K_{sp}].

Appendix B.

Use of muti-collector ICP-MS for studying biogeochemical metal cycling

Introduction

Isotopic analysis of metals (e.g., Li, Mg, Cu, Zn, Mo, Fe) has been performed by geochemists for several decades in order to explore metal cycling in both natural and perturbed environments. With new innovations and developments in analytical methods, the isotope compositions of these metals have been validated in a variety of settings, including both low-temperature (e.g. marine, soil, riverine, lake) and high-temperature environments. The isotopic systematics of some metals is described here to provide a general understanding of the behavior of metals influenced by biogeochemical processes.

Lithium (Li) and magnesium (Mg) isotopes are promising tracers to study key biogeochemical processes. Both Mg and Li are fluid-mobile elements that are not involved in redox reactions.[391] Li isotopes are a useful tracer to study both low-temperature (e.g., silicate weathering)[134] and high-temperature processes (fluid-rock interactions).[392] Natural variation of Li isotope compositions (Table B1) spans a large range (from –20 to 40‰) in terrestrial environments due to the substantial mass difference (~16%) between ^{6}Li and ^{7}Li. Low-temperature weathering could induce Li isotope fractionation between fluids (river, groundwater) and solids (sediment, rock) due to the enrichment of ^{7}Li in fluids.[393]

Table B1 Isotopes, standard materials and natural isotopic compositions for selected elements

Element	Stable isotopes and natural relative abundances (%)	Standard material		Data reporting	Natural isotopic variation
		Name	Composition		
Li	^{6}Li (7.6) ^{7}Li (92.4)	L-SVEC[a] IRMM016[b]	Li carbonate (solid) Li carbonate (solid)	δ^{7}Li	−20 to 40‰

Mg	^{24}Mg (79.0) ^{25}Mg (10.0) ^{26}Mg (11.0)	NIST-SRM980[c] DSM3	Mg chips (solid) Mg in nitric acid (solution)	δ^{26}Mg	−6 to 2‰
Cu	^{63}Cu (69.2) ^{65}Cu (30.8)	NIST-SRM976[a] ERM-AE633	Cu disk (solid) Cu in nitric acid (solution)	δ^{65}Cu	Biotic sample: −1.3 to 1.5‰ Abiotic sample: 0.0 to 0.5‰
Zn	^{64}Zn (49.2) ^{66}Zn (27.8) ^{67}Zn (4.0) ^{68}Zn (18.4) ^{70}Zn (0.6)	JMC3-Lyon[a] IRMM3702	Mg in nitric acid (solution) Mg in nitric acid (solution)	δ^{66}Zn	Biotic sample: −1.0 to 1.5‰ Abiotic sample: 0.5 to 1.0‰
Mo	^{92}Mo (14.8) ^{94}Mo (9.3) ^{95}Mo (15.9) ^{96}Mo (16.7) ^{97}Mo (9.6) ^{98}Mo (24.1) ^{100}Mo (9.6)	NIST-SRM3134	Mo in hydrochloric acid (solution)	δ^{98}Mo	−1.5 to 2.4‰
Fe	^{54}Fe (5.8) ^{56}Fe (91.8) ^{57}Fe (2.1) ^{58}Fe (0.3)	IRMM014[a] IRMM634	Fe wire (solid) Fe in hydrochloric acid (solution)	δ^{56}Fe	−3.6 to 1.2‰

[a]Discontinued: Standard material is no longer available.

[b]IRMM016 has the identical isotope composition to L-SVEC.

[c]NIST-SRM980 was widely used before 2003 and was then replaced by DSM3, a standard developed at the University of Cambridge.

Magnesium is the fifth most abundant element in continental crust and thus, a major component of minerals in different rock types.[394] A variation of >7‰ in Mg isotope compositions (Table B1) is observed in terrestrial samples.[395] Low-temperature weathering (e.g., silicate weathering) can produce significant Mg isotope fractionation, which is due to the partitioning of light Mg (^{24}Mg) into the aqueous phase, and thus, the Mg isotope has been used as a tracer to study weathering processes and water-rock interaction.[396, 397]

Copper (Cu) and zinc (Zn) are redox-sensitive elements affected by biogeochemical processes, making them good tracers to understand complex biological pathways and the fate of contaminants. Copper (Cu) and zinc (Zn) are redox-sensitive elements affected by biogeochemical processes, making them good tracers to understand complex biological pathways and the fate of contaminants. Cu and Zn either form complexes with organic matter or adsorb onto the surface of oxyhydroxides in near-surface environments such as rivers, oceans, and soils.[398] The variation of both Cu and Zn isotopic compositions (Table B1) in natural samples that are involved in biological processes span a range of 2.5‰, while the δ^{66}Zn and δ^{65}Cu of inorganic samples are less variable, with a range less than 0.5‰.[398, 399] Zn and Cu isotopes can also be used as tracers to study processes in high-temperature environments.[398] As the most incompatible chalcophile element, Cu is highly related to the fusion of sulfides during partial melting of the mantle, making it a good tracer to study the role of sulfides during igneous differentiation processes. The moderate volatility and high abundance of Zn in bulk silicate earth makes it a good tracer to understand the volatility processes in rocks. The Cu and Zn isotopic compositions in bulk silicate earth are reported as 0.07 ± 0.10‰[400] and 0.16 ± 0.06‰,[401] respectively.

Molybdenum (Mo) can be used to study redox conditions in near-surface environments due to its redox sensitivity, role in microbiological processes, and relatively large isotopic range in nature (from –1.5‰ to 2.4‰).[402] The largest isotope fractionation (~3‰) is observed from the adsorption of Mo to Mn oxides in oxic seawater by preferentially accumulating lighter isotopes of Mo onto the surface of Mn oxides.[403, 404] Mo is an essential cofactor for enzymes that play an important role in biological nitrate reduction and nitrogen fixation.[402, 405] Bacterial uptake prefers the lighter isotopes of Mo, inducing isotope fractionation with the range of ~0.2 to 1.0‰.[404] Some microorganisms can also utilize oxidized Mo species as electron acceptors in catabolic metabolism when generating energy from chemiosmosis.[406] Thus, Mo isotopes are a good tracer to study redox conditions as well as the evolution of life on Earth[402] and euxinic environments because of the large differences in isotopic fractionation between processes that sequester Mo in sedimentary minerals.

Mass spectrometry is a powerful instrumental technique used to determine the isotopic composition of elements. Types of mass spectrometry used for isotopic analyses are listed in Table B2. Thermal ionization mass spectrometry (TIMS) was first developed for

isotopic analysis of nontraditional isotopes and was widely used before the introduction of inductively coupled plasma mass spectrometry (ICP-MS).[164] The approaches of introducing and ionizing samples are the major differences between the TIMS and ICP-MS methods.[407] The ICP-MS was developed after 1983 and contains three essential components: an ion source, an ion separator, and a detection system. The ion separator used in commercial ICP-MS instrumentation can be classified into three types: quadrupole mass analyzer, double-focusing sector, and time-of-flight mass analyzer. The double-focusing sector can produce higher unit mass resolution, which can result in high precision of isotope ratios, compared with the other two types. An enhanced version of the ICP-MS, the multi-collector (MC)-ICP-MS, was developed on the double-focusing sector field ICP-MS over the following decade[164] and allows the study of isotope abundances of all elements.[408] TIMS is not suitable for elements with high first ionization potentials, whereas MC-ICP-MS is capable of analyzing a wider range of elements (e.g. Mo, Fe, Hf, Hg).[164, 409] More recently, MC-ICP-MS is increasingly used for isotope analysis in many fields (e.g., biogeochemistry, cosmochemistry) due to the advantages of MC-ICP-MS over TIMS (e.g., higher sensitivity, higher ionization efficiency, faster sample throughput, superior precision and accuracy). Common MC-ICP-MS instruments that are commercially available include the Isoprobe from GV Instruments, the Neptune (Plus) from Thermo Fisher Scientific, and the Nu Plasma II and the Nu Plasma 1700 from Nu Instruments.[410]

Table B2 Different types of mass spectrometry for measurement of stable isotope ratios

Mass spectrometry	Ionization	Sample form	Elements of interest
Dual inlet or continuous flow IRMS	Bombard sample with e-beam	Gas	Light elements (e.g., H, C, N, O, S, Cl, Br)
TIMS	Heat by electric current on a filament	Solid or solution	Heavy elements (e.g., Ca, Ti, Cr, Ni, Sr, Pb, Nd)
MC-ICP-MS	Introduce into an inductively coupled argon plasma	Solid or solution	Light and heavy elements (e.g., Li, B, Mg, Si, Ca, Fe, Cu, Zn, Mo, Hf, Hg)
Noble gas MS	Bombard sample with e-beam in the ion gun	Gas	He, Ne, Ar, Kr, Xe

The availability of TIMS or MC-ICP-MS (gradually becoming a widely used instrumental technique) has led to new discoveries in metal cycling. For example, Fe biogeochemistry has been investigated to understand the Fe source, binding environment, and electron transfer and atom exchange pathways. The development of the double spike technique allows high-precision Fe isotope measurements to be achieved.[411-413] The double spike technique is employed to correct and account for instrumental mass fractionation during mass spectrometric analysis. This well-established method is applicable to any element that has four or more isotopes.[414] The double spike technique is being increasingly applied in nontraditional stable isotope research,[407, 415] where it is ideally suited to distinguish between natural and instrumental mass fractionation. MC-ICP-MS is more suitable for nontraditional stable isotope measurements, since its inherent instrumental mass bias is constant and several elements, including Fe, have high ionization efficiency.[244] However, MC-ICP-MS also introduces some new disadvantages, such as isobaric interferences produced by the Ar plasma and interference from other elements (e.g., Ca, Cr, Ni).[244] Great efforts have been made to minimize these interferences.[411, 416, 417] Over the past decade, MC-ICP-MS has been predominantly deployed to study isotope fractionation of a wide range of elements, and to produce high-precision isotope measurements that capture the true naturally occurring mass-dependent variations. Since isotopic analysis for each element and type of sample necessitates detailed method development, this chapter will focus on the application of MC-ICP-MS for studying Fe isotope fractionation in general with specific application in a case study. The overall methods and sample preparation for measuring Fe isotopes are broadly similar for studying other metal isotopes.

Methodology

Instrumentation

Mass resolution(R) is an important parameter of MC-ICP-MS. It estimates the ability of MC-ICP-MS to identify the signals of separated ion beams with slightly different masses:

$$R = m/\Delta m$$

where Δm is the mass difference between two separated ion beams with masses m and $m + \Delta m$,[409] and is indicative of the capability of MC-ICP-MS to separate the neighbor peaks in a mass spectrum. The mass resolution can be calculated in two different ways. In the 10% valley definition, two neighbor peaks (at mass m_1 and mass m_2 in a mass spectrum) with the same height (ion intensity) are separated by a valley whose lowest point is 10% of the peak height. In the peak width definition, the Δm_x is the width of a single peak with mass m at a desired peak height (x% (e.g., 5%) of maximum peak height):[409, 418]

$$R_{\text{10\% valley definition}} = \left(\frac{m_1+m_2}{2}\right)/(m_1 + m_2)$$

$$R_{\text{peak width definition}} = m / \Delta m_x$$

The two definitions are equivalent when the mass resolution is taken at 5% of peak height in peak width definition.

The MC-ICP-MS instrument used for discussion in this chapter is a Nu Plasma II, which is a double-focusing sector field mass spectrometer (Figure B1). The sample is introduced into the system as an aerosol by a nebulizer (CETAC Aridus II Desolvating Nebulizer System) to the inductively coupled argon plasma for ionization. The ions are accelerated first and then separated from other ions in space based on their different mass to charge ratio and introduced into the magnetic sector field of the mass spectrometer. The separated ion beam is subsequently converted into a measurable electrical signal by the detection system.[418] There is a strong negative correlation between the ion transmission efficiency and mass resolution for MC-ICP-MS: the higher the mass resolution, the lower the ion transmission efficiency.[418] For example, reducing the width of the exit slit can increase the mass resolution but decreases the intensity of the ion beam, resulting in low ion transmission efficiency.[409] With high mass resolution, the MC-ICP-MS can separate ions of interest (e.g., Fe) from interfering ions to get accurate and precise isotope ratios.[410] The double-focusing sector, including magnetic and electrostatic sectors, has been developed for

the purpose of producing high mass resolution without significant damage to the ion transmission efficiency. This includes a magnetic sector, which separates ions by the strength of the magnetic field based on their mass to charge ratio (m/z), and an electrostatic sector, which separates ions by acceleration voltage based on their kinetic energy.[418] The double-focusing (energy and directional focusing) sector in spectrometers similar to the Nu Plasma II follows the Nier–Johnson geometry, in which the electrostatic sector is followed by the magnetic sector.[409] The detection system is a combination of Faraday collectors and ion counters. The Faraday collectors are deep buckets that are installed behind the exit slits for collecting the separated ion beams that pass through the exit slits. The ion counters in the Nu Plasma II are discrete dynode secondary electron multipliers, which can improve the sensitivity of mass spectrometers by several orders of magnitude compared with Faraday collectors.[409] The combination of Faraday collectors and ion counters can extend the dynamic range of the detection system and produce accurate and precise isotopic ratios.[410]

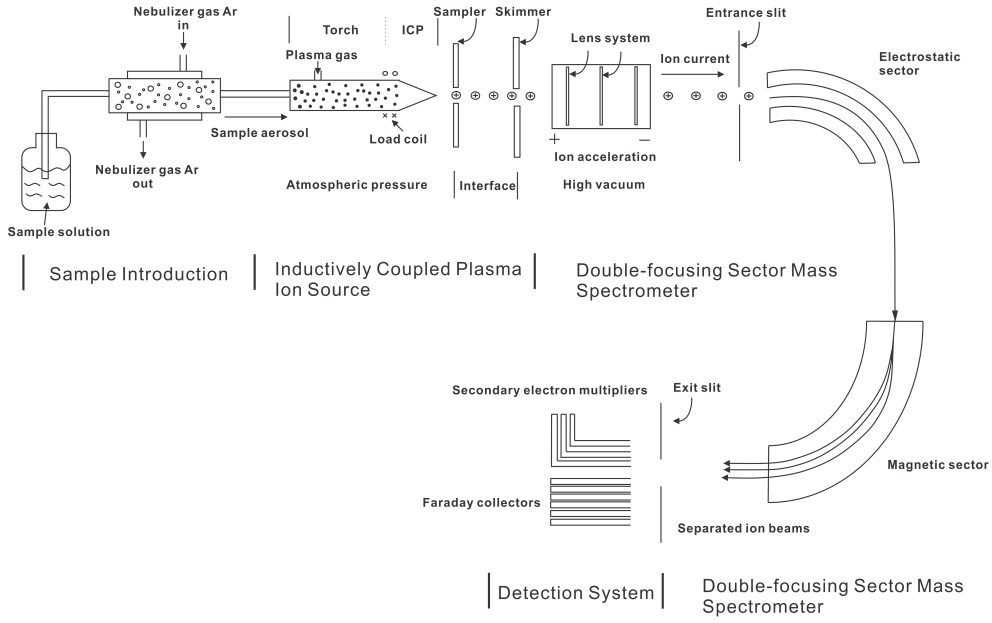


Figure B1 Schematic representation of MC-ICP-MS: Nu Plasma II (coupled with sample introduction system).
Nu Plasma II contains three distinct parts: an inductively coupled plasma ion source, a double-focusing sector mass spectrometer, and a detection system consisting of 16 Faraday collectors (also called Faraday cups), five ion counters (discrete dynode secondary electron multiplier), and a high-abundance sensitivity filter. Modified from Vanhaecke, 2012, with permission of John Wiley and Sons.

Ultrapure deionized water (18.2 MΩ, 4 ppb total organic carbon [TOC] at 25 °C) is used for the preparation of all samples, standards, and test solutions. Dilute nitric acid solutions (0.1% and 2% by volume) are prepared with ultrapure nitric acid (70% w/w, Omni*Trace* Ultra®). Hydrochloric acid is distilled twice, often using the Savillex DST-1000 Acid Purification System, from analytical reagent-grade HCl (Baker Analyzed® A. C. S. Reagent HCl). For the analysis of Fe isotopes, two stock Fe standard solutions are used: IRMM634 (the certified standard replacing IRMM014, from the Institute for Reference Materials and Measurements [IRMM]) and HPS Fe (High-Purity Standards from Delta Scientific Laboratory Products Ltd., 1000 μg/mL Fe solution [source: Fe metal, purity: 99.999%] in 2% HNO_3). The mission of the IRMM is to promote a common and reliable European measurement system in support of EU policies. The standard stock solutions are specific depending on the elemental isotope of interest. For example, the IRMM3702 is the certified reference material for $\delta^{64}Zn$ in 1 M nitric acid. The dilute standard solutions are prepared by dilution of the concentrated standard solutions in 2% nitric acid. Synthetic solutions are prepared that contain the same concentrations of major ions as are present in the samples to be analyzed.

Interference

MC-ICP-MS is usually coupled with ion exchange chromatography in order to eliminate spectral (or isobaric) interferences and nonspectral interferences.[407] Spectral interferences can be further classified into elemental interferences and molecular interferences. Matrix elements such as Cr and Ni can introduce elemental interferences during the Fe isotope measurement.[244] Therefore, care must be taken to limit their possible interference during analysis. For example, ^{54}Fe suffers from the interference of ^{54}Cr and ^{58}Ni because the latter two overlap the ^{58}Fe signal. Some matrix elements such as Ca can form

oxide (or hydroxide) ions such as $^{40}Ca^{16}O$ at ^{56}Fe, $^{40}CaOH^{+}$ at ^{57}Fe, and $^{42}CaO^{+}$ at ^{58}Fe during analysis and result in molecular interferences.[244] These interfering ions will produce significant bias if their concentrations in solutions are an appreciable fraction of the concentration of the target isotope. Albarède and Beard [407] suggest that an interfering ion can bias the true abundance of the target species to result in inaccurate isotopic compositions. In order to erase the effect of these interferences, a strict Fe–matrix separation protocol is applied in the preliminary stages to purify the samples. A correction is also applied to erase the signal of interfering ions based on a standard method.[407]

The MC-ICP-MS instrumental technique also introduces spectral molecular interferences by ionized plasma gas (Ar). The Ar-containing polyatomic ions, $^{40}Ar^{14}N$, $^{40}Ar^{16}O$, and $^{40}Ar^{16}OH$, can overlap signals corresponding to ^{54}Fe, ^{56}Fe, and ^{56}Fe, respectively. However, several approaches (e.g., addition of H_2 gas in collision cell, cool plasma conditions) have been used to remove the interfering effect of these Ar-containing polyatomic ions.[244] Furthermore, the double-focusing sector with which machines similar to Nu Plasma II are equipped can produce both energy-centralized and direction-controlled ion beams, thus reducing the width of source and exit slits in the detection system and further increasing the mass resolution.[418] Similarly, with high mass resolution, the Fe ion beams can be distinguished from other Ar-containing polyatomic ions.

Nonspectral interferences result from the space-charge effect or plasma condition effect.[407] The space-charge effect can cause heavier ions to be more favorably transmitted than lighter ions, resulting in a compositional change of the ion beams (a defocusing effect).[418] The nonspectral interferences are generally coupled with a sensitivity shift of the target ion caused by other elements.[407] Like the spectral interferences, the nonspectral interferences can also produce significant bias in isotopic compositions.

Sample material

MC-ICP-MS has been used to investigate isotopic signatures useful to geomicrobiologists, such as Fe, in various environments such as rivers, oceans, groundwater, and lakes. The sample material in these environmental settings includes porewater and dissolved and particulate phases in the water column, groundwater and sediment. Sediment samples can be dissolved with HF for bulk isotope analysis or treated with sequential acid

extraction to extract different metal phases. Several studies have used sedimentary rock samples to study biogeochemical Fe cycling.[134, 194, 196] Sedimentary rock such as black shales, carbonate rocks, or mudrocks can be effectively dissolved in a mixture of HF–HNO_3–HCl (2:1:1) (HF 29 M: HCl 8 M: HNO_3 14 M; optimal ratio may differ for different types of sedimentary rock).[134]

Sample preparation

Before the samples are introduced into the MC-ICP-MS, they must be purified to separate the ions for isotopic analysis from the background matrix. The matrix contains interfering ions that can induce spectral interferences. In the case of Fe, a strict Fe–matrix chemical separation is required by the standard–sample–standard bracketing approach for mass bias correction.[407]

For Fe isotope analysis, ion exchange chromatography is utilized for the purpose of Fe–matrix separation. Ion exchange resin is an insoluble polymer with exchangeable ions that can exchange with other ions from an aqueous solution, either positively charged ions (cation exchange resin) or negatively charged ions (anion exchange resin). An anion exchange resin (Bio-Rad AG® 1-X4 Resin, Analytical grade, 4% cross-linking, 200–400 mesh) has been used in ion exchange chromatography to separate Fe(III) from other elements in a hydrochloric acid medium.[244, 419] The anion exchange resin is strongly basic, having quaternary ammonium groups ($-N^+(CH_3)_3$) that can absorb hydrochloric acid ($-N^+(CH_3)_3OH^- + Cl^- \rightleftharpoons -N^+(CH_3)_3Cl^- + OH^-$).[420] Fe(III) has high affinity for resin conditioned with concentrated hydrochloric acid and thus forms chloride complexes (e.g., $FeCl_4^-$) with the anion exchange resin.[419] The stabilities of Fe(III)–chlorine complexes increase with increasing hydrochloric acid concentration.[419, 421] Therefore, Fe(III) can be adsorbed to resin in 7 M HCl and eluted from resin in 0.5 M HCl. Prior to use, the anion exchange resin is washed twice using 8 M HCl (distilled twice from analytical reagent-grade HCl) and 10 times using H_2O to rid the column of the finest resin particles,[422] and finally, is filled with H_2O before the sample is loaded onto the column. In order to minimize contamination problems, all procedures are conducted in a laminar flow cabinet located in a metals-free clean room. It has been proven that no isotopic fractionation occurs during the ion exchange chromatography following these procedures.[244, 411] However, it is crucial to

obtain an Fe yield quantitatively close to 100% through chemical separation to avoid mass-dependent fractionation.[407]

Test solutions are carried through ion exchange chromatography to test the accuracy of chemical separation. A certain amount (μg) of high purity standard® (HPS) Fe (in-house standard) is added to synthetic samples, which contain the same major ions as original samples. The amount of HPS Fe should match the range of iron concentrations of the samples to be measured.

MC-ICP-MS Analysis

The required minimal concentrations of measurement solutions introduced into MC-ICP-MS could vary depending on the Fe intensities of different MC-ICP-MS instruments. Samples and Fe standards are prepared at (e.g.) 600 ppb Fe concentration in weak nitric acid (e.g., 0.01%) at the time of the measurement. It is important to keep all samples and standards matched in Fe concentration and acid matrix, since the apparent mass discrimination could change due to any changes of the Fe concentration or acid strength.[423] Different concentrations of HPS Fe (400, 500, 700, and 800 ppb) are also prepared in 0.01% nitric acid for the correction of mass discrimination caused by variation in Fe concentration. These diluted Fe standards are included in each run-set and analyzed as unknown samples. In order to minimize contamination problems, all the sample dilution processes are operated in a laminar flow cabinet that is situated as close to the MC-ICP-MS instrument as possible. The MC-ICP-MS is computer controlled, and each isotopic composition is the average of 40 (varies as desired) 10 s on-peak measurements following a 1 min on-peak measurement of blank acid (0.01% nitric acid).[424] The on-peak measurements of blank acid are conducted in order to use the on-peak zero method (OPZ). This method can eliminate the variation in the background from both the instrumental memory effect and small operational variations, which can cause the accuracy and precision of isotopic ratios to deteriorate (~0.1‰ range).[407] In order to get precise Fe isotope ratios, the peak shapes of Fe isotopes (^{54}Fe, ^{56}Fe, ^{57}Fe, and ^{58}Fe) during a mass scan need to be “flat top” (Figure B1). If not, the collector setting will bias the isotopic ratios.[407] Some instruments, such as Neptune and Nu Plasma II, can produce high-quality “flat top” peak shapes by adjusting independently the width of both source and

exit slits. Reducing the slit width results in high mass resolution by separating analyte peaks from other interferences, therefore producing a large flat-top peak area.

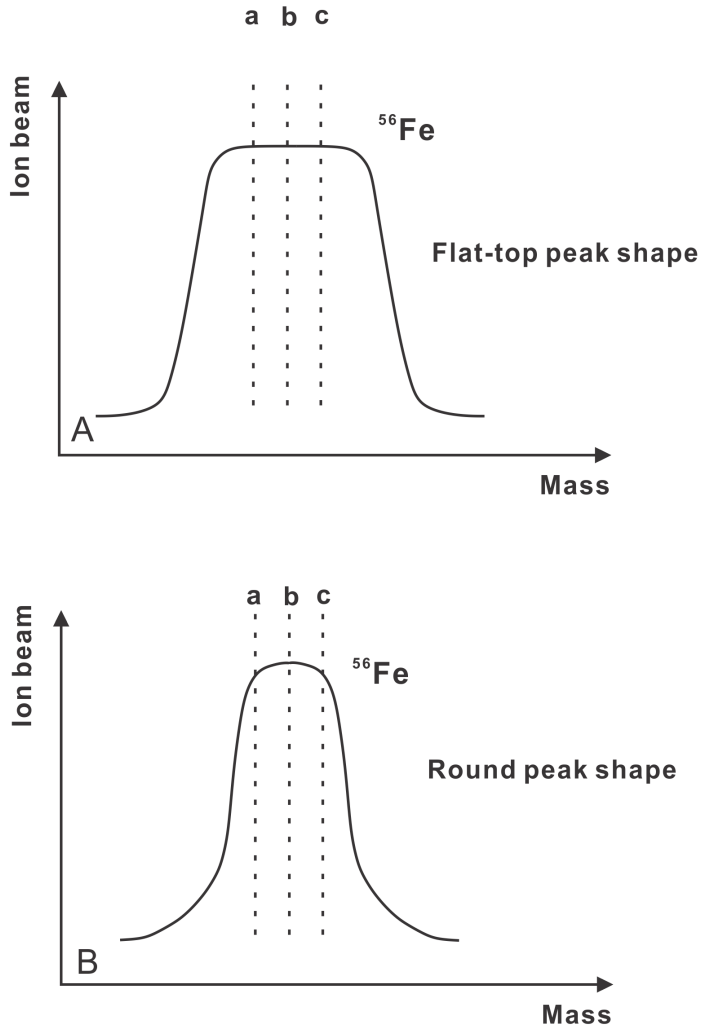


Figure B2 Magnet scans for iron isotope ^{56}Fe in two peak shapes: (A) flat-top peak shape; (B) round peak shape.
The dashed lines (a, b, c) show different analysis mass positions caused by small shifts. In (B), the ion beams (intensity) of ^{56}Fe change with the small variations of mass position (a, b, c), but they remain constant in (A).

An instrumental mass bias (also called mass discrimination effect) between the measured isotope composition and the corresponding true value is created due to the shift of ion beams during transmission from the ion source to the mass spectrometer.[407] Although this bias in isotope measurements is not fully understood, it is likely caused by some processes in

the inductively coupled plasma ion source, such as supersonic expansion of ions and space-charge effect.[425] These processes can cause heavier ions to be more favorably transmitted than lighter ions, which can produce large biases to the measured isotope ratios.[425] The variations in the transmission of samples containing different matrices can also introduce matrix-dependent nonspectral discrimination effects.[425] Therefore, a correction must be applied to correct for the drift, which impacts the instrumental mass discrimination.

Because the mass bias changes slightly during an analysis by MC-MS-ICP, a standard–sample–standard bracketing approach is used for mass bias correction.[244, 424] This approach is designed to erase the drift in measured isotope ratio data due to the instrumental mass bias in order to reveal the natural Fe isotope fractionation inherent in the samples [426]. Before and after each measurement of a sample, the isotopic ratio of Fe standard solution is measured and used to correct the raw data of a sample.[426] This approach can only be used when the matrix difference between samples and Fe reference standards is very small. The matrix difference can introduce drifts in the instrumental mass bias, which can cause inaccurate results during correction.[426] Therefore, a strict chemical separation during the preliminary stage and proper preparation of matrix specific standards are required to eliminate the matrix effect.

Data reporting

Natural mass-dependent variation in Fe isotopes covers a range of ~6‰ (Table B3). Early studies have used the epsilon notation (ε) to report metal isotopic values (ε^{56}Fe, ε^{57}Fe).[427] However, now isotope compositions in most studies are reported as δ values (e.g.: δ^{56}Fe, δ^{57}Fe) given in ‰:

$$\delta^{56}Fe = \left[\left({}^{56}Fe/{}^{54}Fe_{sample}\right)/\left({}^{56}Fe/{}^{54}Fe_{standard}\right) - 1\right] \times 10^3$$

$$\delta^{57}Fe = \left[\left({}^{57}Fe/{}^{54}Fe_{sample}\right)/\left({}^{57}Fe/{}^{54}Fe_{standard}\right) - 1\right] \times 10^3$$

δ^{56}Fe and δ^{57}Fe values are typically normalized to the average of igneous rocks.[244] However, some studies report δ^{56}Fe and δ^{57}Fe values relative to the international standard IRMM014 ($\delta^{56}Fe = -0.09 \pm 0.05$‰ relative to the igneous Fe baseline).[244, 428, 429]

Table B3 Summary of ranges of Fe isotopic compositions in natural environments

Environments		$\delta^{56}Fe^{a}$ (‰)		Reference
		From	To	
Aquifer				
	Groundwater	−3.4	0.58	223, 225, 430, 431
	Sediment	−1.1	0.75	
Lake				
	Porewater	−1.81	0.64	200, 201, 356, 372, 432
	Sediment	−0.72	0.34	
	Water column	−2.14	0.57	
Continental shelf				
	Porewater	−4	1.22	
	Sediment	−0.89	0.15	383, 433-439
	Water column	−3.45	0.04	
Marine				
	Seawater	−0.9	0.71	230, 236, 440-442
	Sediment	−1.8	1	
Soil		−0.64	0.41	184, 203, 222, 258, 443-448
River				
	Dissolved Fe	−0.60	0.51	226, 254, 256, 446, 449
	Suspended Fe	−0.90	0.31	
Human body		−3.6	−0.9	450-452
Total range		−4	1.22	

Reference standards

IRMM certified reference materials, provided by EC-JRC-IRMM (Institute for Reference Materials and Measurements, Belgium), are widely used for inter-laboratory calibration in stable isotope studies. Examples of available reference standards include IRMM014 for Fe and IRMM3702 for Zn (Table B1). When standards like IRMM014 are no longer available (e.g., due to the exhaustion of IRMM014), alternative standards such as IRMM634 are used for Fe isotopic measurements. Other in-house standards (such as HPS Fe; see details in Section 2.2.2), alongside IRMM634, can be additionally employed to test the reliability and reproducibility of data by MC-ICP-MS analysis.

Precision and accuracy

The precision of this technique using the described procedures is ±0.05‰ for $\delta^{56}Fe$ and ±0.07‰ for $\delta^{57}Fe$. To estimate the external reproducibility, at least 10% of the samples are randomly selected to be carried through the entire analytical procedure of sample preparation (different aliquots of the same sample carried through both the ion exchange chromatography and MC-ICP-MS analysis) for replicate measurement. The Fe isotope composition of test solutions should be identical to that of pure standard solutions to ensure that no bias is produced during chemical separations and confirm the accuracy of isotope measurements. The precision and accuracy of isotopic data are evaluated by the standard deviation (2σ) calculated from the repeated analyses of pure standards, test solutions, and samples. The measured external precision is calculated by the average standard deviation of all samples, including the replicates.[205]

Conclusion

MC-ICP-MS is a powerful technique for studying stable metal isotopes providing reliable and rapid isotopic analysis for samples from the natural environment. Application of Fe isotope signatures to biogeochemical Fe cycling is particularly insightful. Fe isotopes can used to investigate constraints on redox conditions and Fe reaction pathways in modern oceans and ancient settings. The advantages of using MC-ICP-MS to analyze stable metal isotope signatures include its high ionization efficiency, low detection limits (ppb concentrations), high precision and rapid analysis. However, MC-ICP-MS is expensive to operate due to large volumes of pure argon gas that are consumed during measurements and the costs of routine instrument maintenance. Due to the variable composition of natural samples, one should bear in mind that a preliminary chemical separation is required to achieve a separation between interfering ions and the metal species of interest and

accompanying standards must be made in the same sample matrix. In addition to standalone MC-ICP-MS techniques, combined MC-ICP-MS with liquid chromatography and MC-ICP-MS with laser ablation are being increasingly explored as powerful analytical techniques for the *in situ* analysis of rock samples.